

**NASA CONTRACTOR
REPORT**

NASA CR-1602



NASA CR-1602
C.1

006085



TECH LIBRARY KAFB, NM

LOAN COPY: RETURN TO
AFWL (WLOL)
KIRTLAND AFB, N MEX

**ANALYTICAL AND
EXPERIMENTAL INVESTIGATION
OF HIGH ENTRAINMENT JET PUMPS**

*by Kenneth E. Hickman, Gerald B. Gilbert,
and John H. Carey*

*Prepared by
DYNATECH R/D COMPANY
Cambridge, Mass.
for Ames Research Center*

NASA CR-1602

TECH LIBRARY KAFB, NM



0060885

ANALYTICAL AND EXPERIMENTAL INVESTIGATION
OF HIGH ENTRAINMENT JET PUMPS

By Kenneth E. Hickman, Gerald B. Gilbert, and John H. Carey

Prepared under Contract No. NAS 2-4824 by

DYNATECH R/D COMPANY

Cambridge, Mass.

for Ames Research Center

NATIONAL AERONAUTICS AND SPACE ADMINISTRATION

For sale by the Clearinghouse for Federal Scientific and Technical Information
Springfield, Virginia 22151 - CFSTI price \$3.00

TABLE OF CONTENTS

<u>Section</u>		<u>Page</u>
	SUMMARY	
1	INTRODUCTION	2
	1.1 Background	2
	1.2 Previous Work	3
	1.3 Purpose	5
2	SYMBOLS	6
	2.1 Symbols Used in the Analysis and Test Results	6
	2.2 Symbols Used in the Computer Program	9
3	ANALYSIS	12
	3.1 Formulation of the Mathematical Model	12
	3.1.1 Assumptions Used in the Analysis	13
	3.1.2 Analysis of the Accommodation Region	13
	3.1.3 Analysis of the Mixing Region	16
	3.1.4 Jet Pump Performance Parameters	18
	3.1.5 Inclusion of Mixing Tube Wall Friction	19
	3.1.6 Dimensionless Formulation	22
	3.1.7 Maximum Entrainment Ratio	28
	3.2 The Computer Program	28
	3.3 Solutions for a Range of Jet Pump Designs	29
	3.4 Jet Pump-Duct Matching Considerations	31
	3.4.1 Representation of Duct Loss Characteristics	31
	3.4.2 Evaluation of the Loss Coefficient, K_L	32
	3.4.3 Development of System Performance Equations	33
	3.4.4 Calculation Procedure for Determining the Operating Point of a Jet Pump in a Duct System	38
	3.4.5 Sample Calculation	40
	3.4.6 Influence of Blowing Duct Area Ratio and Duct Losses Upon Entrainment	42
	3.4.7 Influence of Blowing Duct Area Ratio and Duct Losses Upon Thrust Augmentation	44
	3.4.8 Conclusions	45
4	TEST PROGRAM	47
	4.1 Test Arrangement	47
	4.2 Instrumentation and Data Reduction Procedures	50

TABLE OF CONTENTS (Continued)

<u>Section</u>	<u>Page</u>
4. 2. 1 Instrumentation	50
4. 2. 2 Data Reduction Procedures	51
4. 2. 3 Suction Duct and Nozzle Cluster Losses	53
4. 2. 4 Pressure Loss Due to Wall Friction in the Constant-Area Mixing Tube	56
4. 3 Tabulation of Test Conditions	57
4. 3. 1 Presentation of Data	58
4. 4 Discussion of Test Results	58
4. 4. 1 Comparison of Constant-Area and NAS 2-2518 Varying-Area Mixing Tubes	58
4. 4. 2 Reduced Blockage Nozzle Clusters	63
4. 4. 3 Comparison of Short and Extended Mixing Tubes	66
4. 4. 4 Velocity Profile Investigations	71
5 COMPARISON OF ANALYTICAL AND EXPERIMENTAL RESULTS	74
5. 1 Jet Pump Stagnation Pressure Rise	74
5. 2 Jet Pump Static Pressure Rise	76
6 CONCLUSIONS	78
APPENDIX A - Listing of the Computer Program	81
APPENDIX B Discussion of the Computer Program by Blocks	90
APPENDIX C - Typical Computer Solutions	98
REFERENCES	107
TABLES	110
FIGURES	129

ANALYTICAL AND EXPERIMENTAL INVESTIGATION OF HIGH ENTRAINMENT JET PUMPS

by Kenneth E. Hickman, Gerald B. Gilbert, and John H. Carey

SUMMARY

The use of jet pumps is of increasing interest for boundary layer control or control force augmentation in V/STOL aircraft. In typical applications, a small mass flow of primary air at pressures up to 400 psia can be used to entrain a much larger mass flow of secondary air at ambient conditions. The primary nozzle flow is supersonic while the secondary flow is subsonic. The jet pump system design objectives may be maximum entrainment, maximum thrust augmentation, or some combination of the two. Little information is available in the literature to guide the designer of jet pumps for such applications.

In this investigation, a simple analytical model was developed to predict the performance of high-entrainment compressible flow jet pumps with constant area mixing tubes. While the model is suitable for hand calculation, a computer program was prepared to facilitate calculation of jet pump performance curves and allow comparison of different jet pump designs. Analytical techniques were developed for matching the jet pump design to its associated duct system in order to achieve maximum entrainment or thrust augmentation.

The validity of the analytical model was confirmed by an extensive test program using a multiple-nozzle jet pump with two different mixing tube lengths. The primary-to-secondary flow area ratios were varied from 0.0013 to 0.0067. The primary flow pressure ranged from 55 psia to 350 psia and the primary flow temperature ranged from 200° F to 1200° F. The observed entrainment ratios varied from 15 to 37. The performance of each jet pump geometry was measured over a very broad range of operating conditions in order to develop performance maps for comparison with the analytical predictions.

Section 1

INTRODUCTION

1.1 Background

Jet pumps have been used for many years in industrial applications where a high-pressure gas such as steam is used to pump a lower-pressure gas. The jet pump is a simple low-cost device with no moving parts and is particularly convenient for use with troublesome fluids such as two-phase flows, high-temperature gases, or corrosive gases. Jet pumps are usually employed as low-pressure-rise devices and their thermodynamic efficiency is low, i. e. , under 20%. Because they are low-cost devices of limited performance potential, there has not been a strong incentive for research and development work on industrial jet pumps.

In recent years, applications of jet pumps to boundary layer control systems have become of increasing interest for STOL aircraft. Systems have been proposed which use jet pumps to entrain a large flow of secondary air which is then directed over a deflected flap for lift augmentation. In a configuration patented by F. G. Wagner (references 1 and 2), a jet pump is used to entrain air from one section of the trailing edge of a wing (boundary layer suction upstream of a deflected flap) and then to discharge it over a deflected flap. In this way, the inherent inefficiency of the jet pump is partially balanced by the double employment of the entrained air for boundary layer control. Jet pumps may also have application in VTOL aircraft for direct lift or control force augmentation. The primary, high-pressure flow for the jet pumps can be provided by a bleed from the main engine compressors or by an auxiliary power unit.

The use of jet pumps as primary components of V/STOL aircraft systems places new emphasis upon development of design techniques for these devices. It is essential to be able to minimize the size of jet pumps for particular primary and secondary flow conditions, and to be able to predict the performance of jet pumps over a broad range of operating conditions. However, systematic design and analysis procedures are not available for high-entrainment-ratio compressible-flow jet pumps.

1.2 Previous Work

A number of investigators have carried out analytical and experimental studies of air-to-air jet pumps, primarily for applications requiring high pressure rise or thrust augmentation. The entrainment ratios developed by these jet pumps are low, generally less than 10. Thus, this work is not directly applicable to the high entrainment requirements of V/STOL aircraft systems. Nevertheless, this work provides useful guidance for the development of performance prediction techniques and design rules for high-entrainment jet pumps. A brief review of some of the principal air-to-air jet pump papers follows.

The performance of constant-area jet pumps was analyzed by McClintock and Hood for a range of design and operating conditions in reference 3. The analysis was prepared by assuming incompressible flow but the influence of compressibility was discussed in qualitative terms. Empirical coefficients derived by testing were included in the theory. The influence of mixing length and the use of various multiple-nozzle primary flow geometries were studied experimentally. The jet pumps treated had entrainment ratios of 10 or less; the design goal for the study was achievement of maximum thrust augmentation.

A one-dimensional method of analysis of jet pumps was developed by Keenan, Neumann, and Lustwerk in reference 4. The analysis was applied to both constant-area and constant-pressure mixing processes. Test results were obtained for jet pumps with secondary-to-primary area ratios up to 100, primary-to-secondary pressure ratios up to 200, and a primary-to-secondary temperature ratio of 1.0. The various regimes of operation of jet pumps with supersonic primary flows and both supersonic and subsonic primary flows were described. The analytical results given were for jet pumps developing substantial stagnation pressure rises (e. g. , pressure ratios from 2 to 10) at low entrainment ratios (under 10).

Fabri carried out a number of experiments on jet pumps which supplement the results reported by Keenan, et al. Fabri's results, with supporting analysis, are given in references 5 and 6. These tests also were confined to low entrainment ratio jet pumps. Excellent agreement was obtained between analytical predictions and measured jet pump performance.

An extensive analytical and experimental program was conducted at the University of Minnesota Rosemount Aeronautical Laboratories on jet pumps with secondary-to-primary area ratios up to 36, primary-to-secondary pressure ratios up to 32, and primary-to-secondary temperature ratios up to 3.3. The results are presented in references 7, 8, and 9. Single-nozzle primary flows with constant-area mixing tubes were used in these studies. High entrainment ratios were not an objective of the jet pump design; typical entrainment ratios reported were less than 3. A number of analytical results showing the influence of duct matching upon jet pump and system performance were included in the reports.

An analytical procedure for constant-area jet pumps with subsonic primary flow was developed in reference 10. A computer program was prepared for use in optimizing jet pump design for particular application requirements. An analysis applicable to supersonic primary flows is given in reference 11. The analysis was compared with test results, but was not otherwise applied for jet pump design or optimization.

The performance of a high-entrainment jet pump was measured in the Wagner "Jet Induced Lift" boundary layer control system (figure 1). These tests were performed by the present investigators under NASA contract No. NAS2-2518. The results are reported in reference 12. The jet pump component of the system employed a variable-area mixing tube (designed in an effort to obtain constant pressure mixing) and a 9-nozzle cluster for the primary flow. The jet pump was tested in the system at secondary-to-primary area ratios ranging from 150 to 800, primary-to-secondary pressure ratios up to 26, and primary-to-secondary temperature ratios up to 5.5. The desired constant pressure distribution in the mixing tube was not achieved. The entrainment ratios predicted for the complete system were not attained. The results of the NAS2-2518 program showed that the methods used to design the high-entrainment jet pump and to match it to the duct flow characteristics were inadequate. These results provided the impetus for the present study.

1.3 Purpose

The objectives of this investigation were as follows:

- to develop analytical procedures for predicting the performance of high-entrainment-ratio jet pumps
- to demonstrate the application of these procedures to match a jet pump design to its connecting duct system
- to verify the analytical procedures by testing a jet pump over a broad range of operating conditions and jet pump geometries.

The analysis and experimental work were confined to constant-area mixing tube geometries because both analysis and construction are simplified by this choice. The only other mixing process which can be analyzed without complication is the constant pressure case. However, no reliable methods are available for designing a mixing tube which will actually achieve constant pressure mixing. Furthermore, this condition can be achieved at only one operating point for a jet pump of fixed geometry.

Some of the test results obtained under contract NAS 2-2518 indicated that the design of the nozzle cluster and its position in the mixing tube may have created either high pressure losses in the secondary flow or poor mixing conditions at the mixing tube inlet. The mixing process did not seem to be completed within the length of the mixing tube used. These effects were thought to be partially responsible for the difference between predicted and measured performance for the complete system. Therefore, an additional objective of the present investigation was to test two alternative "low-drag" nozzle cluster designs and an extended mixing tube to determine whether these design changes would lead to significant performance improvements.

Section 2
SYMBOLS

2.1 Symbols Used in the Analysis and Test Results

A	area, ft ²
\bar{A}	area ratio = $A_{th} C_w / A_m$, dimensionless
C	gas specific heat at constant pressure, Btu/lbm-°F
C_w	nozzle flow coefficient, dimensionless
d	duct diameters, inches
f	friction coefficient, dimensionless
g_o	dimensional constant, 32.2 lbm-ft/lbf-sec ²
H	stagnation enthalpy, Btu/lbm
J	conversion factor, 778.2 ft-lbf/Btu
k	gas specific heat ratio, dimensionless
K	duct loss coefficient, dimensionless
L	duct length, inches
m	entrainment ratio = W_s / W_p , dimensionless
m_{max}	maximum entrainment ratio, dimensionless
M	Mach number, dimensionless
P	pressure, psfa or psia
\bar{P}	pressure ratio = P_{po} / P_{so} , dimensionless
P^*	pressure ratio = P_m / P_{so} , dimensionless
q	dynamic head = $\rho V^2 / 2 g_o$, psfa
\bar{q}	dimensionless dynamic head = $\rho V^2 / 2 g_o P_{so}$
r	radius, inches
r_o	outer radius of mixing tube cross section, inches
R	gas constant for air = 53.35 ft-lbf/lbm-°R

T	temperature, °R
\bar{T}	temperature ratio = T_{po}/T_{so} , dimensionless
$\bar{\Pi}$	system thrust augmentation = $W_m V_b / W_p V_{p2}$, dimensionless
V	velocity, ft/sec
\bar{V}	velocity ratio = V_{s2}/V_{p2} , dimensionless
V*	velocity ratio = V_m/V_{p2} , dimensionless
W	mass flow rate, lbm/min
α	parameter defined by equation (34)
β	parameter defined by equation (35)
∂	parameter defined by equation (45)
δ	parameter defined by equation (46)
ΔP	pressure change, psf
ΔP_{ext}	ambient pressure rise imposed upon jet pump system = $P_b - P_{ao}$, psf
ΔP_s	static pressure rise = $P_m - P_{so}$, psf
ΔP_s^*	dimensionless static pressure rise = $(P_m - P_{so})/P_{so}$,
ΔP_t	stagnation pressure rise = $P_{mo} - P_{so}$, psf
ΔP_t^*	dimensionless stagnation pressure rise = $(P_{mo} - P_{so})/P_{so}$
ρ	density, lbm/ft ³
τ	thrust augmentation = $W_m V_m / W_p V_{p2}$, dimensionless
τ_w	wall shearing stress, psi
ϕ	impulse function

Subscripts

a	atmospheric condition
b	blowing duct exit section
d	original conical diffuser exit section
e	test rig diffuser exit section
i	suction duct inlet section
l	overall duct loss coefficient
m	section at end of mixing region
MT	mixing tube
o	stagnation value
p	primary stream variable at nozzle exit
s	secondary stream variable at nozzle exit
SD	section duct
th	primary nozzle throat
1	section at primary nozzle exit
2	section at end of accommodation region

Superscripts

()'	value of parameter at end of frictional mixing tube extension (Section 3.1.5)
$\bar{(\)}$	"mass-momentum" averaged value from test results

2.2 Symbols Used in the Computer Program

<u>Formulation Name</u>	<u>Computer Name</u>	<u>Definition and units</u>
<u>Constants</u>		
g_o	G0	dimensional constant, 32.2 ft-lbm lbf-sec ²
J	CONV	conversion factor, 778 ft-lbf/Btu
R	R	gas constant, ft-lbf/lbm-°R
<u>Variables</u>		
\bar{A}	ABAR1	$A_{th} C_w / A_m$, dimensionless
A_{th}	ATH	nozzle throat area, ft ²
A_p	AP	nozzle exit area, ft ²
A_m	AM	mixing tube area, ft ²
Not Used	ABAR2	A_p / A_m , dimensionless
C_w	CW	nozzle flow coefficient, dimensionless
C_{p2}	CP2	primary specific heat (C_p), location 2, Btu/lbm-°R
C_{s2}	CS2	secondary specific heat (C_p), location 2, Btu/lbm-°R
C_m	CM	specific heat (C_p) at location m, Btu/lbm-°R
H_{p2}	HP2	primary stagnation enthalpy, station 2, Btu/lbm
H_{s2}	HS2	secondary stagnation enthalpy, station 2, Btu/lbm
K_{sd}	FDUCT	suction duct friction coefficient
K_{mt}	FTUBE	mixing tube friction coefficient
M_{p2}	PMOK	primary Mach Number, location 2, dimensionless

<u>Formulation Name</u>	<u>Computer Name</u>	<u>Definition and units</u>
M_{s2}	SMOK	secondary Mach Number, location 2, dimensionless
M_m	EMOK	Mach Number at location m, dimensionless
m	ENTR	entrainment ratio, dimensionless
\bar{P}	PBAR	P_{po}/P_{so} , dimensionless
P_{po}	PPO	primary stagnation process, psi
P_{soi}	PSOI	secondary stagnation pressure at duct inlet, psi
P_{so}	PSO	secondary stagnation pressure at nozzle exit, psi
P_m	PM	static pressure at location m, psi
P_{mo}	PMTOT	stagnation pressure at location m, psi
\bar{T}	TBAR	T_{po}/T_{so} , dimensionless
T_{po}	TPO	primary stagnation temperature, °R
T_{so}	TSO	secondary stagnation temperature, °R
T_{p2}	TP2	primary temperature, location 2, °R
T_{s2}	TS2	secondary temperature, location 2, °R
T_m	TM	temperature at location m, °R
V_{p2}	VP2	primary velocity, location 2, ft/sec
V_{s2}	VS2	secondary velocity, location 2, ft/sec
V_m	VM	velocity at location m, ft/sec
W_p	WP	primary mass flow rate, lbm/min
W_s	WS	secondary mass flow rate, lbm/min
W_m	WM	total mass flow rate, $W_p + W_s$, lbm/min
$P_{mo} - P_{so}$	DELP	stagnation pressure rise, psi

<u>Formulation Name</u>	<u>Computer Name</u>	<u>Definition and Units</u>
$\frac{P_{m0} - P_{so}}{P_{so}}$	DDELP	dimensionless stagnation pressure rise
$P_m - P_{so}$	DSTAT	static pressure change, psi
$\frac{P_m - P_{so}}{P_{so}}$	DDSTAT	dimensionless pressure change
$\frac{\rho_m V_m^2}{2g_o}$	ENER	kinetic energy at location m, lbf/ft ²
$\frac{\rho_m V_m^2}{2g_o P_{so}}$	DENER	dimensionless kinetic energy
τ	AUG	$\frac{W_m V_m}{W_p V_{p2}}$, momentum ratio, dimensionless

Arrays

CHAR1	store solutions for dimensional table
CHAR2	store solutions for dimensionless table
COUNT	store number of solutions for plotting
ENT	store entrainment ratio for plotting
PRISE	store DDELP values for plotting
PTITLE	store title for plotting
SUM	store number of solutions for table
THROS	store AUG values for plotting
TTITLE	store title for plotting

Section 3

ANALYSIS

3.1 Formulation of the Mathematical Model

In this section an analytical model is developed to predict the flow behavior in a compressible flow jet pump with a constant-area mixing tube. The analysis is intended to provide a complete description of the important flow parameters at specific locations within the jet pump and to describe the overall operation of the jet pump as an entrainment and thrust augmentation device. The analysis was prepared for air-to-air jet pumps. The parameters used in the analysis are listed in section 2. The geometrical parameters are shown in figure 2.

The fundamental purpose of the analytical model is to develop the performance characteristics of the jet pump directly. These performance characteristics can be represented by plots of jet pump pressure rise and momentum ratio as functions of entrainment ratio for a number of values of primary jet pressures and temperatures and for various area ratios. The performance characteristics in this form are analogous to head vs. capacity curves or performance maps which are commonly used for pumps and compressors.

The equations describing jet pump performance and flow behavior include the entrainment ratio as an independent parameter. The assumption of a particular value for the entrainment ratio (together with the inlet flow pressures and temperatures and the primary-to-secondary flow area ratio) allows calculation of all of the performance and flow parameters for that operating point. Then another value is assumed for the entrainment ratio and the calculation procedure is repeated. Successive points on the jet pump performance curves are determined in this way until the complete curve is traced out. In the present calculations, the entrainment ratios were limited arbitrarily to the range from 10 to 40. In some cases, the Mach number of the flow in the accommodation region reached 1.0 for an entrainment ratio less than 40. Higher entrainment ratios cannot be achieved in such cases because the constant-area mixing tube chokes when the secondary flow Mach number reaches 1.0.

3. 1. 1 Assumptions Used in the Analysis

The following assumptions are made to simplify the analysis without seriously compromising its accuracy:

1. The values of specific heat at constant pressure (C) and the specific heat ratio (k) are expressed as functions of temperature; otherwise the gas is considered to be a perfect gas.
2. Wall shear forces are assumed to be negligible when compared to the pressure forces and the momentum of the primary and secondary streams. (This assumption is reviewed in section 3. 1. 4.)
3. No heat is transferred across the wall of the jet pump.
4. The mixing tube is assumed to have a constant cross-sectional area along its entire length.
5. When the primary nozzle is operated at an off-design pressure ratio, the primary jet is assumed to expand or contract isentropically until the primary and secondary streams have equal static pressures. This adjustment process is assumed to take place in the accommodation region between sections 1 and 2 (see figure 2) and is assumed to be completed before any mixing takes place between the two streams.
6. The stagnation temperature of the primary flow is assumed to be sufficiently high that moisture condensation shocks do not occur as the flow expands.

3. 1. 2 Analysis of the Accommodation Region

The geometrical parameters and flow conditions in the jet pump are defined as shown in figure 2. The primary stream enters the accommodation region as a very high velocity jet; its Mach number may be as high as 3. 5. The large momentum of the

primary jet induces a secondary flow. In the region defined as the accommodation region, it is assumed that the primary and secondary jets do not mix, but the primary jet expands or contracts until its static pressure matches that of the secondary stream. At the point where the static pressures are equal, denoted as section 2, the accommodation process is assumed to be complete and the flows are parallel. This accommodation process is generally accompanied by a series of oblique expansion and contraction shock waves as the primary flow area adjusts to match the local static pressure outside the jet. However, if the jet pump is operated close to its design conditions, the degree of accommodation is small and the losses caused by the shock waves will be small. A simplified oblique shock analysis indicates that a nozzle designed for 350 psia supply pressure can be operated down to 200 psia with a total pressure loss due to shock waves of only 3%. For the values of supply pressure to be considered here, the error introduced by treating both streams as isentropic flows is negligible. In fact, one of the aims of this research was to show that an assumption of isentropic flow during the accommodation process will produce good results even when the system is operated at conditions quite far from the design point.

As long as the ratio of (P_{po}/P_{so}) is sufficiently high to guarantee a supersonic primary flow, as in the cases being considered here, the primary mass flow rate may be calculated directly using equation (1).

$$W_p = \sqrt{\frac{kg_o}{R} \left(\frac{2}{k+1}\right)^{\frac{k+1}{k-1}}} \frac{144 \times P_{po} (60 \times A_{th} C_w)}{\sqrt{T_{po}}} \quad (1)$$

By specifying an entrainment ratio, $m = W_s/W_p$, the secondary stream mass flow rate can also be found directly.

$$W_s = m W_p \quad (2)$$

In a perfect gas, the local values of total and static pressure are related to the local Mach number by the following equation.

$$P_o/P = \left(1 + \frac{k-1}{2} M^2\right)^{\frac{k}{k-1}} \quad (3)$$

At the end of the accommodation region, the static pressures of the primary and secondary streams are equal. Therefore, at the end of the accommodation region the following relation must be satisfied.

$$P_{po} / \left(1 + \frac{k-1}{2} M_{p2}^2\right)^{\frac{k}{k-1}} = P_{so} / \left(1 + \frac{k-1}{2} M_{s2}^2\right)^{\frac{k}{k-1}} \quad (4)$$

The mass flow rate per unit area for an isentropic flow is given by the relation below:

$$W/A = \sqrt{\frac{k g_o}{R}} \frac{P_o}{\sqrt{T_o}} \left\{ \frac{M}{\left(1 + \frac{k-1}{2} M^2\right)^{\frac{k+1}{2(k-1)}}} \right\} \quad (5)$$

The geometry of the constant area mixing tube requires that $A_{p2} + A_{s2} = A_m$. Using equation (5) to represent A_{p2} and A_{s2} , and inserting the appropriate unit conversion factors, the geometry condition becomes as follows:

$$\frac{W_p}{144 \times 60 \sqrt{\frac{k g_o}{R}}} \left\{ \frac{\sqrt{T_{po}} \left(1 + \frac{k-1}{2} M_{p2}^2\right)^{\frac{k+1}{2(k-1)}}}{P_{po} M_{p2}} + \frac{m \sqrt{T_{so}} \left(1 + \frac{k-1}{2} M_{s2}^2\right)^{\frac{k+1}{2(k-1)}}}{P_{so} M_{s2}} \right\} = A_m \quad (6)$$

When W_p , m , P_{po} , P_{so} , T_{po} , T_{so} and A_m are specified, equations (4) and (6) can be solved simultaneously to obtain M_{p2} and M_{s2} . Equation (5) can be used to find A_{p2} and A_{s2} .

Since the flow of both the primary and secondary streams is assumed to be isentropic in the accommodation region, values of static pressure, temperature, and velocity can be obtained for each stream at location (2) by employing the following equations.

$$P_{p2} = P_{po} / \left(1 + \frac{k-1}{2} M_{p2}^2\right)^{\frac{k}{k-1}} \quad (7)$$

$$T_{p2} = T_{po} / \left(1 + \frac{k-1}{2} M_{p2}^2\right) \quad (8)$$

$$T_{s2} = T_{so} / \left(1 + \frac{k-1}{2} M_{s2}^2\right) \quad (9)$$

$$V_{p2} = \sqrt{\frac{2k}{k-1} \frac{g_o}{R} (T_{po} - T_{p2})} \quad (10)$$

$$V_{s2} = \sqrt{\frac{2k}{k-1} \frac{g_o}{R} (T_{so} - T_{s2})} \quad (11)$$

3.1.3 Analysis of the Mixing Region

The primary and secondary streams enter the mixing region with equal static pressures and parallel velocities. In this region, complete mixing takes place and a uniform flow with constant properties across the channel is obtained at section m. Treating the mixing region as a control volume with completely specified entering flows, the following equations can be applied.

$$\text{Continuity Equation:} \quad W_m = W_p (1 + m) \quad (12)$$

$$\text{Mass Flow Rate:} \quad W_m = 60 \times \rho_m V_m A_m \quad (13)$$

$$\text{Equation of State:} \quad P_m = \rho_m R T_m / 144 \quad (14)$$

Momentum Equation:

$$144 \times 60 \times g_o A_m (P_{s2} - P_m) = W_m V_m - W_p V_{p2} - W_s V_{s2} \quad (15)$$

Energy Equation:

$$W_p H_{p2} + W_s H_{s2} = W_m C_m \left(T_m + \frac{V_m^2}{2g_o J C_m} \right) \quad (16)$$

where H is stagnation enthalpy;

$$H_{p2} = C_{p2} T_{p2} + \frac{V_{p2}^2}{2g_o J}$$

$$H_{s2} = C_{s2} T_{s2} + \frac{V_{s2}^2}{2g_o J}$$

The equation for the specific heat at constant pressure for air as given in the Gas Turbine Engineering Handbook, Gas Turbine Publications, Inc., 1966, page 4, is presented below.

$$C_i = .24916 - .482 \times 10^{-4} T_i + .681 \times 10^{-7} T_i^2 \quad (17)$$

Equations (13) and (14) are combined to give

$$T_m = 60 \times 144 \times (P_m V_m A_m / R W_m) \quad (18)$$

Equation (15) is written in the form

$$V_m = \frac{W_p}{W_m} \left[V_{p2} + m V_{s2} + 60 \times 144 \times \frac{g_o A_m}{W_p} (P_{s2} - P_m) \right] \quad (19)$$

and equations (16) and (18) are combined to yield

$$P_m = \frac{R W_p}{60 \times 144 \times V_m A_m C_m} [H_{p2} + m H_{s2}] - \frac{R W_m V_m}{2 \times 60 \times 144 \times g_o J C_m A_m} \quad (20)$$

Since the values of T_{p2} and T_{s2} are known at the inlet to the mixing region, C_{p2} and C_{s2} can be evaluated directly using equation (17). Equations (12),

(17), (18), (19), and (20) represent five equations for the five unknown exit parameters, W_m , T_m , C_m , P_m and V_m . Therefore, these five equations represent a complete set which describe the properties of the flow leaving the mixing section. In most instances, T_{p2} and T_{s2} are sufficiently close in value to permit the use of a constant specific heat, $C_{p2} = C_{s2} = C_m$. This simplifies the solution by removing equation (17) from the equation set.

3.1.4 Jet Pump Performance Parameters

The jet pump performance parameters which are of particular interest are the stagnation pressure rise and the momentum augmentation. These parameters can be evaluated by using the following expressions.

$$\begin{aligned} \Delta P_t &= P_{mo} - P_{so} \\ \Delta P_t &= P_m \left(1 + \frac{k-1}{2} M_m^2\right)^{\frac{k}{k-1}} - P_{so} \end{aligned} \quad (21)$$

and

$$\begin{aligned} \tau &= \text{outlet momentum/primary momentum} \\ \tau &= \frac{W_m V_m}{\bar{W}_p V_{p2}} = \frac{(m+1) V_m}{V_{p2}} \end{aligned} \quad (22)$$

During the jet pump test program, the measurement of the stagnation pressure rise produced by the jet pump proved to be difficult to accomplish. It was much easier to measure the stagnation-to-static pressure rise in the jet pump. This pressure rise can be used to define another jet pump performance parameter, ΔP_s , which serves as an alternative to the stagnation pressure rise parameter, ΔP_t .

$$\Delta P_s = P_m - P_{so} \quad (23)$$

All of the values needed to compute ΔP_t , ΔP_s , and τ are provided by the analyses of sections 3.1.2 and 3.1.3.

3.1.5 Inclusion of Mixing Tube Wall Friction

The analysis of the mixing region presented in section 3.1.3 neglected the effect of wall friction; this simplifies the equations describing the mixing process. In this section, a procedure is developed to include the effects of wall friction in the jet pump analysis.

The mixing region was assumed to extend from the point where the primary and secondary stream pressures are equal to the point where they have merged into a uniform flow with constant properties across the channel. In reality, the wall friction effects occur in conjunction with the mixing process. Unfortunately, it is difficult with the current state of knowledge to predict wall friction losses accurately in the mixing region. Therefore, rather than adjust the mixing region analysis to include the wall friction effects, we considered that it would be preferable at this time to treat the mixing process and wall friction as independent effects by imagining the mixing tube to extend as shown in figure 3 beyond the point where the mixing process is complete. The flow phenomena occurring in the mixing portion, segment I, is a mixing process without wall friction as analyzed in section 3.1.3. The frictional portion, segment II, represents the effect of wall shear forces upon a uniform adiabatic flow. The hypothetical extension of the mixing tube is meant to represent the friction occurring within the actual mixing tube.

The effect of wall shear forces in ducts is commonly represented by a coefficient of friction defined as follows:

$$f = \frac{\tau_w}{\rho V^2 / 2g_o} \quad (24)$$

where τ_w is the shearing stress exerted upon the stream by the wall. The corresponding stagnation pressure loss is given by equation (25).

$$\Delta P_o = 4 f \frac{L}{D} \frac{\rho V^2}{2g_o} \quad (25)$$

where

L = duct length

D = duct diameter

In many flow analyses, the value of the coefficient of friction is taken from test results for pipe flow. The friction coefficient is a function of wall roughness and Reynolds number. However, in the case of the mixing tube, the wall friction occurs in a very non-uniform flow which has a high level of turbulence. The value of the coefficient of friction for the mixing tube cannot be accurately determined from pipe flow data. Therefore, it is convenient to represent the mixing tube wall friction loss in terms of a head loss factor, K_{MT} , which must be determined experimentally.

$$\Delta P_o \Big)_{\text{mixing tube}} = K_{MT} \frac{\rho_m V_m^2}{2 g_o} \quad (26)$$

The equations for an adiabatic flow in a constant-area tube with a stagnation pressure loss are given below. Primed variables denote parameters at the end of the hypothetical extension of the mixing tube.

Momentum Equation:

$$144 P_m \left(1 + \frac{k-1}{2} M_m^2\right)^{\frac{k}{k-1}} - 144 P_m' \left(1 + \frac{k-1}{2} M_m'^2\right)^{\frac{k}{k-1}} = K_{MT} \frac{\rho_m V_m^2}{2 g_o} \quad (27)$$

Energy Equation:

$$C_m T_m + \frac{V_m^2}{2 g_o} = C_m T_m' + \frac{V_m'^2}{2 g_o} \quad (28)$$

Continuity Equation:

$$\rho_m V_m = \rho_m' V_m' \quad (29)$$

State Equation:

$$P_m = \rho_m R T_m \quad (30)$$

$$P_m' = \rho_m' R T_m' \quad (31)$$

Definition of Mach Number:

$$M_m^2 = \frac{V_m^2}{g_o k R T_m} \quad (32)$$

$$M_m'^2 = \frac{V_m'^2}{g_o k R T_m'} \quad (33)$$

These equations can be combined to give the following results:

$$P_m' \left(1 + \frac{k-1}{2} M_m'^2\right)^{\frac{k}{k-1}} = \alpha \quad (34)$$

$$P_m'^2 M_m'^2 \left(1 + \frac{k-1}{2} M_m'^2\right) = \beta \quad (35)$$

where

$$\alpha = P_m \left\{ \left(1 + \frac{k-1}{2} M_m^2\right)^{\frac{k}{k-1}} - K_{MT} \frac{k M_m^2}{2} \right\} \quad (36)$$

$$\beta = P_m^2 M_m^2 \left(1 + \frac{k-1}{2} M_m^2\right) \quad (37)$$

Eliminating P_m' between equation (34) and equation (35) yields equation (38) which can be used to determine M_m' .

$$\frac{1}{M_m'} \left(1 + \frac{k-1}{2} M_m'^2\right)^{\frac{k+1}{2(k-1)}} = \alpha/\sqrt{\beta} \quad (38)$$

After equation (38) is solved for M_m' , equation (34) can be used to determine P_m' . Combining equations (29), (30), (31), (32), and (33), an equation for T_m' is obtained.

$$T_m' = T_m (P_m'/P_m)^2 (M_m'/M_m)^2 \quad (39)$$

Equation (33) is then used to determine V_m' .

The equations developed in this section can be used to compute the values of P_m' , T_m' , M_m' , and V_m' for a jet pump when the "ideal" analysis of sections 3.1.2 and 3.1.3 is completed and the value of K_{MT} is known or assumed. Alternatively, these equations may be used to deduce the value of K_{MT} when values of P_m' , T_m' , and V_m' are known from test results and values of P_m , T_m , and V_m are computed by using the "ideal" analysis.

3.1.6 Dimensionless Formulation

In this section the equations describing the jet pump operation are formulated in terms of dimensionless variables. The non-dimensional formulation is valuable for two reasons:

- According to the principles of dimensional analysis, a solution in terms of independent non-dimensional groups is a general one. The same solution may be applied for jet pumps having great differences in individual design or operating parameters so long as the independent non-dimensional groups are identical. For example, one such group is the primary-to-secondary flow area ratio, $A_{th} C_w / A_m$; if all other non-dimensional groups are the same, a large-scale and small-scale jet pump having identical area ratios will have identical non-dimensional performance characteristics.
- The non-dimensional formulation permits identification of the minimum number of independent non-dimensional groups

which are required to completely specify a jet pump design and its operating characteristics.

In the derivation which follows, unit conversion factors are not included, and all values of the specific heats (C_p , C_s , C_m) are assumed to be constant and equal.

The equations which apply in the mixing region are given below.

$$\text{Continuity Equation:} \quad W_m = W_p (1 + m) \quad (12)$$

$$\text{Mass Flow Rate:} \quad W_m = \rho_m V_m A_m \quad (40)$$

$$\text{Equation of State:} \quad P_m = \rho_m R T_m \quad (41)$$

Momentum Equation:

$$g_o A_m (P_{s2} - P_m) = W_m V_m - W_p V_{p2} - m W_p V_{s2} \quad (42)$$

Energy Equation:

$$T_{po} + m T_{so} = (m + 1) C \left[T_m + \frac{V_m^2}{2g_o C} \right] \quad (43)$$

The dimensionless variables to be used are defined as follows.

$$V^* = V_m/V_{p2}; \quad P^* = P_m/P_{so}, \quad \bar{P} = P_{po}/P_{so}, \quad (44)$$

$$\bar{T} = T_{po}/T_{so}, \quad \bar{A} = A_{th} C_w/A_m$$

Using these variables, equations (12), (40), (41), (42), and (43) can be combined as follows.

$$P^* = (P_{s2}/P_{so}) + \gamma \left[1 + m (V_{s2}/V_{p2}) - (m + 1) V^* \right] \quad (45)$$

$$V^{*2} + \frac{k}{(k-1)} \frac{2 P^* V^*}{\gamma (m+1)} - \frac{\delta}{(m+1)} \left(1 + \frac{m}{\bar{T}}\right) = 0 \quad (46)$$

where

$$\gamma = W_p V_{p2} / g_o A_m P_{so} \quad (47)$$

and

$$\delta = 2 g_o C T_{po} / V_{p2}^2 \quad (48)$$

Equations (45) and (46) show that P^* and V^* are related through γ , δ , P_{s2}/P_{so} , V_{s2}/V_{p2} , m , k , and \bar{T} .

The equations which govern the flow in the accommodation region are developed next. For an isentropic primary stream,

$$T_{p2}/T_{po} = (P_{p2}/P_{po})^{\frac{k-1}{k}} = \left[\frac{1}{\bar{P}} \frac{P_{s2}}{P_{so}} \right]^{\frac{k-1}{k}} \quad (49)$$

$$W_p = \sqrt{\frac{k g_o}{R} \left(\frac{2}{k+1} \right)^{\frac{k+1}{k-1}} \frac{P_{po}}{\sqrt{T_{po}}} (A_{th} C_w)} \quad (50)$$

and

$$V_{p2} = \sqrt{\frac{2 g_o k R}{k-1} T_{po} (1 - T_{p2}/T_{po})} \quad (51)$$

Equations (49), (50), and (51) can be combined to give

$$\gamma = \frac{\bar{P}}{\bar{A}} \sqrt{\frac{2k^2}{k-1} \left(\frac{2}{k+1} \right)^{\frac{k+1}{k-1}}} \bar{A} \sqrt{1 - \left[\frac{1}{\bar{P}} \left(\frac{P_{s2}}{P_{so}} \right) \right]^{\frac{k-1}{k}}} \quad (52)$$

Similarly, equations (44) and (51) can be used to obtain a value for δ :

$$\delta = 1 / \left\{ 1 - \left[\frac{1}{\bar{P}} \left(\frac{P_{s2}}{P_{so}} \right) \right]^{\frac{k-1}{k}} \right\} \quad (53)$$

Thus, γ and δ are shown to be functions of \bar{P} , \bar{A} , k and P_{s2}/P_{so}

The secondary stream velocity is given by equation (54):

$$V_{s2} = \sqrt{\frac{2 g_o k R}{k-1} T_{so} \left(1 - \frac{T_{s2}}{T_{so}} \right)} \quad (54)$$

Equations (49), (51), and (54) can be combined to yield

$$V_{s2}/V_{p2} = \sqrt{\frac{1}{T}} \sqrt{\frac{1 - \left(\frac{P_{s2}}{P_{so}} \right)^{\frac{k-1}{k}}}{1 - \left[\frac{1}{\bar{P}} \left(\frac{P_{s2}}{P_{so}} \right) \right]^{\frac{k-1}{k}}}} \quad (55)$$

From the definition of total or stagnation pressure,

$$P_{s2}/P_{so} = 1 / \left(1 + \frac{k-1}{2} M_{s2}^2 \right)^{\frac{k}{k-1}} \quad (56)$$

Considering equations (51), (53), (55), and (56) together, it can be seen that the parameters γ , δ , V_{s2}/V_{p2} , and P_{s2}/P_{so} are functions of M_{s2} , \bar{P} , \bar{T} , \bar{A} , m and k only. Equation (5) of section 3.1.2 can be written for the secondary stream as follows.

$$\frac{M_{s2}}{\left(1 + \frac{k-1}{2} M_{s2}^2 \right)^{\frac{k+1}{2(k-1)}}} = \frac{W_s \sqrt{T_{so}}}{P_{so} \sqrt{\frac{k g_o}{R}} (A_m - A_p)} \quad (57)$$

Equation (57) can be combined with equation (50) and written in terms of dimensionless variables as given below.

$$\frac{M_{s2}}{\left(1 + \frac{k-1}{2} M_{s2}^2\right)^{\frac{k+1}{2(k-1)}}} = \frac{m \left(\frac{2}{k+1}\right)^{\frac{k+1}{2(k-1)}} \bar{P} \bar{A}}{\sqrt{\bar{T}} (1 - A_p/A_m)} \quad (58)$$

For high entrainment ratio jet pumps, the term A_p/A_m is of order 0.01. Thus, the term $(1 - A_p/A_m)$ can be approximated as unity. Equation (58) can now be written as follows.

$$\frac{M_{s2}}{\left(1 + \frac{k-1}{2} M_{s2}^2\right)^{\frac{k+1}{2(k-1)}}} = m \left(\frac{2}{k+1}\right)^{\frac{k+1}{2(k-1)}} \frac{\bar{P} \bar{A}}{\sqrt{\bar{T}}} \quad (59)$$

Equation (59) shows that M_{s2} can be determined from m , \bar{P} , \bar{A} , \bar{T} , and k . This indicates that γ , δ , V_{s2}/V_{p2} , and P_{s2}/P_{so} are functions of \bar{P} , \bar{T} , \bar{A} , k and m . Returning to equations (45) and (46), it can be seen that the performance of the jet pump depends upon the parameters \bar{P} , \bar{T} , \bar{A} , k and m . For given values of \bar{P} , \bar{T} , \bar{A} and k , a complete dimensionless solution can be obtained for each specified value of entrainment ratio.

The jet pump performance parameters can be expressed in the form of dimensionless groups using the fundamental dimensionless parameters. The momentum augmentation, τ , is already a dimensionless group:

$$\tau = \frac{W_m V_m}{W_p V_{p2}} = (m + 1) V^* \quad (60)$$

The dimensionless stagnation pressure rise parameter is defined as follows:

$$\Delta P_t^* = \frac{\Delta P_t}{P_{so}} = P^* \left(1 + \frac{k-1}{2} M_m^2\right)^{\frac{k}{k-1}} - 1 \quad (61)$$

To evaluate ΔP_t^* , it is necessary to know M_m^2 . Using the dimensionless variables, M_m^2 is given by equation (62).

$$M_m^2 = \frac{V_m^2}{k g_o R T_m} = \frac{V^*}{P^*} \left(\frac{m+1}{k} \right) \gamma \quad (62)$$

Thus, ΔP_t^* is a function of the fundamental dimensionless variables which determine V^* , P^* , and γ . The static pressure rise parameter, ΔP_s , can be expressed in dimensionless form as follows:

$$\Delta P_s^* = \frac{P_m - P_{so}}{P_{so}} = P^* - 1 \quad (63)$$

Equations (60) through (63) show that the dimensionless jet pump performance parameters are functions of the fundamental independent dimensionless variables \bar{P} , \bar{T} , \bar{A} , k , and m . Five such independent variables and only five have to be specified in order to determine the jet pump performance characteristics in dimensionless terms. (This conclusion is restricted to jet pumps which satisfy the assumptions listed in section 3.1.1 and the additional assumption that the specific heats of all of the streams are equal, i.e., $C = C_{p2} = C_{s2} = C_m$.)

It is possible to use a different set of five independent dimensionless variables. For example, a velocity ratio $\bar{V} = V_{s2}/V_{p2}$ can be used in place of \bar{T} to complete an alternative set of five independent variables, \bar{P} , \bar{V} , \bar{A} , k and m . Another possible set is \bar{P} , \bar{T} , \bar{A} , k , and \bar{V} . The velocity ratio, \bar{V} , was one of the basic design parameters used to select the jet pump geometry for the boundary layer control system tested under contract No. NAS 2-2518.

These remarks can be summarized by the expressions below:

<u>Jet Pump Performance Characteristics</u> (dependent variables)	<u>Design and Operating Conditions</u> (independent variables)
ΔP_t^* , ΔP_s^* , and τ are functions of	$\left\{ \begin{array}{l} \bar{P}, \bar{T}, \bar{A}, k, m \\ \text{or} \\ \bar{P}, \bar{V}, \bar{A}, k, m \\ \text{or} \\ \bar{P}, \bar{T}, \bar{A}, k, \bar{V} \end{array} \right.$

3.1.7 Maximum Entrainment Ratio

Equation (59) can be used to determine the maximum possible entrainment ratio. This maximum occurs when the secondary stream Mach number reaches a value of unity. Setting $M_{s2} = 1$, equation (59) can be written as follows.

$$m_{\max} = \frac{\sqrt{\bar{T}}}{\bar{P} \bar{A}} \quad (64)$$

Thus, the maximum entrainment ratio corresponding to the choking of the secondary stream can be determined directly from the dimensionless initial conditions.

3.2 The Computer Program

A computer program was prepared to predict the performance characteristics of constant area jet pumps using the analytical concepts formulated in the preceding sections. The program was written to develop both dimensional and dimensionless solutions. Values of \bar{P} , \bar{T} , \bar{A} , P_{so} , T_{so} , and A_m are read in as initial conditions. Values of k , R , and m are included within the program. For each value of m , values of τ , ΔP_t , ΔP_s , ΔP_t^* , and ΔP_s^* are calculated. The values of τ , ΔP_t^* , and ΔP_s^* depend only on the dimensionless data, while ΔP_t and ΔP_s depend also upon P_{so} , T_{so} , and A_m .

The program is written in Fortran IV language. The machine used was an IBM System 360/65 with an SC4020 plotter. Automatic plotting of the performance characteristics was obtained by using the subroutine EZPLOT developed by the Missile Systems Division of Avco Corporation, Burlington, Massachusetts.

A block diagram of the computer program is shown in figure 4. For each set of initial conditions, solutions are obtained for values of entrainment ratio between 10.0 and 40.0 in steps of 3.0. The results are printed as each solution corresponding to a particular value of entrainment ratio is determined. The results are also stored in arrays for plotting and for presentation in tabular form. A printout of the entire program is presented in Appendix A. A discussion of the program by blocks is given in Appendix B. Appendix C provides typical computer solutions which indicate the form of the output data.

Certain of the blocks shown in figure 4 and described in Appendix B are denoted as optional, indicating that they can be removed from the program without interfering with the operation of the remaining blocks. Instructions for removing these blocks are given in Appendix B, section B-2.

When frictional effects in the suction duct and mixing tube are to be taken into account in the performance predictions, values of the loss coefficients K_{sd} (defined in Appendix B) and K_{MT} must be provided as input data for the computer solution. These loss coefficients are functions of the flow Reynolds numbers. If values of K_{sd} and K_{MT} have been established for ducts of one size and the computer performance predictions are to be used for ducts of much larger or smaller sizes, it may be advisable to adjust the values of the loss coefficients used by the computer to account for the Reynolds number change.

3.3 Solutions for a Range of Jet Pump Designs

The computer program was applied to develop jet pump performance plots for a broad range of geometries and operating conditions. The range of solutions was selected to encompass all of the test conditions used in this investigation (section 4) and also the range of conditions of interest to NASA for boundary layer control systems and momentum augmentation. The performance plots were developed for use in preliminary design of jet pump systems for matching the jet pump to a duct system and for predicting the resulting system performance characteristics. Techniques for applying the solutions to system design are described in section 3.4.

The range of conditions used to obtain the performance plots were initially defined in dimensional form as follows:

T_{po}	primary flow stagnation temperature	450° F to 3500° F
P_{po}	primary flow stagnation pressure	100 psia to 400 psia
T_{so}	secondary flow stagnation temperature	20° F to 120° F
P_{so}	secondary flow stagnation pressure	1500 psfa to 2116 psfa

The range of values selected for the corresponding dimensionless parameters were as follows:

$$\bar{T} = 1.5 \text{ to } 8.0$$

$$\bar{P} = 5 \text{ to } 40$$

The nozzle and mixing tube geometries available for the test program had area ratio values (\bar{A}) ranging from 0.00125 to 0.0067. The range of values selected for the performance plots is given below:

$$\bar{A} = 0.001 \text{ to } 0.007$$

The ranges of values of \bar{P} , \bar{T} , and \bar{A} given above were used to prepare 9 sets of performance plots showing ΔP_t^* vs. m and τ vs. m for various values of \bar{P} with \bar{T} and \bar{A} fixed; these plots are indexed in table 1 and given in figures 6 through 23. Table 1 includes the values of maximum entrainment ratio attainable for each combination of \bar{P} , \bar{T} , and \bar{A} values. This maximum entrainment ratio is set by choking of the secondary stream as given by equation (64) of section 3.1.7.

Typical computer output sheets for one of the solutions are reproduced in Appendix C. The printed output includes values of jet pump parameters not shown in the plots but required for the jet pump-duct matching techniques described in section 3.4. These parameters are given in dimensional form based upon standard secondary stream inlet conditions, $P_{SO} = 2102$ psfa, $T_{SO} = 70^\circ\text{F}$, and $A_m = 0.08726 \text{ ft}^2$.

In the last six cases, the higher values of \bar{P} cannot be attained because of choking of the flow in the mixing tube. For the cases with $\bar{T} = 1.5$ and 3.5 , choking occurs in the secondary flow ($M_{s2} = 1$) as discussed in section 3.1.7. When \bar{T} was set at 8.0 , choking was predicted to occur first at the mixing tube exit, i. e., $M_m = 1$.

Cross-plots showing ΔP_t^* vs. m and τ vs. m for various values of \bar{A} with \bar{T} and \bar{P} fixed are presented in figures 24 and 25. Lines of constant mixing tube exit Mach number are also shown. These cross-plots provide additional insight on the effect of the area ratio upon jet pump performance.

3.4 Jet Pump-Duct Matching Considerations

The previous sections have developed analytical techniques and a computer program which allow prediction of the performance characteristics of high-entrainment-ratio jet pumps. The performance characteristics take the form of plots of jet pump pressure rise and momentum ratio as functions of entrainment ratio for a number of values of primary jet pressures and temperatures and for various area ratios. These performance characteristics are analogous to head vs. capacity curves or performance maps which are commonly used for pumps and compressors. The actual point (i. e. , entrainment ratio) at which a jet pump will operate when connected to a particular system of inlet and discharge ducts is dictated by the geometry of the duct system.

The resistance curve of a duct system is roughly parabolic as shown in figure 26. A typical jet pump characteristic is also shown on the figure . The actual operating point of the jet pump-duct combination is defined by the intersection of the two curves. The duct characteristic curve is set by the duct geometry and is essentially independent of the jet pump operating conditions. Therefore, if the duct geometry is not changed, the operating point of the system for any jet pump primary flow condition must be located on the parabola. Figure 27 shows how the operating points for a system can be determined if the jet pump performance at various pressure levels is known.

This section establishes a procedure for use to determine the operating points of a jet pump in a duct system when the loss characteristics of the duct system are known. This procedure can be employed as shown by example to match the jet pump design to the duct system so as to achieve maximum entrainment ratio or maximum thrust augmentation for given primary flow conditions.

3.4.1 Representation of Duct Loss Characteristics

When the analytical model developed in sections 3.1 and 3.2 is supplied with values of \bar{P} , \bar{T} and \bar{A} , the performance parameters such as stagnation pressure rise and momentum ratio (thrust augmentation) can be calculated as a function of entrainment ratio. In order to determine the specific value of entrainment ratio which will

be obtained during operation of a given jet pump of fixed geometry, the associated duct system flow characteristics must be taken into account. Using the notation shown in figure 2 , the stagnation pressure rise may be written as follows:

$$\Delta P_t = P_{mo} - P_{so} = (P_{ao} - P_{so}) + (P_{mo} - P_{bo}) + P_{bo} - P_{ao} \quad (65)$$

The two bracketed terms together represent the stagnation pressure loss of the duct system including the inlet duct (first term) and blowing duct (second term).

At low Mach numbers, the stagnation pressure loss due to friction in a duct is proportional to the kinetic energy of the flow. For high entrainment ratio jet pumps, the mass flow rates in the suction and blowing ducts are nearly equal. Therefore, the total pressure loss of the entire ducting system may be related as a first approximation to the kinetic energy of the blowing duct inlet flow by equation (66):

$$(P_{mo} - P_{bo}) + (P_{ao} - P_{so}) = K_\ell \frac{\rho_m V_m^2}{2 g_0} \quad (66)$$

This type of expression has been shown to be accurate for representing frictional losses in duct systems of various shapes.

3.4.2 Evaluation of the Loss Coefficient, K_ℓ

The loss coefficient K_ℓ depends on the geometry of the particular ducts being used and the Mach number level (ref.13). At sufficiently low Mach numbers, (i. e. , under 0.3), compressibility effects can be neglected. For flows at higher Mach numbers, the value of K_ℓ can be corrected for compressibility effects.

Loss coefficients have been presented for a number of duct configurations in references 13 through 26. The configurations reported include ducts of rectangular and circular cross section with varying amounts of diffusion or acceleration. Bends and elbows having a number of different angles of turn are included in these references. The loss coefficients reported were measured for subsonic flow covering a range of Mach numbers up to 1.0.

To provide an example of typical loss data, the influence of Mach number level upon the loss coefficient for straight, conical diffusers is shown in figure 28. The variation of K_ℓ with inlet Mach number is significant for a diffuser of specified geometry.

Because the value of K_ℓ is closely related to the duct configuration and the Mach number level, and values of K_ℓ are readily available for only a few simple duct shapes, the designer of a jet pump and duct system generally will not be able to look up an accurate value for K_ℓ for a new duct design. If optimum matching of the jet pump and ducting is required, the loss coefficient of a new duct geometry will have to be determined experimentally. Testing can be done by using either a full-scale or reduced scale model of the duct. The tests must cover the Mach number range which will be encountered by the actual duct when operating with the jet pump. Flow tests of ducts sometimes have additional value; regions of flow separation or undesirable velocity profiles may be revealed. When the duct geometry is modified to eliminate these problems, the loss coefficient is usually reduced.

3.4.3 Development of System Performance Equations

At the outlet of the blowing duct, the static pressure in the flow must be equal to the local "atmospheric" pressure. The use of a blowing duct having the same cross-sectional area as the constant-area mixing tube will limit the entrainment ratio which can be achieved in the jet pump system. Higher entrainment ratios can be obtained with the same jet pump if a diffuser is added to the blowing duct. The diffuser allows higher velocities and flow rates in the mixing tube. The mixing tube pressures can be sub-atmospheric; the diffuser decelerates the flow to increase its static pressure up to the atmospheric pressure level at the blowing duct exit.

A calculation method can be developed for use to determine the actual operating point (i. e. , entrainment ratio) for a jet pump system as a function of the area ratio selected for the blowing duct diffuser. The calculation method makes use of the generalized jet pump performance characteristics developed by the computer program described in section 3.2 and Appendix B.

The loss coefficient defined in equation (66) is inserted in equation (65) with the following result:

$$\Delta P_t = (P_{bo} - P_{ao}) + K_l q_m \quad (67)$$

where

$$q_m = \frac{\rho_m V_m^2}{2 g_o}$$

Equation (67) may be rewritten as follows:

$$\Delta P_t = (P_b - P_{ao}) + K_l q_m + (P_{bo} - P_b) \quad (68)$$

The term $(P_b - P_{ao})$ represents the external ambient pressure difference imposed upon the jet pump system. This term will be called ΔP_{ext} :

$$\Delta P_{ext} = (P_b - P_{ao}) \quad (69)$$

The value of ΔP_{ext} was zero for the experimental jet pump since both the discharge static pressure (P_b) and inlet stagnation pressure (P_{ao}) for the jet pump system were equal to atmospheric pressure. This term is not necessarily zero for jet pump systems which operate in the presence of an external velocity field. For example, a jet pump used for boundary layer control at the trailing edge of a wing will have its inlet pressure (P_{ao}) established by the flow behavior in the suction slot entry passages and by the local pressure acting on the wing. The discharge pressure (P_b) will be set by the local pressure field on the wing and by the flow behavior from the slot to the deflected flap.

The term $(P_{bo} - P_b)$ in equation (68) represents the dynamic head of the flow at the blowing duct exit. This term is related to the blowing duct exit Mach number as shown in equation (70):

$$(P_{bo} - P_b) = P_b \left(\frac{P_{bo}}{P_b} - 1 \right) = P_b \left[\left(1 + \frac{k-1}{2} M_b^2 \right)^{\frac{k}{k-1}} - 1 \right] \quad (70)$$

In order to evaluate this term, the value of M_b must be calculated using the selected blowing slot area A_b , the exit pressure P_b , and the flow conditions at the discharge of the jet pump mixing tube:

$$M_b \sqrt{1 + \frac{k-1}{2} M_b^2} = \frac{W_m}{A_b} \sqrt{\frac{T_{mo}}{P_b}} \sqrt{\frac{R}{k g_o}} \quad (71)$$

This equation is based upon the assumption that the flow in the blowing duct is adiabatic. The values of T_{mo} and W_m are output values from the jet pump performance calculations described in the previous section. The evaluation of M_b can be made conveniently by using figure 29.

Equations (70) and (71) can be replaced by equation (72) when the blowing duct exit Mach number, M_b , is less than 0.3.

$$P_{bo} - P_b = \frac{\rho_b V_b^2}{2 g_o} \quad (72)$$

The error in using equation (72) in place of equations (70) and (71) is less than 2% of the true $(P_{bo} - P_b)$ difference when M_b is less than 0.3.

A particularly simple jet pump-duct system matching equation can be derived when equation (72) is used. Equation (73) is the continuity relation for the blowing duct:

$$\rho_m V_m A_m = \rho_b V_b A_b \quad (73)$$

The influence of the blowing duct area ratio is introduced when equation (73) is combined with equation (72):

$$P_{bo} - P_b = q_m \left(\frac{A_m}{A_b} \right)^2 \frac{\rho_m}{\rho_b} \quad (74)$$

The jet pump-duct matching equation, equation (75), is derived by combining equations (68), (69) and (74):

$$\Delta P_t = \Delta P_{\text{ext}} + q_m \left[K_l + \left(\frac{A_m}{A_b} \right)^2 \frac{\rho_m}{\rho_b} \right] \quad (75)$$

for

$$M_b \leq 0.3$$

For preliminary design purposes, the value of ρ_m/ρ_b can be taken as 1.0. A more accurate value can be determined as follows:

For a perfect gas,

$$\frac{\rho_m}{\rho_b} = \frac{P_m}{P_b} \frac{T_b}{T_m} \quad (76)$$

With M_b less than 0.3, equation (77) holds with an error of less than 2%:

$$T_b \cong T_{b0} \quad (77)$$

Since the flow in the blowing duct is adiabatic, its stagnation temperature remains constant;

$$T_{b0} = T_{m0} \quad (78)$$

The last relation required is equation (79):

$$\frac{T_{m0}}{T_m} = 1 + \frac{k-1}{2} M_m^2 \quad (79)$$

When equations (76) through (79) are combined, an equation for calculating ρ_m/ρ_b is derived:

$$\frac{\rho_m}{\rho_b} \cong \frac{P_m}{P_b} \left(1 + \frac{k-1}{2} M_m^2 \right) \quad (80)$$

Equations (74), (75), and (80) can be used with small error only if M_b is less than 0.3. If M_b is greater than 0.3, the jet pump-duct matching equation, equation (81), is derived by combining equations (68), (69), and (70):

$$\Delta P_t = \Delta P_{ext} + K_l q_m + P_b \left[\left(1 + \frac{k-1}{2} M_b^2 \right)^{\frac{k}{k-1}} - 1 \right] \quad (81)$$

for all values of M_b

where M_b is computed by using equation(71) and figure 29.

There are two figures of merit which are of interest in the evaluation of jet pump systems for boundary layer control or thrust augmentation applications. These figures of merit are the entrainment ratio and the thrust augmentation. The equations developed above can be used to determine the entrainment ratio at which a jet pump system will operate. Several additional equations are required in order to calculate the thrust augmentation obtained from a jet pump system.

The thrust augmentation obtained with the complete system is defined in equation (82):

$$\begin{aligned} \Pi &= \text{system thrust augmentation} \\ \Pi &= \frac{W_m V_b}{W_p V_{p2}} \end{aligned} \quad (82)$$

The thrust augmentation produced by the jet pump alone was designated as τ in section 3.1.4 (equation 22). The computerized jet pump performance analysis of section 3.2 provides as output data values of τ as a function of entrainment ratio. Thus, once the entrainment ratio is known for a jet pump system, the value of τ is known and the system thrust augmentation can be calculated as follows:

$$\begin{aligned} \tau &= \frac{W_m V_m}{W_p V_{p2}} \\ \text{so} \quad \Pi &= \tau \frac{V_b}{V_m} \end{aligned} \quad (83)$$

The value of V_b/V_m can be related to the blowing duct area ratio by using equation (73):

$$\frac{V_b}{V_m} = \frac{\rho_m}{\rho_b} \frac{A_m}{A_b} \quad (84)$$

The value of ρ_m/ρ_b is given by equation (80) when $M_b \leq 0.3$. When M_b exceeds 0.3, the value of ρ_m/ρ_b is given by equation (85):

$$\frac{\rho_m}{\rho_b} = \frac{p_m}{p_b} \frac{(1 + \frac{k-1}{2} M_m^2)}{(1 + \frac{k-1}{2} M_b^2)}, \quad (85)$$

where the blowing duct flow has been assumed to be adiabatic and the value of M_b is determined by using equation(71) and figure 29.

The equations given above can be used to compute the thrust augmentation parameter once the operating point of the jet pump is known. The next section establishes a procedure for determining the operating point.

3.4.4 Calculation Procedure for Determining the Operating Point of a Jet Pump in a Duct System

The operating point of a given jet pump and duct combination can be determined as follows:

Required Initial Data:

Given: Jet pump design and performance characteristics:

basic jet pump parameters	}	P_{so} P_{po} T_{so} T_{po} $A_{th} C_w$ A_m k
---------------------------	---	--

jet pump performance curves; output data from computer program	}	ΔP_t vs m q_m vs m M_m vs m P_m vs m
values characterizing the particular duct system	}	K_ℓ ΔP_{ext} P_b A_b

Solution technique if $M_b \leq 0.3$:

The specified values of K_ℓ , ΔP_{ext} , P_b , and A_b are inserted into equations (80) and (75). The jet pump performance curves are used to find associated values of ΔP_t , q_m , M_m , and P_m which satisfy equation (75). This is a trial-and-error process which is begun by assuming a value for entrainment ratio, m . The corresponding values of M_m and P_m are determined from the jet pump performance curves and entered into equation (80). The resulting value of ρ_m/ρ_b is entered, together with the value of q_m from the jet pump curves, into the right-hand side of equation (75). If the resulting value of ΔP_t does not agree with the curve value, a new value of m is assumed and the process is repeated. The iteration process is simplified by graphical solution techniques which are described in the section entitled "Sample Calculation". This calculation process finds the value of m at which the jet pump system will operate with the selected value of A_b .

Solution technique if $M_b > 0.3$:

The specified values of K_ℓ , ΔP_{ext} , P_b , and A_b are inserted into equations (81) and (71). The jet pump discharge flow rate, W_m , and the stagnation temperature of the discharge flow, T_{mo} , are plotted as functions of entrainment ratio, m . Values of M_b can be determined as a function of m using equation (71) and figure 29. The solution technique is a trial-and-error process which is begun by assuming a value for m . The jet pump performance curves are used to find values of q_m and

ΔP_t for each value of m assumed. Corresponding values of M_b are determined as above and entered with the q_m values into the right-hand-side of equation (81). If the resulting value of ΔP_t does not agree with the curve value, a new value of m is assumed and the process is repeated. Graphical solution techniques, described in the section below, can reduce the number of iterations required.

Evaluation of thrust augmentation:

The solution techniques described above yield the value of entrainment ratio at which a jet pump will operate in a selected duct system. The performance data provided by the jet pump computer program allows determination of the values of the following jet pump performance parameters at the operating point: τ , P_m , M_m , W_m , and T_{mo} . These values allow calculation of the thrust augmentation, Π , by using the equations presented at the end of section 3.4.3.

Additional Comments:

The values of K_ℓ and P_{so} are not constant for all values of entrainment ratio. At high entrainment ratios, the Mach number levels within the ducts may become sufficiently high that the influence of compressibility upon K_ℓ must be taken into account. Similarly, the value of P_{so} , which is a non-dimensionalizing parameter in the jet pump performance analysis, varies slightly as shown in equation (86) when the entrainment ratio (and secondary stream flow rate) changes.

$$P_{so} = P_{ao} - K_i q_m \quad \text{where } q_m \text{ varies with } m \quad (86)$$

The variations of K_ℓ and P_{so} with entrainment ratio are generally second-order in magnitude. These variations can be neglected in preliminary design calculations, then included for final design if K_ℓ and K_i are known as functions of the Mach number $M_m \cong M_i$.

3.4.5 Sample Calculation

The use of the procedure described above to determine the operating point of a jet pump-duct system is illustrated by the sample calculation which follows:

The jet pump design data is:

$$\begin{array}{l}
 P_{po} = 300 \text{ psia} \\
 P_{so} = 14.9 \text{ psia}
 \end{array}
 \left. \vphantom{\begin{array}{l} P_{po} \\ P_{so} \end{array}} \right\} \bar{P} = 20.13$$

$$\begin{array}{l}
 T_{po} = 1200^\circ \text{ F} \\
 T_{so} = 80^\circ \text{ F}
 \end{array}
 \left. \vphantom{\begin{array}{l} T_{po} \\ T_{so} \end{array}} \right\} \bar{T} = 3.074$$

$$\begin{array}{l}
 A_m = 0.08726 \text{ ft}^2 \\
 A_{th} C_w = 0.000165 \text{ ft}^2
 \end{array}
 \left. \vphantom{\begin{array}{l} A_m \\ A_{th} C_w \end{array}} \right\} \bar{A} = 545.4 \quad (\text{Test value for the Case 4 nozzle})$$

The computer solution for the jet pump performance yielded the values given in table 2 . The values of ΔP_t , P_m , M_m , and q_m are plotted against entrainment ratio in figure 30.

The duct system design conditions were assumed to be as follows:

$$\begin{array}{l}
 \Delta P_{ext} = 0 \quad (\text{i. e. , } P_b = P_{ao}) \\
 K_\ell = 0.1 \\
 P_{ao} = 14.9 \text{ psia}
 \end{array}$$

The blowing slot discharge Mach number, M_b , was assumed to be less than 0.3. Using these values in equation (75) equation (87) was derived.

$$\Delta P_t = q_m \left[0.1 + \left(\frac{A_m}{A_b} \right)^2 \frac{\rho_m}{\rho_b} \right] \quad (87)$$

The calculations were begun for a blowing duct diffuser area ratio, (A_b/A_m) , equal to 1.0. Three values of entrainment ratio, $m = 13, 15, \text{ and } 17$, were selected arbitrarily. The corresponding values of ΔP_t , M_m , q_m , and P_m were read off from figure 30. These values were used to compute ρ_m/ρ_b from

equation (80) and then to compute the right-hand side of equation (87); the right-hand side will be called $\Delta P_t)_{\text{trial}}$. The results are given in the table below.

For $A_b = 1.0$:

m	ΔP_t (psf)	M_m	q_m (psf)	P_m psia	$\frac{\rho_m}{\rho_b}$	$\Delta P_t)_{\text{trial}}$ (psf)
13	99.6	.205	65.3	15.15	1.02	74.9
15	98.5	.235	87	15.00	1.01	96.8
17	97.5	.270	109	14.80	1.01	121

The $\Delta P_t)_{\text{trial}}$ values can be plotted against entrainment ratio as shown in figure 31. The intersection of the $\Delta P_t)_{\text{trial}}$ curve with the ΔP_t jet pump performance curve represents the solution of equation (87) for the selected value of A_b/A_m . This intersection is the operating point of the jet pump in the specified duct system.

3.4.6 Influence of Blowing Duct Area Ratio and Duct Losses Upon Entrainment

Similar calculations were carried out for values of A_b/A_m equal to 2, 3, and 4. The results are shown in figure 31. The entrainment ratio increases as the blowing duct area ratio is increased; the trend is more clearly shown when the results are replotted as in figure 32. For the particular jet pump and system design conditions assumed for this sample calculation, the maximum entrainment ratio is achieved when the mixing tube is choked, i.e., when $M_{s2} = 1.0$.

The influence of the duct loss coefficient was explored by setting $K_\ell = 0.2$ instead of 0.1 as previously assumed. The duct matching calculations were repeated using equation (75); the results are shown in figure 32. Only a small increase in entrainment ratio can be obtained by increasing the area ratio from 4 to 5. This is a consequence of the fact that, by using a sufficiently large area ratio in the blowing duct diffuser, the term $(P_{bo} - P_b)$ in equation (68) can be reduced to almost zero. In that case, equation (75) takes the following form:

$$\Delta P_t \cong \Delta P_{\text{ext}} + K_\ell q_m \quad (88)$$

for small values of A_m/A_b

The maximum value of entrainment ratio is the value for which equation (89) holds:

$$K_\ell q_m = \Delta P_t - \Delta P_{\text{ext}} \quad (89)$$

In the present example, with $K_\ell = 0.2$ and $\Delta P_{\text{ext}} = 0$, the limiting value of entrainment ratio is found by use of figure 30 to be 34. The corresponding mixing tube exit Mach number, M_m , is 0.615.

The results show that the maximum entrainment ratio which can be achieved in a duct system driven by a particular constant-area jet pump is set by one of two conditions:

- by choking at the mixing tube outlet or the suction duct inlet (i. e. , $M_m = 1.0$ or $M_{s2} = 1.0$) if the duct losses are sufficiently low
- or
- by the duct loss limit which is represented by equation (89) if the value of M_m remains below 1.0.

The form of equation (75) is such that, along curves representing constant values of K_ℓ , an increase in blowing duct diffusion always yields an increase in entrainment ratio until the limiting value is reached. In practice, K_ℓ is a variable which depends upon the diffuser area ratio. In jet pump systems with low-loss inlets, the value of K_ℓ is determined primarily by the blowing duct loss coefficient which increases as the area ratio increases. This trend is shown for conical diffusers in figure 28. Examples of the effect of the variation of K_ℓ are shown by the dashed curves in figure 32; these curves represent the loss characteristics of 15° and 20° conical diffusers. The peak entrainment ratio for the 20° diffuser is achieved by using an area ratio of 3; higher area ratios lead to reduced entrainment because of increased losses.

3.4.7 Influence of Blowing Duct Area Ratio and Duct Losses Upon Thrust Augmentation

Figure 33 shows the thrust augmentation parameter, τ , for the jet pump itself. This curve is taken directly from the computer calculations for the jet pump selected in section 3.3.5. In order to determine the values of the system thrust augmentation parameter Π in relation to the blowing duct diffuser area ratio A_b/A_m and the loss coefficient K_ℓ , figure 32 was used to determine the entrainment ratio corresponding to selected values of A_b/A_m and K_ℓ . Then figure 33 was used to find the associated values of τ . The equations of section 3.4.3 permitted calculation of Π .

The variation of system thrust augmentation with blowing duct diffuser area ratio is shown in figure 34. The curve for $K_\ell = 0$ yields maximum thrust augmentation when the mixing tube is choked, i.e., for $M_m = 1.0$. Even with a very low loss in the duct system ($K_\ell = 0.1$), the thrust augmentation reaches a maximum value at a mixing tube Mach number less than 1.0. The curves for $K_\ell = 0.1$ and 0.2 show that the thrust augmentation does not fall off rapidly if the diffuser area ratio is made larger than optimum. This suggests that, when designing a duct system without complete data on duct losses, it is preferable to err on the side of increased diffusion.

The relationship of system thrust augmentation to the entrainment ratio is shown in figure 35. The thrust augmentation peaks on the curve for $K_\ell = 0.1$ and 0.2 and then falls off with increasing entrainment ratio. This is a consequence of the fact that the thrust augmentation is proportional to the product of entrainment ratio and blowing duct exit velocity as follows:

$$\Pi = (m + 1) \frac{V_b}{V_{p2}}$$

where $(m + 1) \approx m$ for high entrainment ratio jet pumps
and $V_{p2} \approx \text{constant}$

so

$$\Pi \approx m V_b \quad (90)$$

In order to achieve entrainment ratios higher than the value at the peak of the Π curve, the diffuser area ratio must be increased. This has the effect of reducing the exit velocity V_b faster than entrainment increases. The net effect is a reduction of the product $m V_b$ and thus Π .

The maximum entrainment ratio attainable is set by the choking limit for the $K_\ell = 0$ and $K_\ell = 0.1$ cases. For the $K_\ell = 0.2$ case, the maximum entrainment value is set by the duct loss limit as represented by equation (84). At this limit, the diffuser area ratio is very large and the duct exit velocity is zero. Consequently, Π must be zero as shown by equation (85). This illustrates the general rule that the thrust augmentation in a jet pump system is always zero at maximum entrainment unless the jet pump mixing tube is choked.

3.4.8 Conclusions

The two previous sections have shown the influence of duct losses and blowing duct diffuser area ratio upon the entrainment ratio and thrust augmentation obtained in a jet pump-duct system. The results shown in figures 32, 34, and 35 are quantitatively valid only for the particular jet pump geometry and operating conditions which were chosen in the section 3.4.5. However, the figures illustrate trends which are qualitatively correct for high entrainment compressible flow jet pumps as a general class.

The results show that the design goals of maximum entrainment and maximum thrust augmentation may require different duct geometries; a system designed for maximum entrainment may have a low value of the thrust augmentation parameter and vice versa. The influence of duct losses is shown to be very strong. Entrainment ratios and thrust augmentation both can be improved significantly by making only minor reductions in the duct loss coefficient. This provides considerable incentive for testing flow models of proposed new duct designs in order to adjust their geometry to achieve minimum losses. Accurate estimates of duct loss coefficients can be obtained from these tests; such estimates are required in order to predict the performance of a new jet pump system and to allow selection of the best diffuser area ratio.

The design problem for a jet pump system often takes the following form:

Given: Primary flow pressure, temperature, and flow rate
 Duct system inlet and discharge pressure levels and
 inlet pressure

Problem: What is the proper mixing tube area and blowing
 duct diffuser area ratio to be used to achieve the
 design goal, e. g. , maximum entrainment or thrust
 augmentation ?

The information provided in plots like figures 32, 34, and 35, together with duct loss estimates, will allow the designer to evaluate the effect of diffuser area ratio upon entrainment ratio and thrust augmentation for a selected mixing tube area. By preparing similar sets of curves for several other values of mixing tube area, the designer can choose the best combination of mixing tube area and diffuser area ratio to meet the design goals. New jet pump performance curves analogous to figures 30 and 32 will be required for each value of mixing tube area to be considered. Data for these performance curves can be obtained by using the computer program described in section 3.2. A series of computer solutions covering a broad range of jet pump geometries and operating conditions is provided in section 3.2 for use in preliminary design calculations.

Section 4

TEST PROGRAM

The test program had two major objectives:

- to provide data for use to evaluate the analytical model
- to determine whether new, reduced-blockage nozzle clusters could be used to improve the performance of the original jet pump

The tests covered a range of operating conditions and nozzle geometries as indicated below:

Primary Flow

pressure range	55 psia to 400 psia
temperature range	200° F to 1200° F
nozzle throat area range	$1.1 \times 10^{-4} \text{ ft}^2$ to $6.0 \times 10^{-4} \text{ ft}^2$
nozzle cluster	three designs
nozzle geometry	four designs

Secondary Flow

inlet pressure	laboratory ambient
inlet temperature	laboratory ambient
mixing tube geometry	constant area = $.087 \text{ ft}^2$, two lengths
pressure rise	regulated by discharge throttling device

This section of the report describes the jet pump test arrangement, the test program, and the results which were obtained.

4.1 Test Arrangement

The jet pump test arrangement with its instrumentation is shown schematically in figure 36. The primary flow supply system employed a 2-stage reciprocating

compressor capable of supplying 7 lbm/min of air at 400 psia. Electrical heaters were used to achieve temperatures up to 1200° F. The primary flow was delivered to a multiple-nozzle cluster directed along the axis of a constant-area circular mixing tube.

The momentum of the primary flow entrains a secondary air flow from the room into the bellmouth inlet and then into the mixing tube. Here, the two streams mix together and the stagnation pressure of the secondary stream is increased. The flow from the mixing tube passes through a conical diffuser and exhausts to the atmosphere through an adjustable throttling cone.

The individual components of the experimental jet pump are described below:

1. Calibrated bellmouth inlet section.

This component consists of a wooden bellmouth, metal connecting tube, and fiberglass primary flow inlet section. The bellmouth differential pressure was calibrated in terms of flow rate by using an orifice and blower available in the laboratory. The calibrated bellmouth permitted direct measurement of secondary mass flow rate for all jet pump tests.

A ceramic insert was used to protect the fiberglass duct from the hot primary flow pipe and flange.

2. Mixing Tube

The original variable-area mixing tube from the previous investigation (ref. 12) was used for the first tests in order to provide baseline performance data. This mixing tube had a length of 6.87" (figure 37). After the initial tests were completed, the mixing tube was bored out to a constant inner diameter of 4.000". A mixing tube extension of the same diameter was also fabricated. The remainder of the test program was completed using both the original mixing tube length of 6.87" and the extended mixing tube length of 18.87".

3. Conical Diffuser

The initial section of the conical diffuser had a length of 10.98" and an area ratio of 1.79. This diffuser section was previously used during the Wagner BLC system tests. An additional section was added to this diffuser to obtain an overall area ratio of 5.0. The purpose of the exhaust diffuser was to maximize the static pressure recovery so that the highest possible system entrainment ratio could be achieved. Changes in the axial positioning of the throttle cone in the diffuser discharge produced a variable system resistance. The jet pump performance characteristic (pressure rise versus entrainment ratio) was generated by varying the system resistance in this manner.

4. Nozzle Cluster Geometry

The nozzle cluster geometry used in the previous investigation (ref. 12) was believed to cause excessive blockage of the secondary flow at the mixing tube inlet, thus causing reduced performance of the jet pump system. Two "reduced-blockage" nozzle cluster configurations were tested in order to determine whether improved performance could be achieved.

The first reduced blockage nozzle cluster was made by placing 2.0" long nozzle extensions between the original nozzle cluster body and each of the nine nozzles. This change moved the cluster body back away from the mixing tube inlet in order to reduce the velocity level around the cluster by increasing the adjacent flow area. This change is shown on figure 38.

The second reduced blockage nozzle cluster was a completely new design consisting of 7 nozzles at the end of small diameter tubes (1/4" dia.). This low drag cluster is shown on figure 39.

5. Primary Nozzle Geometry

Five sets of primary flow nozzles were used in the test program. The throat size, nozzle type, and design conditions are listed in table 3.

The first four nozzle sets listed in table 3 were used with the original nozzle cluster and also the first reduced-blockage configuration (original cluster with 2" extension tubes). The fifth set, Case LD#2-4, consisted of seven nozzles for the second reduced-blockage cluster. The Case LD#2-4 nozzles were designed for the same operating conditions as the Case 4 nozzles of the original cluster.

The nozzle flow coefficients listed in the table were calculated from test results according to the definition below:

$$C_w = \frac{W_p}{W_{p \text{ ideal}}}$$

where

W_p = measured nozzle flow rate at design pressure and temperature

$W_{p \text{ ideal}}$ = isentropic flow rate through nozzle throat at design pressure and temperature; based upon one-dimensional flow assumption

4.2 Instrumentation and Data Reduction Procedures

4.2.1 Instrumentation

The instrumentation used to determine the performance of the experimental jet pump is shown on figure 40 and described in table 4.

The jet pump inlet bellmouth was calibrated for use as a flowmeter. The calibration was accomplished by connecting the bellmouth and the suction duct to the inlet of a blower. An orifice and a throttling arrangement were included in the blower system. The blower permitted calibration of the bellmouth up to a flow rate of 200 lbm/min. The resulting bellmouth flow equation is given on the following page:

$$W_s = 229.5 \sqrt{\rho_b \Delta h_b} \quad (91)$$

where

Δh_b = P_b differential pressure, inches of water gage

ρ_b = inlet density, lbm/ft³

Stagnation pressure traverses were made in the mixing tube and diffuser with a Kiel probe. When the short mixing tube configuration was used, traverses were taken only in the diffuser at the location shown in figure 40. When the mixing tube extension was used, stagnation pressure traverses were taken in the tube 16.4 inches downstream from the primary nozzle exit plane. Additional traverses were made in the diffuser 26.4 inches downstream from the primary nozzle exit plane.

The angular orientation of the traverse locations is shown on figure 40. The same numbering system was used for all traverse locations.

4.2.2 Data Reduction Procedures

The measured data were used to calculate the following jet pump performance parameters.

$$m = \frac{W_s}{W_p} \quad - \quad \text{jet pump entrainment ratio}$$

$$\Delta P_s = \frac{P_m - P_{so}}{P_{so}} \quad - \quad \text{jet pump static pressure parameter}$$

$$\Delta P_t^* = \frac{P_{mo} - P_{so}}{P_{so}} \quad - \quad \text{jet pump stagnation pressure rise parameter}$$

$$V \text{ vs. } \left(\frac{r}{r_o}\right)^2 \quad - \quad \text{velocity profiles}$$

$$P \text{ vs. distance} \quad - \quad \text{jet pump static pressures}$$

$$P \text{ vs. } m \text{ and } P_{po}$$

The static pressure parameter was calculated using the wall static pressure measured at the discharge of the short mixing tube or the maximum static pressure reached within the extended mixing tube. The secondary flow stagnation pressure at the mixing tube inlet (P_{so}) was determined by subtracting the measured bell-mouth inlet and cluster loss (section 4.2.3) from the barometric pressure.

The jet pump stagnation pressure rise parameter, ΔP_t^* , is based upon the secondary flow total pressure P_{so} and upon P_{mo} . Our first tests showed that it was not possible to measure P_{mo} accurately with the "short" mixing tube, i. e., the original 6.87" mixing tube length. Complete mixing was not achieved by the end of this short tube; sharp velocity peaks corresponding to the primary flow jets were observed at the exit section. These peaks were too sharp to be accurately measured by stagnation pressure probes of reasonable size. Therefore, the stagnation probe measurements could not be used to determine P_{mo} with the necessary accuracy.

To obtain an approximate value of P_{mo} for the short mixing tube tests we used the following procedure:

Stagnation pressure probe traverse data was taken at the conical diffuser exit section, P_{do} in figure 40. This data was used to determine an average stagnation pressure (P_{do}) by procedures described below. Then the value of P_{mo} was computed by using equation (92) which accounts for the diffuser stagnation pressure loss.

$$P_{mo} = P_{do} + K \frac{\rho_m V_m^2}{2g_o} \quad (92)$$

The value of K was selected to be 0.05, a value representative of the loss coefficient for a good diffuser.

The procedure used to determine an average stagnation pressure from the stagnation pressure probe readings was the "mass-momentum integral method". The stagnation pressure was measured along a diameter at the diffuser traverse location. A wall static pressure measurement was obtained at that cross-section. Using the ratio of the local stagnation pressure and the wall static pressure at each point along the diameter, the local Mach number was determined. Using a plot of $(1 + kM^2)$ vs. cross-section area (i. e., r^2/r_o^2), the impulse function was determined by graphical integration:

$$\varphi = \text{impulse function} = P \int (1 + kM^2) dA \quad (93)$$

The following equations were used to determine the "mass momentum" averaged properties of this non-uniform compressible flow:

$$\text{- calculate } \bar{M} \text{ from: } \frac{\bar{M} \sqrt{1 + \left(\frac{k-1}{2}\right) \bar{M}^2}}{1 + k \bar{M}^2} = \frac{W_m \sqrt{\frac{RT_{e0}}{kg_o}}}{\varphi} \quad (94)$$

$$\text{- calculate } P \text{ (static) from: } \bar{P} = \frac{\varphi}{(1 + k \bar{M}^2) A} \quad (95)$$

$$\text{- calculate } P_o \text{ (stagnation) from: } \bar{P}_o = \bar{P} \left[1 + \left(\frac{k-1}{2}\right) \bar{M}^2 \right]^{\frac{k}{k-1}} \quad (96)$$

These "mass-momentum average" values of pressure satisfy the measured mass flow rate and integrated momentum of the flow. They correspond to values that would be obtained if the actual non-uniform flow was mixed to a uniform flow in a frictionless, constant area duct.

To calculate P_{mo} for the extended mixing tube, the "mass momentum integral method" was applied to the traverse data taken in the mixing tube 16.4" downstream from the primary nozzle exit plane. No correction for diffuser losses was needed in this case.

The velocity profiles were calculated from the local values of Mach number and the measured jet pump exhaust temperature (T_{e0}).

4.2.3 Suction Duct and Nozzle Cluster Losses

In order to calculate the jet pump pressure rise parameters ΔP_s and ΔP_t^* , the mixing tube inlet stagnation pressure P_{so} is required. The value of P_{so} was determined by subtracting the appropriate suction duct and nozzle cluster

stagnation pressure losses from barometric pressure (the suction duct inlet stagnation pressure). The loss data used for the determination of P_{so} is given below.

Bellmouth Inlet

The stagnation pressure losses in the bellmouth, suction duct, and nozzle cluster configuration used in the test rig (figure 36) were measured for the following four configurations:

1. Original nozzle cluster
2. Original nozzle cluster with 2" nozzle extensions (figure 38)
3. "Low-drag" nozzle cluster (figure 39)
4. No nozzle cluster

The loss measurements were made by connecting the jet pump including the initial section of the conical diffuser (area ratio 1.79) to the suction line of a blower and orifice installation. Air was drawn through the bellmouth and jet pump system by the blower. The stagnation pressure at the end of the constant area mixing tube was calculated using the measured wall static pressure and the Mach number (computed on a one-dimensional basis) at the same measuring station. The stagnation pressure loss was set equal to the difference between this value and the atmospheric pressure. The loss values for the four nozzle configurations are presented on figure 41. These loss values include the suction duct loss, the nozzle cluster loss, and the short mixing tube wall friction loss ($L/d_m = 1.35$).

The results show that the losses are identical for the two reduced blockage clusters #2 and 3. A comparison of the losses for the low blockage clusters to the losses for the original cluster and the minimum possible losses (the "no cluster" curve) shows that the reduced blockage clusters cut the cluster losses by about 42%.

These results were used for two purposes:

1. to guide the selection of the "optimum" nozzle cluster

2. to permit calculation of P_{so} at the jet pump inlet by subtracting the suction tube and nozzle cluster losses from the atmospheric pressure. The P_{so} value was used to calculate the static pressure parameter ΔP_s^* and the stagnation pressure rise parameter ΔP_t^* .

BLC Suction Duct

The data obtained during tests of the Wagner BLC system under the previous contract NAS 2-2518 indicated that the aerodynamic drag of the present nozzle cluster was much higher than had been expected. This drag was considered to be one of the principal reasons for the difference between the predicted and actual performance of the jet pump BLC system. To check this point, the NAS 2-2518 suction duct (figure 42), the short mixing tube, and the initial section of the conical diffuser were connected to the inlet of the blower and orifice system. The original nozzle cluster geometry was installed in the suction duct. The tests results are shown on figure 41. The BLC suction duct produced higher losses than the bellmouth configurations.

Still using the NAS 2-2518 suction duct, the nozzle cluster was dismantled in 3 steps with a loss test made between each step. The nine nozzles only were removed first but no decrease in loss was measured. Next, the cluster body was removed but the elbow was left in place. The measured losses dropped by 13% to the "no cluster" curve shown on figure 41. This amounts to a 5 psf loss reduction for a jet pump entrainment ratio of 20 ($W_s = 128$ lb/min). When the elbow was removed, no further reduction of losses was observed. Therefore, the cluster body with its extensions produced the nozzle cluster losses.

This series of loss tests shows that the nozzle cluster losses are much smaller than had been deduced from the experimental data obtained on the jet pump BLC system. The NAS 2-2518 final report showed suction duct losses to be three times the values shown on figure 41. At that time, a large percentage of these losses were attributed to the nozzle cluster. The results in figure 41 show that this conclusion was incorrect for two reasons:

1. The calculation of suction duct stagnation pressure loss from the BLC system data is sensitive to the choice of the static pressure value at the mixing tube inlet to be used for the calculation. The static pressure data recorded by the first 2 or 3 pressure taps in the first half-inch of the mixing tube always showed a sharp spike of low static pressure at the mixing tube inlet. The static pressure variation becomes more gradual from about the fourth tap onward in the mixing tube. Testing of the mixing tube with the BLC suction duct during the series of loss tests of figure 41 showed this same variation of static pressure even without the nozzle cluster in place. The spike of static pressure must be caused by the local curvature of the streamlines as the flow reaches the mixing tube throat. If suction duct losses are calculated from the third or fourth static pressure tap instead of the first tap measurement, the calculated BLC suction duct losses would compare favorably to the measured losses shown on figure 41.
2. The loss tests on the BLC suction duct showed that the duct itself causes most of the suction duct losses. The nozzle cluster accounts for about 13% of the suction duct loss which may amount to 4% to 8% of the total system resistance.

4.2.4 Pressure Loss Due to Wall Friction in the Constant-Area Mixing Tube

The mixing tube wall friction loss levels must be taken into account when comparing the experimental pressure parameters to the analytical predictions which do not include these losses. Therefore, the pressure loss in the extended mixing tube was measured during the nozzle cluster loss tests which were described in section 4.2.3. The wall static pressure was measured at two points 10.88 inches apart in the constant 4" diameter mixing tube while air was being drawn through the tube by the blower. The total pressure change was calculated using the local Mach numbers (determined on a one-dimensional flow basis) at the two cross sections. The static

pressure change and the stagnation pressure loss as a function of flow rate are given in figure 43. The static pressure change is larger than the stagnation pressure loss because of compressibility effects. The measured loss levels agree well with predictions based upon pipe friction factors for fully-developed turbulent flow.

When the jet pump is operating, the mixing tube velocity profiles differ from the profiles for fully-developed turbulent flow in pipes because of the primary flow - secondary flow interactions. Therefore, wall friction losses in a jet pump mixing tube can be expected to differ somewhat from the losses predicted for fully-developed turbulent flow. No data correlations or analytical procedures are available to allow accurate prediction of wall friction losses in mixing tubes. Thus, pipe friction factor correlations or equivalent test results as in figure 43 must be used as a first approximation in order to estimate mixing tube wall friction losses so that the analytical predictions of jet pump performance can be compared to the experimental results.

4.3 Tabulation of Test Conditions

The jet pump testing was carried out in three series of tests. The configurations used and the test objectives are described below.

Series 1: The jet pump included the calibrated bellmouth inlet, the original short NAS 2-2518 mixing tube with varying area, and the original nozzle cluster. The purpose of this test series was to determine the performance of the jet pump as used in the NAS 2-2518 BLC system tests.

Series 2: The jet pump included the calibrated bellmouth inlet, the short constant-area mixing tube, and three nozzle clusters; the original NAS 2-2518 cluster, the same cluster with 2" nozzle extensions and moved back from the mixing tube throat (i. e. , low-drag cluster #1), and the low-drag nozzle cluster #2 as in figure 39. The objectives of this test series were to determine the effect of nozzle cluster design upon jet pump performance and to determine which cluster would be best for subsequent testing.

Series 3: The jet pump configurations tested included the calibrated bellmouth inlet, both the short and the extended constant-area mixing tubes, and the optimum nozzle cluster selected from the results of test series #2 (the LD#1 cluster). The purpose of this test series was to provide experimental verification of the jet pump performance analysis over a broad range of operating conditions. Each of the four nozzle sets described in table 3 were used; they were operated not only at their design points but also at off-design pressures and temperatures.

A description of the individual tests, operating conditions and configurations is given in table 5.

4.3.1 Presentation of Data

Tabulated data and graphical results are presented for each of the run numbers listed in table 5 . An index to the tables and figures is given in table 6 . The test data is presented in tables 8 to 19 and figures 44 to 84.

4.4 Discussion of Test Results

4.4.1 Comparison of Constant-Area and NAS 2-2518 Varying-Area Mixing Tubes

The original NAS 2-2518 short mixing tube was designed to have a 5.5% contraction in area from inlet to outlet. The tube was intended to have constant-pressure mixing at its design point. Since the jet pump has not been able to produce a flow rate as high as the mixing tube design flow rate, the constant static pressure condition was never achieved. However, a nearly-constant static pressure distribution has been approached near the discharge end of the mixing tube at the higher flow rates obtained during the test program.

The short constant-area mixing tube was made by boring out the NAS 2-2518 mixing tube to a constant internal diameter of 4.00".

Entrainment Ratio Results

Tables 8 and 9 present the primary and secondary flow rates and the entrainment ratio for each test point recorded for the two short mixing tube configurations. For each primary stagnation pressure, the maximum entrainment ratio represents the test where the throttle cone was moved out of the exhaust diffuser as far as it would go. The two test configurations were then completely identical except for the mixing tube. The data shows that use of the NAS 2-2518 mixing tube resulted in maximum entrainment ratios about 6% to 8% higher than the constant-area mixing tube configuration. A basic difference was observed between the measured velocity profiles at the diffuser discharge (see below).

Jet Pump Stagnation and Static Pressure Parameter Results

The experimental results for both mixing tube configurations are compared to the analytical predictions in figure 48. Both the stagnation and static pressure parameters are plotted for four primary pressures.

The experimental stagnation pressure rise values calculated from a single traverse were found to be 13% to 32% below the analytical predictions. The one experimental value calculated from traverses in two perpendicular directions was 8% below the analytical prediction. The differences between the experimental and analytical values are caused by a combination of effects listed below.

- The experimental value is very sensitive to the accuracy and thoroughness of the traversing of the diffuser discharge to determine P_{do} .
- The estimated diffuser losses between the mixing duct exit and the traverse station are added to P_{do} to determine P_{mo} . Since the diffuser inlet flow is highly distorted (the mixing tube is too short and primary nozzle jets persist into the diffuser inlet) the estimated losses may be too low.
- The suction duct and nozzle cluster losses must be subtracted from the barometric pressure in order to determine P_{so} . The

loss characteristics used were obtained by drawing air past the nozzle cluster using a blower at the discharge of the duct system (section 4.2.3). The flow around the cluster may be different when the primary nozzles are in operation. Higher inlet losses may be the result.

- Wall friction losses in the mixing tube (not taken into account in the analytical predictions) reduce the jet pump stagnation pressure rise (section 4.2.4).

The experimental static pressure parameter curves are similar in slope to the curves for the analytical predictions. The experimental curves are shifted to higher negative values of the static pressure parameter. This means that the measured static pressure values are too low just as the integrated stagnation pressure values were too low. There are two reasons why this occurred.

- The data shows that the static pressure is still increasing at the end of the constant-area mixing tube. This means that considerable mixing is still taking place. A longer constant-area mixing tube improves the agreement of the experimental and analytical static pressure parameters as shown in section 4.4.3.
- The suction pipe and nozzle cluster losses, which are used to determine P_{SO} , may not be accurately represented by our measured loss characteristics. This problem was discussed above for the stagnation pressure loss parameter.

To improve the agreement between the experimental and analytical results, the length of the mixing tube was increased using the mixing tube extension piece. The stagnation pressure traverses were then repeated at the end of the extension tube.

Velocity Profiles at the Diffuser Discharge

Velocity profiles were calculated from the stagnation pressure traverse data used to calculate the jet pump discharge stagnation pressure. The velocity profiles measured for the two mixing tubes are presented in figures 44, 45, and 49.

Figure 44 shows velocity profiles taken at four throttle settings at a primary flow pressure of 350 psia using the NAS 2-2518 mixing tube. Three observations can be made from this figure.

- The profiles are generally not symmetrical,
- a sharp dip in velocity occurs at the center of the flow for the higher entrainment ratios,
- the velocity dip becomes less pronounced as entrainment ratio decreases.

Figure 45 shows two velocity profiles for the NAS 2-2518 mixing tube at reduced pressures and one velocity profile measured with an unheated primary flow. In all profiles, a sharp dip in velocity occurs in the center of the tube. The unheated primary flow velocity profile is nearly symmetrical. The asymmetry of all of the heated primary flow velocity profiles is probably caused by a radial shift of the nozzle cluster relative to the mixing tube due to thermal expansion of the elbow which feeds hot air to the cluster. This shift has been measured to be about $1/16$ inch. This situation was corrected in some of the subsequent tests by setting the nozzle cluster off-center at room temperature to compensate for thermal expansion at operating temperature.

Figure 49 presents velocity profiles measured for the short constant-area mixing tube configuration. The velocity profiles are not symmetrical for this mixing tube either. For run 24, two perpendicular velocity traverses were obtained. Both traverses were asymmetrical and both were shifted in the direction which would be expected if caused by elbow thermal expansion (the location of the traverse planes relative to the elbow is shown in figure 40). The dip in velocity at the center of the tube was much smaller for the constant area mixing tube configuration than for the NAS 2-2518 mixing tube. Further discussion of the dip in the velocity profile is presented in section 4.4.4. The presence of the exhaust cone was shown to have no effect on the velocity profile and a wedge probe traverse revealed that a small amount of swirl was present in the flow.

Mixing Tube Static Pressure Distribution

Static pressure data is presented in figures 46, 47, and 50. Figure 47 compares the variation of static pressure along the mixing tube and diffuser for three configurations:

1. NAS 2-2518 mixing tube in the BLC duct system.
2. NAS 2-2518 mixing tube in the Dynatech Test Rig.
3. Constant area mixing tube in the Dynatech Test Rig.

The test conditions for each of the three configurations are listed below. Slight differences in primary temperature and entrainment ratio existed for the three conditions.

Configuration	P_{po} psia	T_{po} ° F	W_p lbm/min	W_s lbm/min	W_m lbm/min	m
1	350	1200°	6.4	118.5	124.9	18.5
2	350	1085°	6.70	118.20	124.9	17.65
3	350	1130°	6.65	118.25	124.9	17.8

The static pressures for configuration 2 are about 2" of water larger than for configuration 1. This shift in the static pressure level is a result of reduced losses in the suction duct and bellmouth as compared to the BLC suction duct. The 2" of water shift is equivalent to a 10.5 psf decrease in suction duct losses. Comparison of this number to figure 41 shows that 10.5 psf is about half of the difference between the measured losses for the two inlet geometries.

The effect of changing from the contracting NAS 2-2518 mixing tube to a constant area tube is shown by configurations 2 and 3 in figure 47. The static pressure rises more rapidly in the constant area tube because of the lower velocity levels. However, the static pressure recovery obtained in the diffuser is substantially larger

for the NAS 2-2518 mixing tube case. This effect may be the result of lower mixing tube stagnation pressure rise or reduced diffuser effectiveness for the constant-area mixing tube case.

Figures 46 and 50 show the variation of static pressure at two locations in the mixing tube for configurations 2 and 3 as a function of the primary pressure and the entrainment ratio. The increase in static pressure for the constant area tube above that of the contracting tube was found to exist for all primary pressure levels and entrainment ratios tested.

4.4.2 Reduced Blockage Nozzle Clusters

Two reduced drag nozzle cluster configurations were tested to determine the influence of the cluster drag upon jet pump performance and to allow selection of the best cluster for further testing. Section 4.1 presents the dimensions of each of the cluster configurations. Table 5 lists the test conditions and table 6 provides an index to the results obtained.

The jet pump performance with the three nozzle cluster configurations (original, original cluster with 2-inch nozzle extension, and the low-drag cluster #2) were compared in the following ways:

1. System performance at minimum throttling (wide open throttle cone)
2. Static pressure parameter
3. Static pressure variation along the mixing tube at a selected total flow rate
4. Velocity profiles
5. Cluster pressure loss characteristics

Entrainment Ratio Results

The system performance at minimum throttling is presented in figure 51 where secondary flow rate is plotted as a function of primary flow rate. Except for the loss characteristics of the nozzle clusters themselves, the system loss characteristics are identical for all three nozzle configurations when the cone is in the wide open position. Both of the modified nozzle clusters show equal improvement with respect to the performance of the original cluster. Both have an increased secondary flow rate for the same primary flow rate.

The LD #2-4 cluster nozzles were designed for a slightly lower primary flow rate at a given pressure and temperature than the Case 4 Nozzles. This difference in design accounts for the shift in data points along the curve for the two reduced drag clusters.

Jet Pump Static Pressure Parameter Results

The analytical and experimental static pressure parameters are compared for the three nozzle clusters in the following figures:

Original Nozzle Cluster: figure 48

LD #1 - Low-Drag Nozzle Cluster: figure 52

LD #2 - Low-Drag Nozzle Cluster: figure 56

The best agreement between analytical and experimental results was obtained for the LD #1 cluster (figure 52). The higher nozzle cluster losses in the original cluster (figure 48) and the less-complete mixing obtained with the 7-nozzle arrangement of the LD #2 cluster (figure 56) are the causes of the poorer agreement between analysis and test results for these clusters.

Velocity Profiles at the Diffuser Discharge

The velocity profiles for the original cluster without and with nozzle extensions are presented in figures 49 and 53. The profiles had two velocity peaks with a dip in the center amounting to 30 to 60 fps. The velocity profiles for the LD #2 cluster are presented in figure 57. Three nearly-equal velocity peaks were obtained

with the LD #2 cluster when traversing along a line passing through three nozzles, and one velocity peak was obtained when traversing along a line passing between nozzles. The difference between the profiles for the original cluster and for the LD #2 cluster appears to be related to the number of nozzles used. The LD #2 nozzle cluster has seven equally-spaced nozzles, each having an equal share of the mixing tube flow cross section to energize. The original cluster has two additional nozzles around the outside, leaving the center nozzle with a larger percentage of the mixing tube flow area to energize. The velocity dip probably was not caused by nozzle cluster losses (i. e., a wake effect) because the LD #1 and LD #2 clusters apparently had similar loss characteristics (figure 51).

Several tests were completed with and without the throttle cone in place. No change in the velocity profile was detected. Therefore, the presence of the throttle cone at the diffuser exit does not seem to be the cause of the dip at the center of the velocity profile when the original nozzle cluster was used. No satisfactory explanation for the dip was developed during this program.

Mixing Tube Static Pressure Distribution

The static pressure variation along the mixing tube is shown for all three clusters in figure 55. The static pressure levels are dictated primarily by the total flow rate, but they are also slightly affected by changes in the mixing process which accompany modifications of the nozzle cluster geometry. The original nozzle cluster produced similar pressure distributions with and without the nozzle extensions. The pressure distribution for the LD #2 cluster shows higher static pressures near the mixing tube inlet because of reduced blockage, and lower static pressures at the mixing tube exit because of less complete mixing (the result of the reduction in number of nozzles from 9 to 7).

Cluster Drag

The cluster loss tests were discussed in section 4.2.3. Both of the low-drag clusters showed equal reduction in loss characteristics relative to the original cluster (figure 41).

Selection of the Optimum Nozzle Cluster

The measured nozzle cluster losses (figure 41) and the jet pump performance characteristics with minimum throttling (figure 51) show that the two low-drag nozzle clusters yield similar results. The comparison of experimental and analytical static pressure parameters and the comparison of static pressure distributions along the mixing tube for both low-drag clusters show that the original cluster with 2 inch nozzle extensions (LD #1) is slightly preferable to the LD #2 cluster.

The original cluster with 2 inch nozzle extensions (LD #1) was selected as the best cluster for the remainder of the test program for the following reasons:

1. The nozzles for the remainder of the test program were already available for this cluster.
2. This cluster gives better agreement between experimental and analytical static pressure values because of the more complete mixing upstream of the measuring station.
3. The LD #2 cluster offers no advantages in comparison to the original cluster with extensions; the measured losses are equal for both clusters and the flow rate curves at the wide-open throttle position are the same.

4. 4. 3 Comparison of Short and Extended Mixing Tubes

Performance data was obtained for both the short and the extended constant-area mixing tubes using each of the four nozzle sets with the LD #1 nozzle cluster. The test results are indexed in table 6 .

The extended mixing tube was found to change the jet pump performance in the following ways:

1. The static and stagnation pressures both reached a maximum value within the extended mixing tube.

This indicates that complete mixing was achieved. The extended mixing tube was superior to the short mixing tube, particularly with respect to static pressure recovery at low entrainment ratios.

2. The wall friction losses in the extended mixing tube were significant in comparison to the stagnation pressure rise developed by the jet pump.
3. The velocity profile at the diffuser inlet was improved by extending the mixing tube.

Identical duct loss characteristics existed for the maximum-entrainment ratio runs for each test number. The throttle cone was withdrawn to a fixed location for these runs. Thus, the performance characteristics of the jet pump as influenced by nozzle design, mixing tube length, and primary flow pressure and temperature can be determined by comparing these maximum-entrainment runs.

Entrainment Ratio Results

A Comparison of the maximum entrainment ratio achieved with the long and short mixing tubes operated with the same nozzles and the same primary flow conditions shows that the short mixing tube configuration achieves a slightly larger entrainment ratio in all cases. The mixing tube extension section allows more complete mixing and improves the diffuser inlet velocity profile. However, the extended tube introduces an additional frictional loss which becomes significant at large flow rates (figure 43). The reduction in entrainment for the extended mixing tube shows that the extra friction losses in the longer tube cancel the effects of improved mixing. The use of a mixing tube length longer than the short tube and shorter than the extended tube would probably lead to a higher entrainment ratio than was developed by either of the tested lengths.

Jet Pump Static Pressure Parameter Results

Table 6 lists the figure numbers which show the static pressure parameters for the eight nozzle and duct configurations tested. The experimental values shown are based upon measured static pressures (P_m or P_{max}) and upon secondary flow stagnation pressures (P_{so}) calculated from the measured inlet losses, cluster losses, and mixing tube losses (figures 41 and 43). The analytical values shown in the figures were calculated by the computer using the ideal jet pump analytical model which neglected inlet, cluster, and mixing tube losses.

The results show that the extended mixing tube test data corresponds more closely to the analytical predictions. The biggest difference between the short and long mixing tubes occurs at low entrainment ratios because the extended mixing tube significantly increases the static and stagnation pressure recovery at low flow rates. At high entrainment ratios, no improvement is produced by the extended mixing tube because the increased frictional losses cancel the potential gains from more thorough mixing.

Inclusion of the inlet and mixing tube losses in the analytical model would give lower (more negative) values of the static pressure parameter which would agree more closely with the experimental values. The biggest changes would occur at high entrainment ratios where the curves are presently furthest apart.

Jet Pump Stagnation Pressure Parameter Results

Table 7 lists all of the experimental stagnation pressure rise parameters which were calculated from the traverse data taken. Traverses were made either at the mixing tube discharge or in the conical diffuser at a station where the area is 1.61 x the inlet area. The stagnation pressure at the traverse station was calculated by the mass-momentum method presented in section 4.2.2. Each result represents the integration of one or two traverses as indicated in the table. The value of P_{mo} was determined from the diffuser exit traverse values (P_{do}) by correcting for the diffuser losses using equation (92) of section 4.2.2.

Figure 59 compares the analytical predictions and experimental values of the stagnation pressure rise parameter for the extended mixing tube tested with the Case 4 nozzles at 300 psia and 1150° F primary flow conditions. The experimental values were obtained as follows:

- ⊙ ☐ The stagnation pressure value P_{mo} was calculated using the diffuser exit stagnation pressure traverse data and correcting for diffuser losses by using equation (92) of section 4.2.2.
- ⊙ ☐ The stagnation pressure P_{mo} was calculated by using stagnation pressure traverse data obtained at the mixing tube exit.
- ⊗ ☒ An additional correction was made to the ⊙ ☐ data to account for mixing tube wall friction effects. The wall friction pressure losses are taken from figure 43 to make this correction.
- ⊗ ☒ The wall friction pressure losses in the mixing tube (figure 43) were added to the ⊙ ☐ data.

The correction of the stagnation pressure rise parameter to account for duct losses places three of the four experimental points within 6 psf of the analytical value. The differences which remain may be due to the factors discussed in section 4.4.1 where similar results were presented for the short mixing tube test.

Additional comparisons of the analytical and experimental stagnation pressure values are made in section 5.1 of this report.

Velocity Profiles at the Diffuser Discharge

Table 6 lists the figure numbers showing the velocity profiles obtained with both the short and long mixing tubes. The effect of extending the mixing tube can be seen clearly on figure 73 where results for both mixing tubes are plotted for the Case 2 nozzles. The centerline depression at the diffuser discharge is much

smaller when the extended mixing tube is used since the flow has a longer flow path for mixing. The tests with the Case 3 and Case 4 nozzles gave the same result. The longer mixing tube improves the symmetry of the flow entering the diffuser and reduces the likelihood of flow separation in the diffuser.

For the Case 3 nozzles with the extended mixing tube, two traverses each were taken at the mixing tube exit and at the diffuser exit. One traverse at each location passed along a diameter through the wake of three nozzles. The second traverse in each location passed through the wake of only the centerline nozzle (figure 79). The four traverses show the flow to be reasonably symmetrical. A reduced velocity exists along the centerline while two peaks of velocity appear on either side. The velocity profiles in the two planes at one station were nearly identical. Further discussion of the velocity profiles is included in section 4.4.4.

Mixing Tube Static Pressure Distribution

Table 6 lists the figures showing the static pressure variation along the mixing tube. These variations are plotted only for the extended mixing tube tests. The static pressure at each location in the duct is a result of the interaction of the following factors:

1. The local Mach number of the flow,
2. The stagnation pressure rise achieved by mixing of the two streams,
3. The frictional losses on the walls.

The data in figures 71, 75, and 81 show that the static pressure reaches a maximum at the middle or near the end of the mixing tube extension. In the duct upstream of the location of maximum static pressure, the increase in stagnation pressure due to mixing is larger than the reduction in stagnation pressure due to wall friction. Beyond the maximum point, the added wall friction loss becomes dominant. The location of the maximum static pressure point is closer to the mixing tube inlet for the high flow rate test points because of the increased magnitude of frictional pressure loss which accompanies the increased velocity levels.

These results show that an optimum mixing tube length exists which will produce the maximum static pressure. This optimum length is a function of flow rate.

4.4.4 Velocity Profile Investigations

As mentioned in other portions of section 4.4, the velocity profiles measured at the mixing tube exit and the discharge of the initial diffuser section have shown various degrees of distortion. This distortion is due to the following causes:

1. Angular and/or radial misalignment of the nozzle cluster and mixing tube centerlines.
2. Non-uniform pumping.

The alignment of the nozzle cluster elbow with the mixing tube centerline was accomplished with a special centering plug which was inserted snugly into both the elbow and the mixing tube. The original centering plug aligned the elbow and tube concentrically with the elbow at room temperature. Traverses taken with low primary air temperatures (from ambient to 200° F) gave velocity profiles which were quite symmetrical about the centerline, thus indicating good alignment. However, when the primary flow was heated to 1150° F, the elbow flange-to-centerline dimension increased by about 1/16" due to thermal expansion. The high velocity region in the velocity profile shifted noticeably in the same direction (an example is given by figure 49).

To compensate for the thermal expansion, an offset plug was made to position the two centerlines 1/16 inch apart when the elbow was at room temperature. The offset plug was used to position the cluster for all of the high temperature tests performed subsequent to test No. 16. Even with the offset plug, some of the short constant area mixing tube tests showed distorted velocity profiles indicating that the mixing process in the short tube is highly sensitive to slight misalignments. All of the velocity profiles for the extended mixing tube tests were reasonably symmetrical showing that the mixing process in the longer tube is relatively insensitive to misalignment.

Most of the velocity profiles exhibited a slight depression of the centerline velocity below the velocity of the surrounding flow. This depression was less pronounced when the extended mixing tube was used (an example is given by figure 73). To determine the reason for the slight depression of velocity along the centerline, the following series of tests were run:

1. Velocity profiles were obtained with the Kiel probe with and without the throttle cone in place. The same primary flow conditions were maintained for both tests.
2. A wedge probe was used to measure local static pressure and flow direction for comparison with a Kiel probe measurement.
3. A nozzle arrangement using 8 Case 2 nozzles around the circumference of the cluster and 1 Case 4 nozzle located in the center was tested to explore the effect of increasing the momentum in the center of the mixing tube.

The first test described above showed conclusively that the throttle cone does not influence the flow at the traverse station. There was no detectable difference in the traverse results with and without the cone.

The traverse results for tests 2 and 3 above are shown on figure 85. The wedge probe results, like the Kiel probe results, show the depression in velocity along the centerline. Associated with this depression in velocity was a reduction in static pressure of about 1 inch of water and a departure of the velocity from the axial direction by roughly $\pm 2^\circ$ all along the diameter. These results indicate that a slight swirl exists in the flow.

The third test above employed a center nozzle with a throat area about 50% larger than that of the surrounding eight nozzles. The velocity profile still shows a centerline depression. Thus, the depression cannot be accounted for as only a primary flow momentum deficiency in the center of the mixing tube.

The small amount of swirl that appears to be present in the flow is not likely to have a significant effect on the test results. This small amount of swirl could be caused by one or more of the primary nozzles being bent at a small angle to the axis, by the presence of the primary nozzle elbow, or by wakes shed off of objects in the laboratory outside the jet pump.

No satisfactory explanation for the centerline depression in the velocity profile remained after these tests were completed. The cause of the depression is unknown.

Section 5

COMPARISON OF ANALYTICAL AND EXPERIMENTAL RESULTS

5.1 Jet Pump Stagnation Pressure Rise

The experimental measurements of the jet pump stagnation pressure rise parameter, ΔP_t^* , generally fell below the analytical predictions. Examples are given in section 4.4.1 (figure 48) and section 4.4.3 (figure 59). Additional values of ΔP_t^* were measured in other tests and the results are given in table 7.

The analytical values of ΔP_t^* were predicted by neglecting wall friction losses in the mixing tube, by assuming complete mixing, and by neglecting suction duct losses and conical diffuser losses. Thus, the analytical values represent "ideal" jet pump performance. The measured performance fell below the "ideal" values for the following reasons:

- the experimental value is very sensitive to traversing thoroughness and accuracy
- mixing tube wall friction losses were not included in the analysis; these losses are not negligible
- in many tests, the stagnation pressure traverses were made in the conical diffuser. The test results were corrected to account for diffuser losses between the measuring section and the mixing tube exit. These corrections may be inaccurate.
- to determine the measured value of $\Delta P_t = P_{mo} - P_{so}$, the value of P_{so} had to be estimated by subtracting suction duct and nozzle cluster losses from the atmospheric pressure. These losses cannot be measured under the conditions which exist during jet pump operation so the corrections may be inaccurate.

- the adjustment of the supersonic primary flow to match the secondary flow static pressure was assumed to be isentropic in the analysis. When the primary flow at the nozzle exit is appreciably over- or under-expanded, the flow is non-isentropic and stagnation pressure losses occur in the primary flow adjustment process.

The effects of mixing tube wall friction can be estimated by using the loss measurements of figure 43. The analytical values of ΔP_t^* were reduced by the appropriate loss taken from figure 43 to derive the column in table 7 entitled "Corrected for Duct Friction". The corrected analytical values were used to prepare the right-hand column which shows the percentage error between the corrected analytical value and the test measurement of ΔP_t^* , i. e. :

$$\frac{\left. \begin{array}{l} P_{mo} \\ \text{analytical} \\ \text{corrected} \end{array} \right) - \left. \begin{array}{l} P_{mo} \\ \text{experimental} \end{array} \right)}{\left. \begin{array}{l} P_{mo} \\ \text{analytical} \\ \text{corrected} \end{array} \right) - P_{so}}$$

The table shows that the difference between the corrected analytical value and the test value of ΔP_t^* is 10% or less when traverses in two directions were made during the test. The difference can be 20% or more if only one traverse was made, particularly when the short mixing tube was used or distorted velocity profiles were observed.

The remaining differences between the corrected analytical value and the test value are due to incomplete traversing and possible inaccuracies in the conical diffuser and suction duct loss corrections. Furthermore, the pressure loss measurements shown in figure 43 were made by drawing air through the mixing tube with a blower. The wall friction losses may be different when the jet pump is operating because the mixing action changes the velocity profiles considerably. Thus, even the mixing tube wall friction corrections may not be exact.

5.2 Jet Pump Static Pressure Rise

The experimental measurements of the jet pump static pressure rise parameter, ΔP_s^* , fell consistently below the analytical predictions. The measured static pressure values at the mixing tube exit were lower than predicted. The reasons for this discrepancy were as follows:

- mixing tube wall friction losses were not included in the analysis; these losses are not negligible
- in the case of the short mixing tube, the tests showed that mixing was not completed within the tube. Thus, the static pressure did not reach its mixed-out value, the value which the computer program seeks to predict.
- the distorted velocity profiles existing in the actual mixing tube lead to lower static pressures than the uniform velocity profiles assumed in the computer analysis.
- to determine the measured value of $\Delta P_s = P_m - P_{so}$, the value of P_{so} was estimated by subtracting suction duct and nozzle cluster losses from the atmospheric pressure. These loss corrections may not be exact.
- the primary flow is not isentropic in the accommodation region when the primary flow is over- or under-expanded at the primary nozzle exit. Isentropic accommodation is assumed in the analysis.

The differences between the experimental measurements and the analytical predictions are most pronounced at low entrainment ratios when poor mixing occurred, when the short mixing tube was used, and particularly with the 7-nozzle LD#2 nozzle cluster. The extended mixing tube improved the recovery of static and stagnation pressure at low flow rates. At high flow rates (high entrainment ratios), the increased frictional losses in the extended mixing tube cancel the potential gains from more thorough mixing.

The computer program was modified as described in sections 3.1.5 and appendix B.1 to allow inclusion of mixing tube wall friction and suction duct losses in the analytical performance predictions. Preliminary values of K_{MT} and K_{sd} can be obtained by loss tests as in figures 41 and 43, or by estimates using duct loss correlations available in the literature. More accurate values of K_{MT} and K_{sd} must be obtained empirically from jet pump testing.

An example of the empirical approach is shown in figure 86. Test values of ΔP_s^* are replotted for the 260 psia operating condition from figure 72. A number of alternative values of K_{MT} were assumed and used as input data for the computer performance analysis. The value of K_{sd} was assumed to be 0.006 for all calculations. The results show that selection of $K_{MT} = 0.055$ makes the analytical prediction agree closely with the test results. The loss coefficient K_{MT} as used here includes not only the effect of mixing tube wall friction, but also the effects of the other sources of discrepancies mentioned above. The mixing tube loss coefficient measured by drawing air through the mixing tube with a blower (figure 43) was $K_{MT} = 0.053$.

This good agreement between the value of K_{MT} measured in the blower test and the value of K_{MT} deduced from the computer calculations suggests that the blower test method may afford a simple and accurate way to determine K_{MT} for a new jet pump design. However, the mixing action which occurs when the jet pump is operating may cause the mixing tube wall friction characteristics to vary when the primary flow pressure and temperature are changed. To determine whether such variations of K_{MT} are significant, more of the test results of section 4 could be analyzed by the computer to determine the appropriate values of K_{MT} . These "jet-pump-derived" values of K_{MT} could be compared to K_{MT} as measured by the blower test method to determine whether serious discrepancies can occur. This report includes sufficient data to make such comparisons.

Section 6

CONCLUSIONS

The conclusions which may be reached as a result of this investigation are listed below:

1. **Validity of the Analysis:**

The analytical model developed in section 3.1 for high-entrainment compressible-flow jet pumps with constant area mixing tubes is based upon the simplifying assumption that the supersonic primary nozzle flow adjusts isentropically to match the secondary flow static pressure. The analytical predictions of jet pump pressure rise and thrust augmentation based upon this assumption agree closely with test results when mixing tube wall friction effects are taken into account. The agreement is good over a very broad range of operating conditions.

2. **Mixing Tube Wall Friction:**

The stagnation pressure losses which occur in the mixing tube due to wall friction are significant in comparison to the stagnation pressure rise developed by a high-entrainment jet pump. Measurement of the wall friction losses by drawing air through the mixing tube with a blower may yield values of the friction loss coefficient which are accurate enough for design purposes. Further analysis of the data in this report is required to check this point.

3. **Jet Pump-Duct System Matching:**

A technique for selecting the optimum design for a jet pump to match given operating conditions was presented in section 3.4. For the same primary flow conditions, the jet pump geometry to achieve maximum entrainment was shown to be different from the geometry

required to achieve maximum thrust augmentation. In order to match a jet pump to its associated duct system to obtain peak performance, it is essential that the loss coefficients of the duct components be estimated as accurately as possible.

4. Optimum Mixing Tube Length:

The mixing tube length must be selected to balance the increased pressure recovery resulting from more complete mixing in a longer tube against the increased wall friction losses in the longer tube. The results of this investigation suggest that no simple length-to-diameter rule is applicable to mixing tube design. The optimum mixing tube length is a function of the primary flow conditions and the entrainment ratio at the operating point. This entrainment ratio is set by the loss characteristics of the jet pump duct system.

5. Nozzle Cluster Design:

The original position of the nozzle cluster close to the mixing tube inlet led to increased losses and inferior jet pump performance. When the nozzle cluster was moved upstream away from the mixing tube inlet, its pressure loss and blockage effects were minimized and the performance of the jet pump was measurably improved. A special "low-drag" nozzle cluster design was no better than the original cluster when both were-positioned away from the mixing tube inlet.

A reduced centerline velocity appeared in most of the velocity profiles measured at the mixing tube exit and in the conical diffuser. The cause of the reduced centerline velocity is unknown.

6. Performance of the Wagner Jet Induced Lift System:

The loss characteristics of the suction duct and nozzle cluster arrangement used in the NAS 2-2518 test program were measured during this program. The high suction duct and nozzle cluster losses, incomplete mixing in the too-short mixing tube, and non-optimum matching of the jet pump to the duct system all acted to reduce the entrainment ratios achieved with the system substantially below the peak values attainable.

7. Mixing Tube Design:

The original mixing tube geometry, which had a small reduction in cross-sectional area along its length, produced a slightly higher entrainment ratio than the constant-area mixing tube under similar test conditions. Further analytical and experimental work should be carried out to determine the performance characteristics of a variety of mixing tube shapes. Significant performance improvements may be possible if mixing tubes other than the conveniently-analyzed constant area and constant pressure designs are used.

APPENDIX A

Listing of the Computer Program

An "*" before a line indicates that it can be removed if there is to be no plotting with the EZPLOT subroutine.

```

0001          DIMENSION PRISE(11,15),THRUS(11,15),ENT(11,15),ARRAY(11,15)
0002          DIMENSION COUNT(15),X(15),Y(15),PTITLE(15),TTITLE(15),NC(9)
0003          DIMENSION CHAR1(11,6),CHAR2(11,5)
0004          DATA NC/38,63,16,55,44,19,24,52/
           C   CLEAR ARRAYS
0005          DO 26 K=1,15
0006          COUNT(K)=0
0007          X(K)=0
0008          Y(K)=0
0009          PTITLE(K)=0
0010          TTITLE(K)=0
0011          DO 25 J=1,11
0012          PRISE(J,K)=0
0013          THRUS(J,K)=0
0014          ENT(J,K)=0
0015          ARRAY(J,K)=0
0016          25 CONTINUE
0017          26 CONTINUE
           C   CALL IDFRMV REMOVED FROM PROGRAM HERE
0018   Line 1   READ(5,350)NTP,(PTITLE(I),I=1,15)
0019   Line 2   READ(5,450)NTT,(TTITLE(I),I=1,15)
0020   Line 3   READ(5,52)N
0021          G=1.4
0022          G0=32.2
0023          R=53.35
0024          CONV=778.16
0025          K=0
           C   BEGIN OUTER LOOP, EACH LOOP USES A NEW SET OF INITIAL CONDITIONS
0026          1 WRITE(6,100)
0027          DO 761 J=1,11
0028          DO 760 M=1,5
0029          CHAR1(J,M)=0
0030          CHAR2(J,M)=0
0031          760 CONTINUE
0032          761 CONTINUE
0033          CHAR1(11,6)=0
0034          K=K+1
           C   READ DIMENSIONLESS INITIAL CONDITIONS
0035   Line 4   READ(5,50,END=300)PBAR,TBAR,ABAR1,ABAR2
           C   READ DIMENSIONAL INITIAL CONDITIONS
0036   Line 5   READ(5,51)PSOI,TSO,AM
0037   Line 6   READ(5,455)FDUCT,FTUBE
0038          WRITE(6,101)PBAR,TBAR
0039          WRITE(6,102)ABAR1,ABAR2
0040          WRITE(6,103)PSOI,TSO,AM
0041          WRITE(6,456)FDUCT,FTUBE
           C   CALCULATE OTHER DIMENSIONAL VALUES FROM DIMENSIONLESS VALUES
0042          PPO=PBAR*PSOI

```

```

0043      TPO=TBAR*TSO
0044      ATH=ABAR1*AM
0045      AP=ABAR2*AM
          C      BEGIN INNER LOOP, EACH TIME THROUGH GIVES A SET OF SOLUTIONS
          C      FOR A DIFFERENT VALUE OF ENTRAINMENT RATIO.
0046 Line 7      DD 13 J=1,11
0047      ENTR=7.0+J*3.0
0048      WRITE(6,105)J,ENTR
          C      CALCULATE PRIMARY AND SECONDARY MASS FLOW RATES
0049      WP=G*GO*(1/R)*(2.0/(G+1))**((G+1)/(G-1))
0050      WP=SQRT(WP)*144.0*60.0*PPD*ATH/SQRT(TPO)
0051      WS=ENTR*WP
0052 Line 8      PSO=PSOI-FDUCT*WS*WS*R*TSO
          1/(3600.0*2.0*GO*PSOI*AM*AM*144.0*144.0)
Line 9 C      ITERATE TO FIND SECONDARY MACH NUMBER
0053      820 I=0
0054      GUESS=0.2
0055      Z=W*S*SQRT(TSO)/(60.0*144.0*PSO*(AM-AP)*SQRT(G*GO/R))
0056      2 PARAM=1+(G-1)/2.0*GUESS*GUESS
0057      ZCALC=GUESS/PARAM**((G+1)/(2.0*(G-1)))
0058 Line 10     IF(GUESS-1.0)14,14,15
0059      14 IF(I-100)3,3,5
0060      3 IF(ABS(ZCALC-Z)-.0005)6,6,4
0061      4 DERIV=PARAM**(-(G+1)/(2.0*(G-1)))-(G+1)/2.0*GUESS*GUESS
          1*PARAM**((1-3.0*G)/(2.0*(G-1)))
0062      GUESS=GUESS-(ZCALC-Z)/DERIV
0063      I=I+1
0064      GO TO 2
0065      5 WRITE(6,66)
0066      GO TO 405
0067      15 WRITE(6,115)
0068      GO TO 13
0069      6 CONTINUE
0070      SMOK=GUESS
0071      PS=PSO/(1+(G-1)/2.0*SMOK*SMOK)**(G/(G-1))
0072      TS=TSO/(1+(G-1)/2.0*SMOK*SMOK)
0073      VS=2.0*G*GO*R*(TSO-TS)/(G-1)
0074      VS=SQRT(VS)
0075      PSOR=PSOI-FDUCT*VS*VS*PS/(2.0*GO*R*TS )
0076      IF(ABS((PSOR-PSO)/PSOR)-.0005) 800,800,810
0077      810 PSO=PSOR
0078      GO TO 820
0079      800 PSO=PSOR
0080      WRITE(6,457)PSO
0081      WRITE(6,600)I
          C      MAKE CORRECTION FOR UNDER OR OVER EXPANSION
          I=0
0082      16 PMOK=(1+(G-1)/2.0*SMOK*SMOK)*(PPD/PSO)**((G-1)/G)-1.0
0083      PMOK=SQRT(2.0*PMOK/(G-1))
0084      AM2=W*S*SQRT(TSO)*(1+(G-1)/2.0*SMOK*SMOK)**((G+1)/(2.0*(G-1)))
          1/(PSO*SMOK)
0086      AM2=AM2+WP*SQRT(TPO)*(1+(G-1)/2.0*PMOK*PMOK)**((G+1)/(2.0*(G-1)))
          1/(PPD*PMOK)

```

```

0087          AM2=AM2*SQR(T(R/(G*G0)))/(144.0*60.0)
0088          IF(ABS(AM2-AM)-.00005) 19,19,17
0089          17 SMOK=SMOK+((AM2-AM)/ABS(AM2-AM))*EXP(5.2*SMOK*SMOK)*5.E-5
0090          IF(I-200) 18,5,5
0091          18 CONTINUE
0092          I=I+1
0093          GO TO 16
0094          19 CONTINUE
0095          WRITE(6,601)I
0096          AP=(1+(G-1)/2.0*PMOK*PMOK)**((G+1)/(2.0*(G-1)))
0097          AP=AP*WP*SQR(TPO)/(144.0*60.0*PP0*PMOK*SQR(T(G*G0/R)))
C          CALCULATE CONDITIONS AT END OF ACCOMMODATION REGION
0098          PS2=PS0/(1+(G-1)/2.0*SMOK*SMOK)**(G/(G-1))
0099          TS2=TS0/(1+(G-1)/2.0*SMOK*SMOK)
0100          VS2=2.0*G*G0*R*(TS0-TS2)/(G-1)
0101          VS2=SQR(T(VS2))
0102          PP2=PS2
0103          TP2=TPO*(PP2/PP0)**((G-1)/G)
0104          VP2=2.0*G*G0*R*(TPO-TP2)/(G-1)
0105          VP2=SQR(T(VP2))
0106          C2=SQR(T(G*G0*R*TP2))
0107          PMDK=VP2/C2
Line 11 C          BEGIN ITERATION TO FIND OUTLET CONDITIONS
0108          WM=WP*(1+ENTR)
0109          CP2=.24914
0110          CS2=.24914
0111          I=0
0112          HP2=CP2*TP2+VP2*VP2/(2.0*G0*CONV)
0113          HS2=CS2*TS2+VS2*VS2/(2.0*G0*CONV)
0114          INT=0
0115          PMG=PS2+.4
0116          7 VM=VP2+ENTR*VS2+60.0*144.0*G0*AM*(PS2-PMG)/WP
0117          VM=VM*WP/WM
0118          TM=60.0*144.0*PMG*VM*AM/(R*WM)
0119          CM=.24914
0120          PM=(HP2+ENTR*HS2)*R*WP/(60.0*144.0*VM*AM*CM)
0121          PM=PM-R*WM*VM/(2.0*144.0*60.0*G0*CONV*CM*AM)
0122          IF(I-800) 8,8,15
0123          8 IF(ABS(PMG-PM)-.01) 11,11,9
0124          9 IF(PM .GT. PMG) GO TO 20
0125          IF(INT .EQ. 1 ) GO TO 11
0126          PMG=PMG+(PMG-PM)/PMG
0127          I=I+1
0128          GO TO 7
0129          20 INT=1
0130          PMG=PMG-.001
0131          I=I+1
0132          GO TO 7
0133          10 WRITE(6,66)
0134          GO TO 405
0135          11 CONTINUE
0136          WRITE(6,602)I
0137          PM=PMG

```

```

0138          EMOK=VM/SQRT(G*G0*R*TM)
Line 12 C    CALCULATE THE EFFECT OF WALL FRICTION
0139          GAM1=1.0+(G-1)/2.0*EMOK*EMOK
0140          ALPH=144.0*PM*(GAM1**(G/(G-1))-FTUBE*EMOK*EMOK*G/2.0)
0141          BETA=ALPH/SQRT(144.0*PM*144.0*PM*EMOK*EMOK*GAM1)
0142          I=1
0143          GMOK=EMOK
0144          700 GAM2=1.0+(G-1)/2.0*GMOK*GMOK
0145          A=(1/GMOK)*GAM2**((G+1)/(2.0*(G-1)))
0146          DA=(G+1)/2.0*GAM2**((3-G)/(2.0*(G-1)))
0147          DA=DA-(1/(GMOK*GMOK))*GAM2**((G+1)/(2.0*(G-1)))
0148          IF(I .GT. 200)GO TO 10
0149          IF(GMOK-1.0)701,701,15
0150          701 IF(ABS(A-BETA)-.0001)703,703,702
0151          702 I=I+1
0152          GMOK=GMOK-(A-BETA)/DA
0153          GO TO 700
0154          703 CONTINUE
0155          WRITE(6,604)I
0156          P2=(1/144.0)*ALPH/GAM2**(G/(G-1))
0157          TM=TM*(P2/PM)**2.0*(GMOK/EMOK)**2.0
Line 13 C    CALCULATE OUTLET PARAMETERS
0158          VM=GMOK*SQRT(G*G0*R*TM)
0159          PM=P2
0160          EMOK=GMOK
0161          PMTOT=144.0*PM*(1.0+(G-1)/2.0*EMOK*EMOK)**(G/(G-1))
0162          DELP=PMTOT-144.0*PSO
0163          DDELP=DELP/(144.0*PSO)
0164          DSTAT=144.0*(PM-PSO)
0165          DDSTA=(PM-PSO)/PSO
0166          AUG=WM*VM/(WP*VP2)
0167          ENER=144.0*PM*VM*VM/(2.0*G0*R*TM)
0168          DENER=ENER/(144.0*PSO)
0169          NDELP=DELP
0170          IF (NDELP .LE. 0) GO TO 1
C           STORE SOLUTIONS FOR TABLE PRESENTATION
0171          SUM=J
0172          CHAR1(J,1)=ENTR
0173          CHAR1(J,2)=DDELP
0174          CHAR1(J,3)=DDSTA
0175          CHAR1(J,4)=EMOK
0176          CHAR1(J,5)=DENER
0177          CHAR1(J,6)=AUG
0178          CHAR2(J,1)=ENTR
0179          CHAR2(J,2)=PM
0180          CHAR2(J,3)=DELP
0181          CHAR2(J,4)=DSTAT
0182          CHAR2(J,5)=ENER
C           STORE SOLUTIONS IN ARRAYS TO BE PLOTTED LATER
0183          PRISE(J,K)=DDELP
0184          THRU(J,K)=AUG
0185          ENT(J,K)=ENTR
0186          COUNT(K)=J

```

```

0187          WRITE(6,106)
0188          WRITE(6,107)
0189          WRITE(6,108)PP2,PS2,PM
0190          WRITE(6,109)TP2,TS2,TM
0191          WRITE(6,110)VP2,VS2,VM
0192          WRITE(6,111)PMOK,SMOK,EMOK
0193          WRITE(6,112)WP,WS,WM
0194          WRITE(6,116)AP
0195          WRITE(6,113)DELP
0196          WRITE(6,120)DDELP
0197          WRITE(6,603)DDSTA
0198          WRITE(6,114)AUG
          C    END OF INNER LOOP
0199 Line 14  C    13 CONTINUE
          C    PRINT OUT TABLE OF RESULTS
0200          765 WRITE(6,707)
0201          WRITE(6,710)
0202          WRITE(6,751)PBAR,TBAR,ABAR1
0203          WRITE(6,707)
0204          WRITE(6,720)
0205          WRITE(6,730)
0206          M=SUM
0207          DO 725 J=1,M
0208          WRITE(6,704)CHAR1(J,1),CHAR1(J,2),CHAR1(J,3),CHAR1(J,4),CHAR1(J,5)
          1,CHAR1(J,6)
0209          725 CONTINUE
0210          WRITE(6,707)
0211          WRITE(6,750)
0212          WRITE(6,751)PBAR,TBAR,ABAR1
0213          WRITE(6,752)PSO,TSO,AM
0214          WRITE(6,707)
0215          WRITE(6,753)
0216          WRITE(6,754)
0217          DO 726 J=1,M
0218          WRITE(6,755)CHAR2(J,1),CHAR2(J,2),CHAR2(J,3),CHAR2(J,4),CHAR2(J,5)
0219          726 CONTINUE
          C    END OF OUTER LOOP
0220 Line 15  C    IF(K .GE. N) GO TO 300
0221          GO TO 1
0222          300 CONTINUE
          C    FIND LARGEST VALUES IN ARRAYS PRISE AND THRUS
0223          PMAX=TOP(PRISE)
0224          TMAX=TOP(THRUS)
          C    ENTER PLOTTING SECTION OF THE PROGRAM
0225          K=1
0226          NA=17
0227          NO=27
0228          NF=1
0229          GO TO 303
0230          301 NTP=0
0231          NA=0
0232          NO=0
0233          NF=2

```

```

0234      302 K=K+1
0235      303 M=COUNT(K)
0236          DO 305 J=1,11
0237          X(J)=0
0238          Y(J)=0
0239      305 CONTINUE
0240          DO 304 J=1,M
0241          X(J)=ENT(J,K)
0242          Y(J)=PRISE(J,K)
0243      304 CONTINUE
0244          NP=COUNT(K)
0245      C CALL EZPLOT REMOVED FROM DECK HERE
0246          IF(K .GE. N)GO TO 400
0247          IF(K-2)301,302,302
0248      400 K=1
0249          NA=17
0250          NO=28
0251          NF=1
0252          GO TO 403
0253      401 NTT=0
0254          NA=0
0255          NO=0
0256          NF=2
0257      402 K=K+1
0258      403 M=COUNT(K)
0259          DO 406 J=1,11
0260          X(J)=0
0261          Y(J)=0
0262      406 CONTINUE
0263          DO 404 J=1,M
0264          X(J)=ENT(J,K)
0265          Y(J)=THRUS(J,K)
0266      404 CONTINUE
0267          LAST=1
0268          IF(K .GE. N)LAST=2
0269      C CALL EZPLOT REMOVED FROM DECK HERE
0270          IF(K .GE. N) GO TO 405
0271          IF(K-2)401,402,402
0272      C CALL PLTND REMOVED FROM DECK HERE
0273      405 CONTINUE
0274          50 FORMAT(4F10.5)
0275          51 FORMAT(3F10.5)
0276          52 FORMAT(I10)
0277          100 FORMAT(//25X,65H***** THE FOLLOWING CASES WILL USE THESE INITIAL C
0278          101 FORMAT(/2X,15HPRESSURE RATIO=,E10.4,10X,18HTEMPERATURE RATIO=,
0279          1E10.4)
0280          102 FORMAT(/2X,12H(ATH*CW/AM)=,E10.4,13X,6HAP/AM=,E10.4)
0281          103 FORMAT(/2X,19HSECONDARY PRESSURE=,E10.4,3X,22HSECONDARY TEMPERATUR

```



```
0312      457 FORMAT(/5X,39HSECONDARY TOTAL PRESSURE BEFORE MIXING=,E10.4)
0313      END
0001      FUNCTION TOP(ARRAY)
0002      DIMENSION ARRAY(11,15)
0003      TOP=ARRAY(1,1)
0004      DO 501 L=1,11
0005      DO 500 M=1,15
0006      IF(TOP .LT. ARRAY(L,M)) TOP=ARRAY(L,M)
0007      500 CONTINUE
0008      501 CONTINUE
0009      RETURN
0010      END
```

APPENDIX B

B.1 Discussion of Computer Program by Blocks

Block 1 - Declare and Clear Arrays, Set Values of Constants:

To make sure that the storage arrays used in the program are all empty, zeroes are placed in every location by this block of the program.

Numerical values of G, GO, R, and CONV are also defined in this section of the program. The numerical values are not read in as input; they are defined within the program. To change them, the appropriate cards in the deck must be changed.

Block 2 - Read Initial Conditions and Initialize Parameters:

In the segment of the program between line 1 and 6, the initial conditions are read in and prepared for further calculations. These initial conditions include data required by the plotting routine.

Titles for plots of dimensionless pressure rise and momentum ratio as functions of entrainment ratio (PTITLE, TTITLE) and the number of cases to be solved (N) are introduced in lines 1, 2 and 3 respectively. The number preceding each title is the number of characters and spaces in the title. Dimensionless initial conditions (PBAR, TBAR, ABAR1 and ABAR2) are read in on line 4. Although

ABAR2 has not been used in the formulation, it is used as an initial guess for an iteration loop as described in more detail in the discussion of block 5. Since a value of k has been specified in block 1, the initial conditions for a dimensionless solution are complete at this point.

Values of PSOI, TSO and AM are read in on line 5, and values of friction coefficients (FDUCT, FTUBE) are introduced at line 6. This completes the information required to begin calculations. Specific values of PPO, TOI, ATH and AM are obtained by multiplying the dimensional initial conditions by the non-dimensional initial conditions.

Block 3 - Calculation of Suction Duct Pressure Loss:

The performance of a jet pump is dependent upon the stagnation pressure of the secondary flow at the exit of the primary nozzles, PSO. It is difficult to measure this pressure in an experimental jet pump. Instead, the suction duct inlet stagnation pressure can be measured and the loss between the inlet section and the primary nozzle exit section can be accounted for by the following equation:

$$\Delta P_t \Big)_{\text{suction duct}} = K_{sd} \frac{\rho_s V_s^2}{2 g_o} \tag{97}$$

The loss coefficient K_{sd} can be evaluated by drawing air through the suction duct with a blower and plotting $(\Delta P_t)_{\text{suction duct}}$ vs. $\rho_s V_s^2 / 2 g_o$ on a Cartesian graph. The slope of the resulting curve is equal to K_{sd} .

The correction for suction duct pressure loss begins on line 8 of the program. The equation for this correction is given below.

$$P_{so} = P_{soi} - K_{sd} \frac{\rho_s V_s^2}{2 g_o} \tag{98}$$

where P_{soi} is the secondary flow stagnation pressure at the suction duct inlet.

Blocks 4 and 10 - Specification of Entrainment Ratio:

Line 7 initiates a DO loop which encloses all statements down to line 14 (statement number 13). The entrainment ratio (ENTR) is initially set equal to 10.0 and the loop is repeated, increasing ENTR by 3.0 each time through, until a value of 40.0 has been reached. The integer J is used to count the number of loops completed.

Block 5 - Solution of Equations for the Accommodation Region:

Block 4 extends between line 9 and line 11. Primary and secondary mass flow rates (WP, WS) are calculated using equations (1) and (2). The value of the secondary flow Mach number (SMOK) is obtained by solving equation (57). Equation (57) is solved using Newton's method. A series of values of M_{s2} are tried until one is found which makes the left side of equation (57) sufficiently close in value to the right side. The numerical criterion for acceptable convergence is agreement within 0.0005, which gives a secondary flow rate accurate to within 0.5 lbm/min.

The primary mass flow rate and the entrainment ratio are specified in this program before the secondary Mach number is evaluated. There exists a maximum possible secondary mass flow rate corresponding to a secondary Mach number of 1.0. Thus, for given initial conditions, the jet pump will have a maximum permissible value of entrainment ratio, which can be calculated from equation (64). The statement on line 10 was inserted to recognize trial values of M_{s2} which are greater than 1.0. If the program tries to obtain a solution for an entrainment ratio greater than the maximum possible for the system, a message "This value of entrainment ratio is inaccessible" is printed and the program proceeds to block 9 (line number 15) to look for another set of initial conditions.

When the secondary Mach number has been determined, the static pressure at the end of the accommodation region ($P_{p2} = P_{s2}$) is calculated using P_{s0} and M_{s2} in equation (3). Then equation (3) is used with P_{p0} and P_{p2} to calculate M_{p2} . This procedure neglects the effect of primary stream expansion or contraction upon the secondary stream area. Equation (6) is used to correct for primary flow area

changes as follows. The calculated values of M_{p2} and M_{s2} are substituted into the left side of equation (6) and the result is compared with the actual mixing tube area. If the values are not sufficiently close, the value of M_{s2} is changed slightly, a new value of M_{p2} is determined from equation (3), and the test to see if equation (6) is satisfied is repeated. When values of M_{s2} and M_{p2} which satisfy equation (6) are determined, equations (7), (8), (9), (10), and (11) are employed to calculate the pressure, temperature and velocity for each stream at the end of the accommodation region.

The solution of equation (57) for M_{s2} requires a value of A_p , the area of the primary nozzle flow, which is introduced as an initial condition through the dimensionless area ratio ABAR2. However, this value of M_{s2} is used only temporarily; it is eventually modified as the effect of primary area changes is considered. Therefore, even though the analytical formulation did not make use of ABAR2, the program is made more efficient by using it to obtain a preliminary value of M_{s2} .

Block 6 - Solution of Equations Representing the Mixing Region:

The segment of the program which solves the mixing region equation extends from line 11 to line 12. The solution is obtained by an iteration technique in which the value of one variable is assumed and the equations are solved to obtain a calculated value of that variable. When the trial value is sufficiently close to the calculated value, an acceptable solution has been determined.

Values of stagnation enthalpy ($HP2$, $HS2$) are calculated for the primary and secondary streams using their properties at the end of the accommodation region. A trial value of PM ($PMG = PSO + 0.4$) is chosen and equations (19), (18), (17) and (20) are solved sequentially to determine a calculated value of PM . If the trial and calculated values satisfy the criterion below, the trial value is accepted as the solution.

$$|PMG - PM| \leq 0.01$$

If this convergence criterion is not satisfied, a new trial value is chosen and the procedure is repeated. The convergence criterion corresponds to an error of less than 0.1%.

The integer I keeps track of the number of iterations performed in order to limit their number to 400. Convergence is generally obtained in less than 100 iterations. In some cases, the trial value will oscillate about the calculated value without quite converging. When this occurs, the trial value is within a region very close to convergence. Therefore, the logical variable INT is used to detect this condition, stop the iteration, and accept the current trial value as a satisfactory solution.

In the course of the development of a satisfactory value of PM, corresponding values of VM and TM are determined. These three values completely specify the conditions at the end of the mixing region. If no frictional effects are included, all the desired jet pump performance parameters such as stagnation pressure rise, static pressure change and momentum ratio can be determined from PM, VM, and TM.

For the temperature ranges of interest, the variation of specific heat with temperature has been found to have a negligible effect on the results (figure 5). This computer program, therefore, has been written to treat specific heat and k as constants. As a result, equation (17) has not been used in the program. If it is desired to include a variable specific heat, an equation such as (17) can be added to the existing program without altering its basic structure.

Block 7 - Solution of Equations Representing Mixing Region Friction Effects:

Block 7, from lines 12 to 13, corrects the values of M_m , P_m , T_m and V_m for frictional effects. Equation (38) is used to accomplish this. For a specified value of mixing duct friction coefficient, K_{MT} , both α and β can be determined from the results of block 6. Equation (38) is then solved using Newton's method to give a new value of Mach number at location m . A new value of pressure is obtained from equation (34). Corrected values of temperature and velocity are then determined using equations (39) and (33).

Block 8 - Print Solutions for One Value of Entrainment Ratio:

When a solution for a particular value of entrainment ratio is obtained, all variables are printed together with appropriate titles. Data internal to the program

is also printed, e.g., the number of iterations required for convergence in each section in which an iterative method is used. When a new set of initial conditions are used, this is indicated by an appropriate statement and a list of the new initial conditions.

Block 9 - Store Solutions for Plots and Tabular Presentation:

The results which are printed as each solution is obtained are also summarized in tabular form. To allow the tabular form to be printed, arrays are filled with the numbers from each solution.

Arrays of the same type are used to store solutions for the plotting routine. These arrays are larger because the plotter is used for several sets of initial conditions whereas the tabular results are printed for each individual set of initial conditions.

Block 11 - Print Solutions in Tabular Form:

After a set of solutions for one set of initial conditions has been obtained and stored in the arrays of block 9, the results are printed in a table. Values of the desired performance parameters are printed vs. entrainment ratio. Two tables are printed; one presents dimensionless variables and the other presents dimensional variables. The dimensionless solutions are independent of the dimensional initial conditions unless frictional effects have been included in the solution.

Block 13 - Plot Dimensionless Pressure Rise and Momentum Ratio:

Values which have been stored in the arrays PRISE and THRUS in block 9 are plotted as functions of entrainment ratio. Two plots are obtained; dimensionless pressure rise and momentum ratio vs. entrainment ratio. If it is desired to plot variables other than these, this may be done by storing the desired variables in the PRISE and THRUS arrays in place of the dimensionless pressure rise and momentum ratio values.

The plotting system is too complex to discuss in detail here. Unless the user has access to the EZPLOT routine used in this program, it is unlikely that he

will be able to use the plotting section directly. However, the storage arrays developed within the program should be useful for providing data to any other plotting device which may be available.

B.2 Using the Computer Program

This section discusses the various options which may be exercised when using the program and the tasks which must be performed to set them up.

The Complete Program:

The complete program includes suction duct and mixing tube frictional effects and plotting of the results. Values of PBAR, TBAR, ABAR1, ABAR2, PSOI, TSO, and AM must be provided as input data together with empirically-determined values of FDUCT and FTUBE. A value of N equal to the number of cases to be solved must be included to maintain control within the plotting block. It is best to vary only one parameter such as \bar{A} in a single set of solutions. The plot titles (which are provided as input data) can then denote this parameter on the plots as illustrated in the sample solutions provided in section 3.3.

If variables other than DDELP and AUG are to be plotted, this may be done by storing them in the PRISE and THRUS arrays.

Omission of Frictional Effects:

Frictional effects may be omitted by inputting zero values for FDUCT and/or FTUBE, depending on which frictional effect is to be eliminated.

Omission of the Plotting Section:

The plotting function may be temporarily omitted by punching a character in the first column of the "CALL EZPLOT" cards. The necessary input data for plotting must still be read-in or else the input format will not function correctly.

If the plotting section is to be removed permanently, it is best to remove all cards associated with the plotting function. This includes READ statements, logic for data manipulation, storage arrays, and the function TOP (ARRAY). The cards which may be removed are noted by an asterisk on the program listing of Appendix A.

APPENDIX C
Typical Computer Solutions

***** THE FOLLOWING CASES WILL USE THESE INITIAL CONDITIONS *****

PRESSURE RATIO=0.3000E 02 TEMPERATURE RATIO=0.1500E 01
 (ATH*CW/AM)=0.1000E-02 AP/AM=0.8000E-02
 SECONDARY PRESSURE=0.1440E 02 SECONDARY TEMPERATURE=0.5300E 03 MIXING TURE APFA=0.8726E-01

**** CASE 1 ENTRAINMENT RATIO= 10.00000 ****

MACH NUMBER ITERATIONS= 2
 PRIMARY AREA ITERATIONS= 10
 PRESSURE ITERATIONS= 73

	ACCOMMODATION REGION		*	OUTLET
	PRIMARY	SECONDARY		
PRESSURE, PSIA	0.1439E 02	0.1439E 02	•	0.1493E 02
TEMPERATURE	0.2996E 03	0.5278E 03	•	0.5498E 03
VELOCITY, FT/SEC	0.2441E 04	0.1624E 03	•	0.1786E 03
MACH NUMBER	0.2875E 01	0.1441E 00	•	0.1553E 00
MASS FLOW RATE, POUND/MIN	0.6230E 01	0.6230E 02	•	0.6853E 02

THE PRIMARY STREAM AREA AFTER ACCOMODATION=0.3282E-02 SQ. FEET
 TOTAL PRESSURE RISE=0.8384E 02 POUND/SQ. FOOT
 DIMENSIONLESS PRESSURE RISE=0.3988E-01
 DIMENSIONLESS STATIC PRESSURE CHANGE=0.2251E-01
 MOMENTUM RATIO=0.8049E 00

**** CASE 2 ENTRAINMENT RATIO= 13.00000 ****

MACH NUMBER ITERATIONS= 1
 PRIMARY AREA ITERATIONS= 0
 PRESSURE ITERATIONS= 4

	ACCOMMODATION REGION		*	OUTLET
	PRIMARY	SECONDARY		
PRESSURE, PSIA	0.1424E 02	0.1424E 02	•	0.1476E 02
TEMPERATURE	0.2987E 03	0.5262E 03	•	0.5433E 03
VELOCITY, FT/SEC	0.2443E 04	0.2125E 03	•	0.2272E 03
MACH NUMBER	0.2882E 01	0.1889E 00	•	0.1987E 00
MASS FLOW RATE, POUND/MIN	0.6230E 01	0.8099E 02	•	0.8772E 02

THE PRIMARY STREAM AREA AFTER ACCOMODATION=0.3303E-03 SQ. FEET
 TOTAL PRESSURE RISE=0.8251E 02 POUND/SQ. FOOT
 DIMENSIONLESS PRESSURE RISE=0.3925E-01
 DIMENSIONLESS STATIC PRESSURE CHANGE=0.1102E-01
 MOMENTUM RATIO=0.1302E 01

**** CASE 3 ENTRAINMENT RATIO= 16.0000 ****

MACH NUMBER ITERATIONS= 1

PRIMARY AREA ITERATIONS= 6

PRESSURE ITERATIONS= 4

	ACCOMMODATION REGION		●	OUTLET
	PRIMARY	SECONDARY		
PRESSURE, PSIA	0.1405E 02	0.1405E 02	●	0.1455E 02
TEMPERATURE	0.2975E 03	0.5242E 03	●	0.5383E 03
VELOCITY, FT/SEC	0.2446E 04	0.2641E 03	●	0.2773E 03
MACH NUMBER	0.2891E 01	0.2352E 00	●	0.2437E 00
MASS FLOW RATE, POUND/MIN	0.6230E 01	0.9968E 02	●	0.1052E 03

THE PRIMARY STREAM AREA AFTER ACCOMMODATION=0.3331E-03 SQ. FEET

TOTAL PRESSURE RISE=0.8131E 02 POUND/SQ. FOOT

DIMENSIONLESS PRESSURE RISE=0.3867E-01

DIMENSIONLESS STATIC PRESSURE CHANGE=-.3367E-02

MOMENTUM RATIO=0.1927E 01

**** CASE 4 ENTRAINMENT RATIO= 19.0000 ****

MACH NUMBER ITERATIONS= 2

PRIMARY AREA ITERATIONS= 0

PRESSURE ITERATIONS= 6

	ACCOMMODATION REGION		●	OUTLET
	PRIMARY	SECONDARY		
PRESSURE, PSIA	0.1381E 02	0.1381E 02	●	0.1429E 02
TEMPERATURE	0.2961E 03	0.5216E 03	●	0.5336E 03
VELOCITY, FT/SEC	0.2449E 04	0.3177E 03	●	0.3291E 03
MACH NUMBER	0.2903E 01	0.2836E 00	●	0.2905E 00
MASS FLOW RATE, POUND/MIN	0.6230E 01	0.1184E 03	●	0.1246E 03

THE PRIMARY STREAM AREA AFTER ACCOMMODATION=0.3368E-03 SQ. FEET

TOTAL PRESSURE RISE=0.8030E 02 POUND/SQ. FOOT

DIMENSIONLESS PRESSURE RISE=0.3919E-01

DIMENSIONLESS STATIC PRESSURE CHANGE=-.2089E-01

MOMENTUM RATIO=0.2688E 01

**** CASE 5 ENTRAINMENT RATIO= 22.0000 ****

MACH NUMBER ITERATIONS= 2
PRIMARY AREA ITERATIONS= 0
PRESSURE ITERATIONS= 8

	ACCOMMODATION REGION		*	OUTLET
	PRIMARY	SECONDARY		
PRESSURE, PSIA	0.1351E 02	0.1351E 02	*	0.1399E 02
TEMPERATURE	0.2943E 03	0.5184E 03	0	0.5289E 03
VELOCITY, FT/SEC	0.2454E 04	0.3735E 03	0	0.3824E 03
MACH NUMBER	0.2917E 01	0.3345E 00	0	0.3399E 00
MASS FLOW RATE, POUND/MIN	0.6230E 01	0.1371E 03	0	0.1433E 03

THE PRIMARY STREAM AREA AFTER ACCOMMODATION=0.3414E-02 SQ. FEET

TOTAL PRESSURE RISE=0.7946E 02 POUND/SQ. FOOT

DIMENSIONLESS PRESSURE RISE=0.3780E-01

DIMENSIONLESS STATIC PRESSURE CHANGE=-.4197E-01

MOMENTUM RATIO=0.1593E 01

**** CASE 6 ENTRAINMENT RATIO= 25.0000 ****

MACH NUMBER ITERATIONS= 2
PRIMARY AREA ITERATIONS= 0
PRESSURE ITERATIONS= 10

	ACCOMMODATION REGION		*	OUTLET
	PRIMARY	SECONDARY		
PRESSURE, PSIA	0.1315E 02	0.1315E 02	0	0.1362E 02
TEMPERATURE	0.2920E 03	0.5144E 03	0	0.5237E 03
VELOCITY, FT/SEC	0.2459E 04	0.4326E 03	0	0.4408E 03
MACH NUMBER	0.2935E 01	0.3889E 00	0	0.3927E 00
MASS FLOW RATE, POUND/MIN	0.6230E 01	0.1559E 03	0	0.1620E 03

THE PRIMARY STREAM AREA AFTER ACCOMMODATION=0.3472E-02 SQ. FEET

TOTAL PRESSURE RISE=0.7884E 02 POUND/SQ. FOOT

DIMENSIONLESS PRESSURE RISE=0.3750E-01

DIMENSIONLESS STATIC PRESSURE CHANGE=-.6717E-01

MOMENTUM RATIO=0.4460E 01

**** CASE 7 ENTRAINMENT RATIO= 28.0000 ****

MACH NUMBER ITERATIONS= 3
 PRIMARY AREA ITERATIONS= 0
 PRESSURE ITERATIONS= 12

	ACCOMODATION REGION		*	OUTLET
	PRIMARY	SECONDARY		
PRESSURE, PSIA	0.1272E 02	0.1272E 02	*	0.1318E 02
TEMPERATURE	0.2892E 03	0.5095E 03	*	0.5179E 03
VELOCITY, FT/SEC	0.2466E 04	0.4965E 03	*	0.5024E 02
MACH NUMBER	0.2957E 01	0.4486E 00	*	0.4502E 00
MASS FLOW RATE, POUND/MIN	0.6230E 01	0.1744E 03	*	0.1807E 02

THE PRIMARY STREAM AREA AFTER ACCOMODATION=0.3547E-02 SQ. FEET

TOTAL PRESSURE RISE=0.7848E 02 POUND/SQ. FOOT

DIMENSIONLESS PRESSURE RISE=0.3733E-01

DIMENSIONLESS STATIC PRESSURE CHANGE=-.9734E-01

MOMENTUM RATIO=0.5908E 01

**** CASE 8 ENTRAINMENT RATIO= 31.0000 ****

MACH NUMBER ITERATIONS= 3
 PRIMARY AREA ITERATIONS= 0
 PRESSURE ITERATIONS= 16

	ACCOMODATION REGION		*	OUTLET
	PRIMARY	SECONDARY		
PRESSURE, PSIA	0.1218E 02	0.1218E 02	*	0.1264E 02
TEMPERATURE	0.2857E 03	0.5033E 03	*	0.5111E 03
VELOCITY, FT/SEC	0.2475E 04	0.5669E 03	*	0.5702E 03
MACH NUMBER	0.2986E 01	0.5153E 00	*	0.5143E 00
MASS FLOW RATE, POUND/MIN	0.6230E 01	0.1931E 03	*	0.1994E 03

THE PRIMARY STREAM AREA AFTER ACCOMODATION=0.3645E-02 SQ. FEET

TOTAL PRESSURE RISE=0.7839E 02 POUND/SQ. FOOT

DIMENSIONLESS PRESSURE RISE=0.3729E-01

DIMENSIONLESS STATIC PRESSURE CHANGE=-.1340E 00

MOMENTUM RATIO=0.7371E 01

**** CASE 9 ENTRAINMENT RATIO= 36.00000 ****

MACH NUMBER ITERATIONS= 2
 PRIMARY AREA ITERATIONS= 0
 PRESSURE ITERATIONS= 21

	ACCOMMODATION REGION		*	OUTLET
	PRIMARY	SECONDARY		
PRESSURE, PSIA	0.1150E 02	0.1150E 02	*	0.1198E 02
TEMPERATURE	0.2810E 03	0.4951E 03	*	0.5026E 03
VELOCITY, FT/SEC	0.7496E 04	0.5478E 03	*	0.6474E 03
MACH NUMBER	0.3024E 01	0.5937E 00	*	0.5889E 00
MASS FLOW RATE, POUND/MIN	0.6230E 01	0.2119E 03	*	0.2181E 03

THE PRIMARY STREAM AREA AFTER ACCOMMODATION=0.3790E-02 SQ. FEET
 TOTAL PRESSURE RISE=0.7875E 02 POUND/SQ. FOOT
 DIMENSIONLESS PRESSURE RISE=0.3746E-01
 DIMENSIONLESS STATIC PRESSURE CHANGE=-.1796E 00
 MOMENTUM RATIO=0.9115E 01

**** CASE 10 ENTRAINMENT RATIO= 27.00000 ****

MACH NUMBER ITERATIONS= 2
 PRIMARY AREA ITERATIONS= 1
 PRESSURE ITERATIONS= 20

	ACCOMMODATION REGION		*	OUTLET
	PRIMARY	SECONDARY		
PRESSURE, PSIA	0.1059E 02	0.1059E 02	*	0.1110E 02
TEMPERATURE	0.2744E 03	0.4834E 03	*	0.4912E 03
VELOCITY, FT/SEC	0.2502E 04	0.7483E 03	*	0.7413E 03
MACH NUMBER	0.3080E 01	0.4939E 00	*	0.4871E 00
MASS FLOW RATE, POUND/MIN	0.6230E 01	0.2205E 03	*	0.2267E 03

THE PRIMARY STREAM AREA AFTER ACCOMMODATION=0.3997E-02 SQ. FEET
 TOTAL PRESSURE RISE=0.7992E 02 POUND/SQ. FOOT
 DIMENSIONLESS PRESSURE RISE=0.3811E-01
 DIMENSIONLESS STATIC PRESSURE CHANGE=-.2197E 00
 MOMENTUM RATIO=0.1124E 02

**** CASE 11 ENTRAINMENT RATIO= 40.00000 ****

MACH NUMBER ITERATIONS= 4

PRIMARY AREA ITERATIONS= 1

PRESSURE ITERATIONS= 80

	ACCOMODATION REGION PRIMARY	REGION SECONDARY	* *	OUTLET
PRESSURE, PSIA	0.8932E 01	0.8932E 01	*	0.9727E 01
TEMPERATURE	0.2614E 03	0.4606E 03	*	0.4723E 03
VELOCITY, FT/SEC	0.2533E 04	0.9137E 03	*	0.8776E 03
MACH NUMBER	0.3194E 01	0.8681E 00	*	0.8234E 00
MASS FLOW RATE, POUND/MIN	0.6230E 01	0.2492E 03	*	0.2554E 03

THE PRIMARY STREAM AREA AFTER ACCOMODATION=0.4445E-03 SQ. FEET

TOTAL PRESSURE RISE=0.8365E 02 POUND/SQ. FOOT

DIMENSIONLESS PRESSURE RISE=0.3979E-01

DIMENSIONLESS STATIC PRESSURE CHANGE=-.3337E 00

MOMENTUM RATIO=0.1420E 02

DIMENSIONLESS SOLUTION USING THESE INITIAL CONDITIONS,
 PRESSURE RATIO=30.00 TEMPERATURE RATIO= 1.50 (ATH*CW/AM)=0.001000

ENTRAINMENT RATIO	* DIMENSIONLESS TOTAL PRESSURE RISE	* DIMENSIONLESS STATIC PRESSURE CHANGE	* MACH NUMBER	* DIMENSIONLESS KINETIC ENERGY	* MOMENTUM RATIO
10.0	0.03988	0.02251	0.155	0.0173	0.805
12.0	0.03925	0.01102	0.199	0.0280	1.302
16.0	0.03867	-0.00327	0.244	0.0414	1.927
19.0	0.03819	-0.02089	0.291	0.0579	2.688
22.0	0.03780	-0.04197	0.340	0.0775	3.593
25.0	0.03750	-0.06717	0.393	0.1007	4.660
28.0	0.03733	-0.09724	0.450	0.1281	5.908
31.0	0.03729	-0.13397	0.514	0.1604	7.373
34.0	0.03746	-0.17957	0.589	0.1992	9.115
37.0	0.03801	-0.23973	0.682	0.2476	11.259
40.0	0.03979	-0.33374	0.823	0.3162	14.205

DIMENSIONAL SOLUTION USING THESE INITIAL CONDITIONS,
 PRESSURE RATIO=30.00 TEMPERATURE RATIO= 1.50 (ATH*CW/AM)=0.001000

SECONDARY PRESSURE=14.60 PSI SECONDARY TEMPERATURE= 530.00 DEGREE RANKINE MIXING TUBE AREA=0.087260 SQ. FT.

ENTRAINMENT RATIO	* *	EXIT STATIC PRESSURE (PSI)	* *	TOTAL PRESSURE RISE (PSF)	* *	STATIC PRESSURE CHANGE (PSF)	* *	KINETIC ENERGY (PSF)
10.0	*	14.93	*	82.84	*	47.3240	*	36.30
13.0	*	14.76	*	82.51	*	23.1685	*	59.76
16.0	*	14.55	*	81.31	*	-7.0784	*	87.09
19.0	*	14.29	*	80.30	*	-43.9244	*	121.64
22.0	*	13.99	*	79.46	*	-88.2290	*	162.93
25.0	*	13.62	*	78.84	*	-141.2129	*	211.76
28.0	*	13.18	*	78.48	*	-204.6518	*	269.21
31.0	*	12.64	*	78.39	*	-281.6621	*	337.16
34.0	*	11.98	*	78.75	*	-377.5278	*	418.71
37.0	*	11.10	*	79.92	*	-504.0132	*	520.54
40.0	*	9.73	*	83.65	*	-701.6533	*	664.84

REFERENCES

1. United States Letter Patent #3,093,349, Fred G. Wagner, Inventor: "Duct Arrangement for Aircraft Boundary Layer Control."
2. United States Letter Patent #3,085,740, Fred G. Wagner, Inventor: "End Inlet Jet Pump for Boundary Layer Control System."
3. Mc Clintock, F. A., and Hood, J. Hall: "Aircraft Ejector Performance," Journal of the Aeronautical Sciences, November, 1946.
4. Keenan, J. H., Neumann, E. P., and Lustwerk, F.: "An Investigation of Jet Pump Design by Analysis and Experiment", Journal of Applied Mechanics, Volume 17 (1950).
5. Fabri, J. and Paulon, J.: "Theory and Experiments on Supersonic Air-to-Air Ejectors", NACA TM 1410, September, 1958.
6. Fabri, J. and Siestrunk, R.: "Supersonic Air Ejectors", in Advances in Applied Mechanics, Volume V., Academic Press, N. Y., 1958.
7. De Leo, Richard V. and Wood, Richard D." "An Experimental Investigation of the Use of Hot Gas Ejectors for Boundary Layer Control", WADC TR 52-128, Part 1 (April, 1952), Part 2 (December, 1953), Part 3 (June, 1958).
8. De Leo, Richard V., and Rose, R. E.: "An Experimental Investigation of the Use of Supersonic Driving Jets for Ejector Pumps", WADC TR 57-357, December, 1958.
9. De Leo, Richard V., Rose, R. E., and Dart, R. S.: "An Experimental Investigation of the Use of Supersonic Driving Jets for Ejector Pumps", Transactions of the ASME, J. E. P., 61-HTD-13.
10. Traksal, J.: "Simplified Ejector and Jet Thrust Augmentor Theory", Report No. 14898, Lockheed Aircraft Corporation, California Division, January, 1963.

11. Van der Lingen, T. W. : "A Jet Pump Design Theory", Transactions of the ASME, J.B.E., December, 1960.
12. Seaver, R. J., "Development of a Hot Jet Pump BLC System (Jet Induced Lift System), Phase I: Bench Testing of An Experimental Jet Pump", final report, NASA Contract No. NAS 2-2518, prepared by Sunrise Aircraft Corporation of America, November, 1966.
13. Society of Automotive Engineers, Aero-Space Applied Thermodynamics Manual, 1960.
14. Wirt, L., "New Data for the Design of Elbows in Duct Systems", G. E. Review, Volume 30, 1927, p. 286.
15. American Society of Heating, Refrigerating and Air Conditioning Engineers, Guide and Data Book, Systems and Equipment Volume, 1967.
16. Lamb, O. P., and Holdhusen, J. S., "Investigation of Aircraft Ducting Components at High Subsonic Speeds," WADC TR 56-187, September, 1957.
17. Dynatech Report No. 261, "Pressure Loss Calculation Procedures for High Speed Gas Flow in Ducts", prepared for U.S. Navy Bureau of Ships, Contract No. Nobs-84282, June, 1961.
18. Henry, J. R., "Design of Power Plant Installations; Pressure-Loss Characteristics of Duct Components," NACA WR L-208, 1944.
19. Hall, W. B., and Orme, E.M., "Flow of a Compressible Fluid Through a Sudden Enlargement in a Pipe," Proceedings of the Institute of Mechanical Engineers, Volume 169, No. 49, 1955.
20. Cole, B. N. and Mills, B., "Theory of Sudden Enlargements Applied to the Poppet Exhaust-Pulse Scavenging," Proceedings of the Institute of Mechanical Engineers, Vol. 1B, p. 364.

21. Patterson, G. N., "Modern Diffuser Design," Aircraft Engineering, September 1938.
22. Young, A. D., and Green, G. L., "Tests of High-Speed Flow in Diffusers of Rectangular Cross-Section," R & M No. 2201, British A.R.C., July, 1944.
23. Little, B.H., Jr., and Wilbur, S. W., "Performance and Boundary Layer Data from 12° and 23° Conical Diffusers of Area Ratio 2.0 at Mach Numbers up to Choking and Reynolds Numbers up to 7.5×10^6 ," NACA Report 1201, 1954.
24. Young, A.D., Green, G.L., and Owen, P.R., "Tests of High-Speed Flow in Right-Angled Pipe Bends of Rectangular Cross-Section," R & M No. 2066, British A. R. C., October, 1943.
25. Higginbotham, J. T., Wood, C. C., and Valentine, E. F., "A Study of the High-Speed Performance Characteristics of 90° Bends in Circular Ducts," NACA TN 3696, June, 1956.
26. Friedman, D., and Westphal, W.R., "Experimental Investigation of a 90° Cascade Diffusing Bend with An Area Ratio of 1.45:1 and with Several Inlet Boundary Layers," NACA TN 2668, April, 1952.

\bar{A}	\bar{T}	Values of P and Corresponding Maximum Entrainment Ratios, m_{max}					Fig. Nos.	
.001 ↓	1.5	\bar{P} : 25	30	35	40	45	6, 7	
		m_{max} : 49	41	35	30.5	27		
	3.5	\bar{P} : 40	45	50	55	60	65	8, 9
		m_{max} : 47	41.5	37.5	34	31	29	
	8.0	\bar{P} : 60	70	80	90		10, 11	
		m_{max} : 47	40.5	35	31.5			
.003 ↓	1.5	\bar{P} : 9	10	11	12	13	14	12, 13
		m_{max} : 45.5	41	37	34	31.5	29	
	3.5	\bar{P} : 20	22	24	26	28		14, 15
		m_{max} : 47	43	39	36	34		
	8.0	\bar{P} : 20	22	24	26	28		16, 17
		m_{max} : 47	43	39	36	34		
.007 ↓	1.5	\bar{P} : 4	4.5	5	5.5	6		18, 19
		m_{max} : 44	39	35	32	29		
	3.5	\bar{P} : 5	6	7	8	9		20, 21
		m_{max} : 53.5	44.5	38	33.5	30.0		
	8.0	\bar{P} : 9	10	11	12	13	14	22, 23
		m_{max} : 45	40.5	37	33.5	31	29	

Table 1: Index to Analytical Jet Pump Performance Plots

Entrainment Ratio (m)	Jet Pump Total Pressure Rise psf (ΔP_t)	Mixing Tube. Outlet Static Pressure psia (P_m)	Mixing Tube Dynamic Head psf $\left(\frac{\rho_m V_m^2}{2 g_o}\right)$	Mixing Tube Exit Mach No. M_m
10.0	101.5	15.32	40.83	.163
13.0	99.59	15.13	65.30	.206
16.0	97.86	14.90	96.04	.255
19.0	96.35	14.62	133.47	.300
22.0	95.05	14.29	178.30	.352
25.0	93.96	13.88	231.09	.407
28.0	93.12	13.40	293.75	.469
31.0	92.61	12.81	368.10	.535
34.0	92.60	12.06	458.39	.615
37.0	93.52	11.03	573.92	.722

Table 2 - Jet Pump Performance Characteristics from Computer Output

Nozzle	Nozzle Throat Diameter inches	Nozzle Throat Area ft ² x10 ⁴	Nozzle Type	Design Pressure psia	Design Temp. °F	Flow Coefficient C _w	Flow Rate at Design W _p
Case 2	0.047	1.089	converging-diverging	350	200°F	.938	6.39 lbm/min
Case 3	0.1109	6.05	converging-diverging	100	1200°F	.965	6.52 lbm/min
Case 4	0.0596	1.75	converging-diverging	350	1200°F	.965.	6.60 lbm/min
Case 4A	0.063	1.952	converging	350	1200°F	.935	7.11 lbm/min
Case LD-4	0.0658	1.650	converging-diverging	350	1200°F	.941	6.08 lbm/min

Table 3. Primary Nozzle Characteristics

	Flow Parameter	Instrumentation Used to Measure Parameter	How Recorded	Required for Determining	Data Reduction Procedure
Primary Flow	P_{po}	Bourdon Tube Gage	Manually and Photographically	Jet Pump Input Conditions	None needed
	T_{po}	Thermocouple and Bridge	Manually	Jet Pump Input Conditions	None needed
	W_p	Orifice Flow Meter and Panel Gage	Manually	Jet Pump Input Conditions	Standard calibration curves provided by flowmeter manufacturer
Secondary Flow	T_{so}	Dial Gage In Suction Duct	Manually	Secondary Flow Temperature	None needed
	P_{atm}	Mercury Barometer	Manually	Atmospheric Pressure	None needed
	P_b	Manometers	Manually and Photographically	Secondary Flow Rate	See below
	W_s	Calibrated Bellmouth	Manually	Secondary Flow Rate in lb/min	Equation (91)
Mixing Tube and Diffuser	P vs. length	Manometer Board	Photographically	Mixing Tube and Diffuser Static Pressures	None needed
	P_{mo} P_{do} }	Kiel Probe Traverse	Manually	Discharge Stagnation Pressure for Jet Pump	"Mass-momentum" method for Compressible Flow (See Text)
	T_{eo}	Dial Gage Near End of Diffuser	Manually	Jet Pump Discharge Temperature	None needed

Table 4. Measured Parameters and Instrumentation

Test No.	Run No.	Nozzle Set	Primary Flow Pressure (psia)	Primary Flow Temperature (° F)	Secondary Flow Rate	Discharge Configuration	Cluster Configuration			
Test Series #1: Reference Test										
114	1	1-5	350	1085°	4 values	NAS2-2518 mixing tube	Original			
	2	6-9	300	1160°	4 values					
	3	10-14	260	1185°	5 values					
	4	15-18	225	1145°	4 values					
Test Series #2: Nozzle Cluster Performance Comparison										
	5	19-22	350	1130°	4 values	Constant-area short mixing tube	Original			
	6	23-26	300	1160°	4 values					
	7	27-31	260	1165°						
	8	32-35	225	1158°						
	9	36-39	350	1160°						
	10	40-43	300	1180°	4 values					
	11	44-47	260	1200°						
	12	48-51	225	1200°						
	13	52-55	350	1130°						
	14	56-59	300	1195°	4 values					
	15	60-63	260	1190°						
	16	64-67	225	1180°						
	13	52-55	LD#2-4							
	Test Series #3: Final Performance Tests									
		17	96-99	350	1110°			4 values	Constant-area long mixing tube	LD#1
		18	100-103	300	1150°					
19		104-107	260	1200°						
20		108-111	225	1200°						
21		80-83	300	750°						
22		84-87	260							
23		88-91	225							
24		92-95	175							
25		68-71	260	455°						
26		72-75	225	460°						
27		76-79	175	460°						

Table 5. Jet Pump Test Program



Test No.	Run No.	Nozzle Set	Primary Flow Pressure (psia)	Primary Flow Temperature (° F)	Secondary Flow Rate	Discharge Configuration	Cluster Configuration	
28	242-245	4A	350	1160°	4 values	Constant-area short mixing tube	LD#1	
29	246-249 (converging)	↓	300	1150°-1100°				
30	250-253		260	1150°				
31	254-257		225	1150°				
32	140-143		350	1160°				
33	144-147		300	1150°				
34	148-151		260	1095°-1031°				
35	152-155		225	1020°				
36	124-127		300	750°				
37	128-131		260	↓				
38	132-135		225					
39	136-139		175	745°				
40	112-115		260	455°				
41	116-119	225	455°					
42	120-123	175	460°					
43	180-183	2	350	200°	4 values	Constant-area long mixing tube	LD#1	
44	184-187	↓	300	↓				
45	188-191		260					
46	192-195		225					
47	196-199		400					455°
48	200-203		350					455°
49	204-207		260					450°
50	208-211		225					450°
51	212-215		400					460°
52	216-219		350					455°
53	220-223		260					450°
54	224-227		225					450°
55	168-171		3		100	1160°-1115°	4 values	Constant area long mixing tube
56	172-175	↓	85	1140°				
57	176-179		70	1145°				
58	156-159		85	755°				
59	160-163		70	750°				
60	164-167		55	745°				
61	228-231		100	1150°-1110°				
62	232-235		85	1155°				
63	236-239		70	1155°				

Table 5. Jet Pump Test Program (Continued)

Test Date	Test Nos.	Run Nos.	Constant Area Mixing Tube	Nozzle Case No.	Tabulated Data	Static Pressure Parameter $\frac{P_m - P_{so}}{P_{so}}$	Stagnation Pressure Rise Parameter $\frac{P_{mo} - P_{so}}{P_{so}}$	Velocity Profiles	Static Pressures vs. P_{po} and m	Static Pressures vs. Distance	Thrust Augmentation Parameter τ
25 July 1968	1-4	1-18	short	4 no extension	Table 8		Table 7 Figure 48	Figure 44 Figure 45	Figure 46	Figure 47	
31 July 1968	5-8	19-35	short	4 no extension	Table 9	Figure 48	Table 7 Figure 48	Figure 49	Figure 50	Figure 47	
13 August 1968	9-12	36-51	short	4	Table 10	Figure 52	Table 7	Figure 53	Figure 54	Figure 55	
19 August 1968	13-16	52-67	short	LD#2-4	Table 11	Figure 56	Table 7	Figure 57	Figure 58	Figure 55	
28 August 1968	17-27	68-111	extended	4	Table 12	Figure 59 Figure 60	Table 7 Figure 59	Figure 61 Figure 62	Figure 63	Figure 64	Table 12
13 Sept. 1968	28-31	242-259	short	4A	Table 13	Figure 65	Table 7	Figure 66	Figure 67		
3 Sept. 1968	32-42	112-155	extended	4A	Table 14	Figure 68 Figure 69			Figure 70	Figure 71	Table 14
11 Sept. 1968	43-50	180-211	extended	2	Table 15	Figure 72	Table 7	Figure 73	Figure 74	Figure 75	Table 15
11 Sept. 1968	51-54	212-227	short	2	Table 16	Figure 76	Table 7	Figure 73	Figure 77		
10 Sept. 1968	55-60	156-179	extended	3	Table 17	Figure 78	Table 7	Figure 79	Figure 80	Figure 81	Table 17
12 Sept. 1968	61-63	228-241	short	3	Table 18	Figure 82	Table 7	Figure 83	Figure 84		

Table 6
Index to Test Results

Test No.	Run No.	Traverse Location and Number of Traverses	Nozzles	Cluster Configuration	Duct Configuration	P _{po} psia	T _{po} °F	m	P _{do} psf Diffuser	Experimental			Analytical				Comments on Results	
										P _{mo} psf ← Mixing Tube →	P _{so} psf	P _{mo} - P _{so} P _{so}		P _{mo} - P _{so} P _{so}				
1	1	Diffuser 1	Case 4	Original Cluster	Short Converging Mixing Tube	350	1094	26.2	2189.5	2187.9	2093.3	.01519	.0538	.0503	10.70	+10.2	short mixing tube one traverse incomplete mixing	
1	2	Diffuser 1	Case 4			350	1086	22.5	2171.2	2184.0	2100.3	.03985	.0540	.0514	24.26	+22.5		
1	4	Diffuser 1	Case 4			350	1084	18.4	2180.6	2189.0	2107.0	.03891	.0555	.0536	30.95	+27.4		
1	5	Diffuser 1	Case 4			350	1085	15.6	2196.9	2203.0	2110.7	.04372	.0561	.0547	23.18	+20.07		
2	7	Diffuser 1	Case 4			300	1158	25.4	2169.4	2180.8	2102.4	.03729	.0459	.0435	13.06	+14.28		
3	11	Diffuser 1	Case 4			260	1186	29.7	2157.8	2189.1	2102.2	.03182	.0391	.0387	10.28	+13.30		
5	20	Diffuser 1	Case 4	Original Cluster	Short Constant Area Mixing Tube	350	1131	22.4	2214.6	2225.8	2128.0	.04595	.0541	.0515	11.81	+10.78		
6	24	Diffuser 2	Case 4			300	1174	24.9	2216.4	2225.8	2129.4	.04527	.0460	.0437	-3.34	- 3.59		
7	27	Diffuser 1	Case 4			260	1164	29.13	2192.5	2201.8	2128.1	.03463	.0393	.0371	5.28	+ 6.66		
10	41	Diffuser 1	Case 4	LD#1	Short Constant Area Mixing Tube	300	1187	25.6	2192.1	2202.4	2117.2	.0402	.0458	.0434	6.96	+ 7.60		
14	37	Diffuser 2	Case LD2-4	LD#2	Short Constant Area Mixing Tube	300	1198	27.4	2216.3	2226.5	2105.8	.0573	.0427	.0403	-35.80	-42.18	Not as well mixed as other clusters. Traverses through nozzles significantly larger than traverses set through nozzles.	
18	101	Mixing Tube 2	Case 4	LD#1	Extended Constant Area Mixing Tube	300	1154	26.5	-----	2204.1	2126.7	.03639	.0455	.0376	2.57	+ 3.22	extended mixing tube two traverses good mixing	
18	101	Diffuser 2	Case 4			300	1154	26.5	2190.4	2202.1	2126.7	.0355	.0455	.0376	4.47	+ 5.59		
18	102	Mixing Tube 2	Case 4			300	1158	22.1	-----	2208.9	2131.25	.0355	.0465	.0409	11.51	+13.20		
18	102	Diffuser 2	Case 4			300	1158	22.1	2204.9	2212.9	2131.3	.03828	.0465	.0409	5.58	+ 6.40		
56	173	Mixing Tube 2	Case 3			85	1138	23.6	-----	2188.7	2127.8	.02862	.0360	.0298	2.51	+ 3.96		
56	173	Diffuser 2	Case 3			85	1138	26.6	2178.1	2187.8	2127.8	.02782	.0360	.0298	4.21	+ 6.64		
48	200	Diffuser 1	Case 2			350	444	28.5	2124.0	2136.1	2088.6	.02274	.0350	.0269	8.89	+15.46	extended mixing tube one traverse	
52	217	Diffuser 1	Case 2		Short Constant Area Mixing Tube	350	452	27.3	2156.1	2166.6	2089.2	.03704	.0349	.0325	9.48	-13.97	short mixing tube one traverse distorted velocity profile	
63	240	Diffuser 1	Case 3			85	1159	26.1	2142.3	2153.7	2088.7	.03111	.0354	.0325	3.53	+ 5.15		
29	258	Diffuser 1	Case 4A			300	1193	26.6	2143.5	2157.4	2093.9	.03002	.0490	.0170	32.62	+33.94	short mixing tube one traverse distorted velocity profile	

Table 7. Tabulation of Stagnation Pressure Results

Test No.	Run	P _{po} psia	T _{po} ° F	W _p lbm/min	T _{so} ° F	W _s lbm/min	m
1 ↓	1	350	1094	6.69	95	175.5	26.2
	2	↓	1086	6.70	93	150.8	22.5
	4	↓	1084	6.66	95	122.8	18.4
	5	↓	1085	6.70	95	104.4	15.6
2 ↓	6	300	1164	5.66	93	163.4	28.9
	7	↓	1158	5.66	94	143.5	25.35
	8	↓	1158	5.65	95	124.0	21.95
	9	↓	1160	5.67	95	99.0	17.45
3 ↓	10	260	1185	4.91	91	153.5	31.3
	11	↓	1186	4.87	93	144.8	29.7
	12	↓	1185	4.87	93	128.1	26.3
	13	↓	1184	4.89	92	108.3	22.15
	14	↓	1185	4.90	92	92.0	18.8
4 ↓	15	225	1139	4.39	93	143.2	32.6
	16	↓	1158	4.20	92	128.0	30.5
	17	↓	1158	4.34	93	112.6	25.9
	18	↓	1145	4.40	93	94.1	21.4

Table 8
Jet Pump Test Results
NAS 2-2518 Mixing Tube
Original Nozzle Cluster
Case 4 Nozzles

Test No.	Run	P _{po} psia	T _{po} ° F	W _p lbm/min	T _{so} ° F	W _s lbm/min	m
5 ↓	19	350 ↓	1162	6.57	89	162.5	24.74
	20		1131	6.75	88	151.4	22.43
	21		1124	6.66	86	125.4	18.83
	22		1130	6.63	82	104.6	15.78
6 ↓	23	300 ↓	1158	5.70	90	151.4	26.57
	24		1162	5.70	88	145.7	25.56
	25		1162	5.70	88	124.4	21.83
	26		1160	5.70	88	99.9	17.52
7 ↓	27	260 ↓	1166	4.84	89	141.0	29.13
	29		1165	4.84	89	129.2	26.68
	30		1165	4.84	89	110.2	22.76
	31		1166	4.84	89	91.8	18.97
8 ↓	32	225 ↓	1156	4.33	90	132.6	30.63
	33		1158	4.29	89	128.1	29.85
	34		1158	4.29	89	111.5	25.98
	35		1158	4.29	88	92.4	21.54

Table 9

Jet Pump Test Results
Short Constant Area Mixing Tube
Original Nozzle Cluster
Case 4 Nozzles

Test No.	Run	P _{po} psia	T _{po} °F	W _p lbm/min	T _{so} °F	W _s lbm/min	m
9	36	350	1164	6.82	88	182.0	26.7
	37	↓	1158	6.82	87	149.5	21.95
	38	↓	1158	6.82	86	125.0	18.35
	39	↓	1158	6.82	87	107.4	15.80
10	40	300	1209	5.72	85	170.0	29.8
	41	↓	1187	5.75	86	146.9	25.6
	42	↓	1160	5.78	85	125.0	21.6
	43	↓	1161	5.78	85	98.5	17.0
11	46	260	1207	4.95	86	160.0	32.3
	47	↓	1201	4.98	86	139.7	28.1
	44	↓	1200	4.98	86	112.5	22.6
	45	↓	1202	4.98	86	93.6	18.8
12	48	225	1188	4.32	86	151.0	35.0
	49	↓	1196	4.32	86	129.0	29.9
	50	↓	1201	4.27	85	113.1	26.5
	51	↓	1203	4.32	85	95.5	22.1

Table 10
 Jet Pump Test Results
 Short Constant Area Mixing Tube
 LD#1 Nozzle Cluster
 Case 4 Nozzles

Test No.	Run	P _{po} psia	T _{po} °F	W _p lbm/min	T _{so} °F	W _s lbm/min	m
13 ↓	52	350 ↓	1137	6.18	82	177.4	28.7
	53		1128	6.21	80	153.1	24.7
	54		1125	6.21	82	125.1	20.2
	55		1122	6.20	83	105.0	16.9
14 ↓	56	300 ↓	1195	5.24	85	164.3	31.4
	57		1160	5.34	83	146.1	27.4
	58		1194	5.21	82	125.1	24.0
	59		1194	5.23	82	100.4	19.2
15 ↓	60	260 ↓	1192	4.63	84	154.7	33.4
	61		1191	4.61	84	129.7	28.1
	62		1190	4.58	84	109.8	24.0
	63		1190	4.59	84	93.3	20.3
16 ↓	64	225 ↓	1184	3.99	84	144.3	36.2
	65		1183	3.99	84	129.4	32.4
	66		1182	3.96	82	115.1	29.1
	67		1182	3.96	84	95.3	24.1

Table 11

Jet Pump Test Results
Short Constant Area Mixing Tube
LD#2 Nozzle Cluster
LD#2-4 Nozzles (7 Nozzles)

Test No.	Run	P _{po} psia	T _{po} °F	W _p lbm/min	T _{so} °F	W _s lbm/min	m	τ
25	68	260	453	6.48	78	163.4	25.2	5.06
↓	69	↓	452	6.48	↓	140.4	21.7	3.64
↓	70	↓	453	6.46	↓	122.9	19.0	2.77
↓	71	↓	455	6.48	↓	110.5	17.1	2.24
26	72	225	454	5.67	78	153.2	27.0	5.05
↓	73	↓	456	5.67	79	139.3	24.6	4.11
↓	74	↓	460	5.65	79	124.7	22.1	3.28
↓	75	↓	462	5.64	77	104.2	18.5	2.28
27	76	175	459	4.43	78	133.8	30.2	4.92
↓	77	↓	459	4.43	79	121.6	27.5	4.04
↓	78	↓	463	4.43	79	106.8	24.1	3.09
↓	79	↓	463	4.42	79	94.3	21.3	2.42
21	80	300	753	6.63	82	172.3	26.0	4.96
↓	81	↓	753	6.60	↓	153.2	23.2	3.81
↓	82	↓	752	6.59	↓	130.0	19.7	2.71
↓	83	↓	752	6.59	↓	111.4	16.9	1.99
22	84	260	749	5.66	81	161.8	28.6	5.07
↓	85	↓	745	5.65	80	142.2	25.2	3.81
↓	86	↓	749	5.64	80	123.5	21.9	2.86
↓	87	↓	752	5.62	80	107.6	19.2	2.19
23	88	225	753	5.03	82	150.4	29.9	4.89
↓	89	↓	750	5.02	80	134.3	26.7	3.83
↓	90	↓	749	5.01	81	117.8	23.5	2.94
↓	91	↓	748	5.02	81	103.9	20.7	2.28
24	92	175	744	4.0	82	132.2	33.1	4.77
↓	93	↓	745	3.96	80	119.9	30.3	3.92
↓	94	↓	745	3.94	83	107.3	27.2	3.15
↓	95	↓	748	3.94	80	95.7	24.3	2.50
17	96	350	1116	6.82	88	179.8	26.4	4.85
↓	97	↓	1115	6.81	88	153.0	22.5	3.35
↓	98	↓	1112	6.76	88	129.7	19.2	2.39
↓	99	↓	1105	6.77	89	117.3	17.3	1.96
18	100	300	1147	5.78	88	167.3	28.9	4.76
↓	101	↓	1149	5.78	87	153.1	26.5	3.91
↓	102	↓	1154	5.77	86	127.7	22.1	2.68
↓	103	↓	1159	5.73	86	112.7	19.7	2.08
19	104	260	1195	5.01	83	156.7	31.3	4.67
↓	105	↓	1198	4.98	83	137.4	27.6	3.54
↓	106	↓	1199	4.98	83	115.1	23.1	2.47
↓	107	↓	1203	4.96	80	106.7	21.5	2.13
20	108	225	1198	4.35	83	145.5	33.4	4.61
↓	109	↓	1203	4.35	82	134.7	31.0	3.92
↓	110	↓	1205	4.26	81	119.0	27.9	3.09
↓	111	↓	1204	4.30	81	101.0	23.5	2.22

Table 12

Jet Pump Test Results
Extended Constant Area Mixing Tube
LD#1 Nozzle Cluster
Case 4 Nozzles

Test No.	Run	P _{po} psia	T _{po} °F	W _p lbm/min	T _{so} °F	W _s lbm/min	m
28 ↓	242	350 ↓	1160	7.25	86	175.3	24.17
	243		1139	7.24	86	156.4	21.60
	244		1156	7.25	86	134.3	18.53
	245		1156	7.24	85	105.5	14.57
29 ↓	246	300 ↓	1165	6.31	85	166.0	26.30
	247		1154	6.24	85	148.0	23.71
	248		1143	6.23	85	127.3	20.43
	249		1126	6.23	84	101.0	16.21
	258		1103	6.26	87	166.8	26.64
	259		1103	6.30	88	167.7	26.62
30 ↓	250	260 ↓	1149	5.44	85	157.7	28.99
	251		1149	5.41	85	142.5	26.35
	252		1149	5.38	85	122.0	22.68
	253		1150	5.38	84	100.5	18.68
31 ↓	254	225 ↓	1148	4.70	84	150.0	31.91
	255		1150	4.69	84	136.6	29.13
	256		1150	4.66	84	119.0	25.54
	257		1150	4.64	83	95.3	20.53

Table 13
 Jet Pump Test Results
 Short Constant Area Mixing Tube
 LD#1 Nozzle Cluster
 Case 4A Nozzles

Test No.	Run	P _{po} psia	T _{po} °F	W _p lbm/min	T _{so} °F	W _s lbm/min	m	τ
40	112	260	453	6.96	78	165.6	23.8	4.93
	113		457	6.92	78	142.8	20.6	3.57
	114		459	6.91	79	125.2	18.1	2.72
	115		462	6.89	79	108.3	15.7	2.05
41	116	225	456	6.05	79	155.4	25.7	4.96
	117		455	6.02	80	138.5	23.0	3.89
	118		456	5.98	80	124.3	20.8	3.12
	119		457	5.98	80	103.2	17.3	2.16
42	120	175	458	4.81	80	140.2	29.1	5.06
	121		462	4.81		123.5	25.7	3.89
	122		463	4.78		107.3	22.5	2.94
	123		464	4.78		96.5	20.2	2.38
36	124	300	753	7.10	84	172.1	24.2	4.73
	125		750	7.10		150.4	21.2	3.50
	126		749	7.08		128.7	18.2	2.54
	127		750	7.07		111.7	15.8	1.92
37	128	260	751	6.20	85	161.9	26.1	4.75
	129		752	6.19		140.5	22.7	3.49
	130		754	6.17		123.7	20.1	2.70
	131		756	6.17		106.8	17.3	2.01
38	132	225	745	5.35	86	152.6	28.5	4.86
	133		743	5.35	86	134.2	25.1	3.69
	134		744	5.36	85	117.8	22.0	2.82
	135		746	5.35	85	103.2	19.3	2.17
39	136	175	739	4.26	86	137.0	32.2	4.94
	137		743	4.24		119.7	28.2	3.73
	138		746	4.23		105.4	24.9	2.89
	139		748	4.22		95.9	22.7	2.40
32	140	350	1175	7.26	92	174.6	24.1	4.34
	141		1162	7.18		151.1	21.1	3.17
	142		1158	7.17		124.5	17.4	2.13
	143		1140	7.18		115.5	16.1	1.83
33	144	300	1146	6.26	94	165.1	26.4	4.43
	145		1149	6.23		145.2	23.3	3.35
	146		1148	6.28		124.6	19.8	2.43
	147		1124	6.27		110.7	17.7	1.93
34	148	260	1094	5.52	94	156.8	28.4	4.60
	149		1057	5.55		129.7	23.4	3.05
	150		1048	5.56		112.8	20.3	2.30
	151		1031	5.58		105.1	18.8	1.99
35	152	225	1021	4.95	94	148.7	30.0	4.62
	153		1021	4.94		129.7	26.3	3.47
	154		1021	4.94		114.5	23.2	2.70
	155		1021	4.93		101.9	20.7	2.14

Table 14
Jet Pump Test Results
Extended Constant Area Mixing Tube
LD#1 Nozzle Cluster
Case 4A Nozzles

Test No.	Run	P _{po} psia	T _{po} °F	W _p lbm/min	T _{so} °F	W _s lbm/min	m	τ
43 ↓	180	350 ↓	201	6.35	78 ↓	158.7	25.0	5.55
	181		199	6.38		140.2	22.0	4.21
	182		199	6.39		123.3	19.3	3.21
	183		200	6.39		106.4	16.7	2.38
44 ↓	184	300 ↓	200	5.51	79 ↓	148.8	27.0	5.53
	185		205	5.47		137.0	25.0	4.68
	186		204	5.45		123.6	22.7	3.79
	187		205	5.44		101.3	18.6	2.53
45 ↓	188	260 ↓	201	4.80	79 ↓	138.4	28.8	5.52
	189		203	4.79		126.3	26.4	4.56
	190		201	4.78		114.1	23.9	3.70
	191		201	4.78		96.4	20.2	2.63
46 ↓	192	225 ↓	197	4.14	79 ↓	128.4	31.0	5.52
	193		197	4.14		118.9	28.7	4.70
	194		196	4.14		108.1	26.1	3.86
	195		199	4.12		93.9	22.8	2.92
47 ↓	196	400 ↓	456	6.30	81 ↓	167.7	26.6	5.43
	197		453	6.30		147.3	23.4	4.06
	198		455	6.29		129.3	20.6	3.09
	199		454	6.29		110.5	17.6	2.24
48 ↓	200	350 ↓	444	5.56	81 ↓	158.3	28.5	5.43
	201		454	5.54		140.8	25.4	4.21
	202		454	5.54		126.4	22.8	3.36
	203		454	5.52		104.8	19.0	2.31
49 ↓	204	260 ↓	449	4.07	82 ↓	137.0	33.7	5.50
	205		450	4.08		126.7	31.0	4.63
	206		451	4.08		115.4	28.3	3.82
	207		452	4.08		97.2	23.8	2.70
50 ↓	208	225 ↓	447	3.58	82 ↓	127.8	35.7	5.45
	209		447	3.58		116.2	32.5	4.47
	210		449	3.59		106.5	29.7	3.73
	211		450	3.58		93.2	26.0	2.85

Table 15
Jet Pump Test Results
Extended Constant Area Mixing Tube
LD#1 Nozzle Cluster
Case 2 Nozzles

Test No.	Run	P _{po} psia	T _{po} °F	W _p lbm/min	T _{so} °F	W _s lbm/min	m
51 ↓	212	400 ↓	456	6.25	85	171.4	27.4
	213		459	6.26	85	149.6	23.9
	214		458	6.25	85	127.4	20.4
	215		458	6.24	86	133.7	15.8
52 ↓	216	350 ↓	451	5.52	86	161.3	29.2
	217		452	5.52	85	150.8	27.3
	218		456	5.50	84	128.3	23.3
	219		457	5.49	83	96.6	17.6
53 ↓	220	260 ↓	451	4.12	81	142.5	34.6
	221		451	4.12	81	128.6	31.2
	222		451	4.09	82	109.5	26.8
	223		451	4.09	82	92.1	22.5
54 ↓	224	225 ↓	449	3.57	83	133.4	37.4
	225		448	3.58	83	120.9	33.8
	226		448	3.58	83	105.9	29.6
	227		448	3.58	83	88.9	24.8

Table 16

Jet Pump Test Results
Short Constant Area Mixing Tube
LD#1 Nozzle Cluster
Case 2 Nozzles

Test No.	Run	P _{po} psia	T _{po} °F	W _p lbm/min	T _{so} °F	W _s lbm/min	m	τ
58 ↓	156	85 ↓	755	6.64	540	158.3	23.8	4.95
	157		758	6.59	541	138.6	21.0	3.75
	158		758	6.59	542	124.3	18.9	3.02
	159		758	6.58	543	105.5	16.0	2.18
59 ↓	160	70 ↓	751	5.44	542	141.9	26.1	4.97
	161		748	5.42	542	128.9	23.8	4.07
	162		748	5.43	542	113.4	20.9	3.13
	163		749	5.41	542	98.0	18.1	2.35
60 ↓	164	55 ↓	743	4.40	542	121.6	27.6	4.68
	165		743	4.40	543	114.2	26.0	4.16
	166		744	4.40	543	105.0	23.9	3.52
	167		746	4.40	543	90.2	20.5	2.59
55 ↓	168	100 ↓	1158	6.61	550	161.2	24.4	4.62
	169		1140	6.66	550	146.1	21.9	3.68
	170		1128	6.68	550	128.3	19.2	2.81
	171		1116	6.67	550	107.9	16.2	2.00
56 ↓	172	85 ↓	1141	5.74	549	149.4	26.0	4.58
	173		1138	5.75	550	134.5	23.4	3.67
	174		1138	5.76	550	120.7	21.0	2.94
	175		1138	5.76	550	104.3	18.1	2.20
57 ↓	176	70 ↓	1141	4.81	549	133.4	27.7	4.41
	177		1146	4.80	548	120.5	25.1	3.58
	178		1148	4.76	548	110.7	23.3	3.06
	179		1154	4.77	549	96.4	20.2	2.33

Table 17
Jet Pump Test Results
Extended Constant Area Mixing Tube
LD#1 Nozzle Cluster
Case 3 Nozzles

Test No.	Run	P _{po} psia	T _{po} °F	W _p lbm/min	T _{so} °F	W _s lbm/min	m
61 ↓	228	100 ↓	1151	6.80	88	167.6	24.65
	229		1130	6.80	87	148.0	21.76
	230		1124	6.79	87	124.6	18.34
	231		1110	6.77	87	99.1	14.63
62 ↓	232	85 ↓	1161	5.82	86	156.3	26.86
	233		1159	5.81	81	143.7	24.74
	234		1154	5.80	83	121.6	20.96
	235		1153	5.80	85	98.3	16.95
	240		1159	5.73	92	150.4	26.25
	241		1149	5.76	93	152.1	26.40
63 ↓	236	70 ↓	1158	4.81	86	141.8	29.47
	237		1155	4.81	86	126.2	26.23
	238		1152	4.81	86	112.5	23.38
	239		1152	4.81	86	92.8	19.29

Table 18

Jet Pump Test Results
Short Constant Area Mixing Tube
LD#1 Nozzle Cluster
Case 3 Nozzles

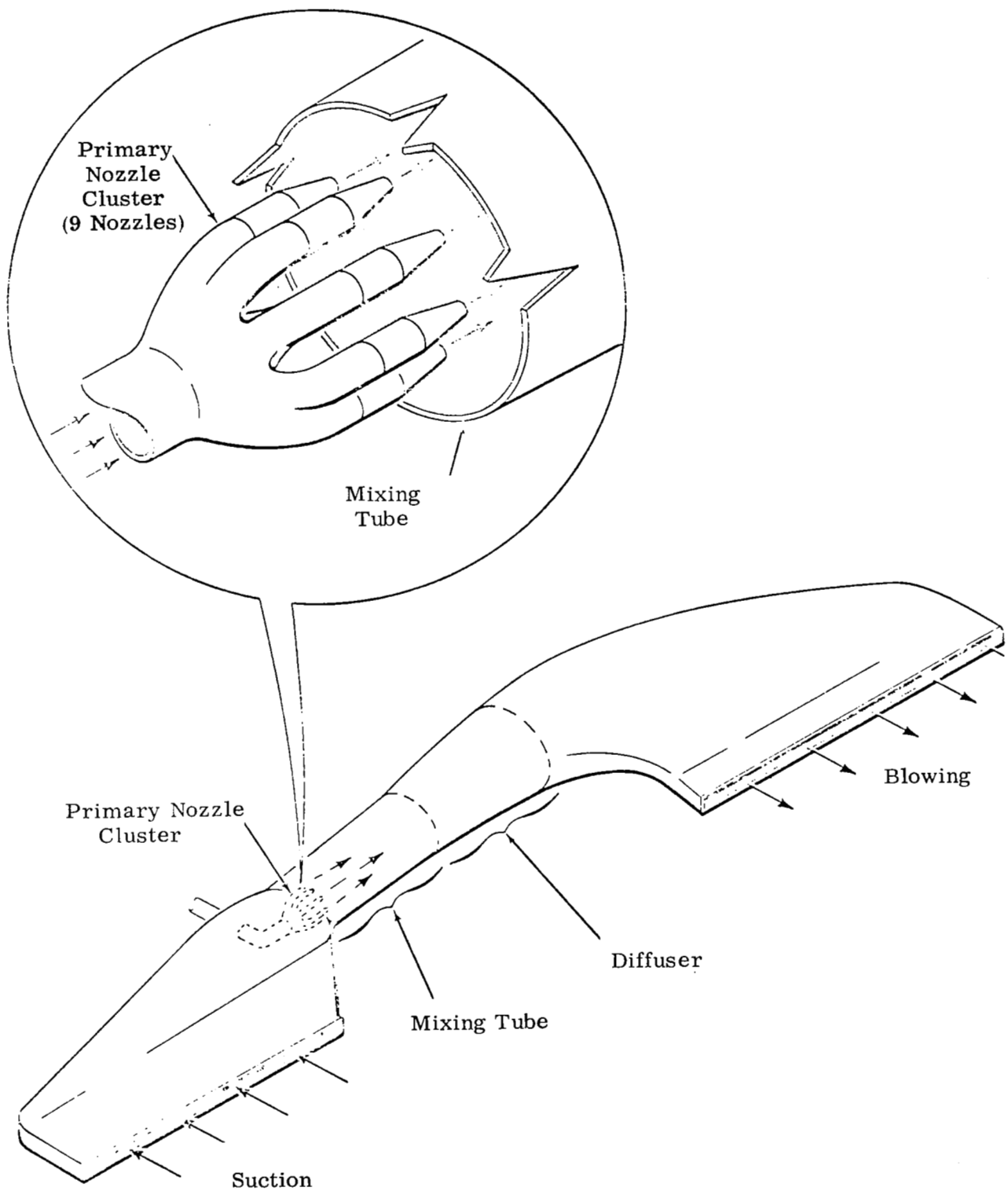


Figure 1
 BLC Jet Pump Duct Arrangement

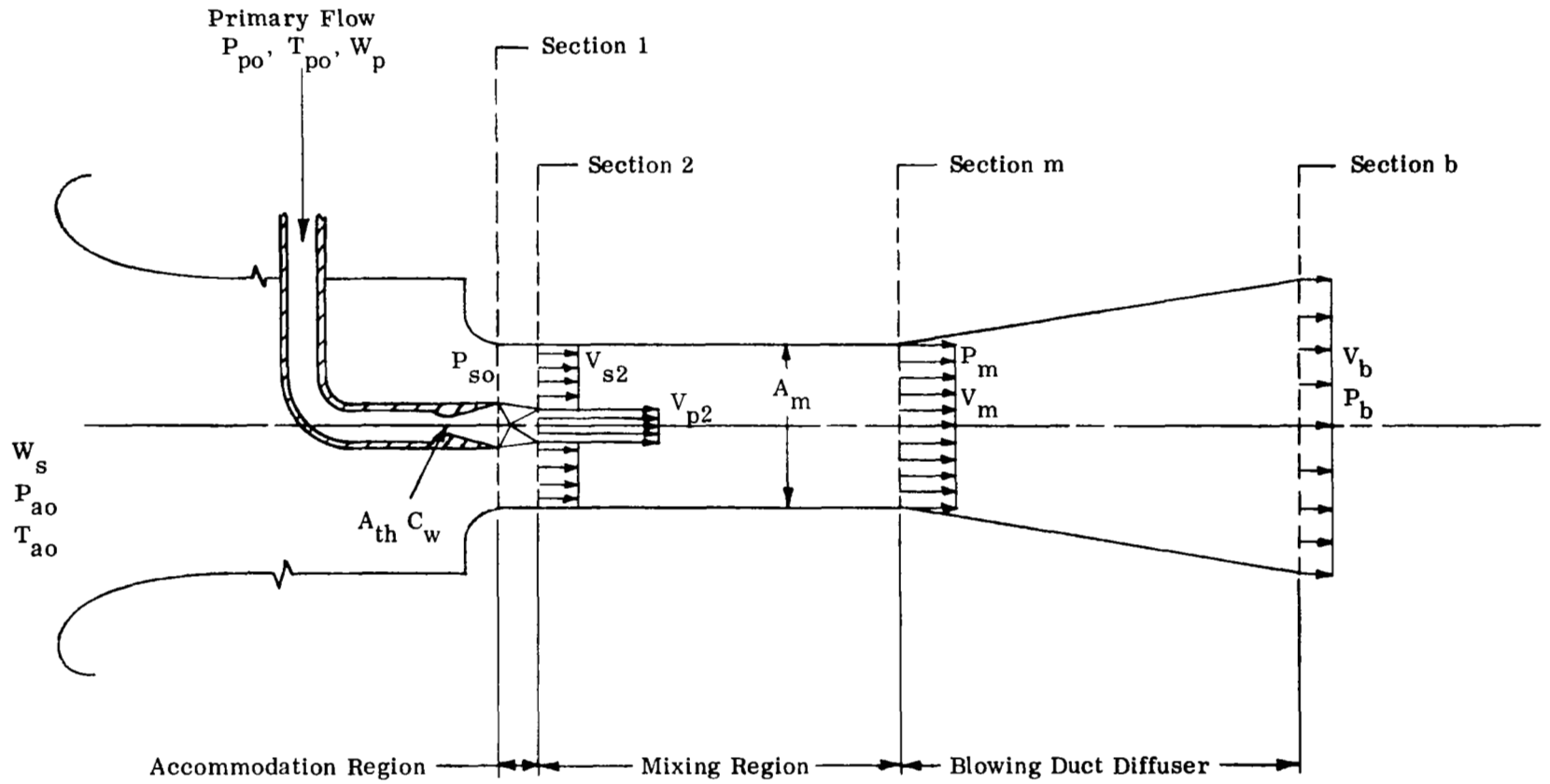


Figure 2
Jet Pump Definitions

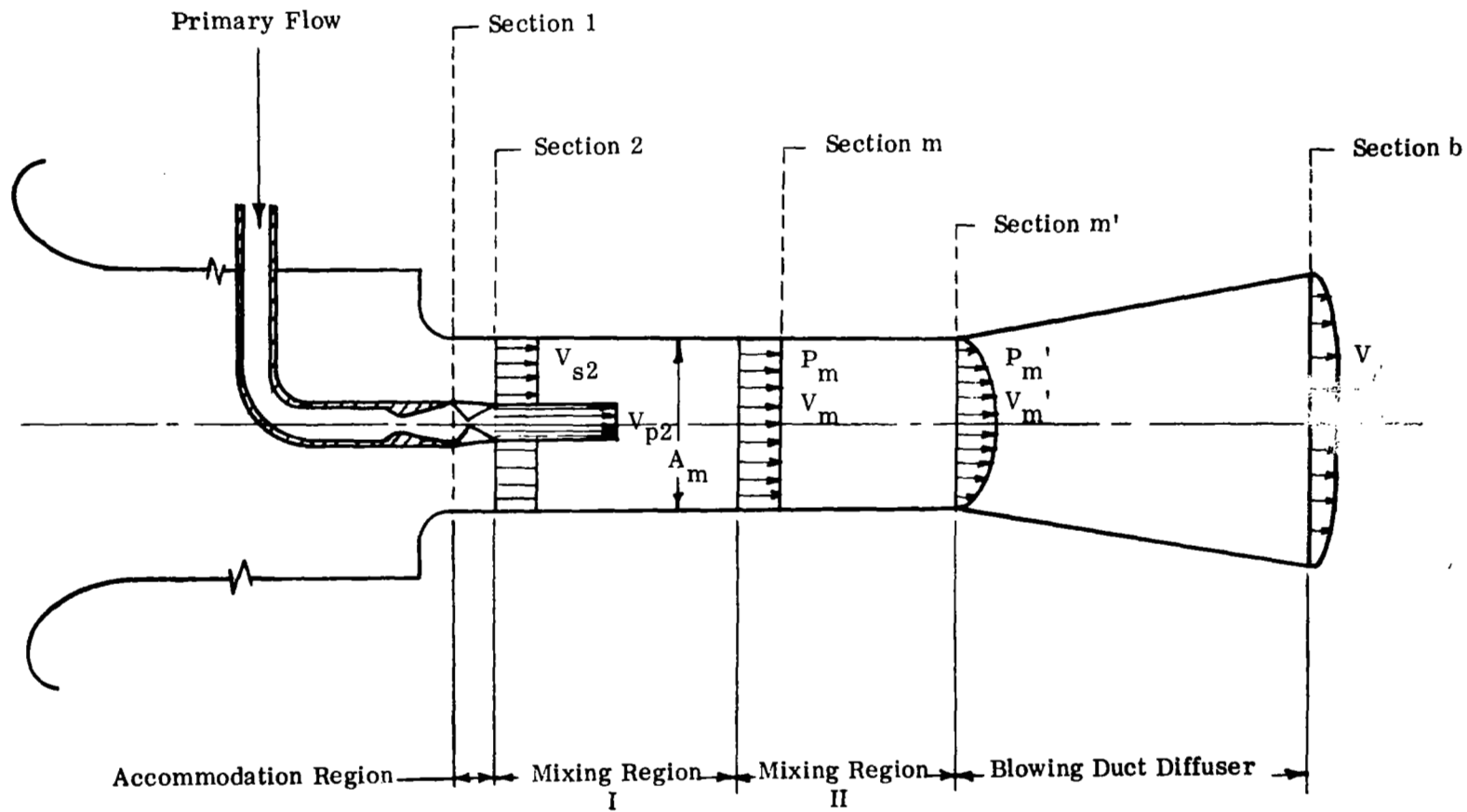


Figure 3

Mixing Tube Wall Friction Approximation

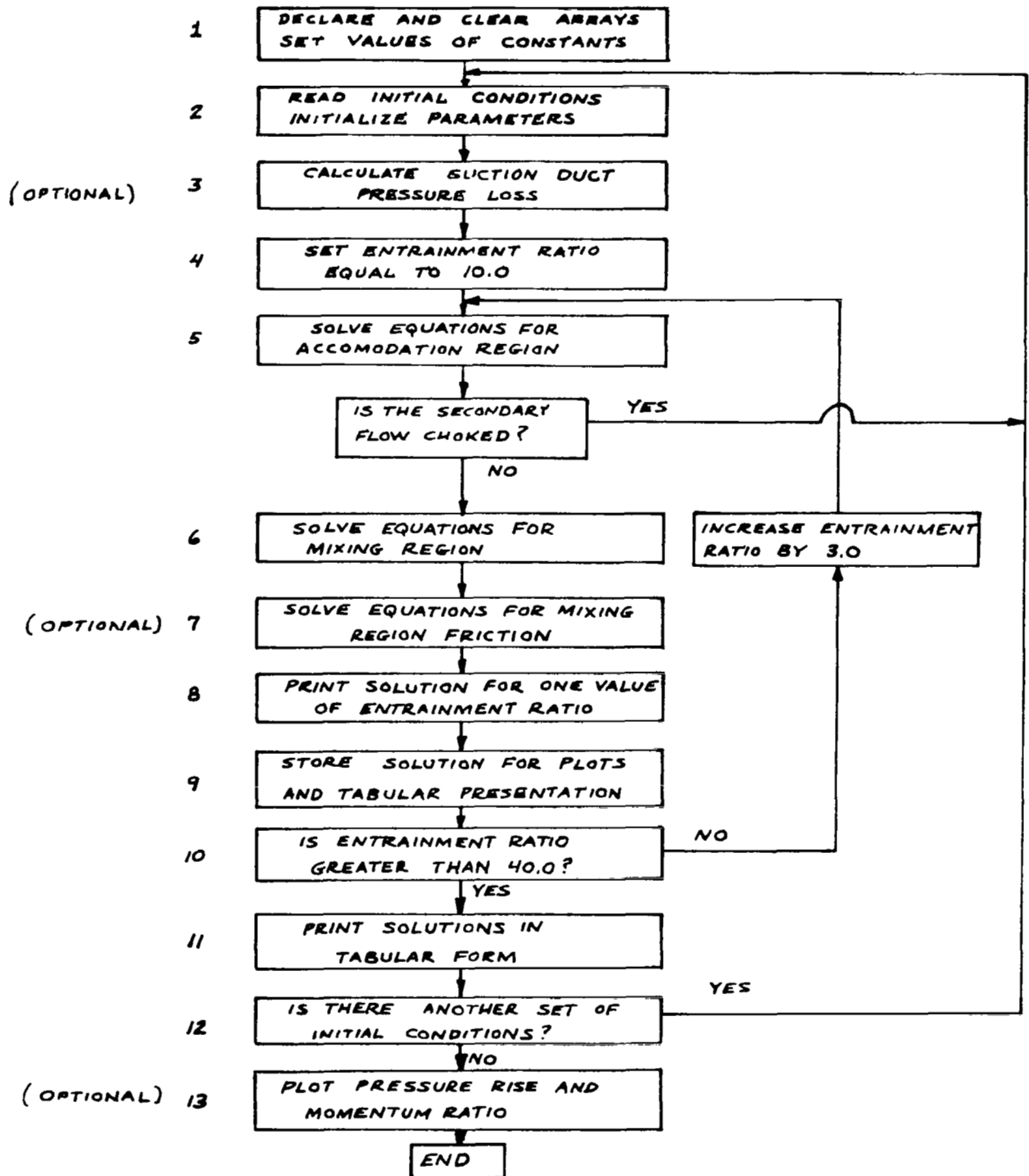
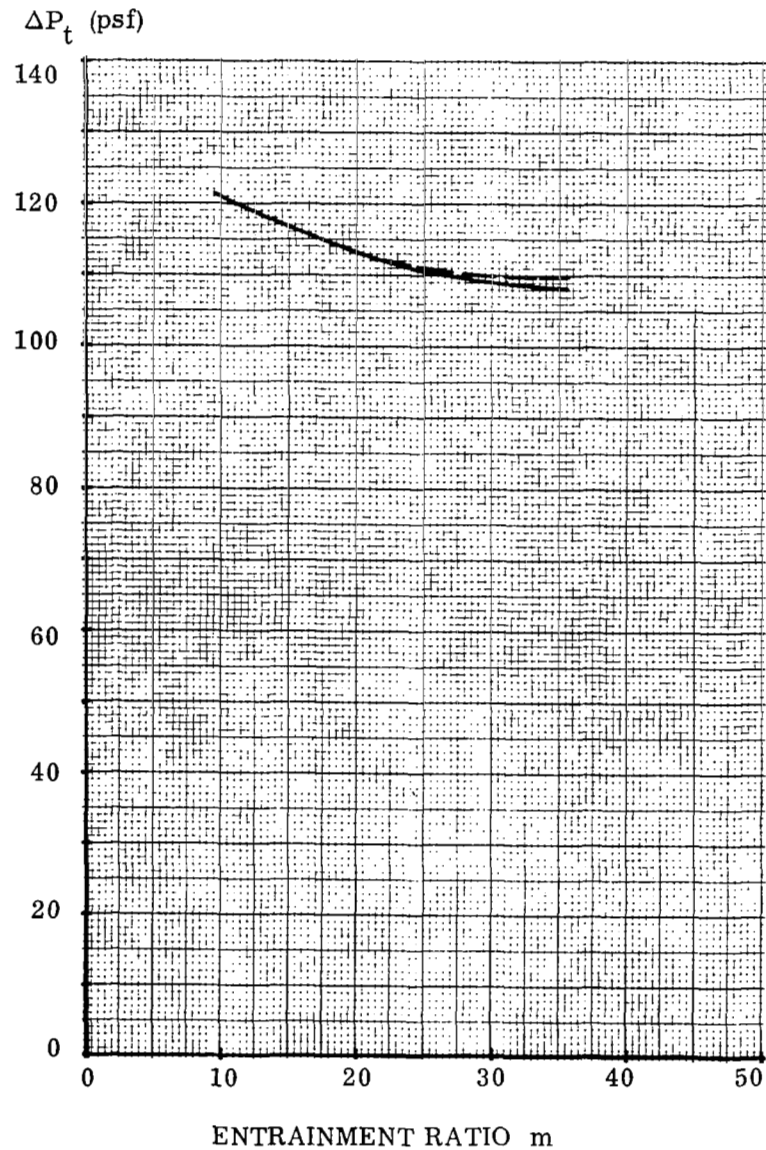


Figure 4

Block Diagram of the Computer Program



————— Constant C_p
 - - - - - C_p as a function of temperature

Solution Conditions

$T_{po} = 1200^\circ \text{ F}$	$T_{so} = 70^\circ \text{ F}$
$P_{po} = 350 \text{ psia}$	$P_{so} = 14.6 \text{ psia}$
$A_{th} = 0.000175 \text{ ft}^2$	$C_w = 0.935$
$A_m = 0.08726 \text{ ft}^2$	

Figure 5
Influence of the Constant Specific Heat Assumption

PUMP CHARACTERISTICS. PARAMETER IS PRESSURE RATIO

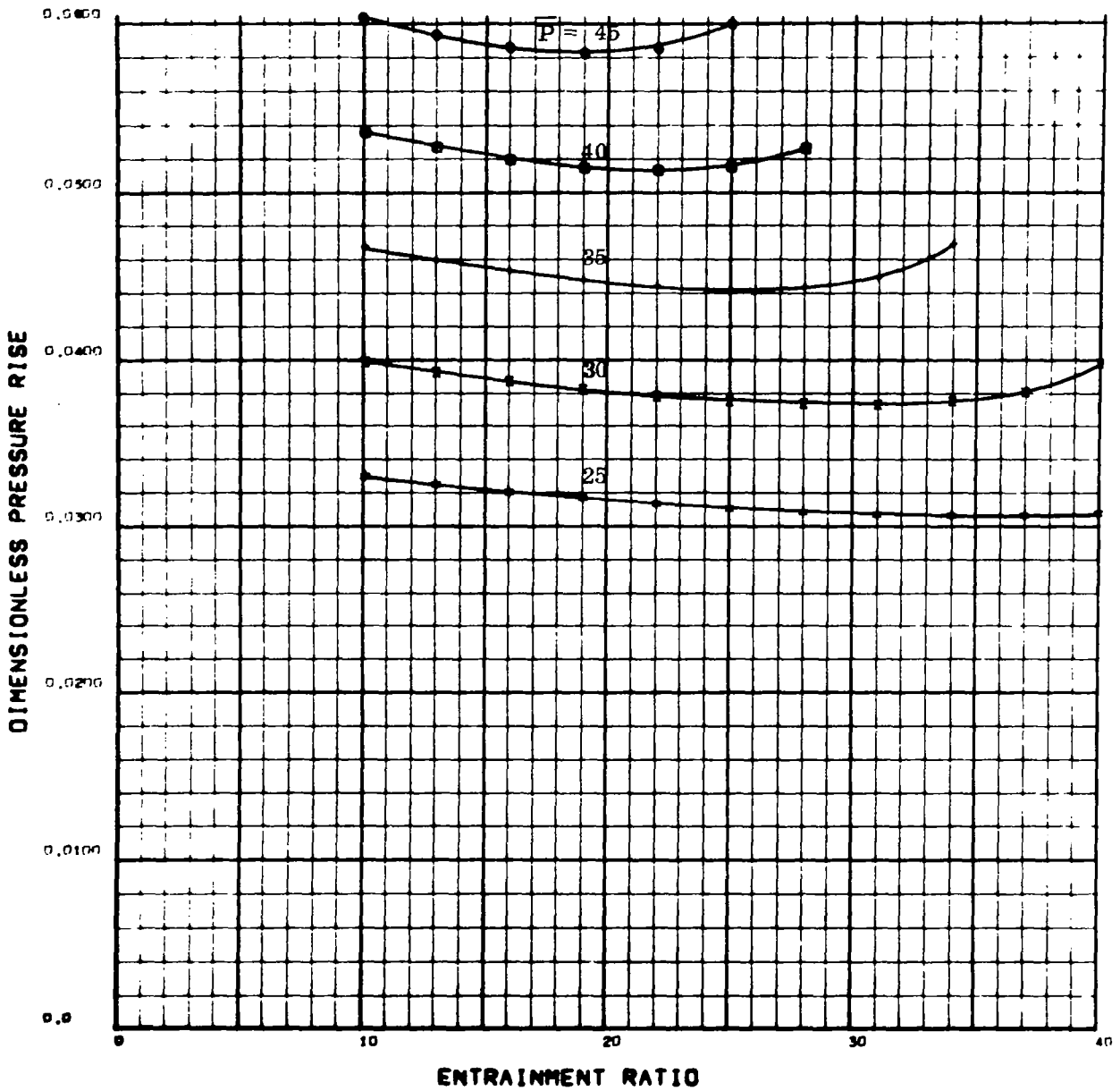


Figure 6

Jet Pump Performance Characteristics
 Dimensionless Pressure Rise (ΔP_t^*) vs. Entrainment Ratio

$$\bar{A} = 0.001$$

$$\bar{T} = 1.5$$

$$P = 25, 30, 35, 40, 45$$

MOMENTUM RATIO, PARAMETER IS PRESSURE RATIO

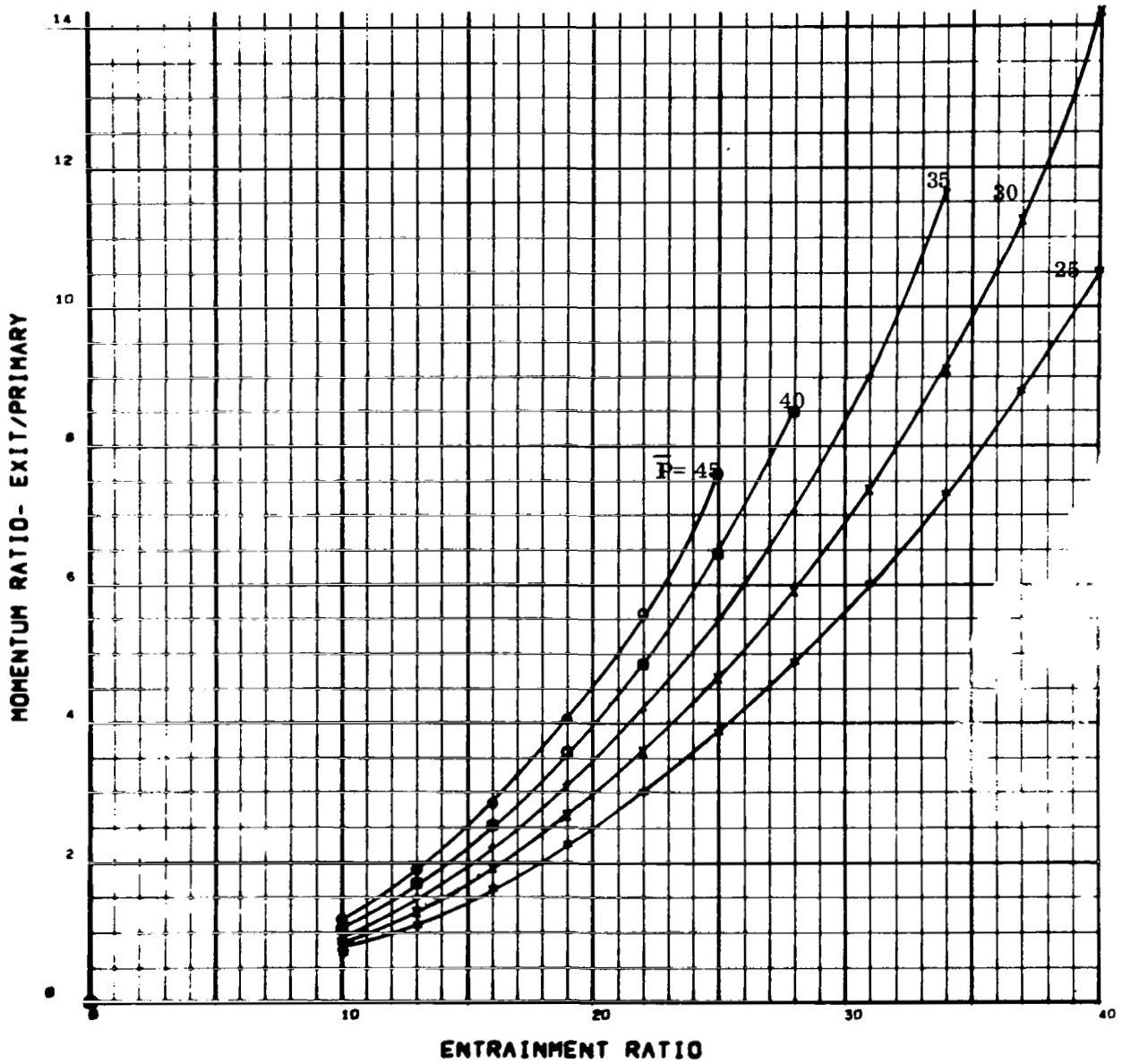


Figure 7

Jet Pump Performance Characteristics
Momentum Augmentation (τ) vs. Entrainment Ratio

$$\bar{A} = 0.001$$

$$\bar{T} = 1.5$$

$$\bar{P} = 25, 30, 35, 40, 45$$

PUMP CHARACTERISTICS. PARAMETER IS PRESSURE RATIO

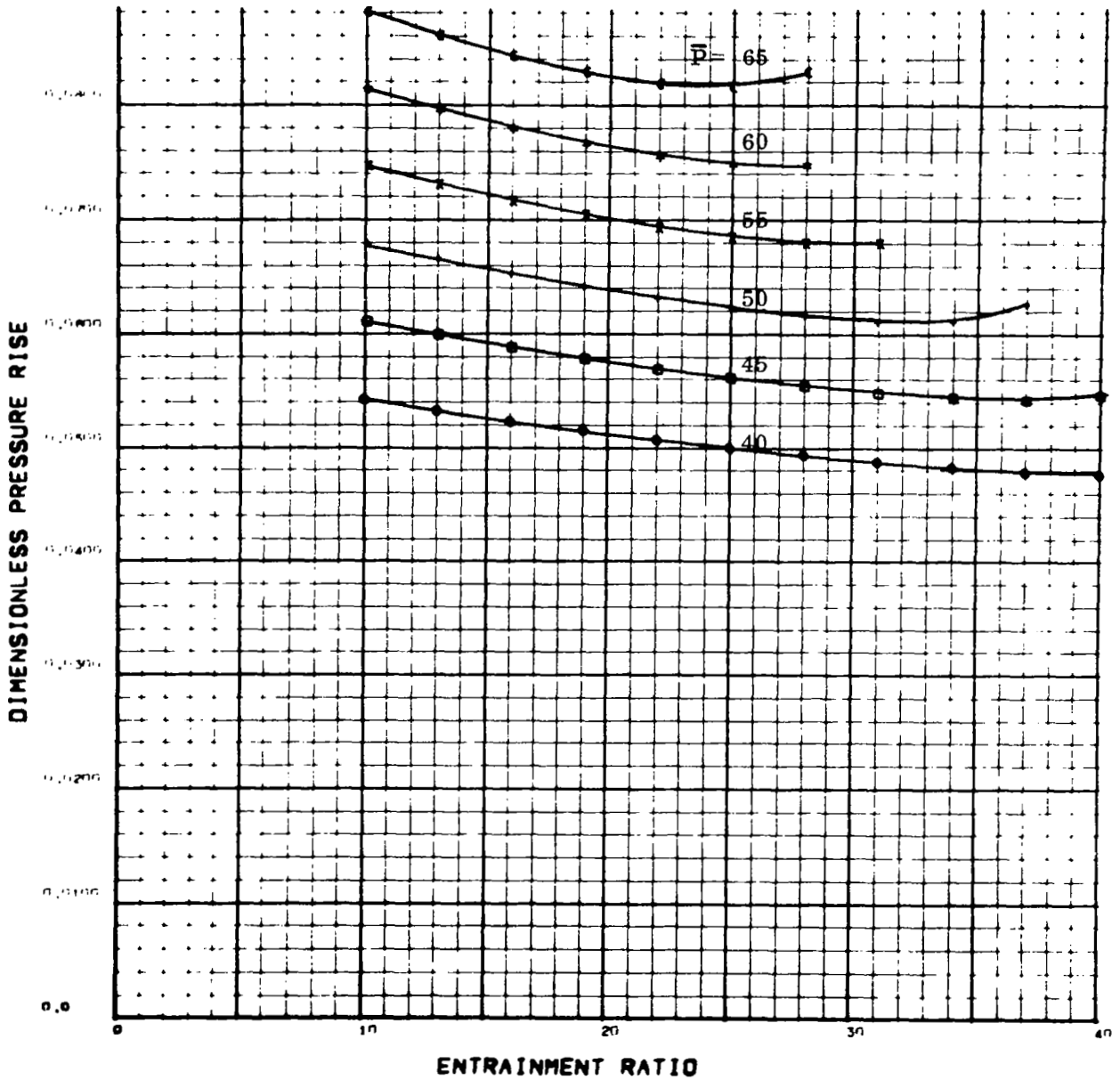


Figure 8
 Jet Pump Performance Characteristics
 Dimensionless Pressure Rise (ΔP_t^*) vs. Entrainment Ratio

$\bar{A} = 0.001$

$\bar{T} = 3.5$

$\bar{P} = 40, 45, 50, 55, 60, 65$

MOMENTUM RATIO. PARAMETER IS PRESSURE RATIO

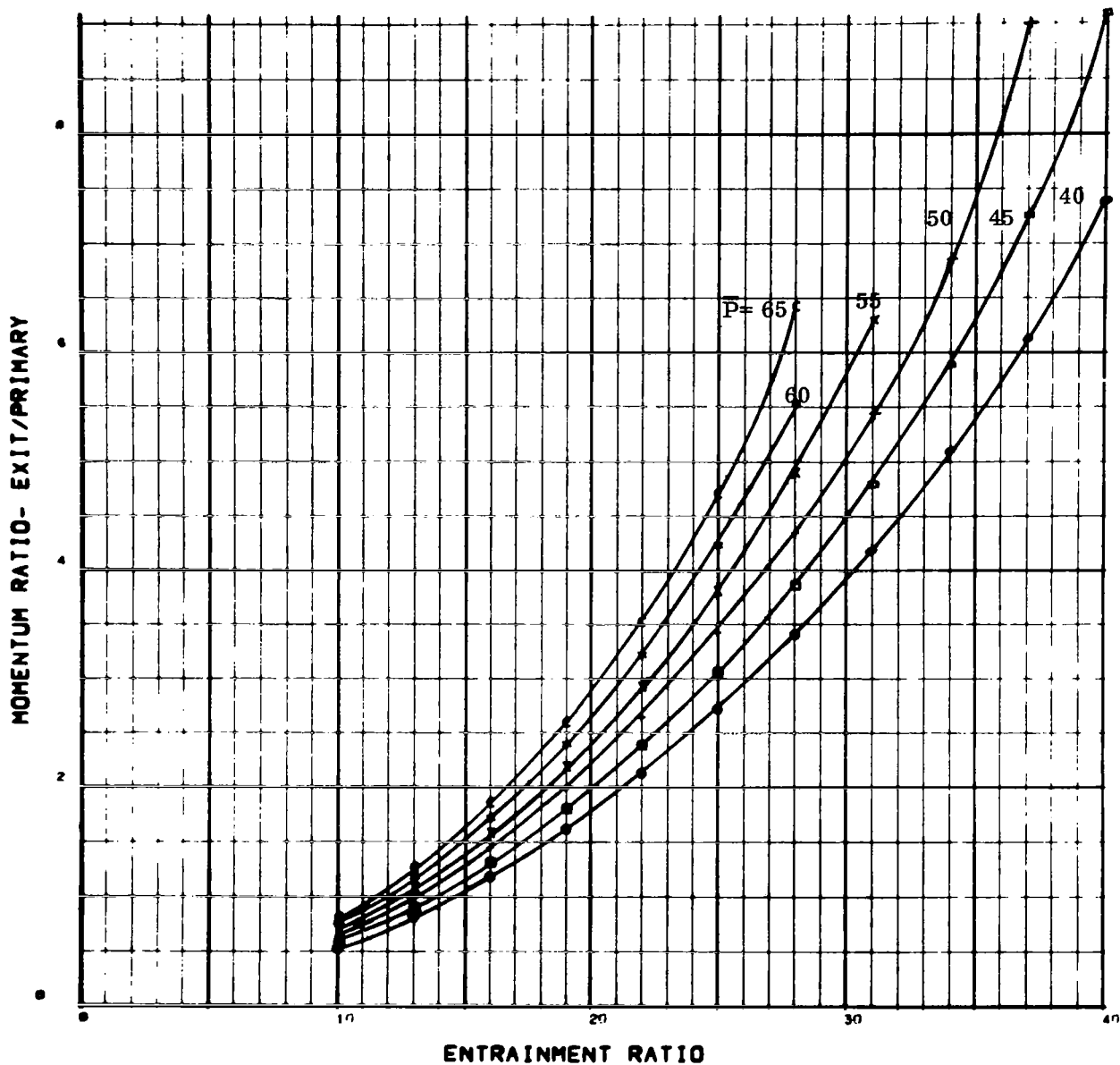


Figure 9
 Jet Pump Performance Characteristics
 Momentum Augmentation (τ) vs. Entrainment Ratio

$\bar{A} = 0.001$
 $\bar{T} = 3.5$
 $\bar{P} = 40, 45, 50, 55, 60, 65$

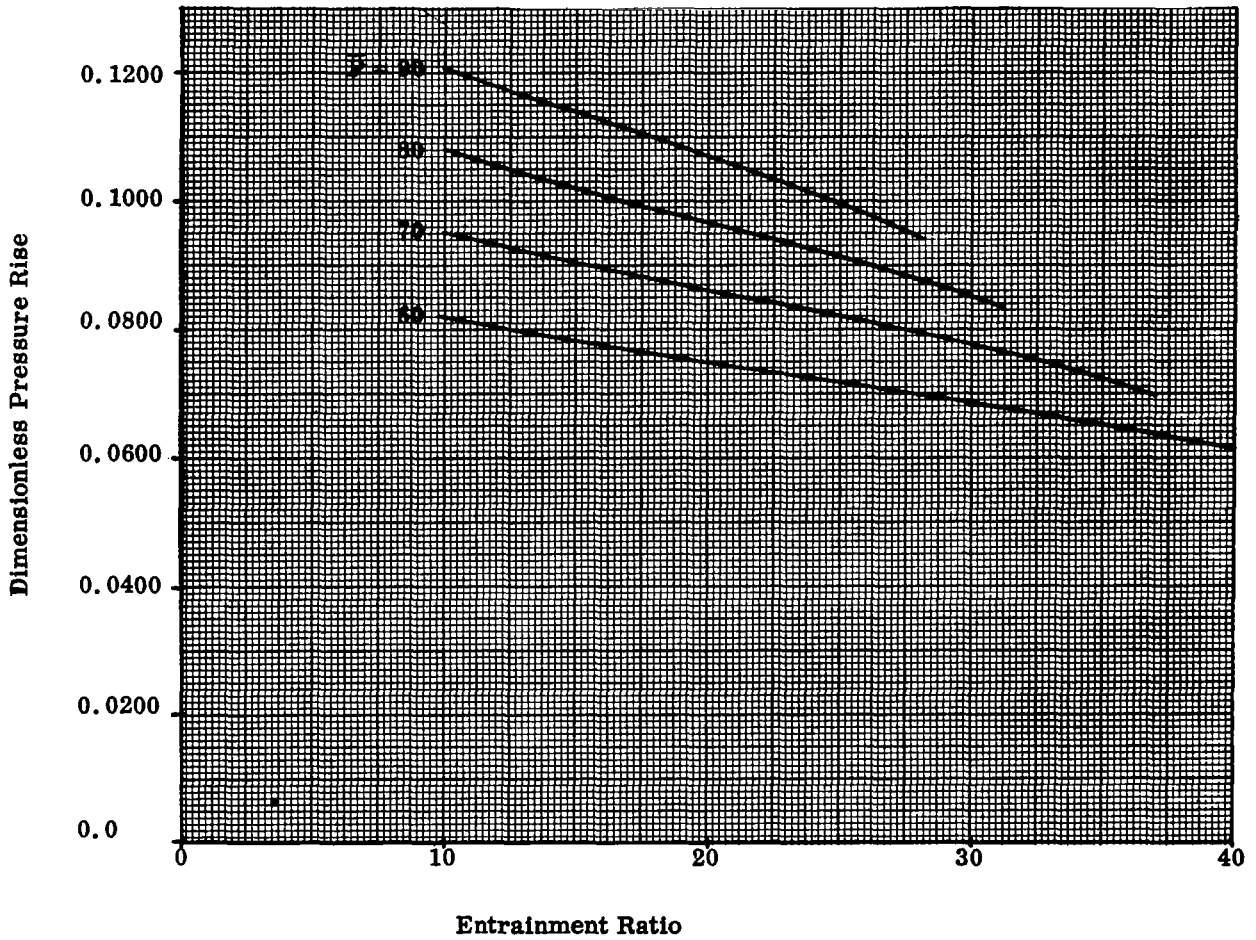


Figure 10
 Jet Pump Performance Characteristics
 Dimensionless Pressure Rise (ΔP_t^*) vs. Entrainment Ratio
 $\bar{A} = 0.001$
 $\bar{T} = 8.0$
 $\bar{P} = 60, 70, 80, 90$

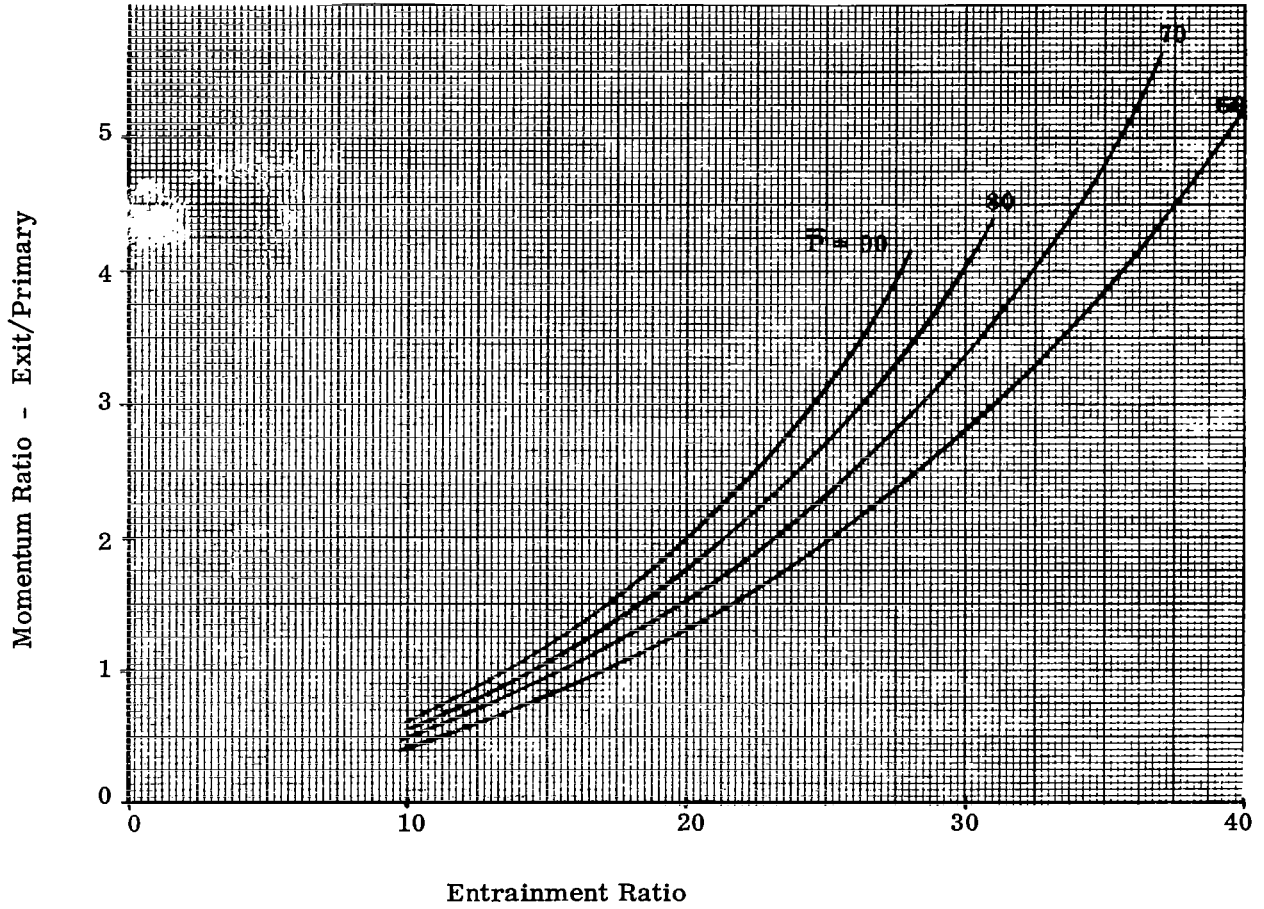


Figure 11
 Jet Pump Performance Characteristics

Momentum Augmentation (τ) vs. Entrainment Ratio

$$\bar{A} = 0.001$$

$$\bar{T} = 8.0$$

$$\bar{P} = 60, 70, 80, 90$$

PUMP CHARACTERISTICS. PARAMETER IS PRESSURE RATIO

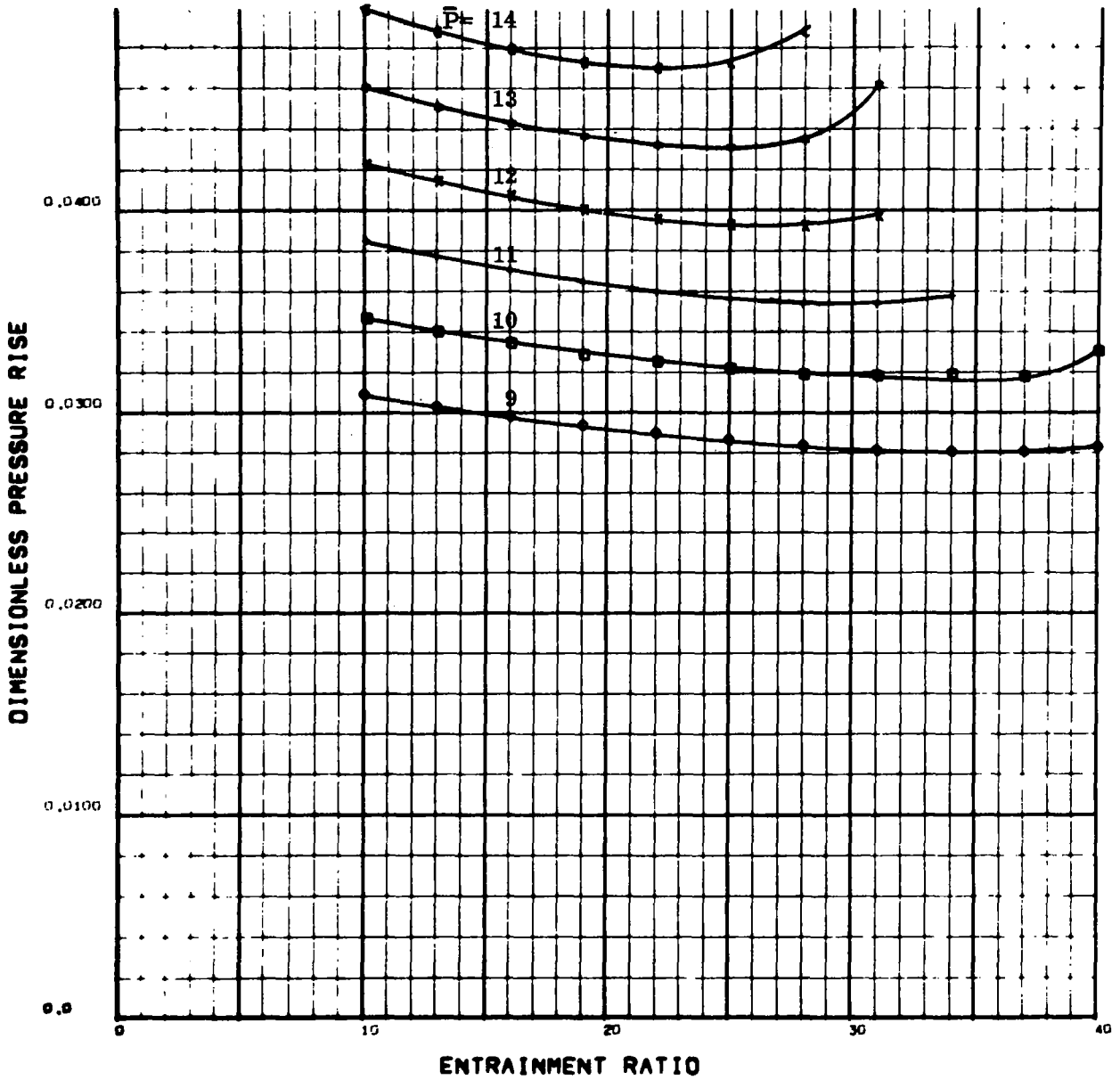


Figure 12

Jet Pump Performance Characteristics
 Dimensionless Pressure Rise (ΔP_t^*) vs. Entrainment Ratio

$$\bar{A} = 0.003$$

$$\bar{T} = 1.5$$

$$\bar{P} = 9, 10, 11, 12, 13, 14$$

MOMENTUM RATIO, PARAMETER IS PRESSURE RATIO

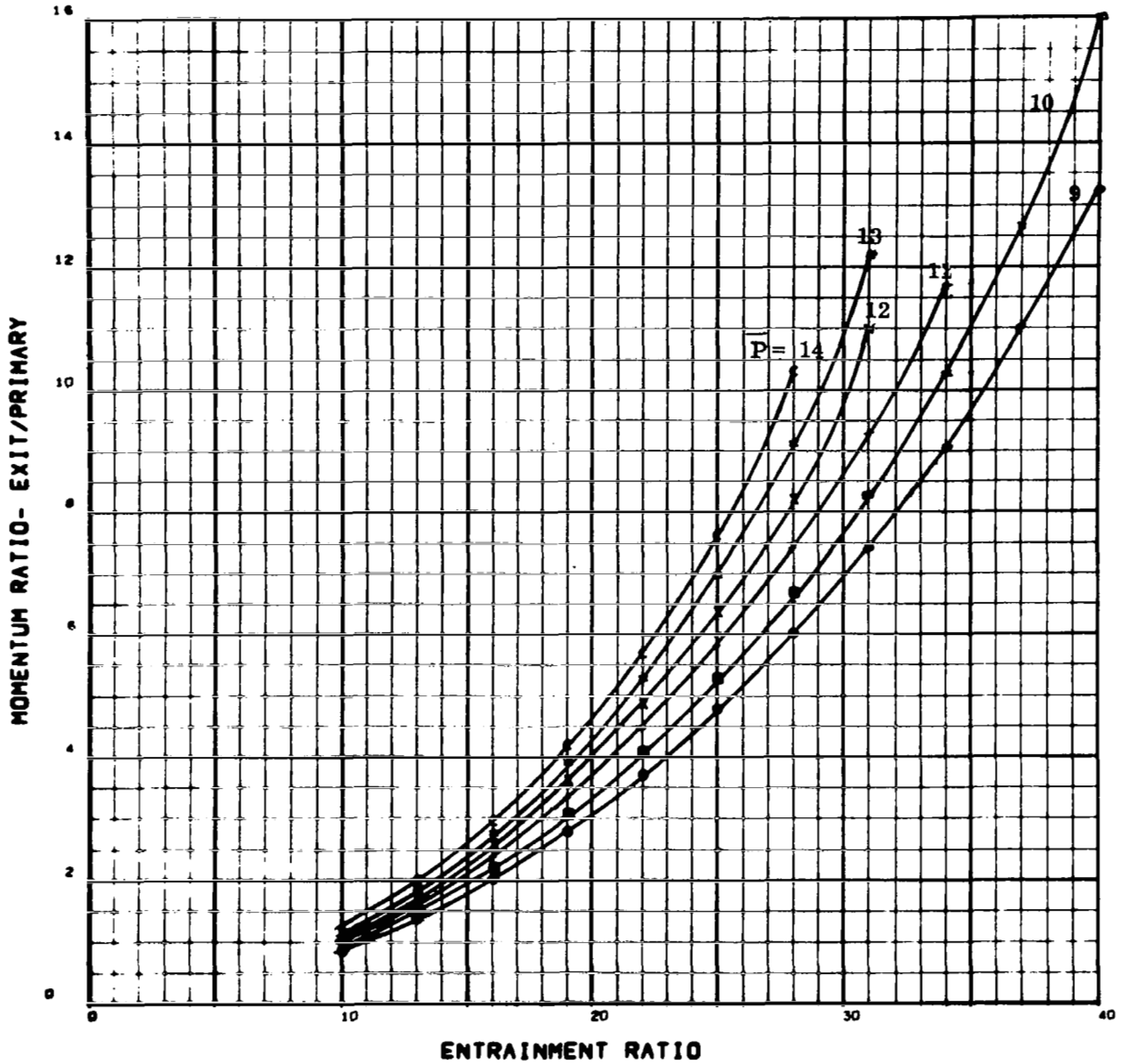


Figure 13

Jet Pump Performance Characteristics
Momentum Augmentation (τ) vs. Entrainment Ratio

$$\frac{\bar{A}}{\bar{T}} = 0.003$$

$$\frac{\bar{T}}{\bar{P}} = 1.5$$

$$\bar{P} = 9, 10, 11, 12, 13, 14$$

PUMP CHARACTERISTICS. PARAMETER IS PRESSURE RATIO

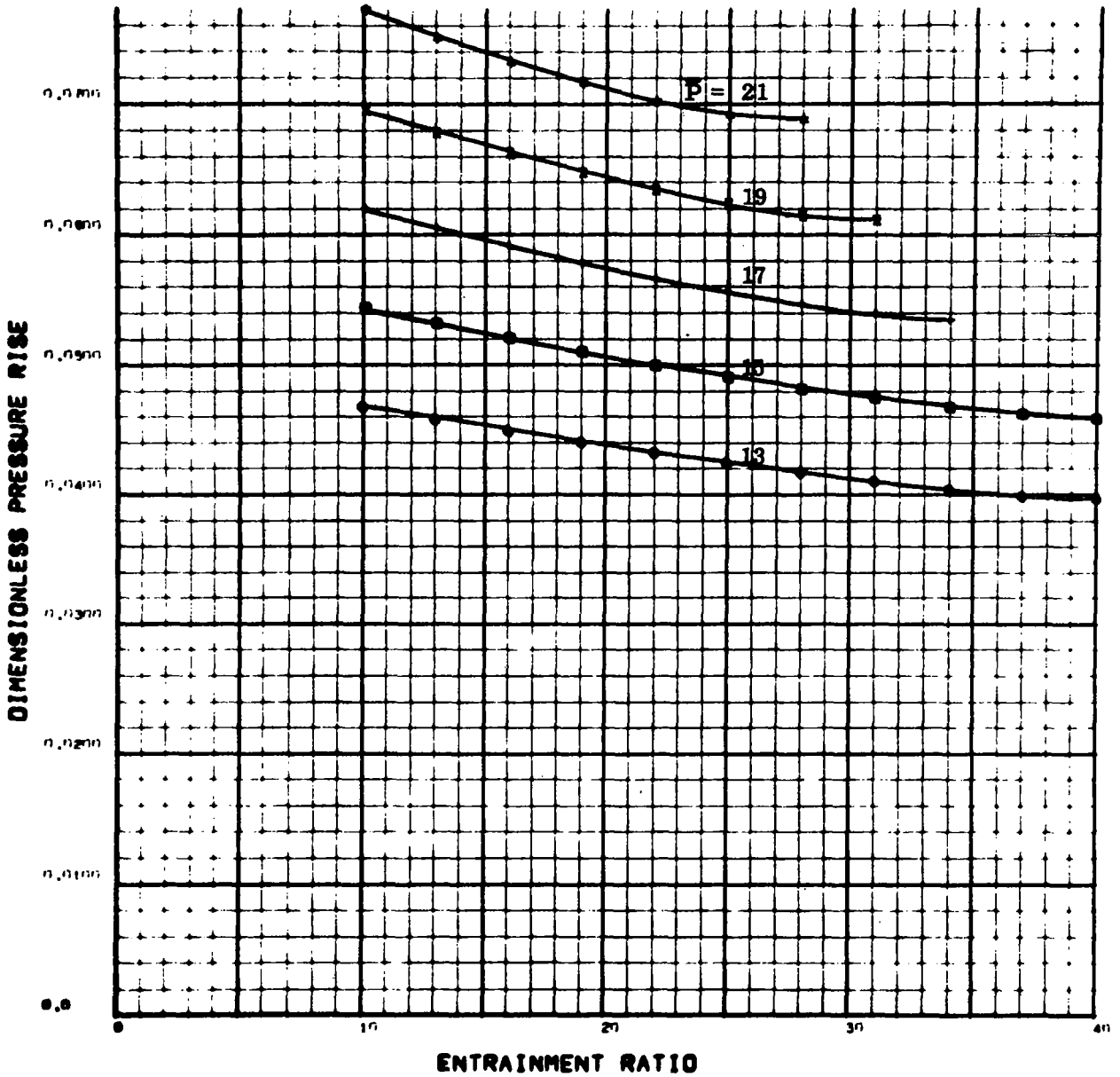


Figure 14

Jet Pump Performance Characteristics
 Dimensionless Pressure Rise (ΔP_t^*) vs. Entrainment Ratio

$$\begin{aligned} \bar{A} &= 0.003 \\ \bar{T} &= 3.5 \\ \bar{P} &= 13, 15, 17, 19, 21 \end{aligned}$$

MOMENTUM RATIO. PARAMETER IS PRESSURE RATIO

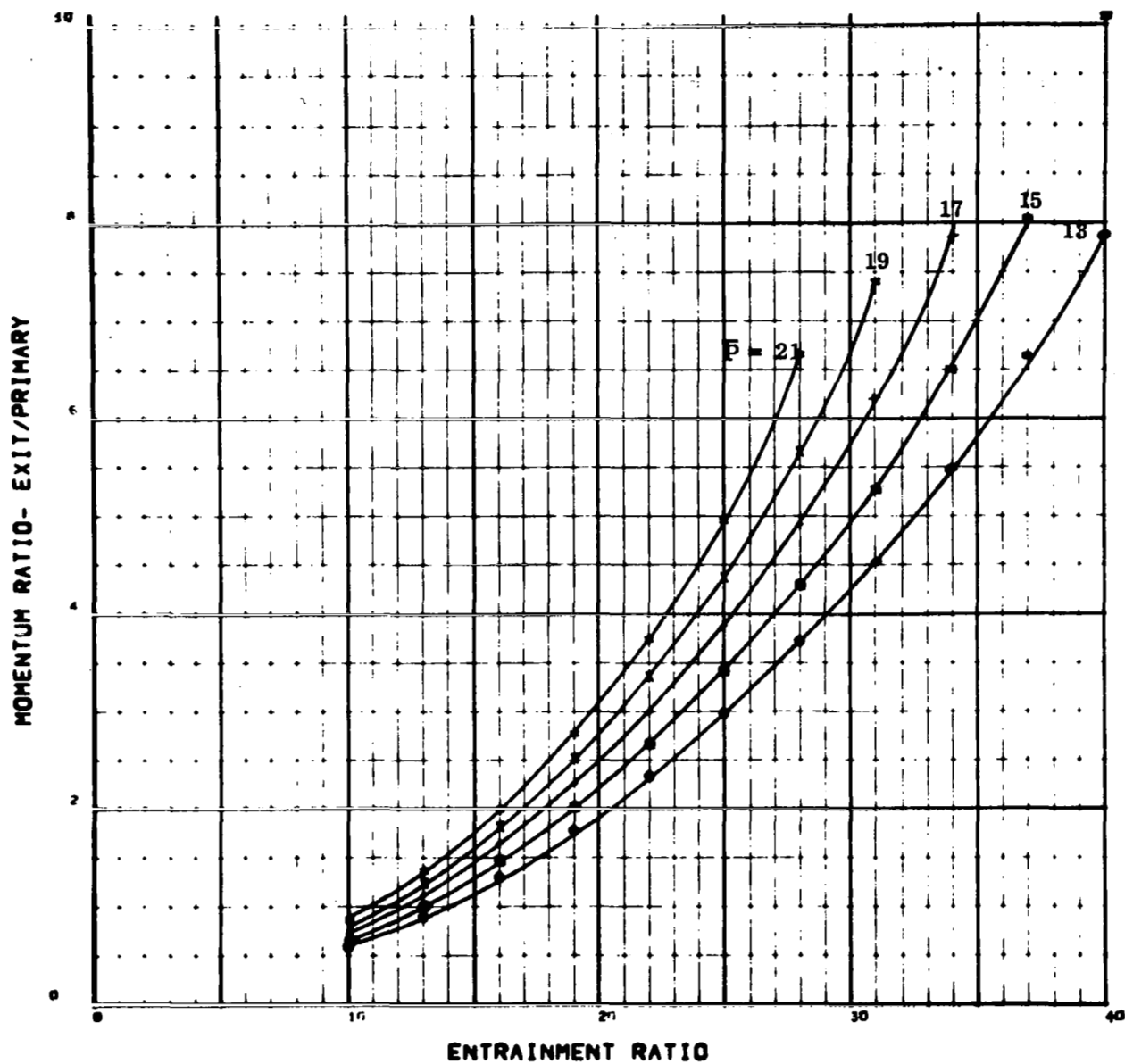


Figure 15
 Jet Pump Performance Characteristics
 Momentum Augmentation (τ) vs. Entrainment Ratio

$\bar{A} = 0.003$
 $\bar{T} = 3.5$
 $\bar{P} = 13, 15, 17, 19, 21$

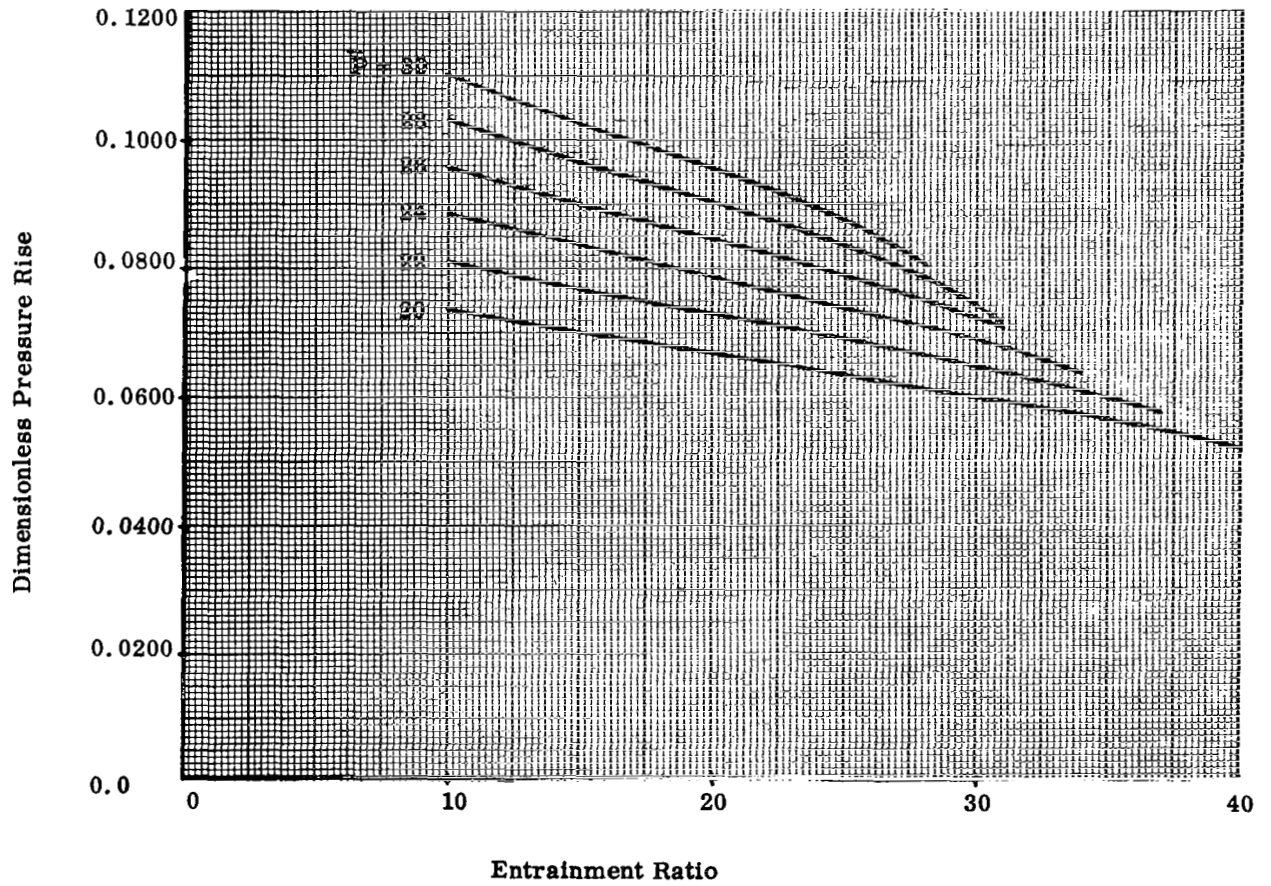


Figure 16
 Jet Pump Performance Characteristics
 Dimensionless Pressure Rise (ΔP_t^*) vs. Entrainment Ratio

$$\bar{A} = 0.003$$

$$\bar{T} = 8.0$$

$$\bar{P} = 20, 22, 24, 26, 28, 30$$

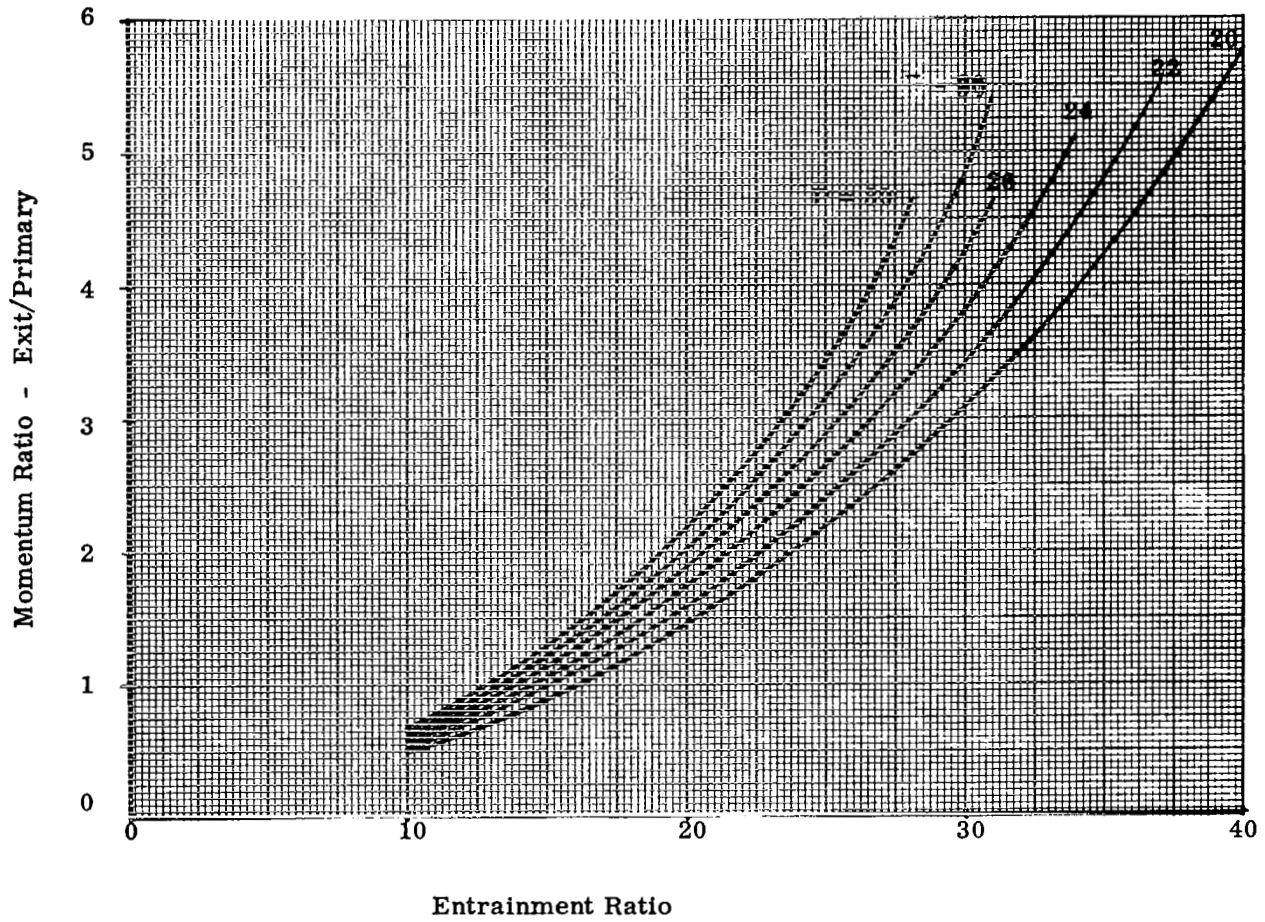


Figure 17
 Jet Pump Performance Characteristics

Momentum Augmentation (τ) vs. Entrainment Ratio

$$\bar{A} = 0.003$$

$$\bar{T} = 8.0$$

$$\bar{P} = 20, 22, 24, 26, 28, 30$$

PUMP CHARACTERISTICS. PARAMETER IS PRESSURE RATIO

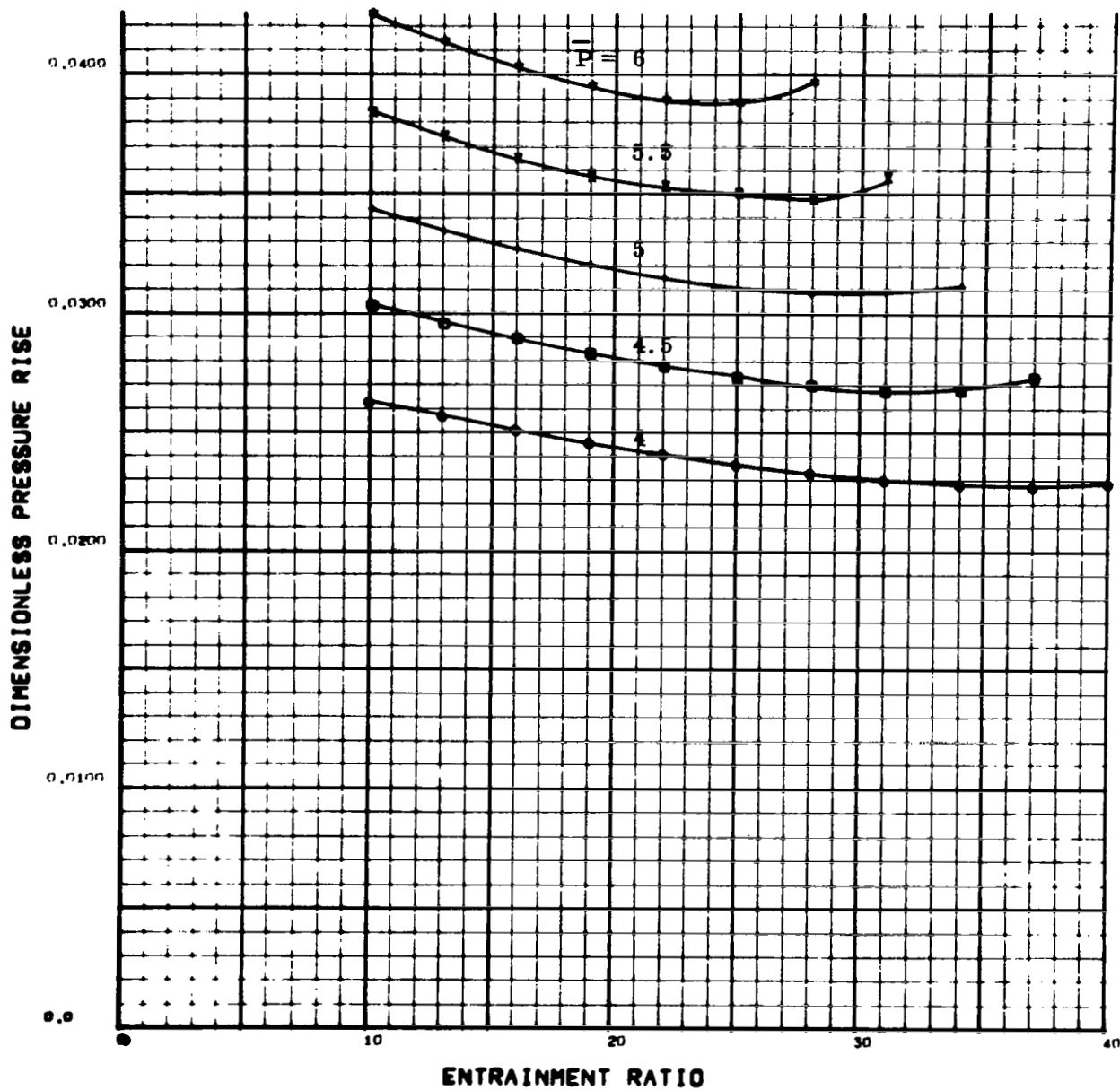


Figure 18

Jet Pump Performance Characteristics
Dimensionless Pressure Rise (ΔP_t^*) vs. Entrainment Ratio

$$\bar{A} = 0.007$$

$$\bar{T} = 1.5$$

$$\bar{P} = 4, 4.5, 5, 5.5, 6$$

MOMENTUM RATIO. PARAMETER IS PRESSURE RATIO

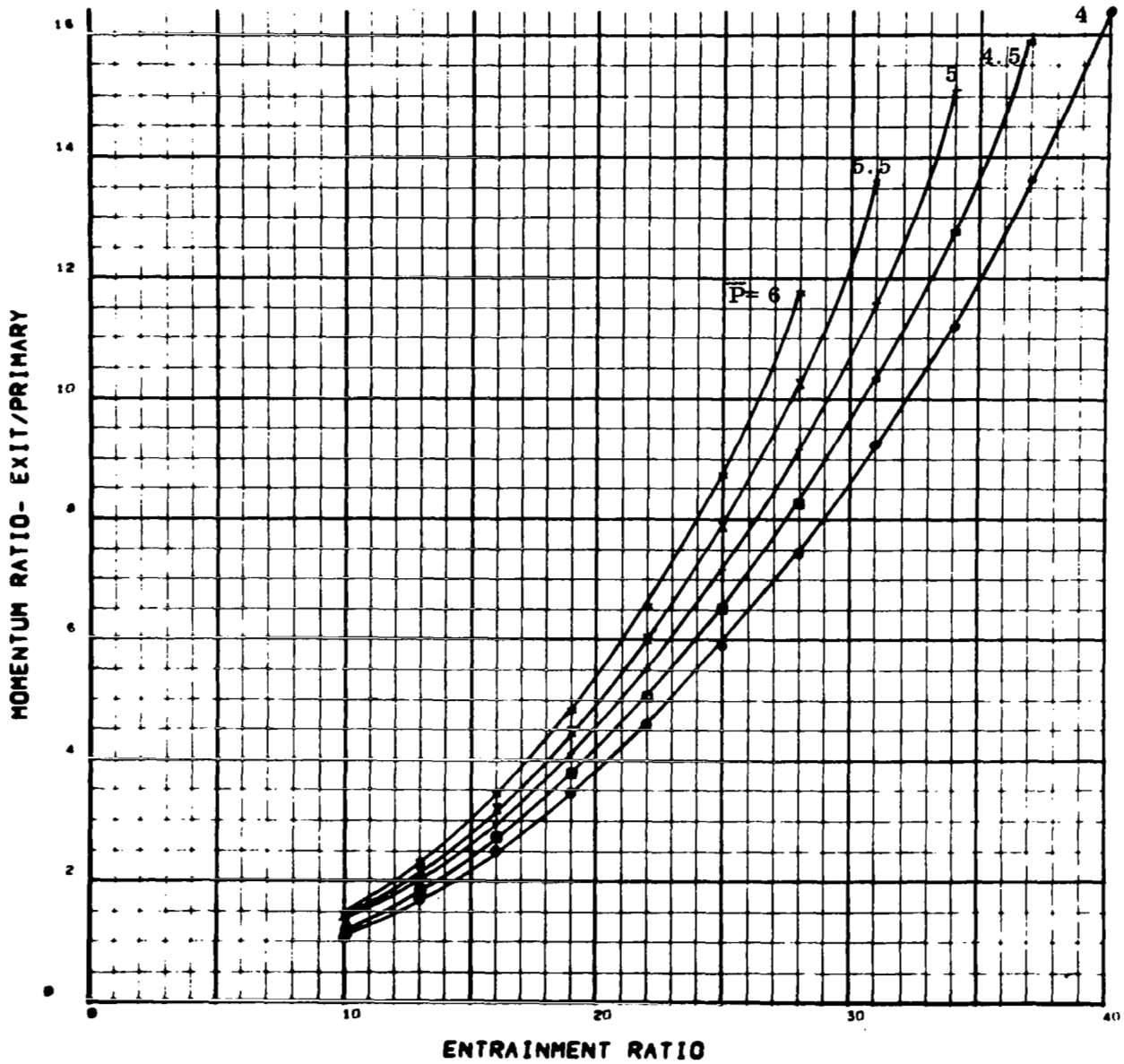


Figure 19

Jet Pump Performance Characteristics
Momentum Augmentation (τ) vs. Entrainment Ratio

$$\frac{A}{P} = 0.007$$

$$\frac{T}{P} = 1.5$$

$$P = 4, 4.5, 5, 5.5, 6$$

PUMP CHARACTERISTICS. PARAMETER IS PRESSURE RATIO

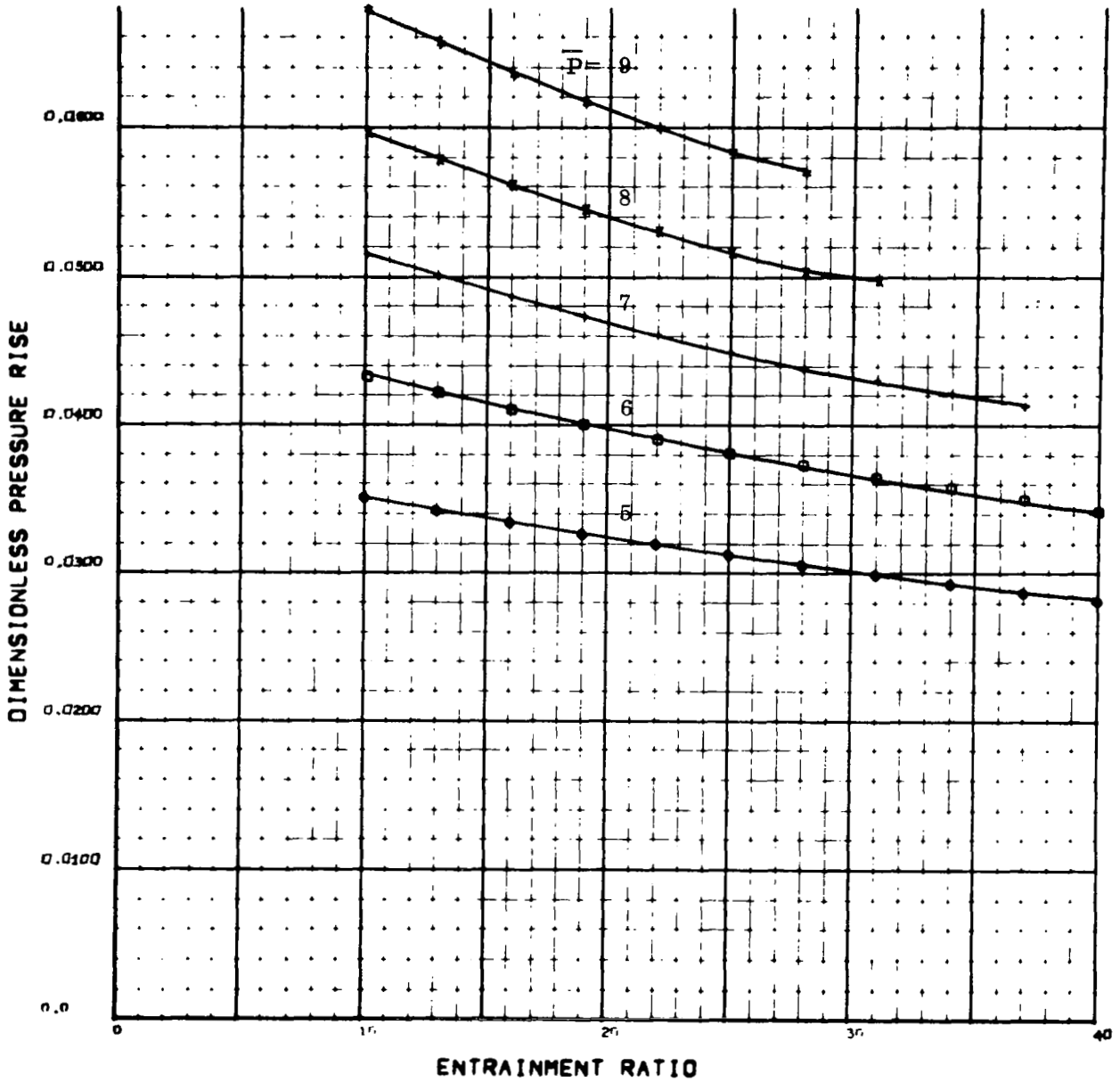


Figure 20

Jet Pump Performance Characteristics
 Dimensionless Pressure Rise (ΔP_t^*) vs. Entrainment Ratio

$\bar{A} = 0.007$
 $\bar{T} = 3.5$
 $\bar{P} = 5, 6, 7, 8, 9$

MOMENTUM RATIO. PARAMETER IS PRESSURE RATIO

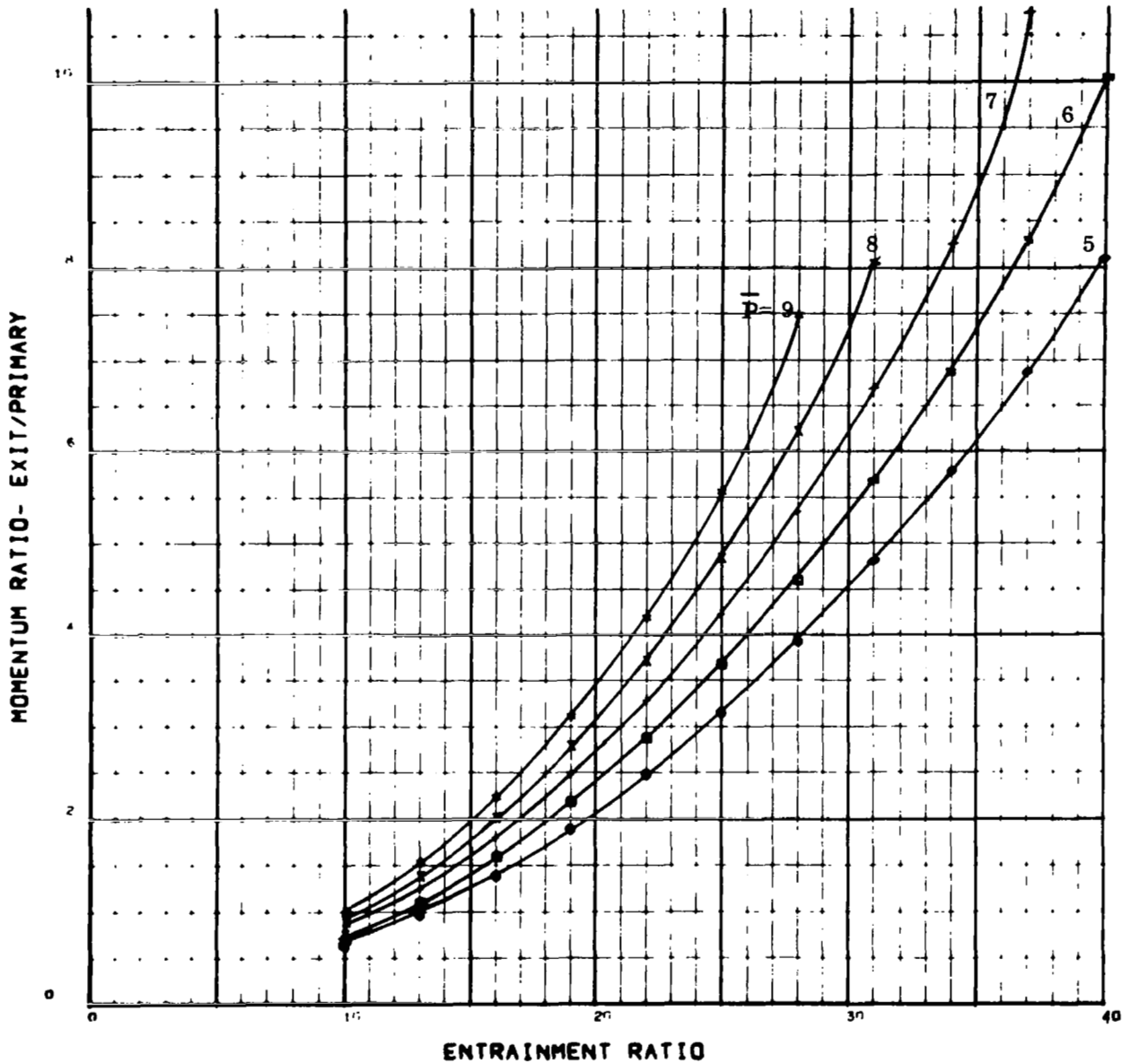


Figure 21

Jet Pump Performance Characteristics
Momentum Augmentation (τ) vs. Entrainment Ratio

$$\bar{A} = 0.007$$

$$\bar{T} = 3.5$$

$$\bar{P} = 5, 6, 7, 8, 9$$

PUMP CHARACTERISTICS. PARAMETER IS PRESSURE RATIO

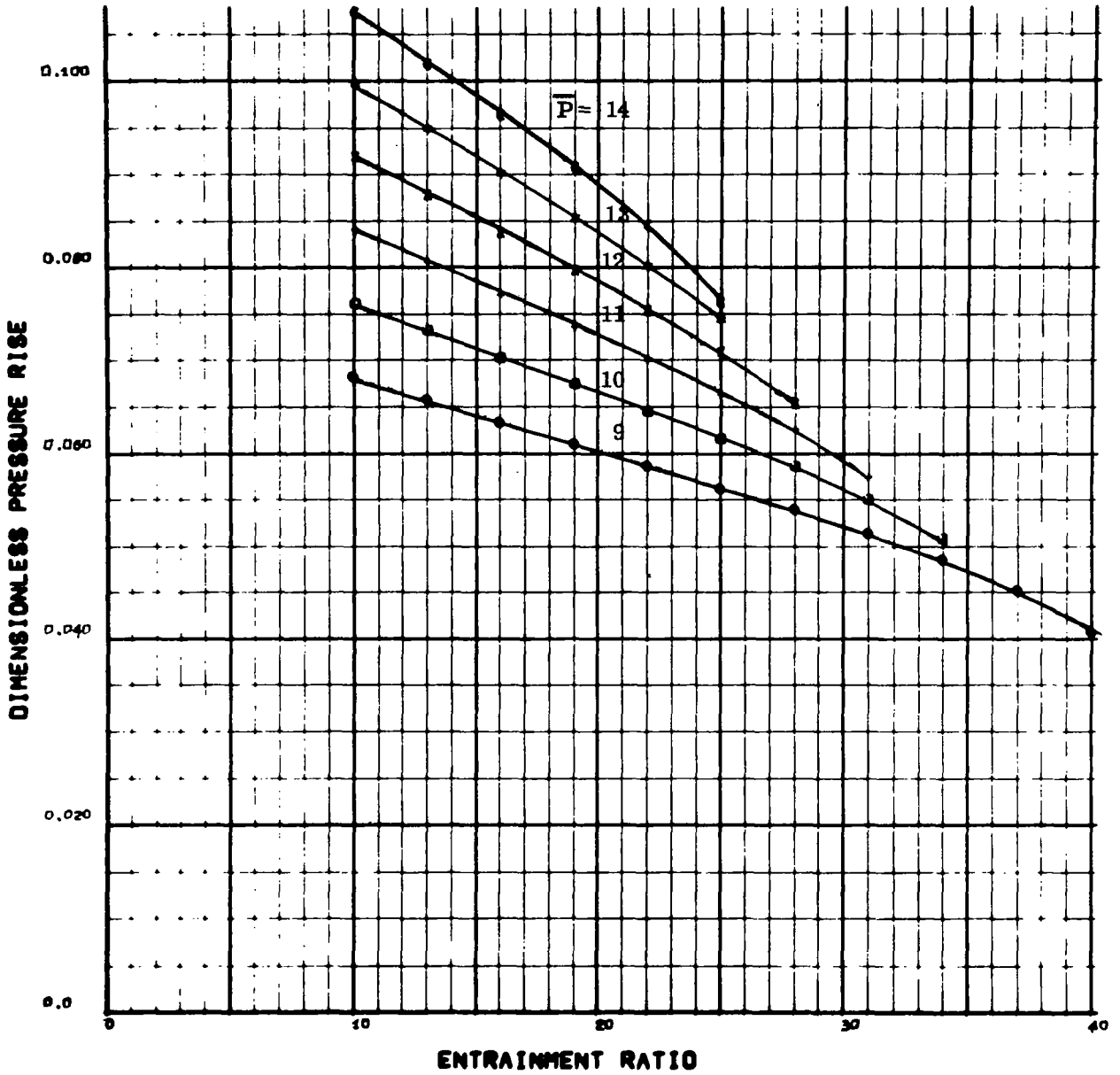


Figure 22

Jet Pump Performance Characteristics
 Dimensionless Pressure Rise (ΔP_t^*) vs. Entrainment Ratio

$\bar{A} = 0.007$

$\bar{T} = 8.0$

$\bar{P} = 9, 10, 11, 12, 13, 14$

MOMENTUM RATIO. PARAMETER IS PRESSURE RATIO

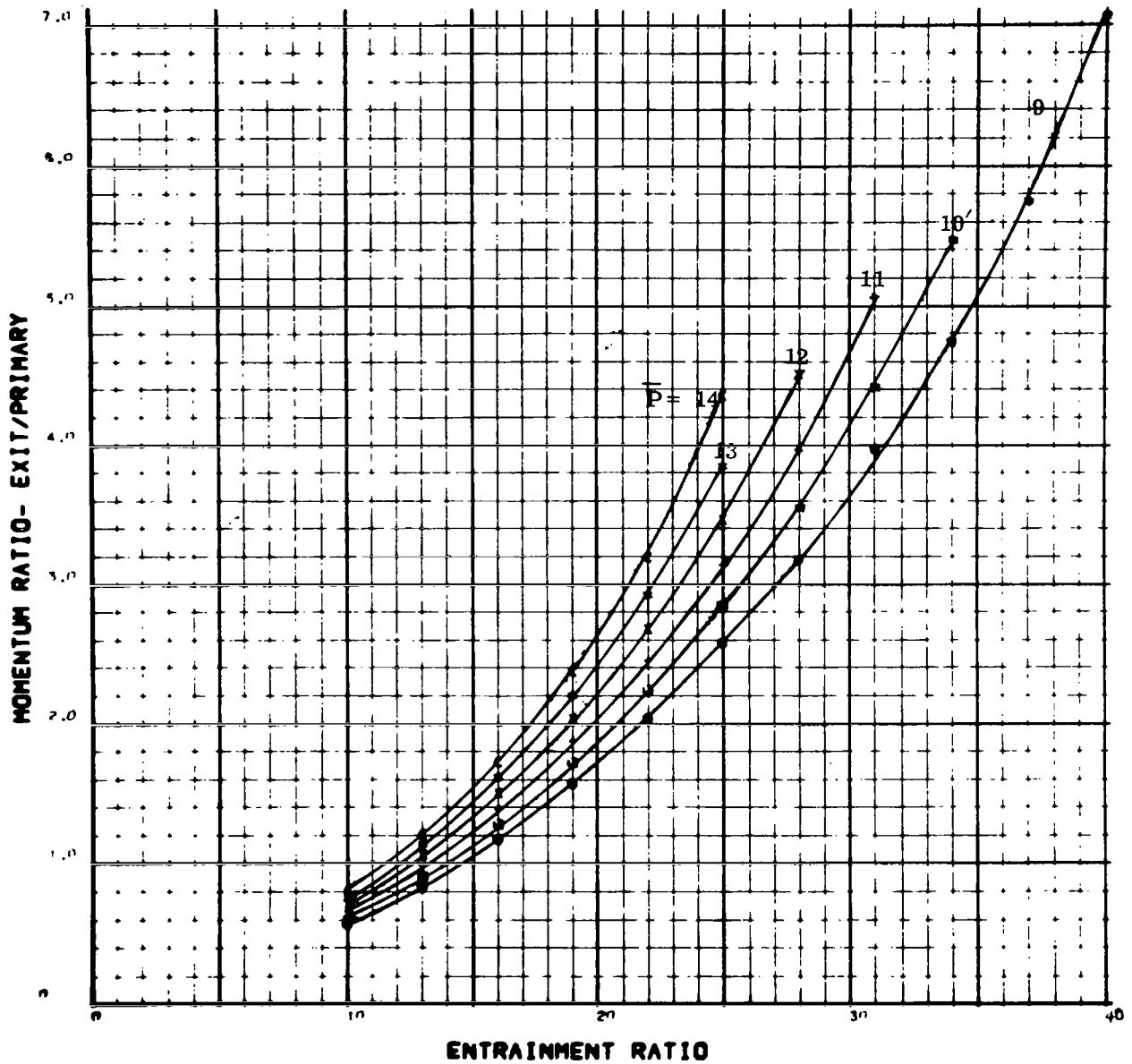


Figure 23

Jet Pump Performance Characteristics
Momentum Augmentation (τ) vs. Entrainment Ratio

$$\bar{A} = 0.007$$

$$\bar{T} = 8.0$$

$$\bar{P} = 9, 10, 11, 12, 13, 14$$

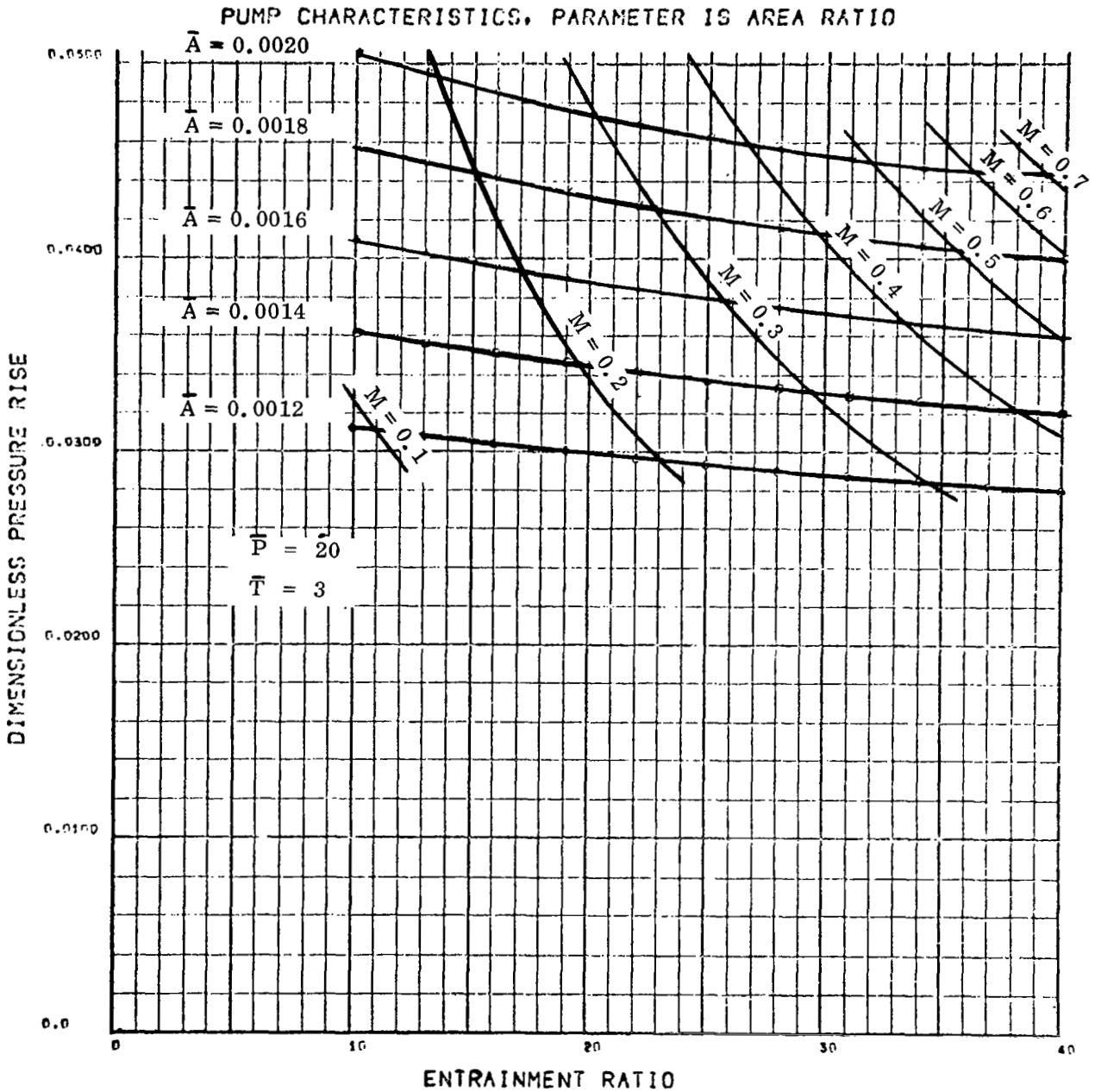


Figure 24
Jet Pump Pressure Rise in Relation to
Geometry (\bar{A}_1) and Mixing Tube Exit Mach Number

MOMENTUM RATIO, PARAMETER IS AREA RATIO

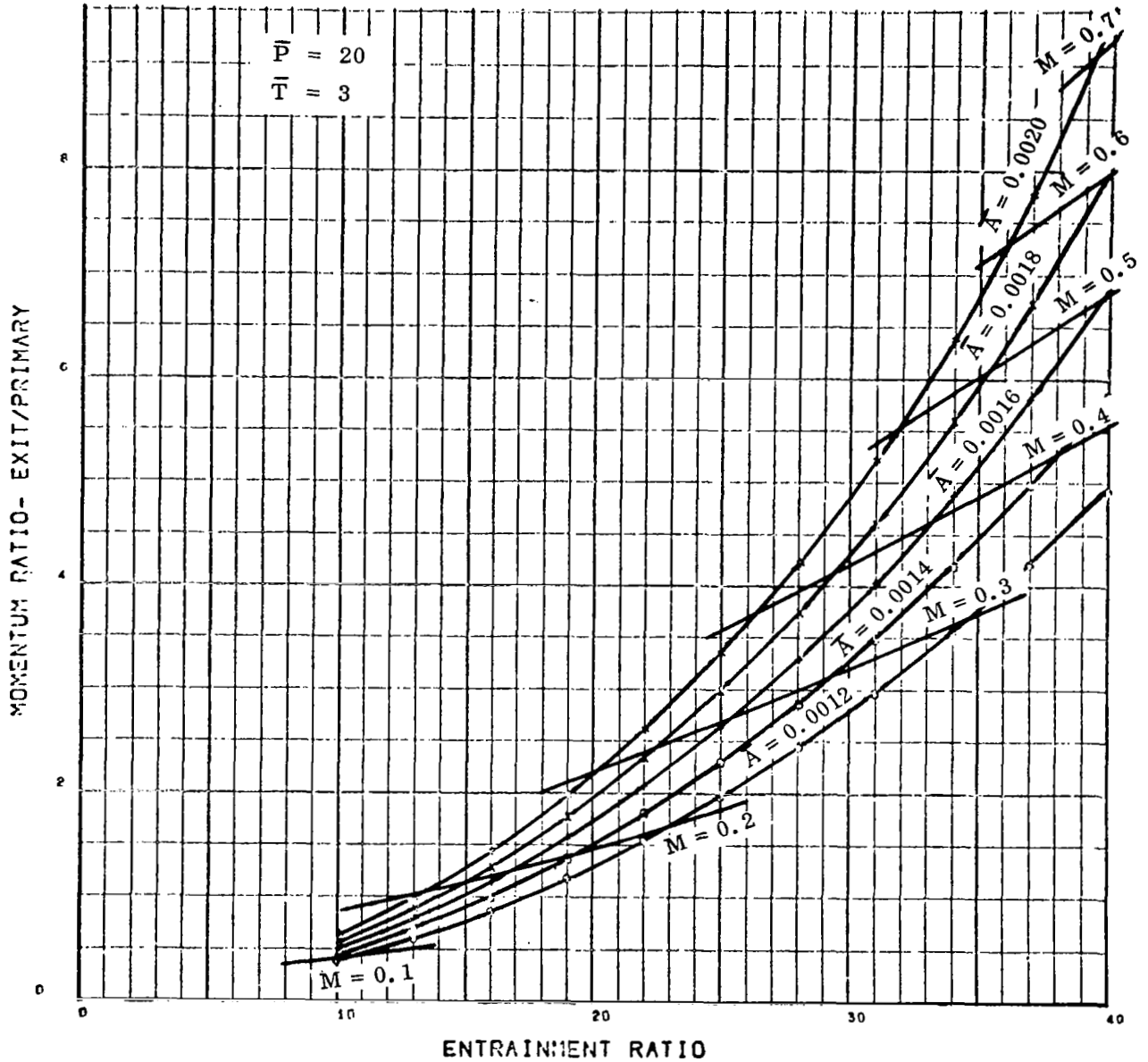


Figure 25
 Jet Pump Momentum Ratio in Relation to Geometry (\bar{A}_1)
 and Mixing Tube Exit Mach Number

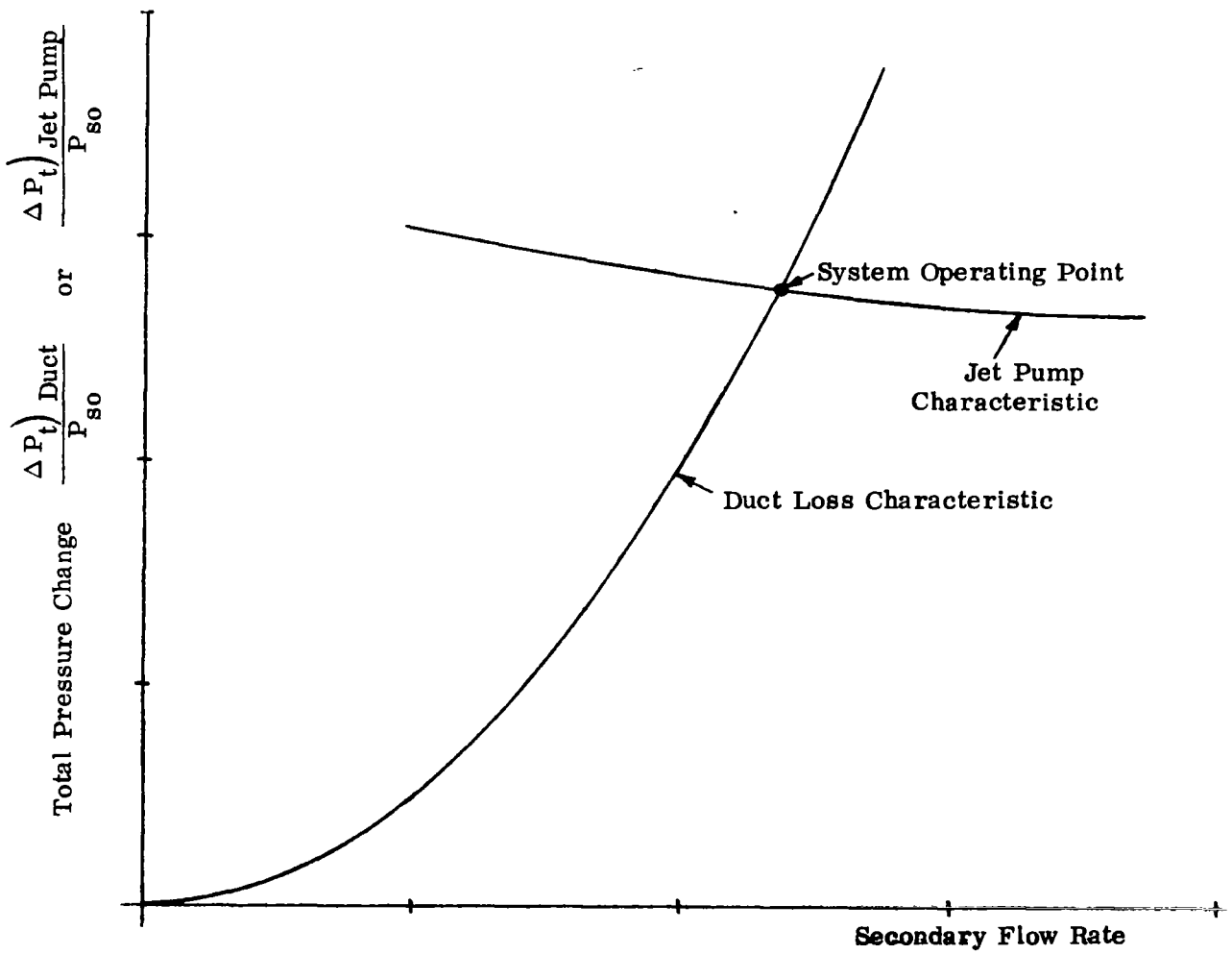


Figure 26
 Jet Pump System Operating Point

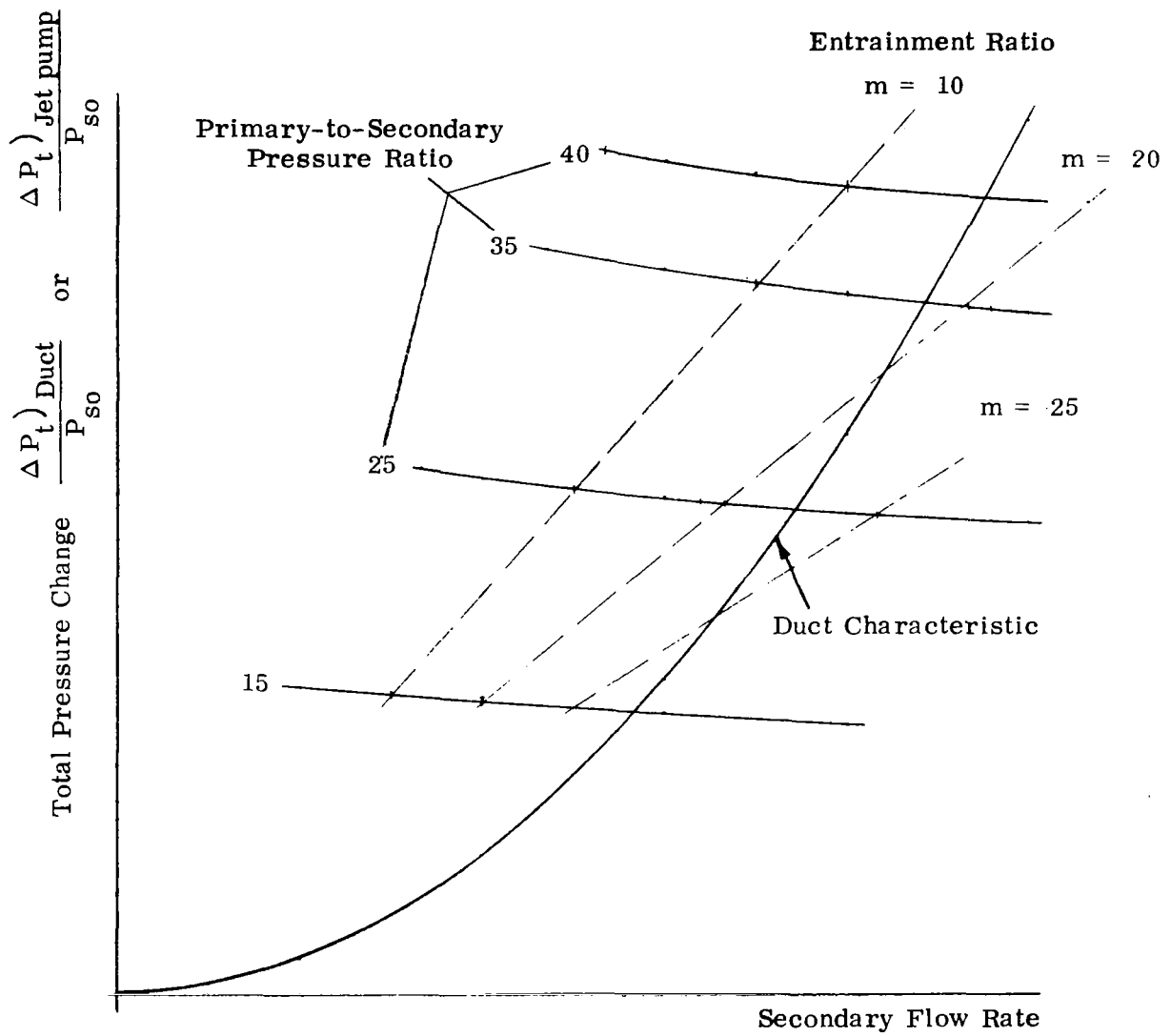


Figure 27
 Influence of Pressure Ratio on Jet Pump-System
 Operating Points

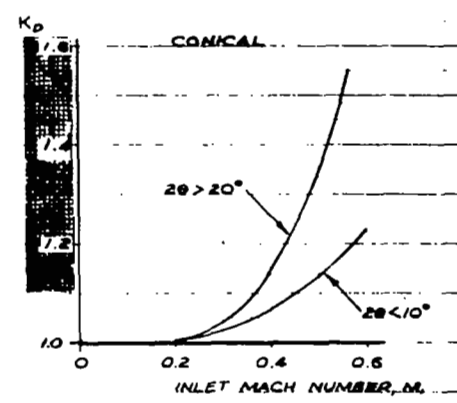
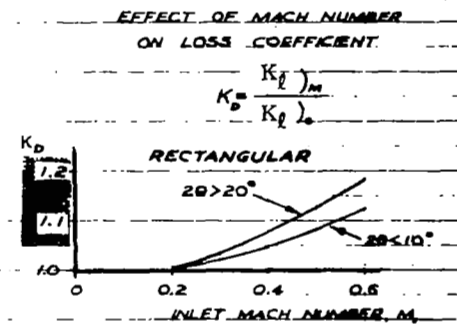
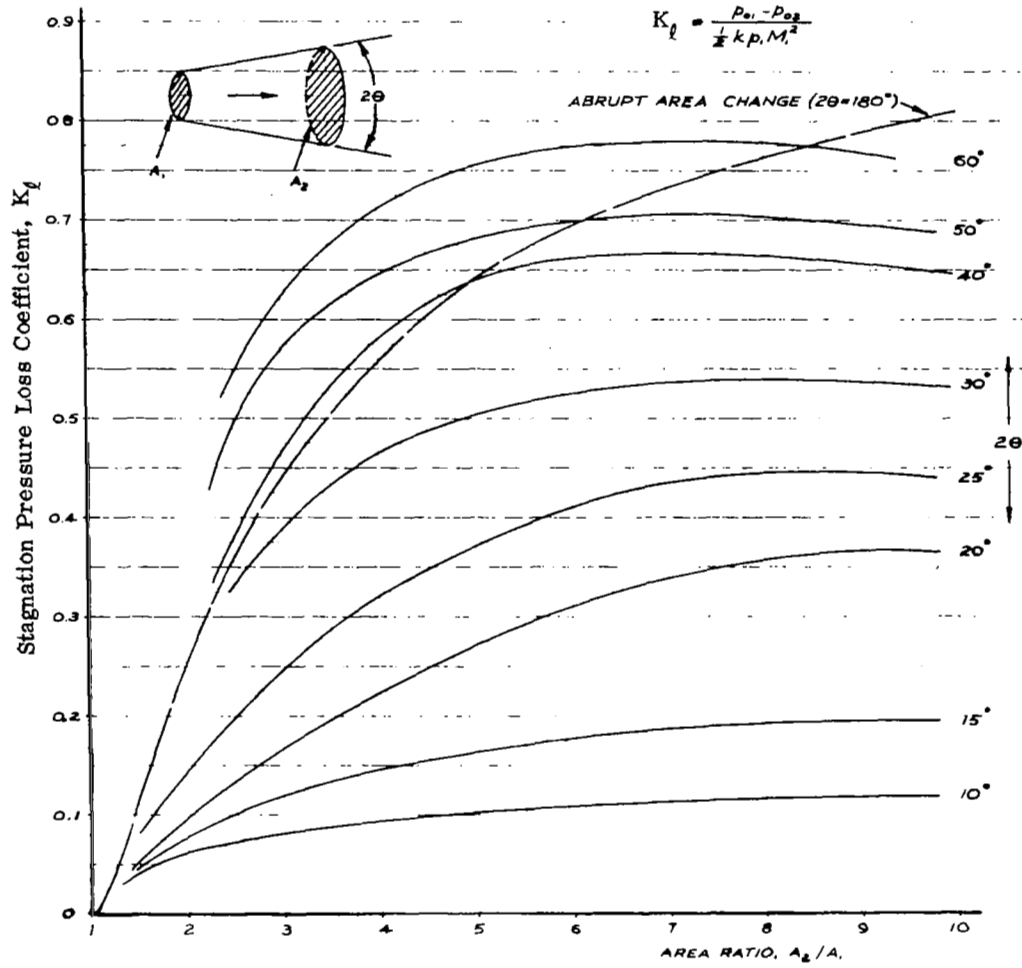


Figure 28
Loss Coefficients for Straight Conical Diffusers

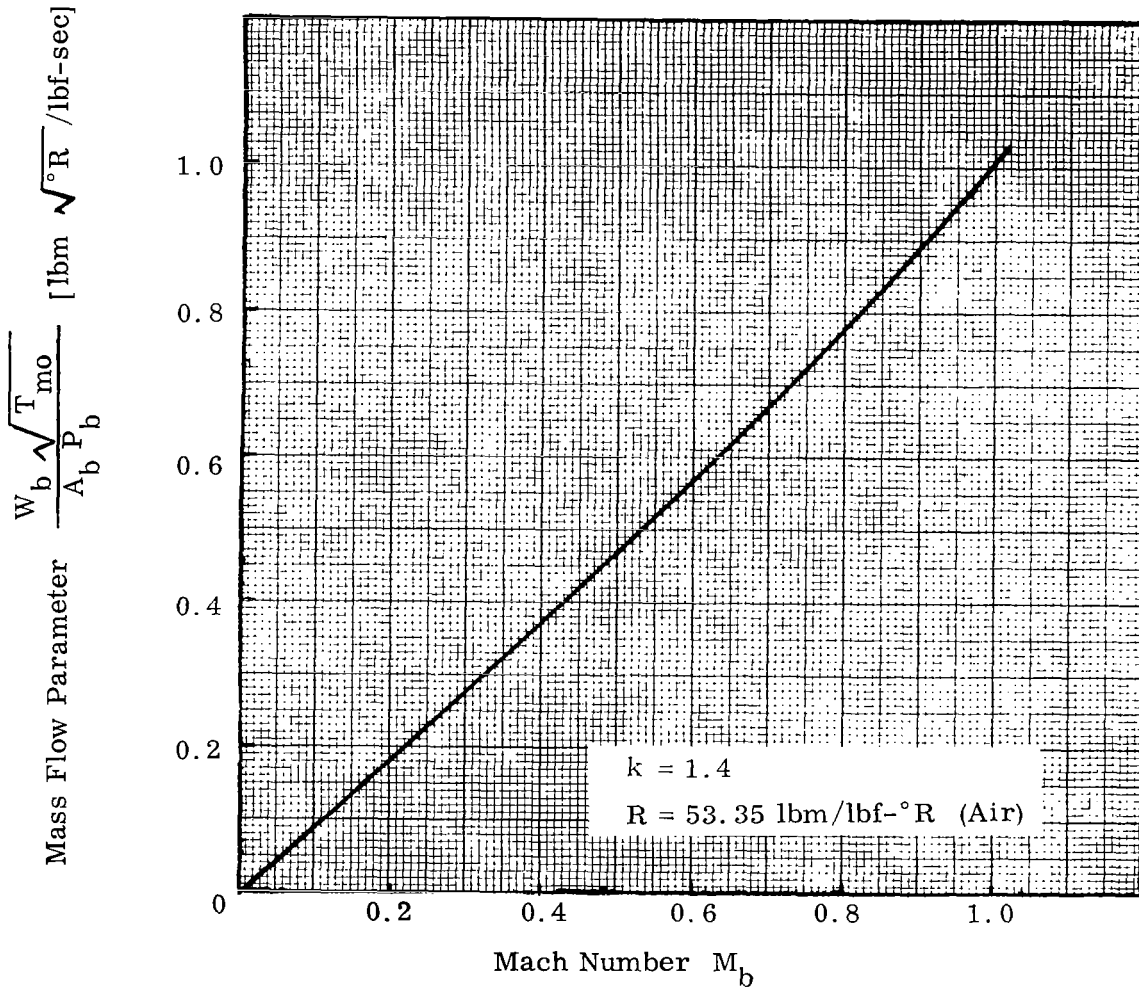


Figure 29

Chart for Determining M_b (Equation 66)

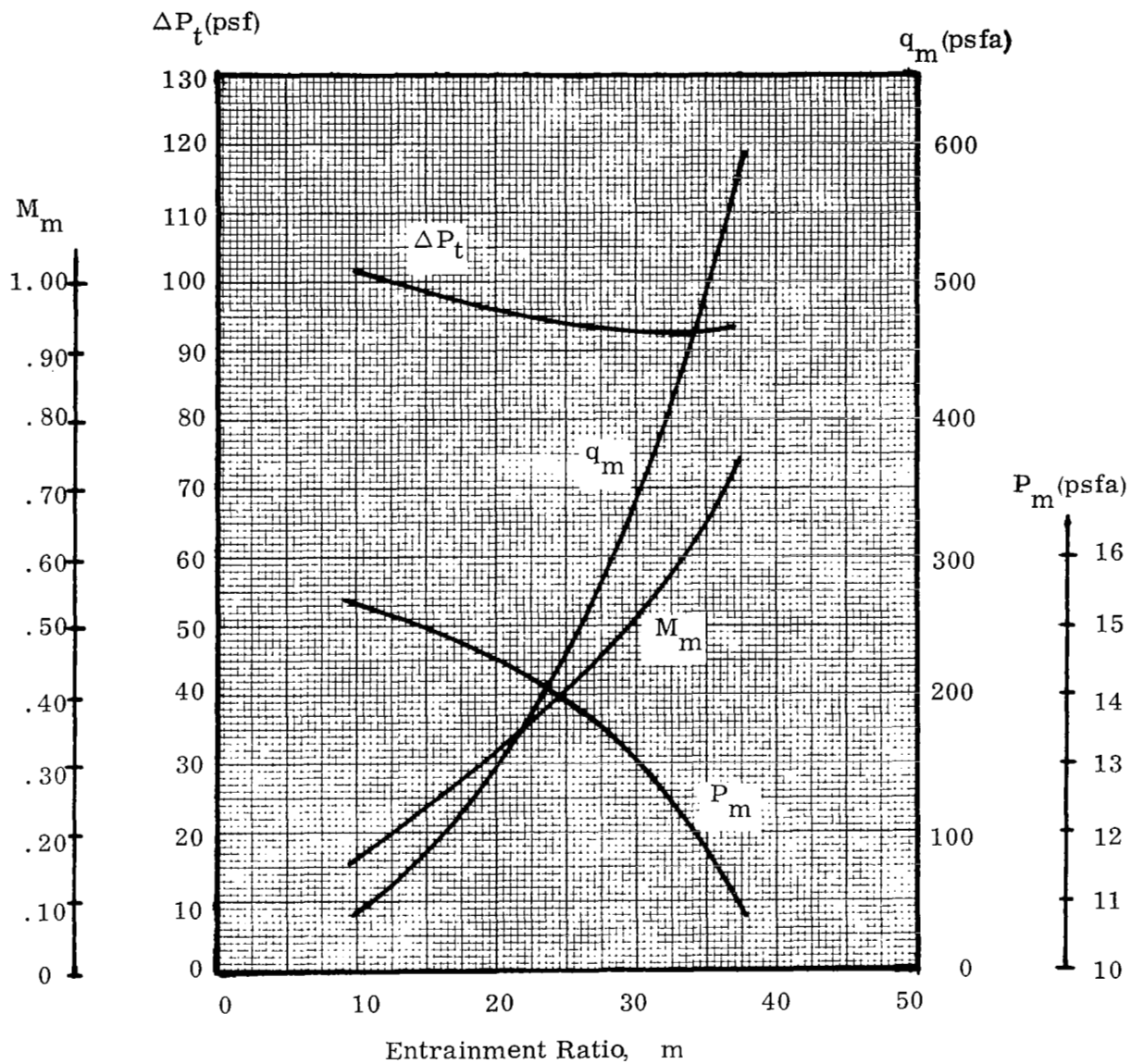


Figure 30

Jet Pump Operating Characteristics

ΔP_t (psf)

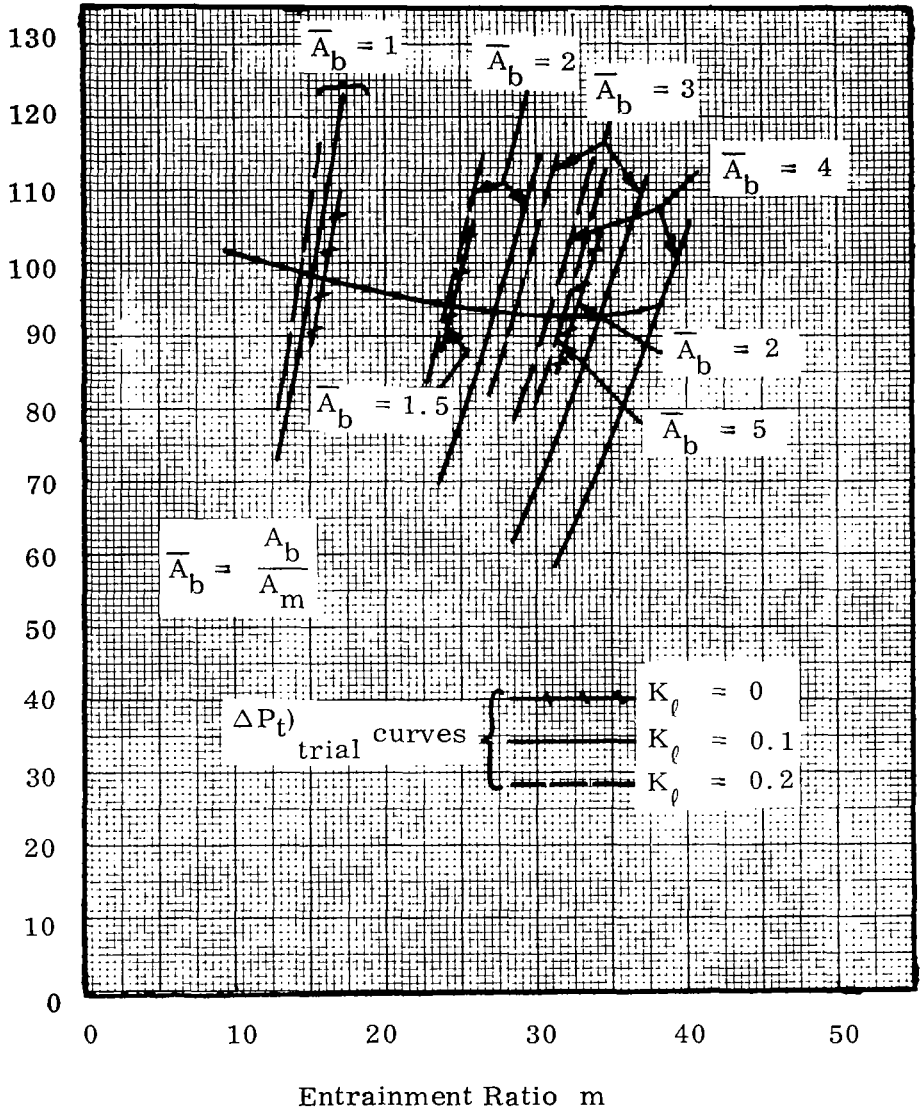


Figure 31

Determination of System Operating Points

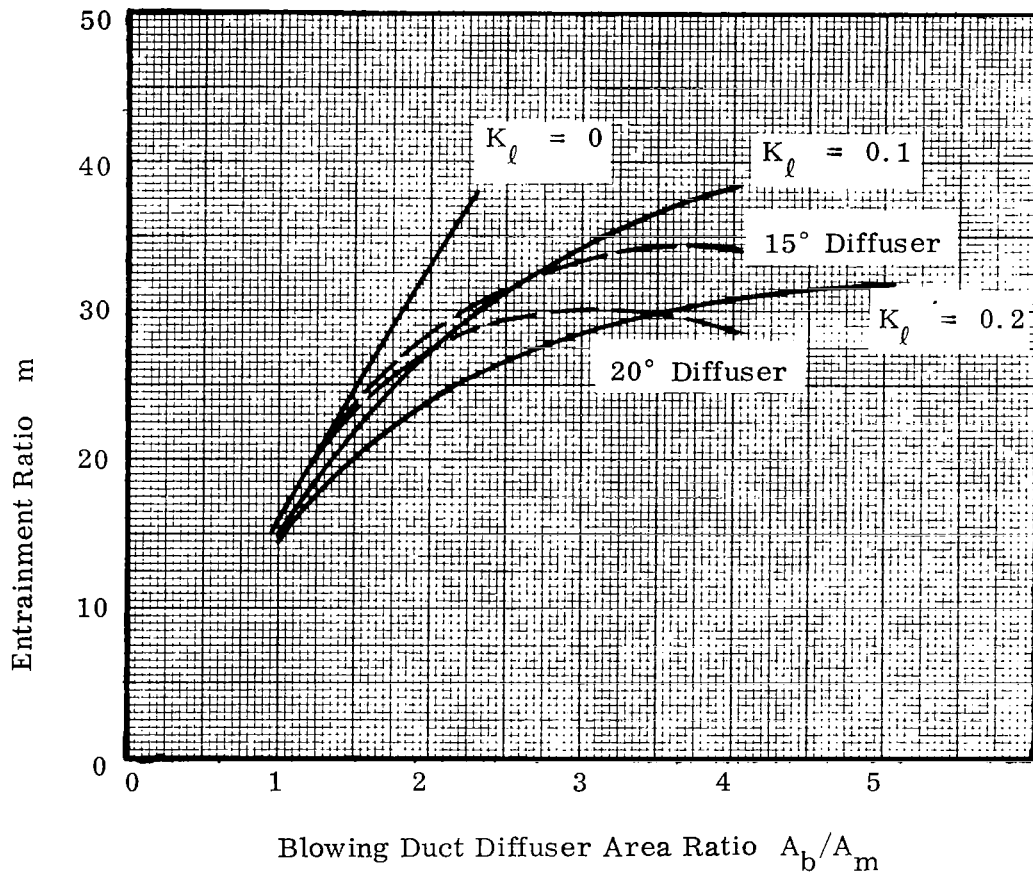


Figure 32

Influence of Blowing Duct Diffusion Upon Entrainment Ratio

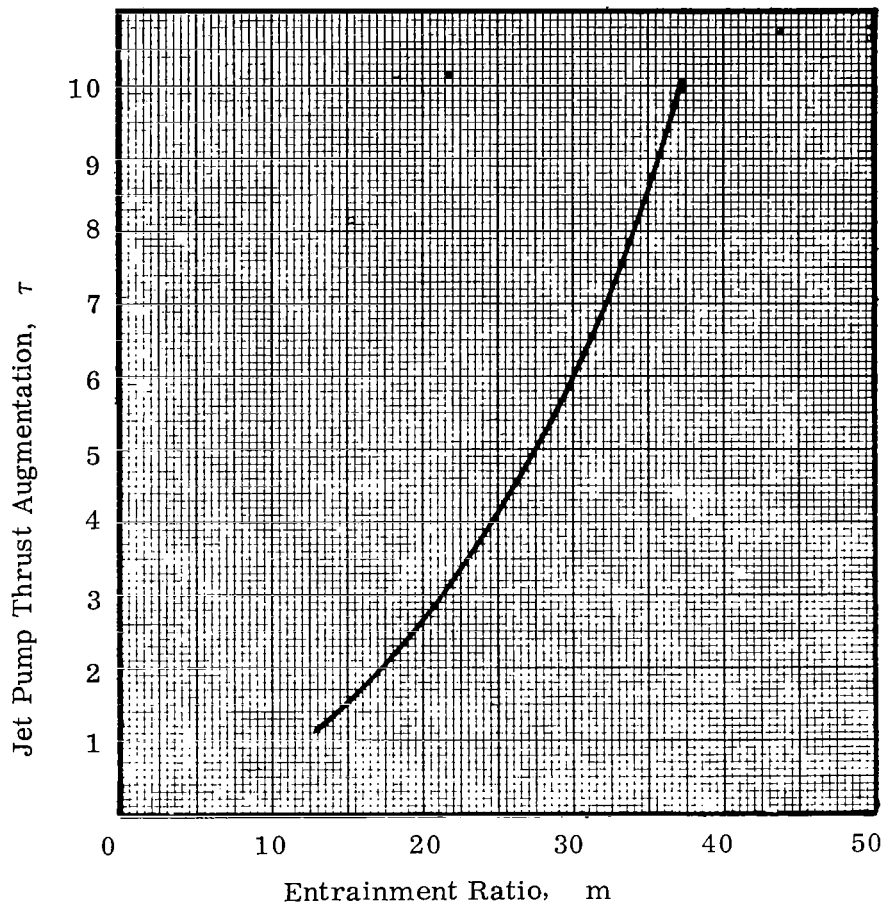


Figure 33
 Jet Pump Thrust Augmentation Characteristic

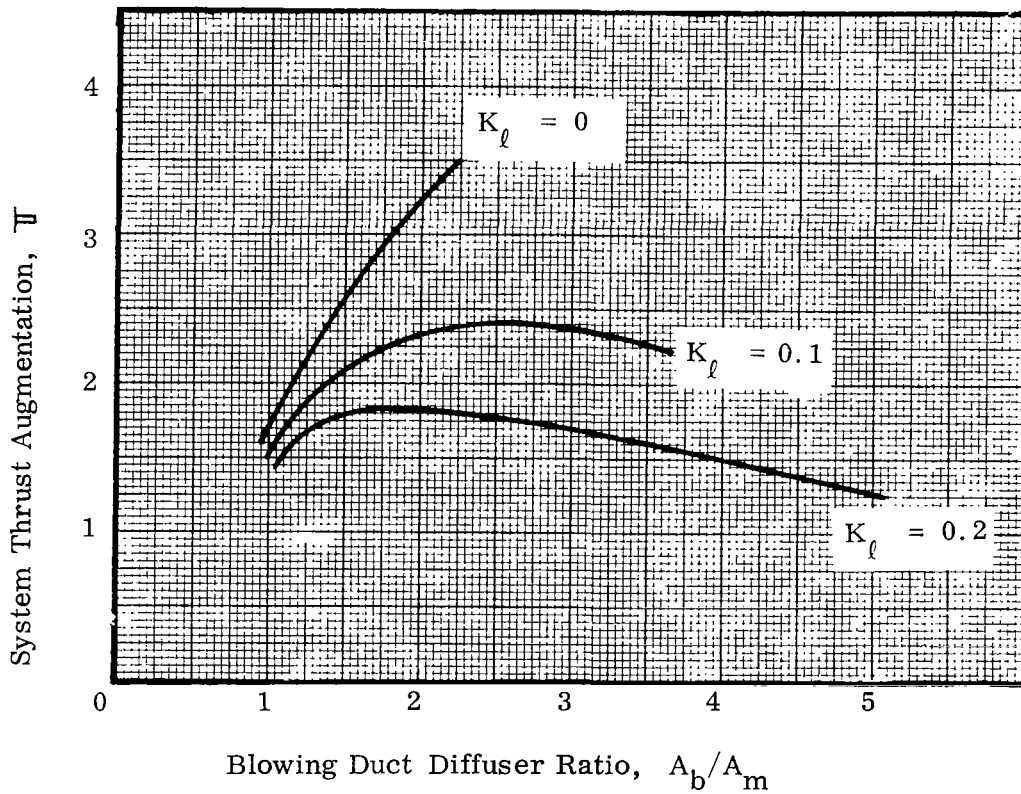


Figure 34

Influence of Blowing Duct Diffusion Upon System Thrust Augmentation

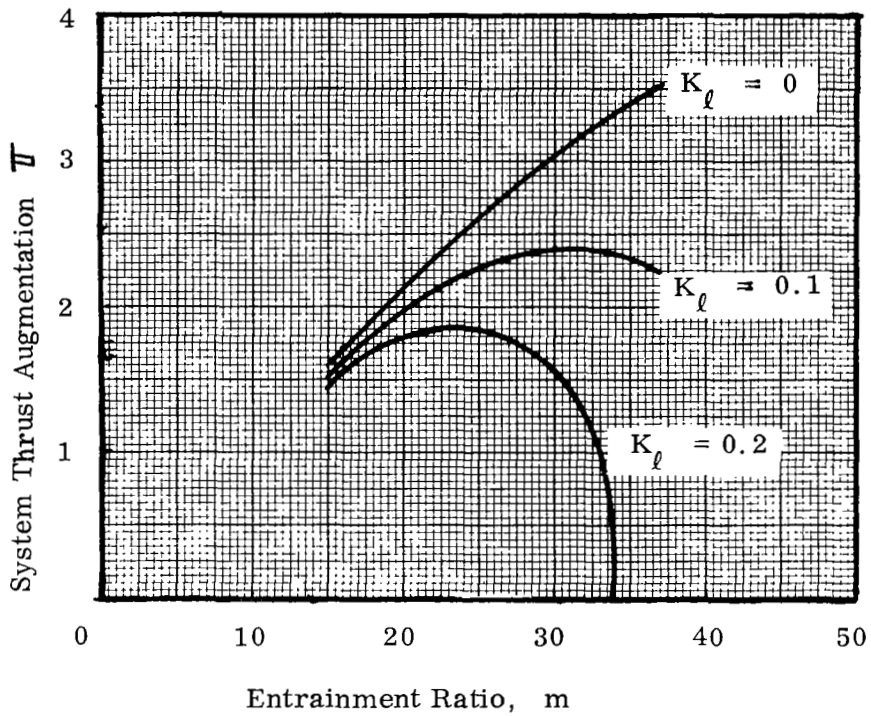


Figure 35

Relationship of Thrust Augmentation to Entrainment Ratio

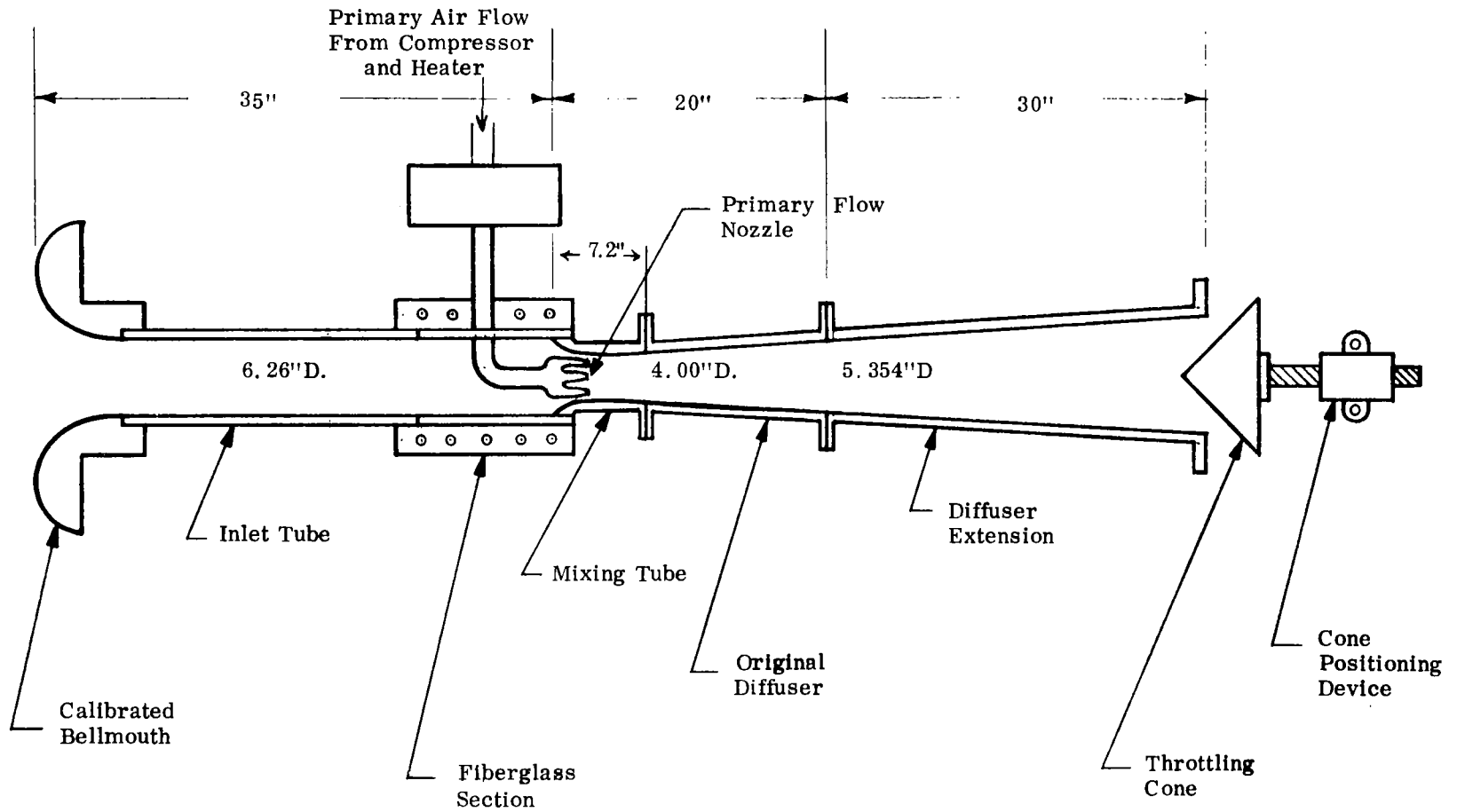


Figure 36
Jet Pump Test Rig

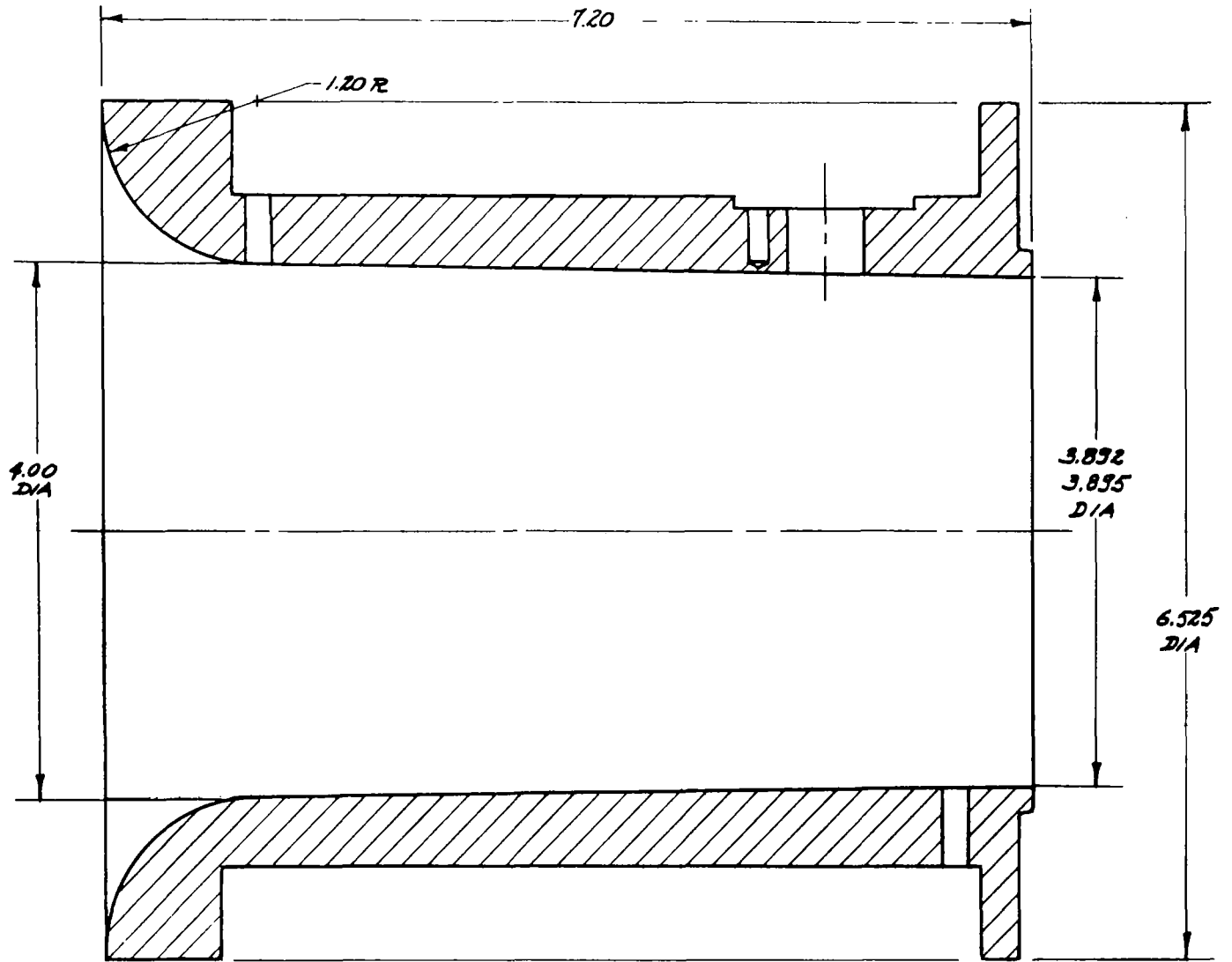
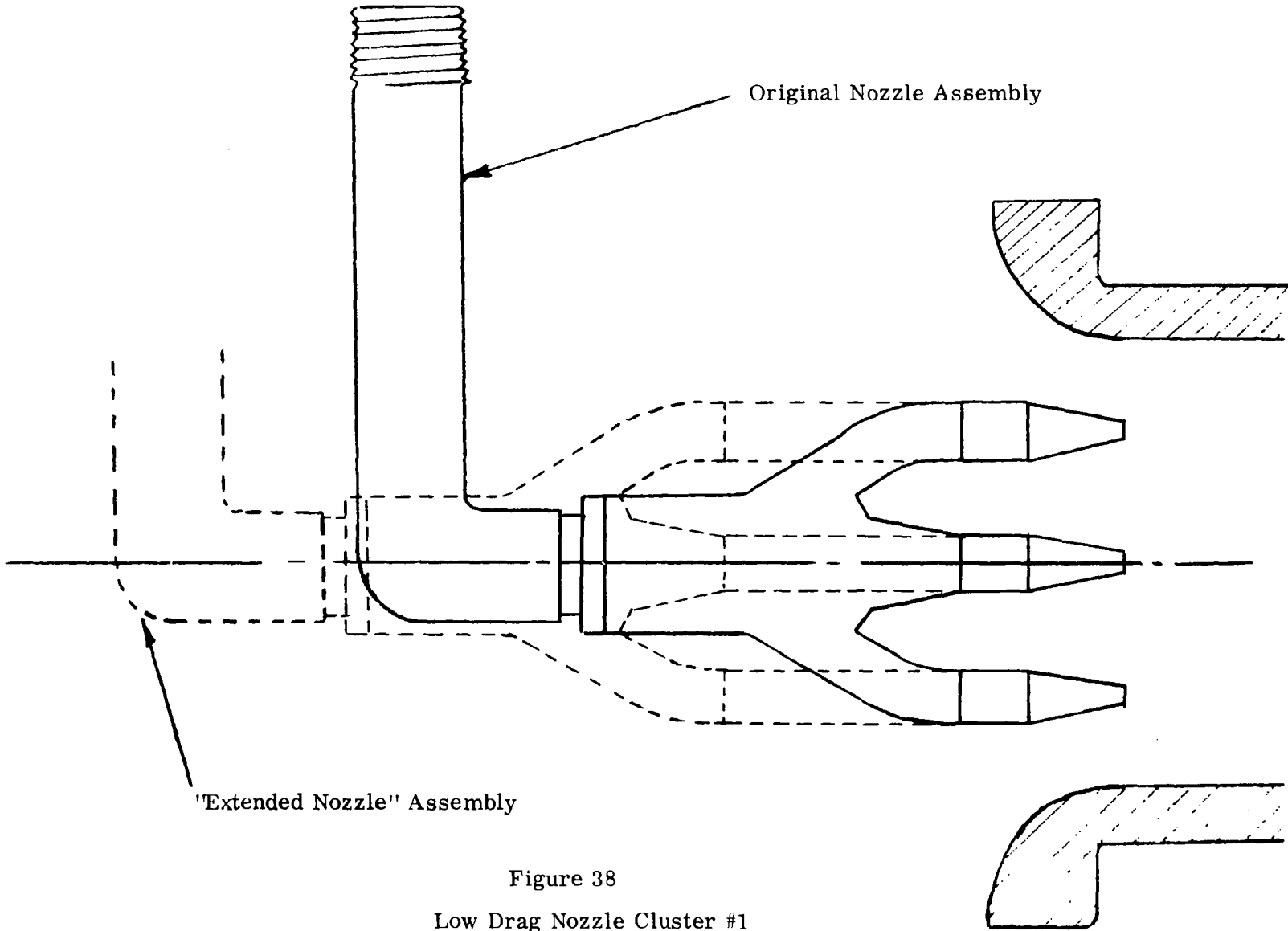


Figure 37
Original Mixing Tube Geometry



'Extended Nozzle' Assembly

Original Nozzle Assembly

Figure 38
Low Drag Nozzle Cluster #1

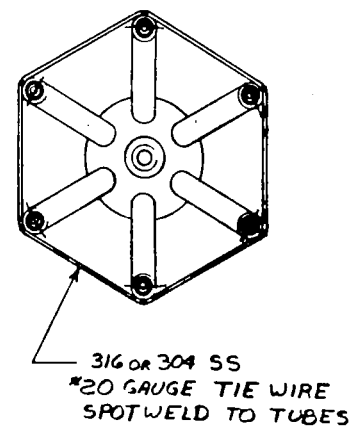
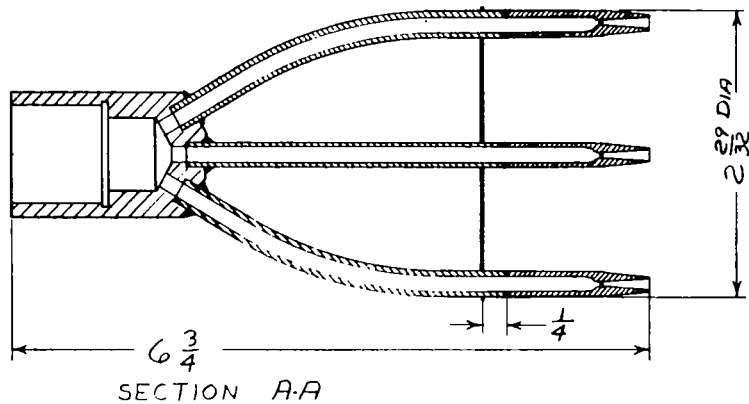
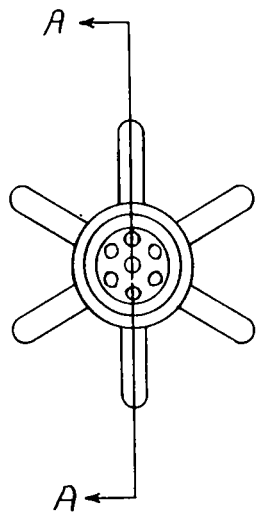


Figure 39
Low-Drag Nozzle Cluster #2

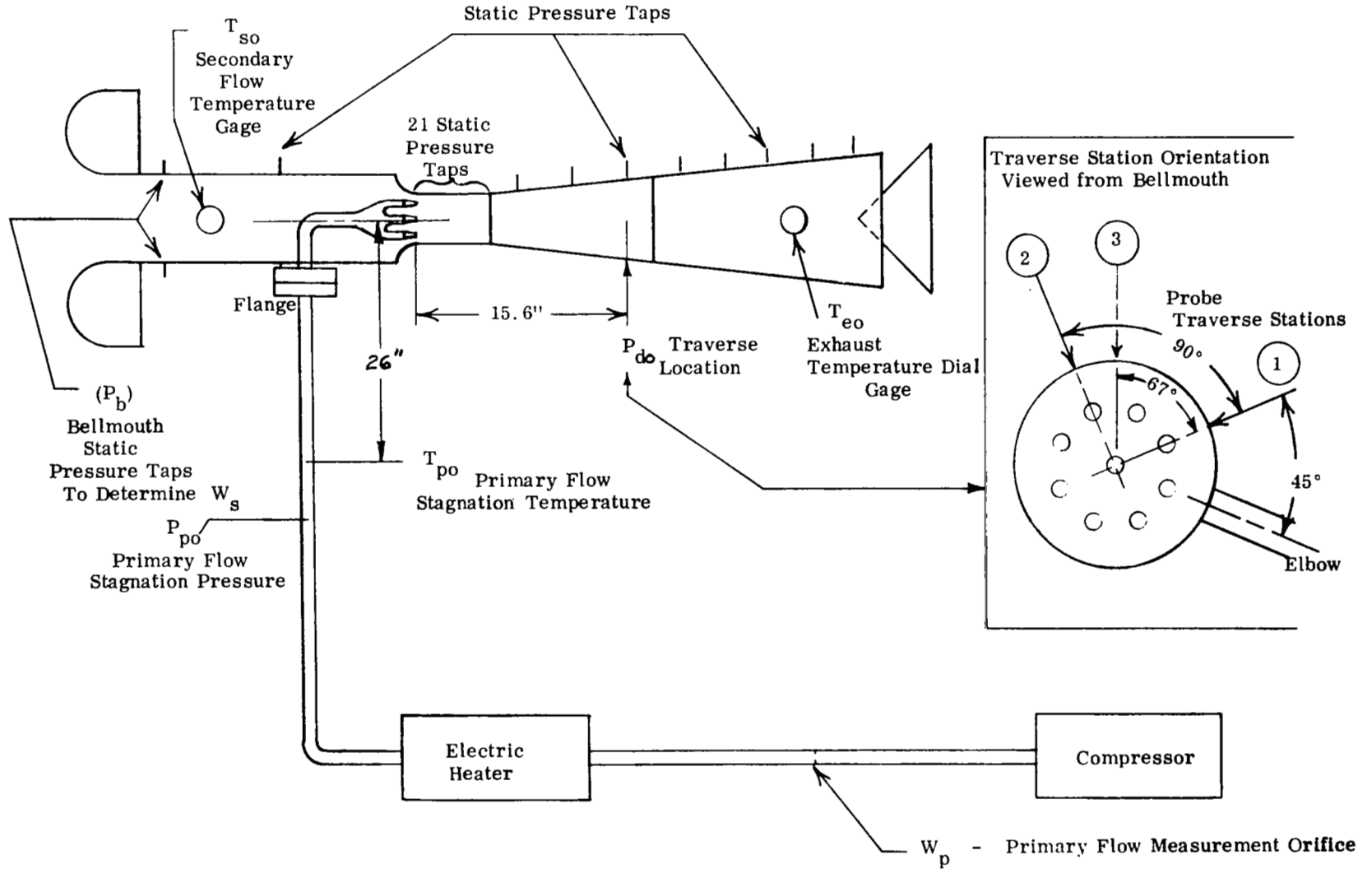
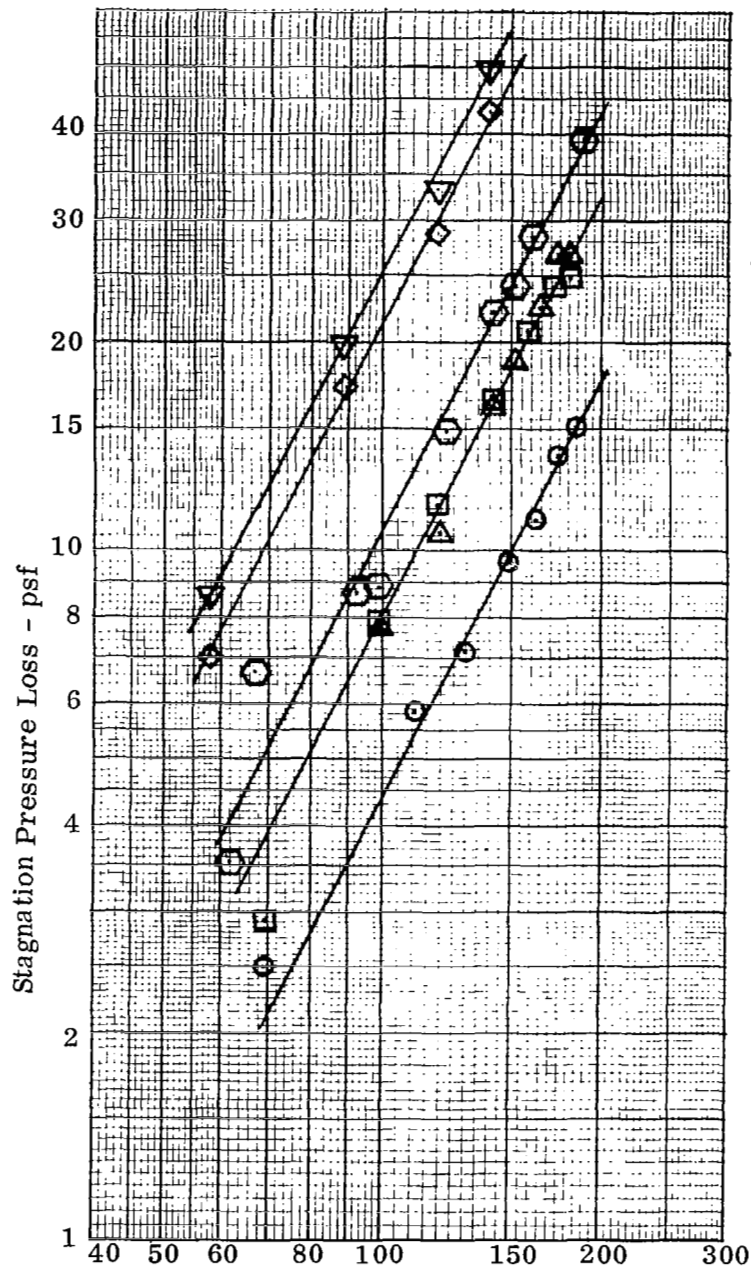


Figure 40
 Dynatech Jet Pump Test Instrumentation



W_s - Secondary Flow Rate - lbm/min

Figure 41

Pressure Loss Characteristics

Four Inlet Duct and Nozzle Cluster Configurations

(Measurements Made at End of Short
Mixing Tube, $L/d_m = 1.35$)

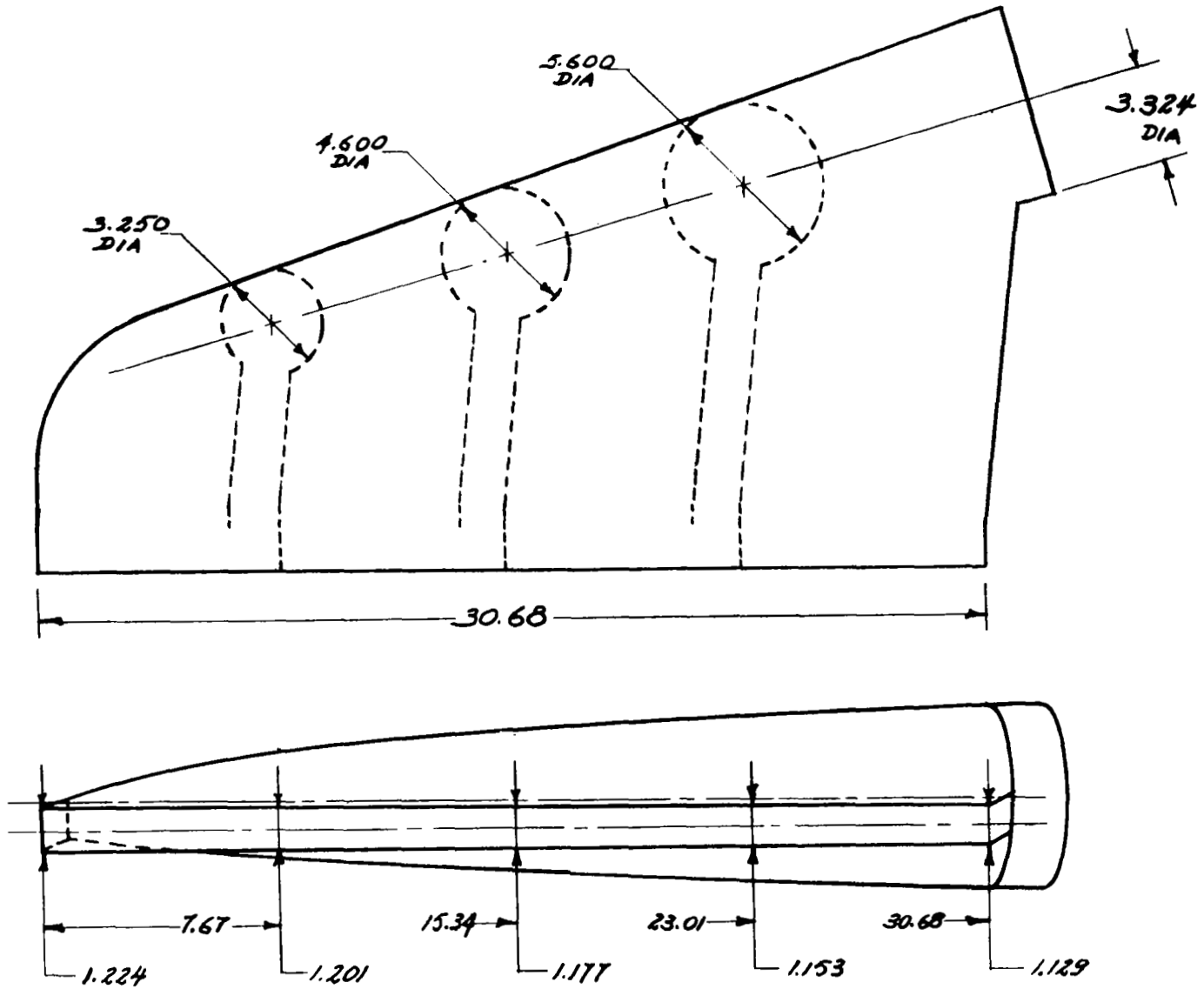


Figure 42
NAS 2-2518 BLC System Suction Duct



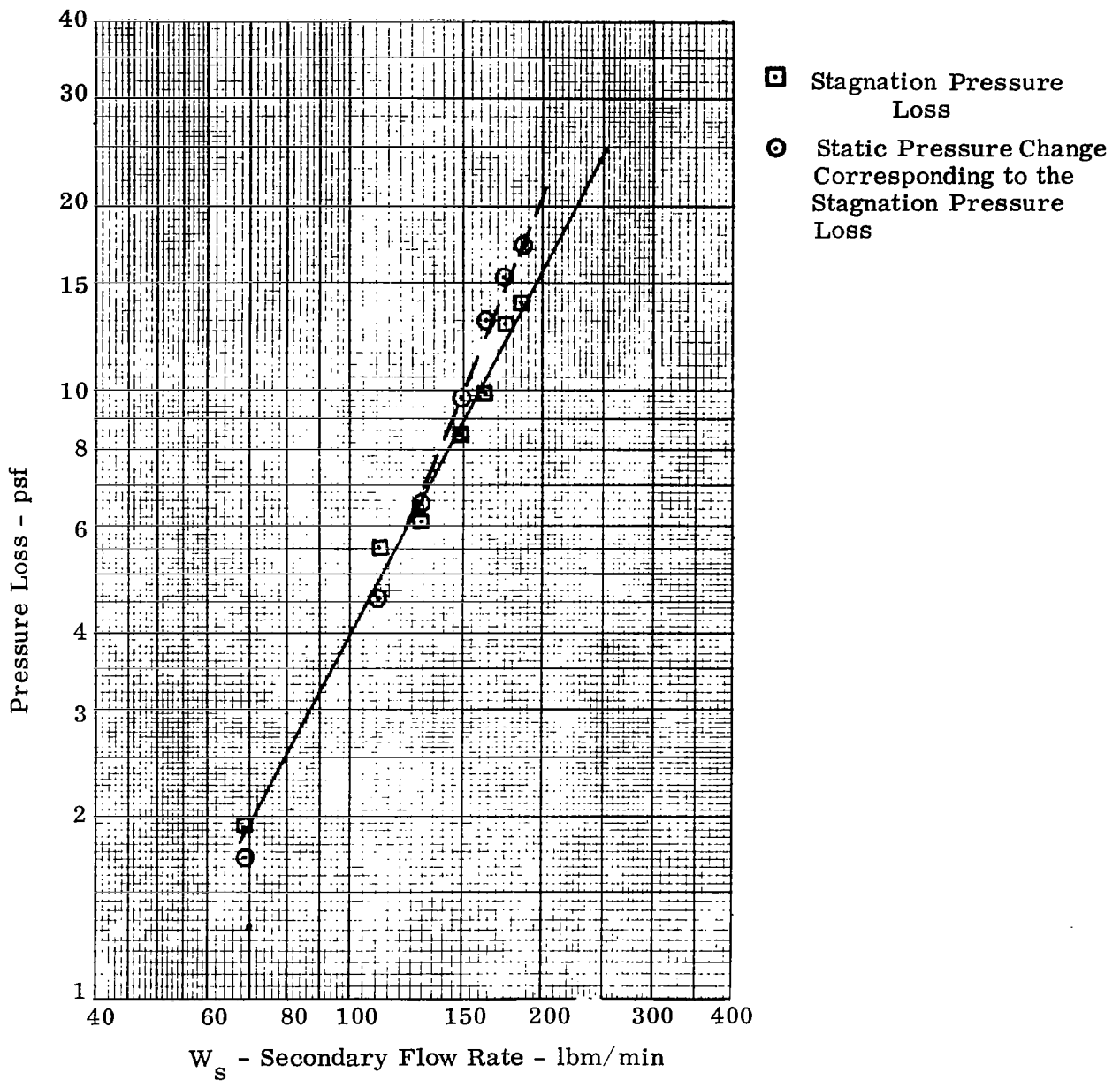


Figure 43

Pressure Loss Characteristics of the
 Extended Constant Diameter Mixing Tube

(Pressure Measurements Taken
 2.72 Duct Diameters Apart ;
 $d_m = 4.0$ Inches)

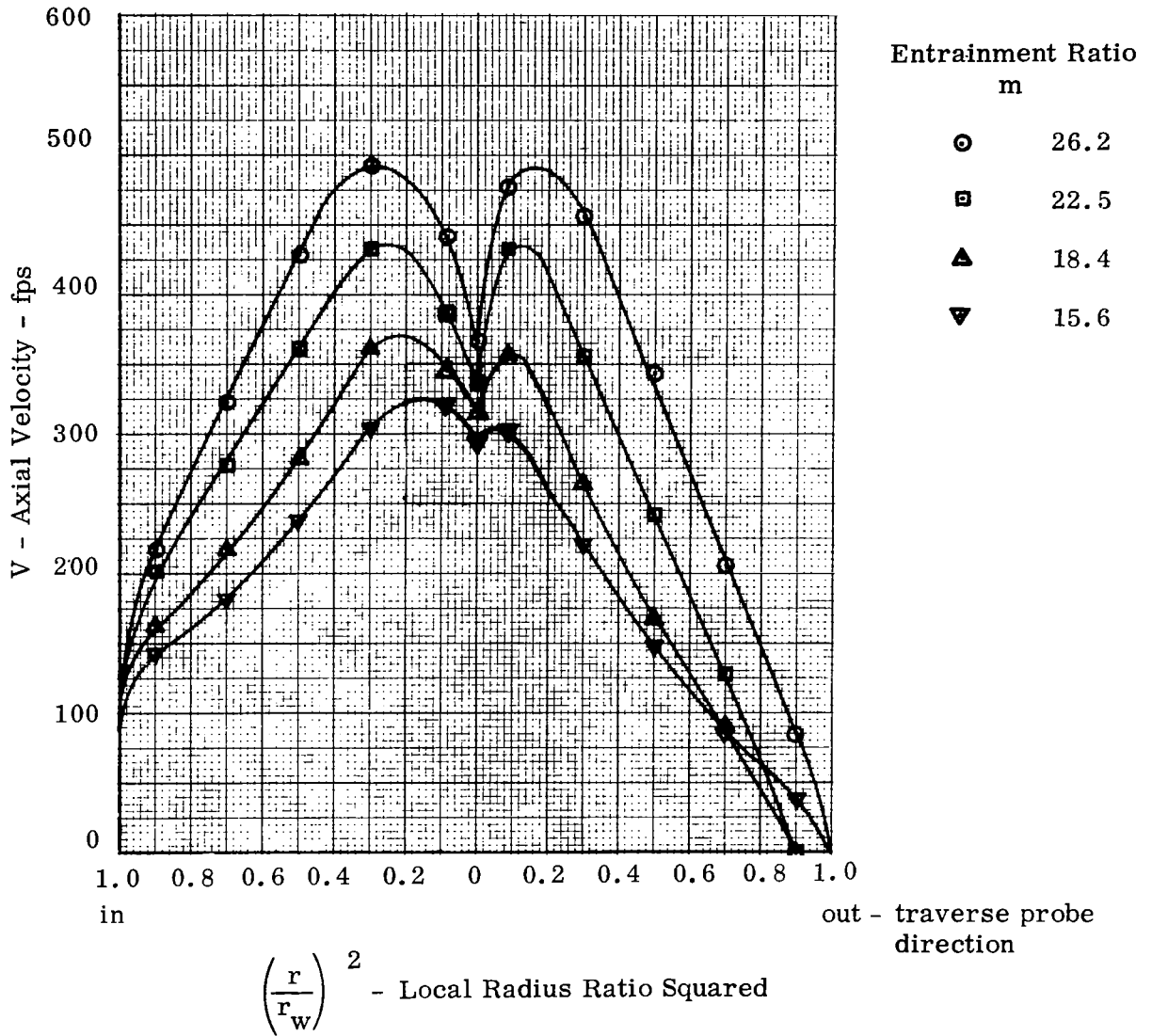


Figure 44

Velocity Profiles at Diffuser Discharge

$$d = 5.084" \quad \frac{A_d}{A_m} = 1.71$$

NAS 2-2518 Mixing Tube
 Original Nozzle Cluster
 Case 4 Nozzles (350 psia, 1090°F)

$$W_p = 6.69 \text{ lbm/min}$$

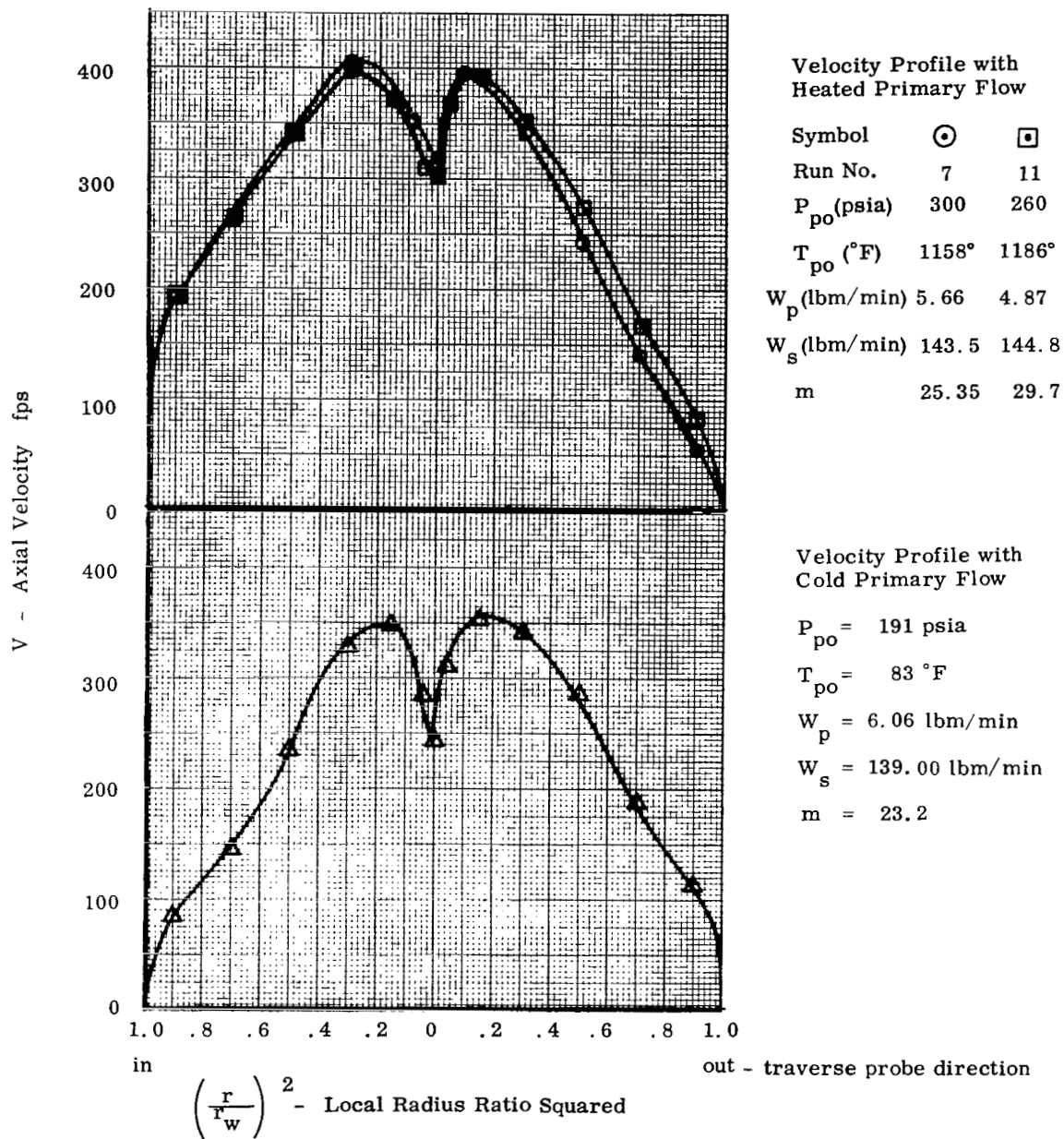


Figure 45

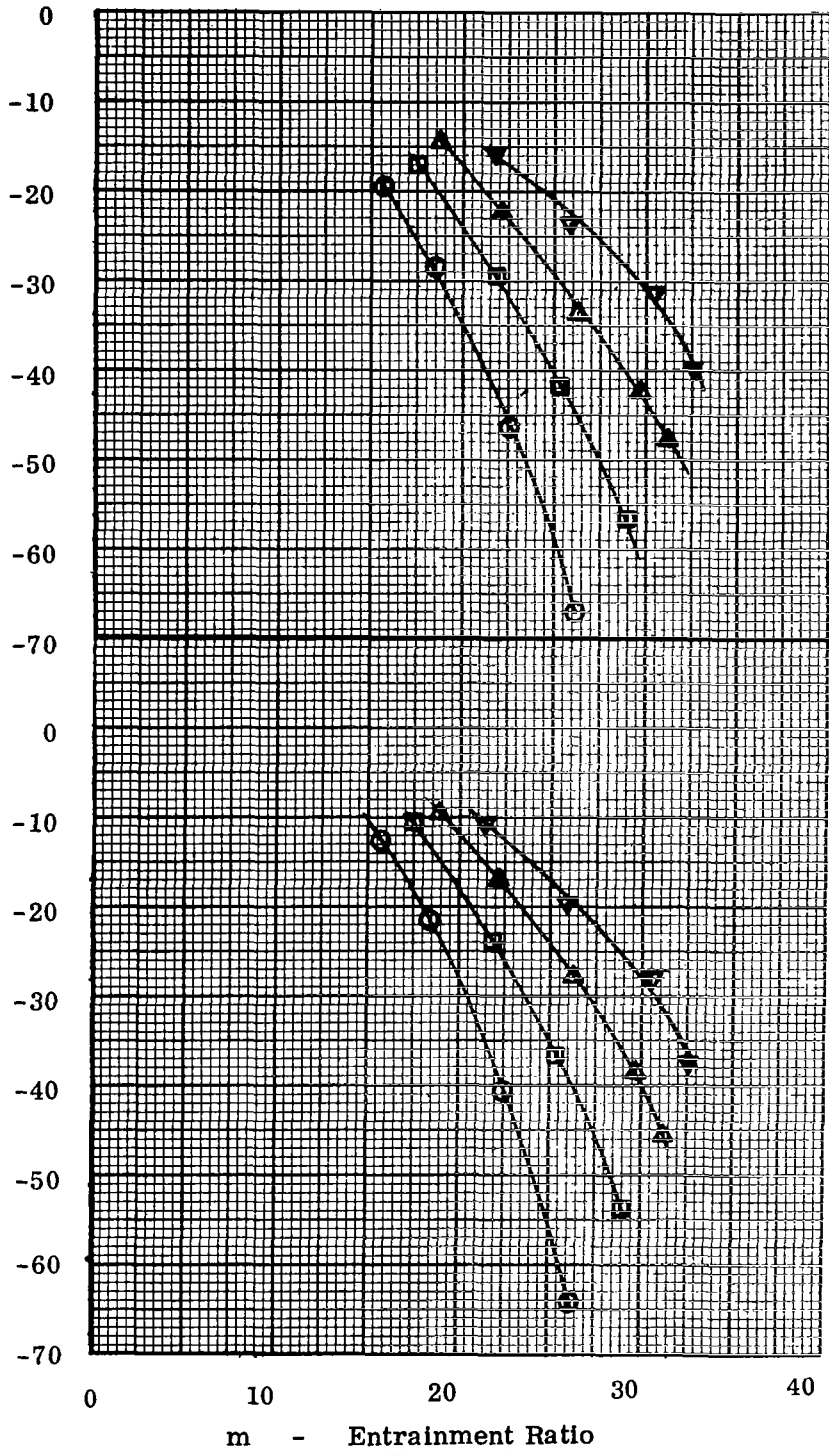
Velocity Profiles at Diffuser Discharge

$$d = 5.084'' \quad \frac{A_d}{A_m} = 1.71$$

NAS 2-2518 Mixing Tube
 Original Nozzle Cluster
 Case 4 Nozzles

P - Static Pressure 0.81 Inches Down-
stream of Primary Nozzle Discharge
Inches of Water Gage

P - Static Pressure At
Mixing Tube Discharge
Inches Water
Gage



	P_{po} psia	T_{po} ° F
○	350	1085°
□	300	1160°
△	260	1185°
▽	225	1145°

Figure 46
Static Pressure in NAS 2-2518 Mixing Tube
Original Nozzle Cluster
Case 4 Nozzles

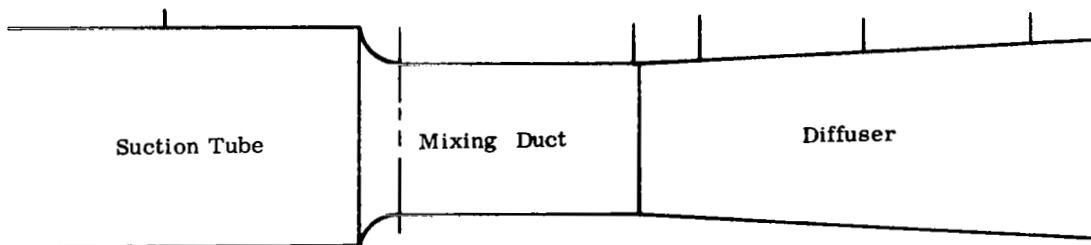
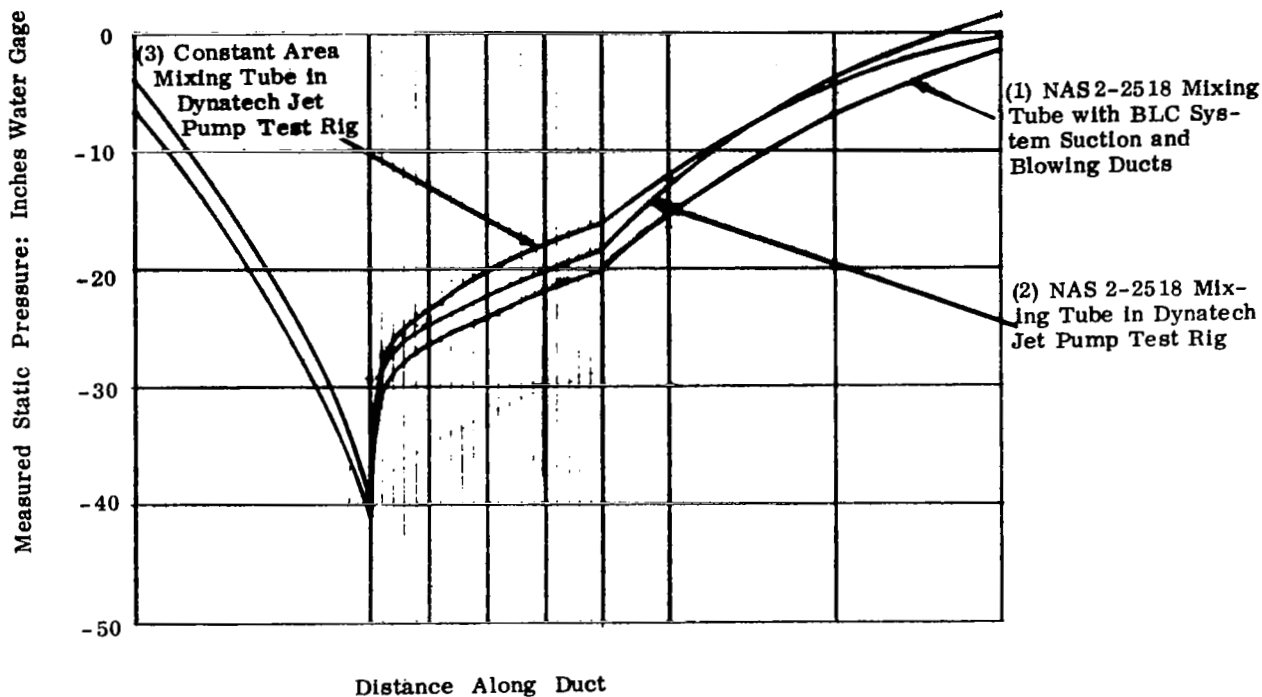


Figure 47
Variation of Static Pressure in Mixing Tube and Diffuser
For Three Configurations
Case 4 Nozzles

$$\begin{aligned}
 P_{po} &= 350 \text{ psia} \\
 T_{po} &= 1100^\circ \text{ F to } 1200^\circ \text{ F} \\
 W_m &= 124.9 \text{ lbm/min}
 \end{aligned}$$

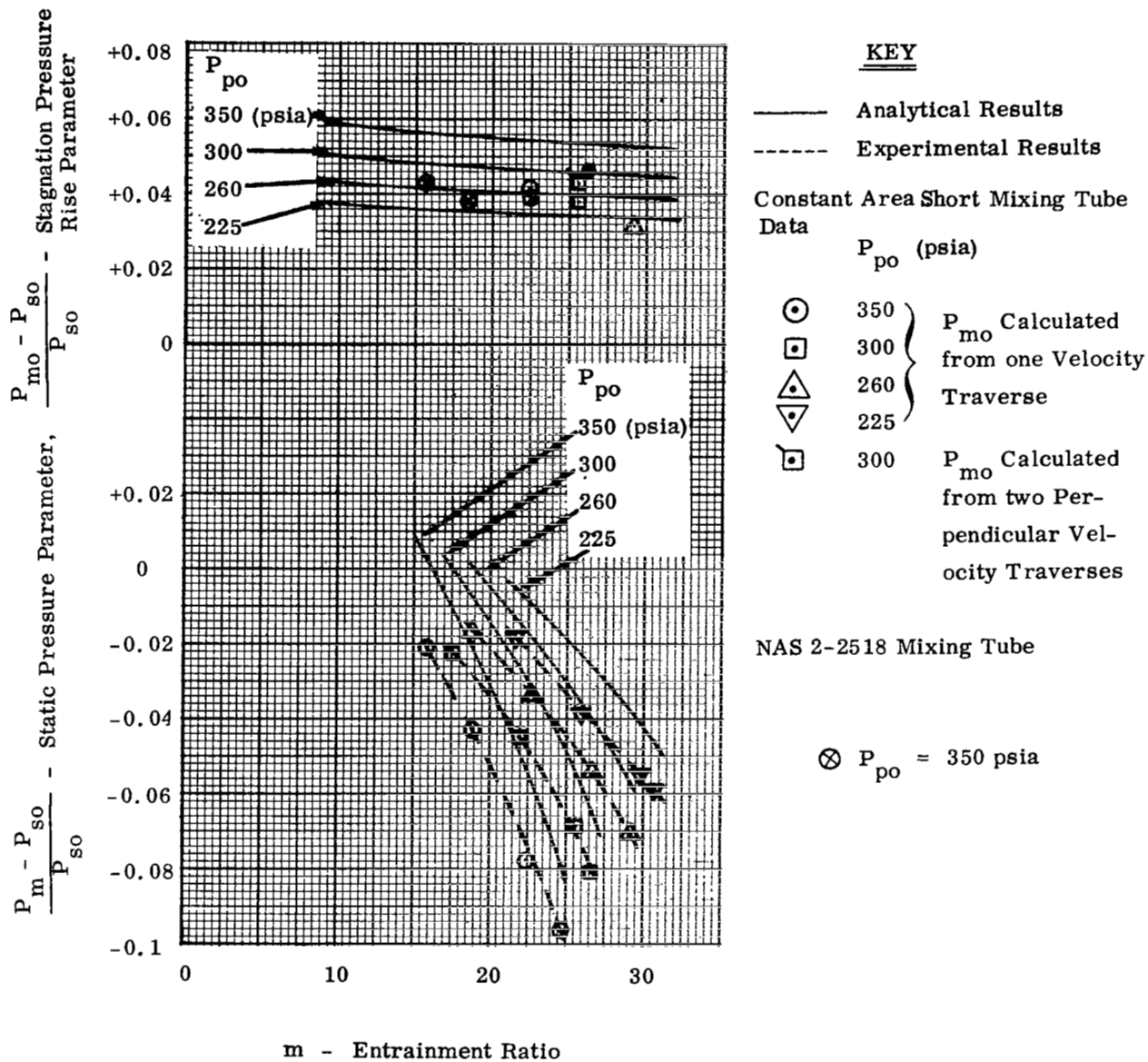


Figure 48
 Jet Pump Pressure Rise Parameters Calculated at
 Mixing Tube Discharge
 Original Nozzle Cluster
 Case 4 Nozzles

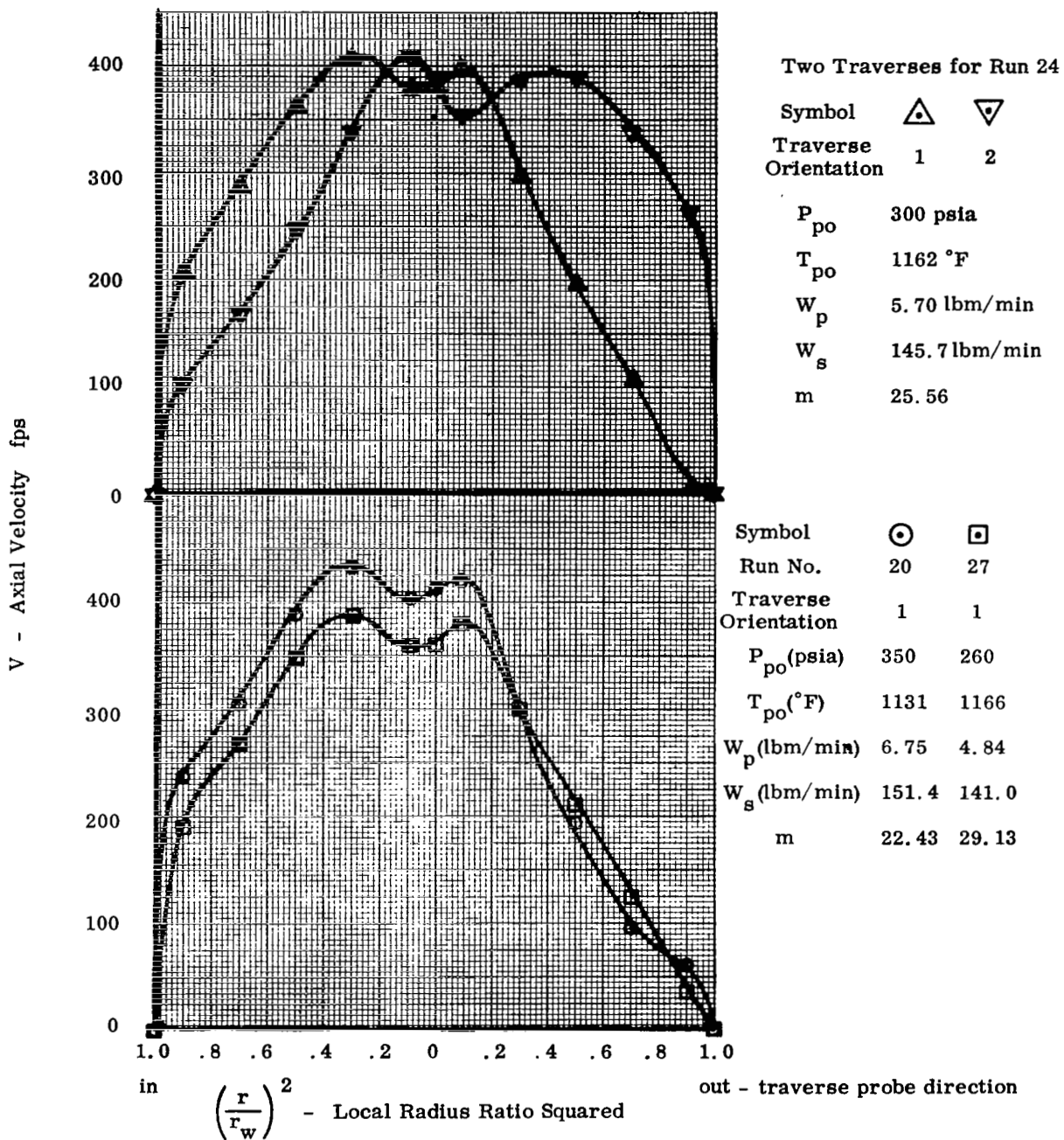


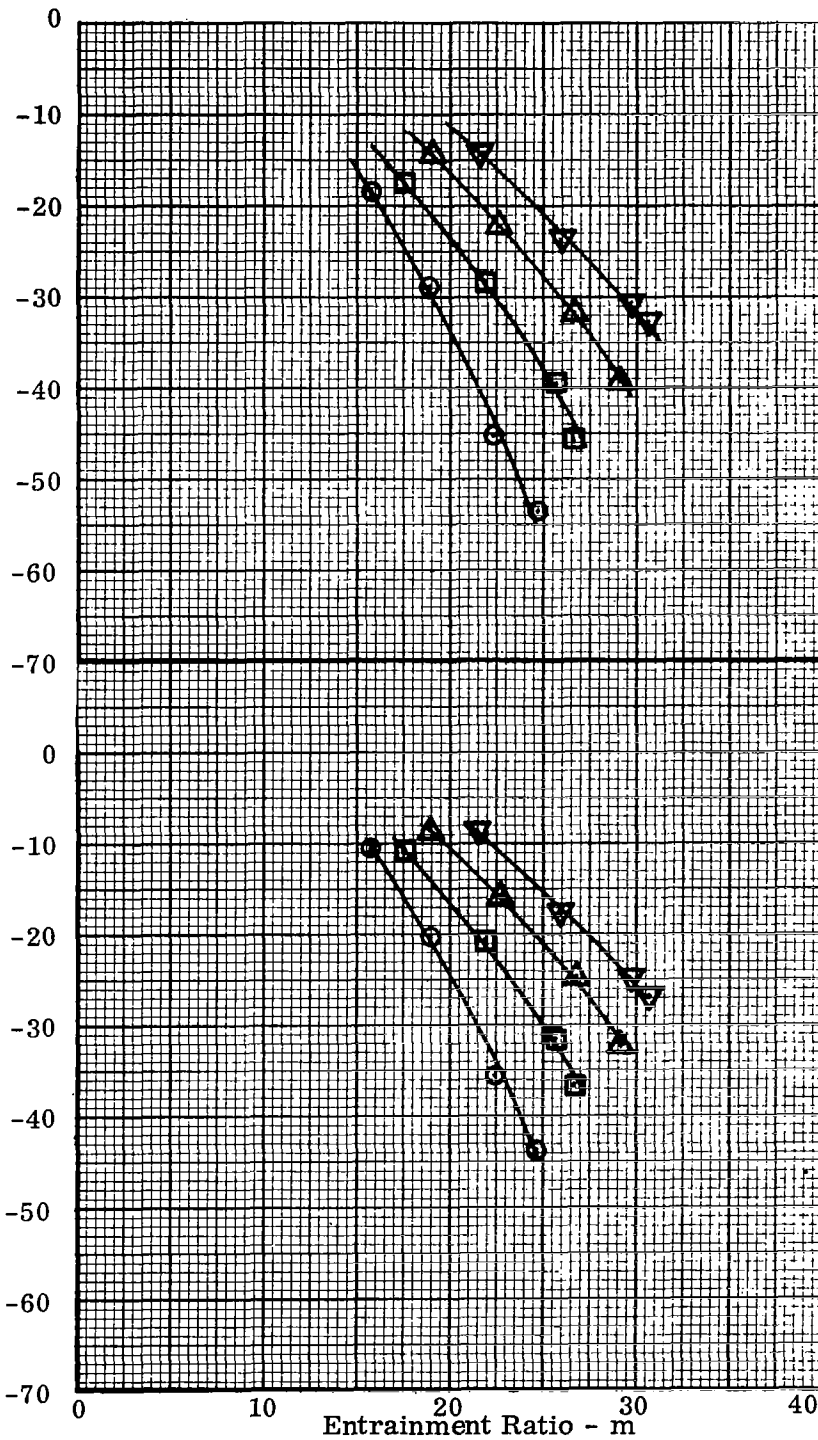
Figure 49
Velocity Profiles at Diffuser Discharge

$$d = 5.084'' \quad \frac{A_d}{A_m} = 1.61$$

Short Constant Area Mixing Tube
 Original Nozzle Cluster - Case 4 Nozzles

P - Static Pressure 0.81 Inches Downstream
of Primary Nozzle Discharge - Inches of
Water Gage (tap #18)

P - Static Pressure At - Inches Water
Mixing Tube Discharge
Gage



	P _{po} psia	T _{po} ° F
○	350	1130°
□	300	1160°
△	260	1165°
▽	225	1158°

Figure 50

Static Pressures in Mixing Tube
Short Constant Area Mixing Tube
Original Nozzle Cluster
Case 4 Nozzles

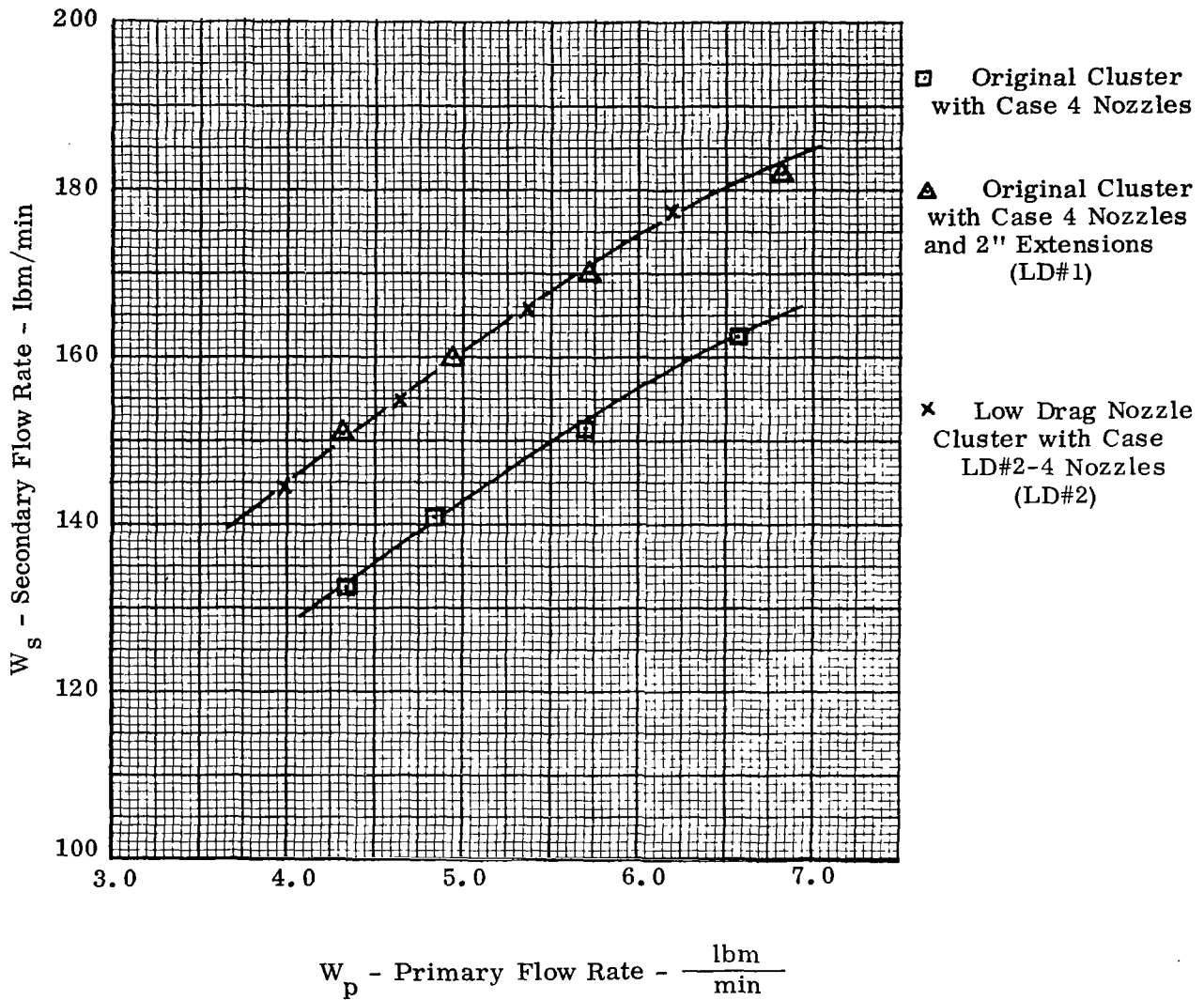


Figure 51
 Secondary Flow Vs. Primary Flow
 Wide Open Throttle Condition
 Short Constant Area Mixing Tube

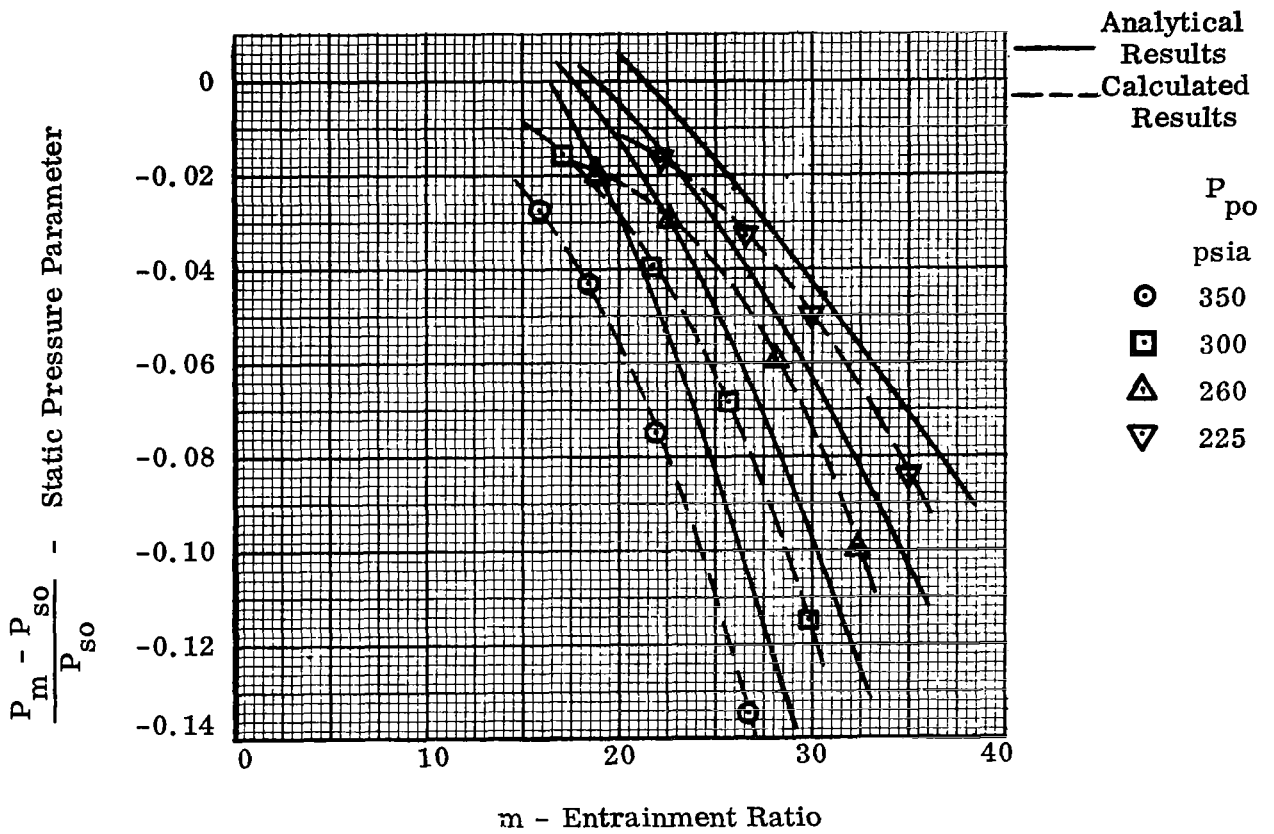
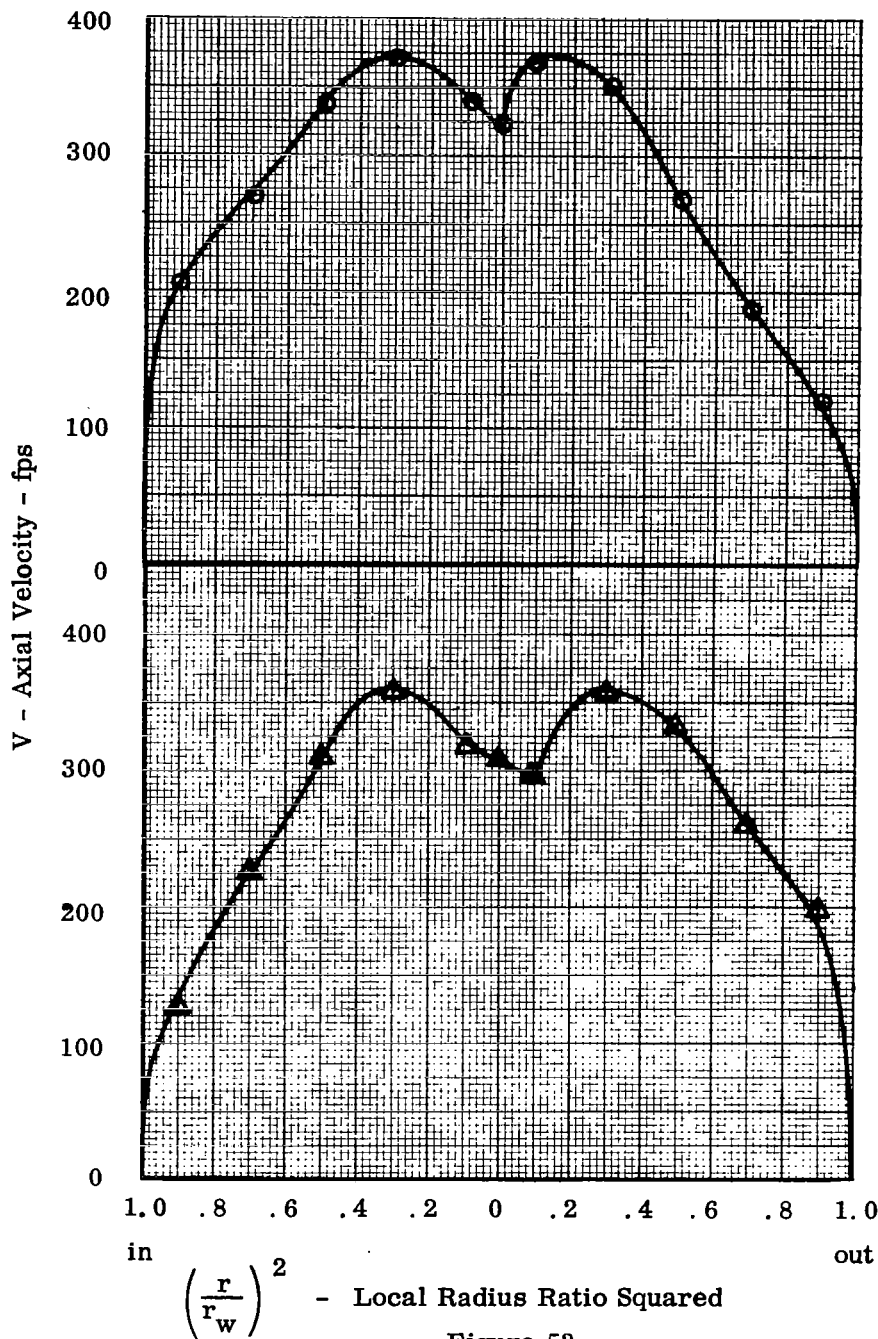


Figure 52

Jet Pump Static Pressure Parameter Calculated at
Mixing Tube Discharge

Short Constant Area Mixing Tube
Low-Drag Nozzle Cluster #1
Case 4 Nozzles



Velocity Profile with Heated Primary Flow

Run 41

- $P_{po} = 300$ psia
- $T_{po} = 1187$ °F
- $W_p = 5.75$ lbm/min
- $W_s = 146.9$ lbm/min
- $m = 25.6$

Velocity Profile with Unheated Primary Flow

- $P_{po} = 197$ psia
- $T_{po} = 92$ °F
- $W_p = 6.26$ lbm/min
- $W_s = 143$ lbm/min
- $m = 22.85$

Figure 53

Velocity Profiles at Diffuser Discharge

$$d = 5.084'' \quad \frac{A_d}{A_m} = 1.61$$

Short Constant Area Mixing Tube
LD#1 Nozzle Cluster
Case 4 Nozzles

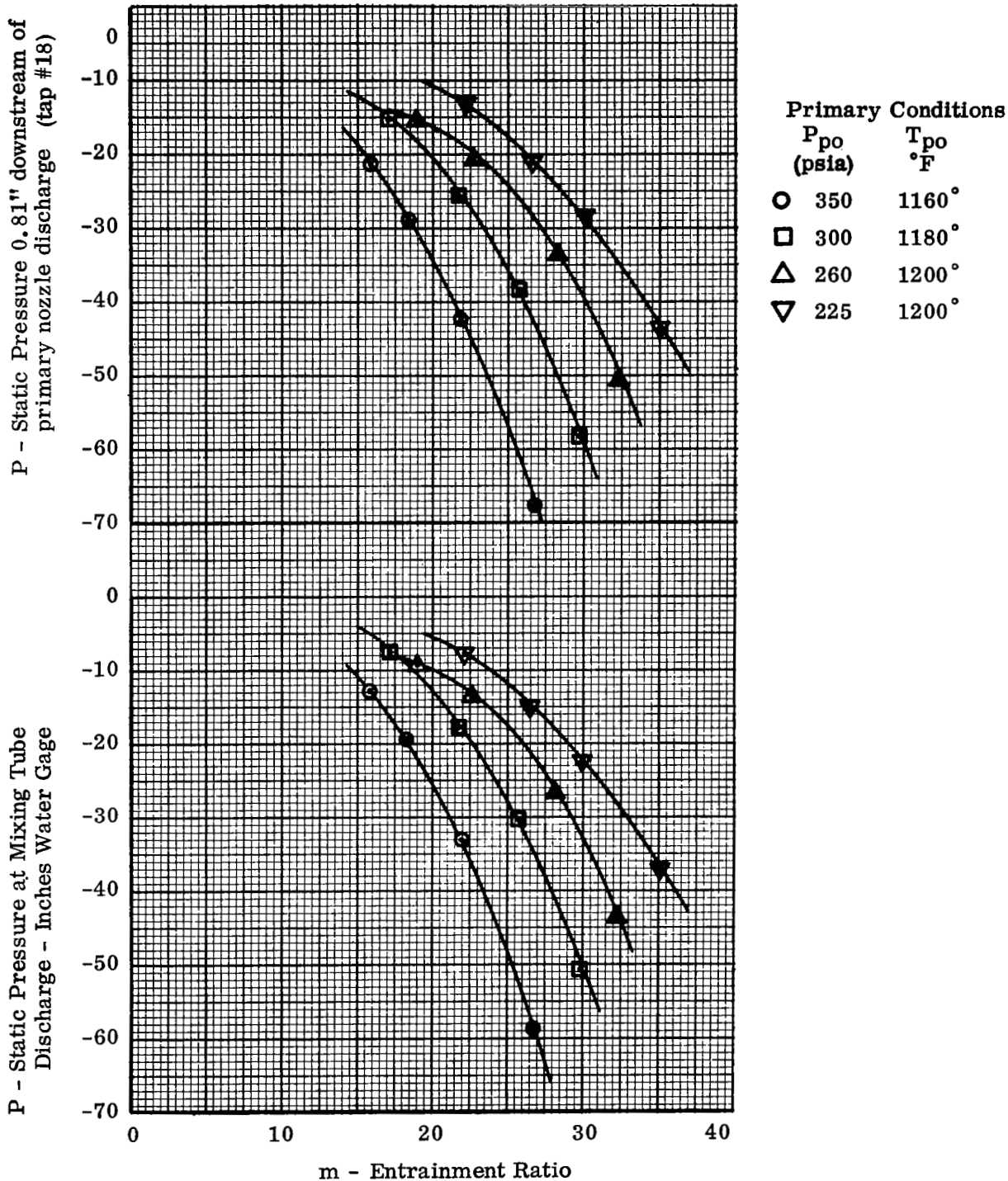


Figure 54
 Static Pressures in Mixing Tube
 Short Constant Area Mixing Tube
 LD #1 Nozzle Cluster
 Case 4 Nozzles

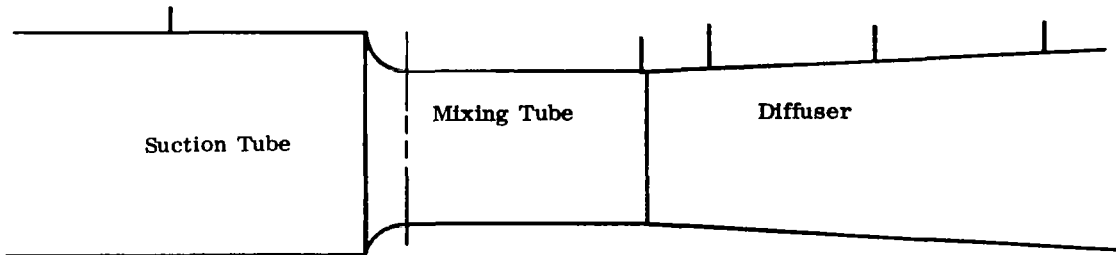
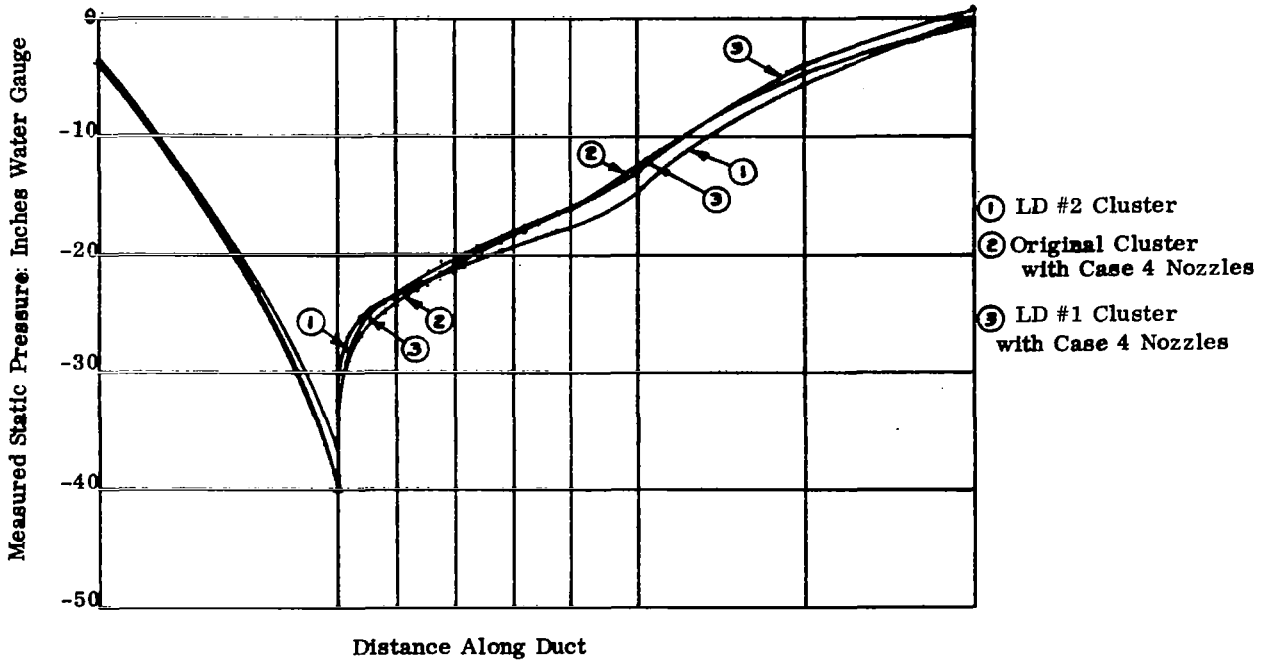


Figure 55

Variation of Static Pressure in Mixing Tube and Diffuser
for Three Nozzle Clusters

$$\begin{aligned}
 P_{po} &= 350 \text{ psia} \\
 T_{po} &= 1100^\circ \text{ F to } 1200^\circ \text{ F} \\
 W_m &= 124.9 \text{ lbm/min}
 \end{aligned}$$

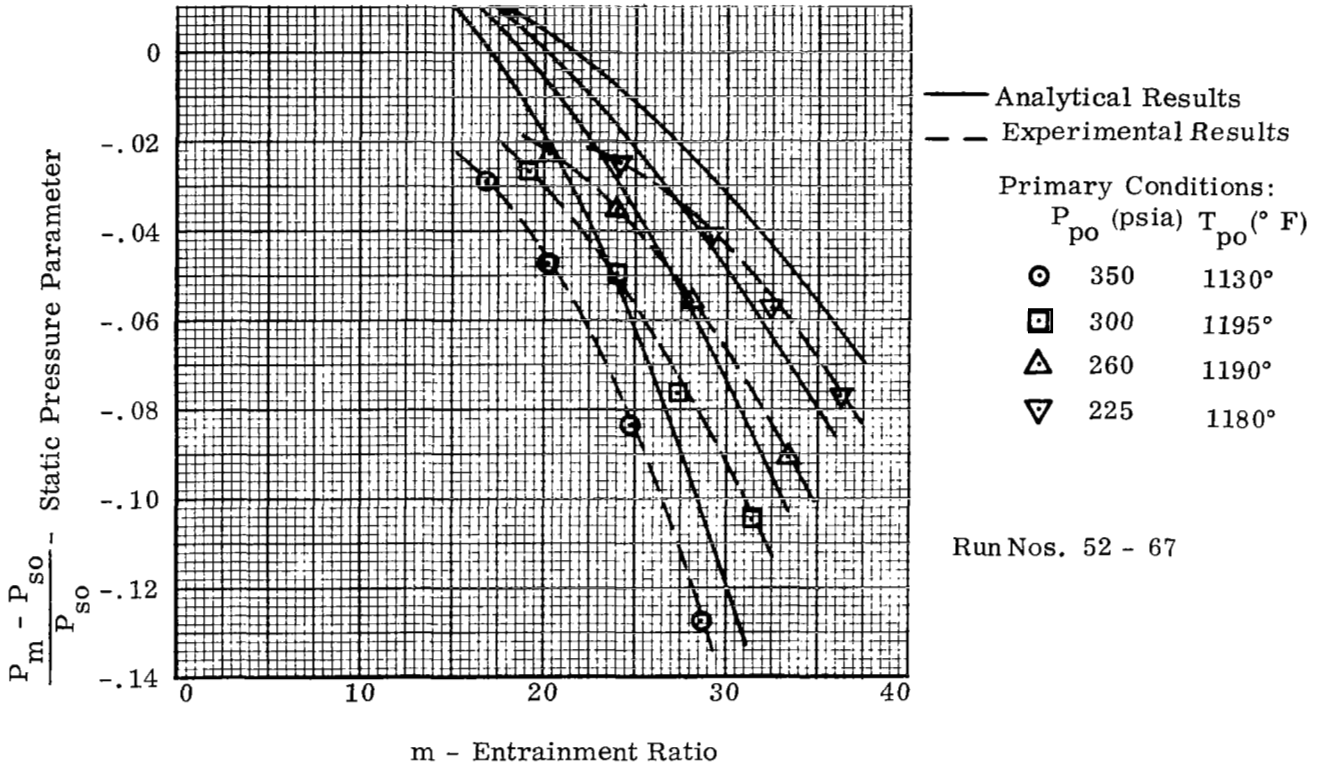


Figure 56

Jet Pump Static Pressure Parameters Calculated at
 Mixing Tube Discharge
 Short Constant Area Mixing Tube
 Low-Drag Nozzle Cluster #2
 LD #2-4 Nozzles (7 Nozzles)

Traverse Station
Orientation Viewed from
Bellmouth

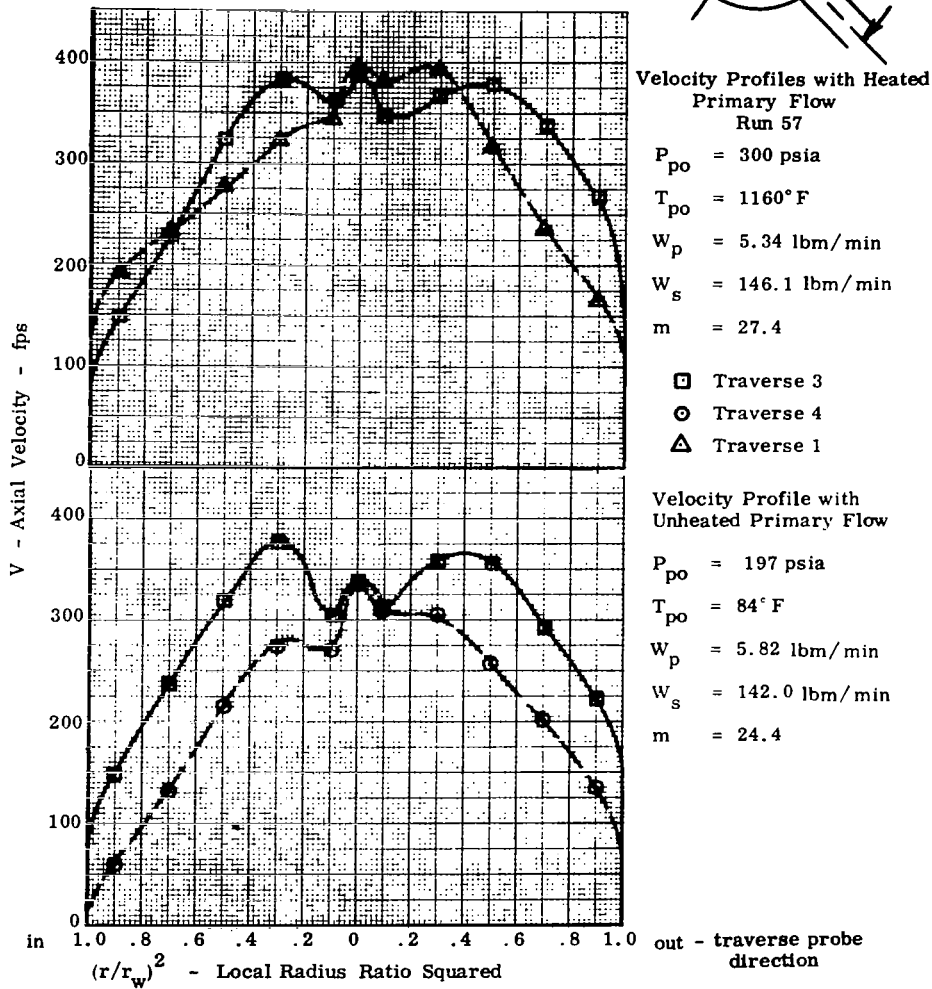
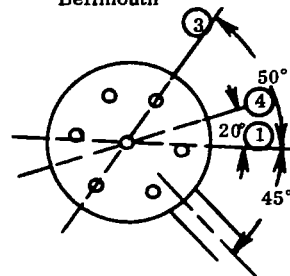


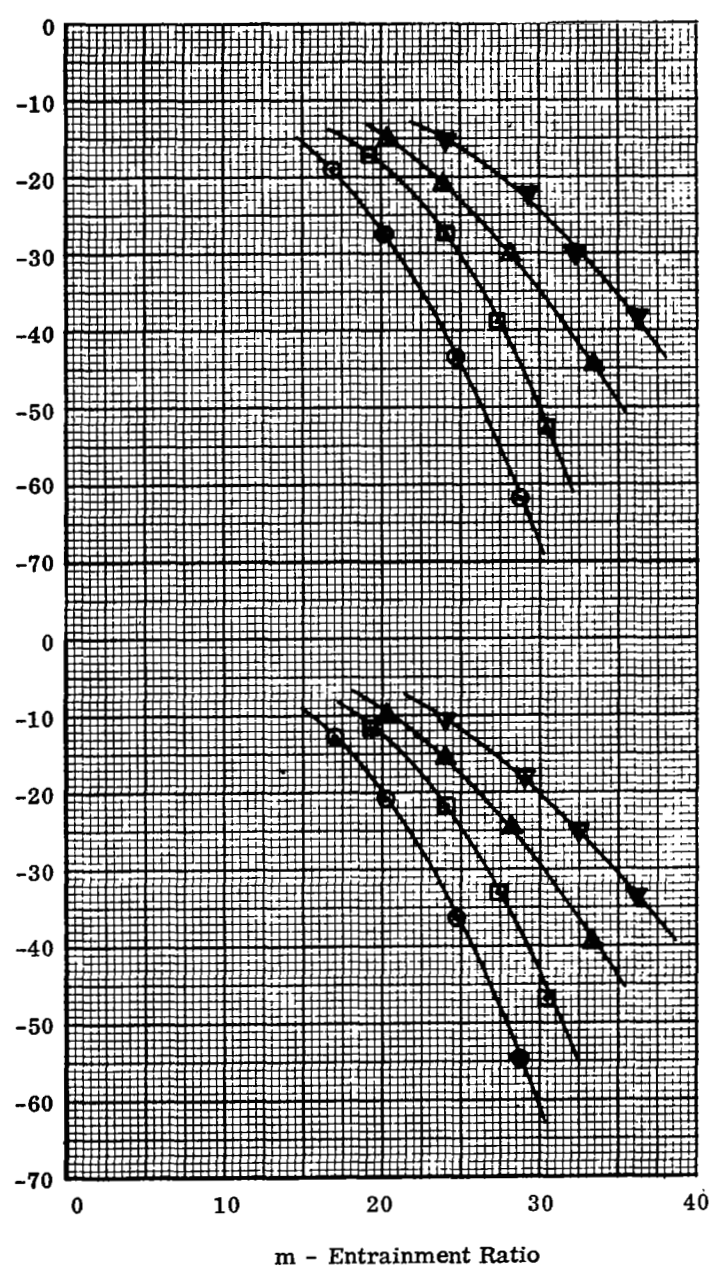
Figure 57
Velocity Profiles at Diffuser Discharge

$$d = 5.084'' \quad \frac{A_d}{A_m} = 1.61$$

Short Constant Area Mixing Tube
LD #2 Nozzle Cluster
LD #2-4 Nozzles

P - Static Pressure 0.81" downstream of primary nozzle
discharge - Inches Water Gage (tap #18)

P - Static Pressure at Mixing Tube
Discharge - Inches Water Gage



Primary Conditions	
P_{po} (psia)	T_{po} °F
○ 350	1130°
□ 300	1195°
△ 260	1190°
▽ 225	1185°

m - Entrainment Ratio
Figure 58

Static Pressures in Mixing Tube
Short Constant Area Mixing Tube
LD #2 Nozzle Cluster
LD #2-4 Nozzles

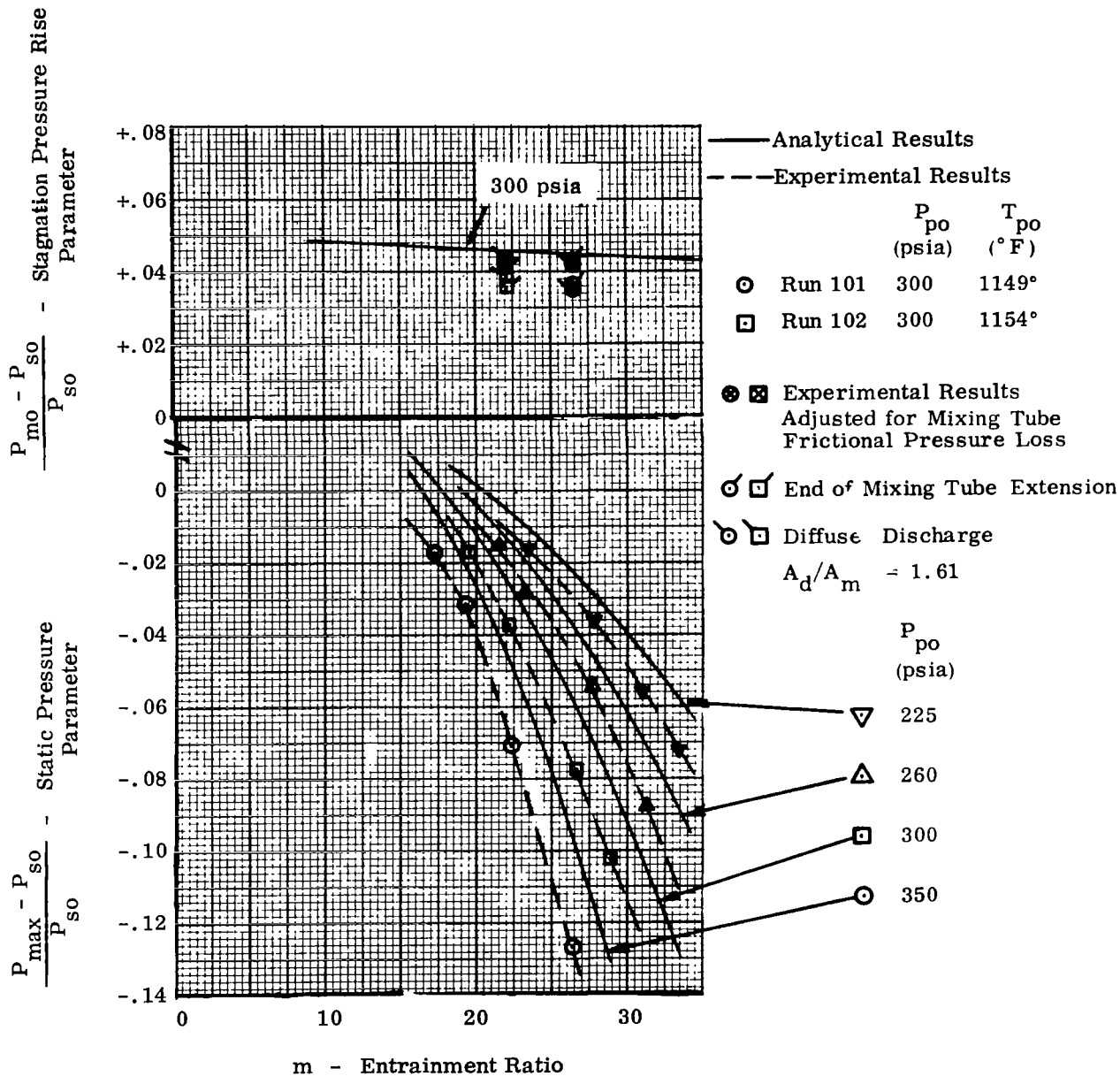


Figure 59
 Jet Pump Pressure Parameters
 Extended Constant Area Mixing Tube
 LD#1 Nozzle Cluster
 Case 4 Nozzles

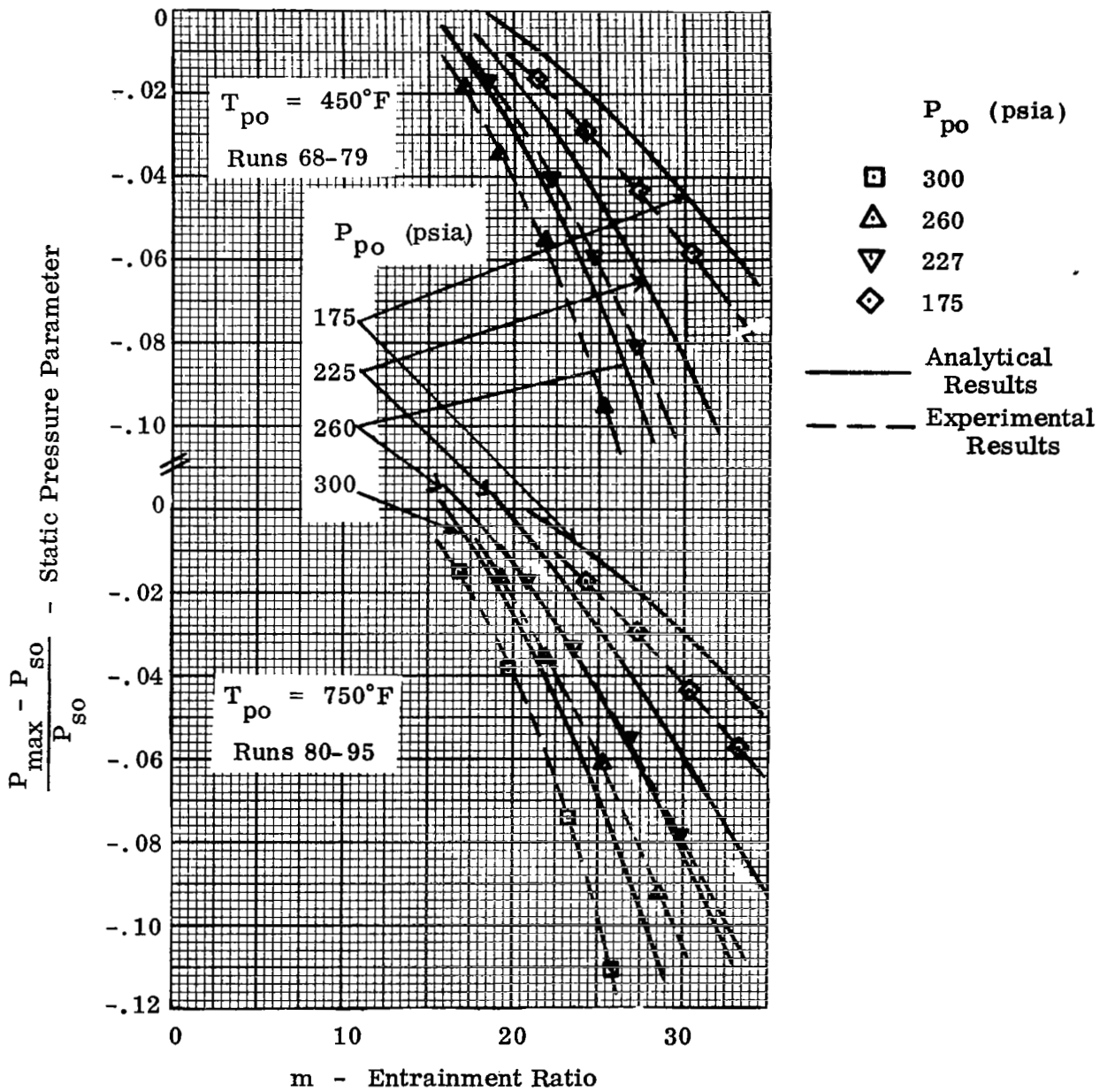


Figure 60

Jet Pump Static Pressure Parameter
 Extended Constant Area Mixing Tube
 LD #1 Nozzle Cluster
 Case 4 Nozzles

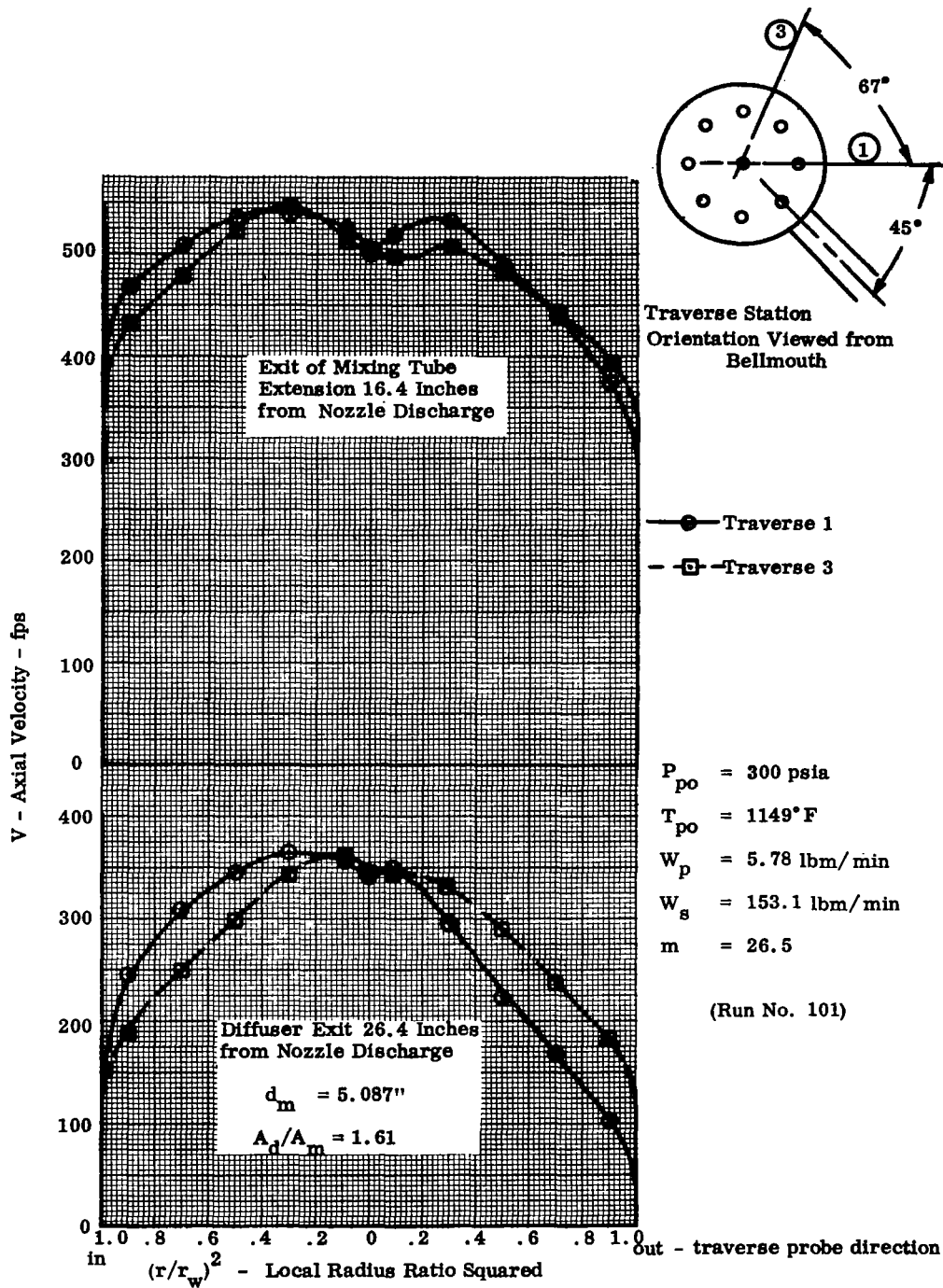


Figure 61
Velocity Profiles
Extended Constant Area Mixing Tube
LD#1 Nozzle Cluster — Case 4 Nozzles

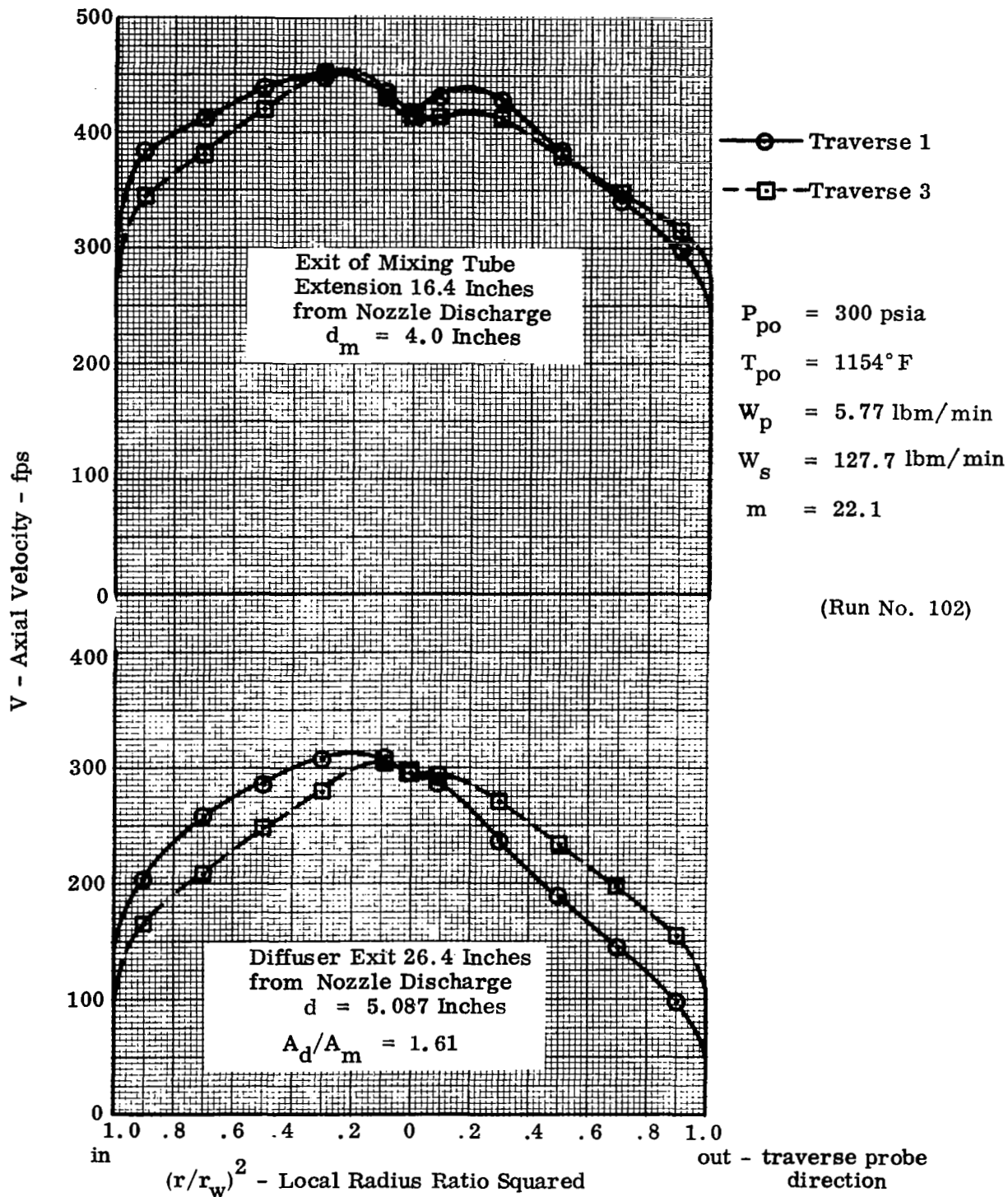


Figure 62
 Velocity Profiles
 Extended Constant Area Mixing Tube
 LD #1 Nozzle Cluster - Case 4 Nozzles

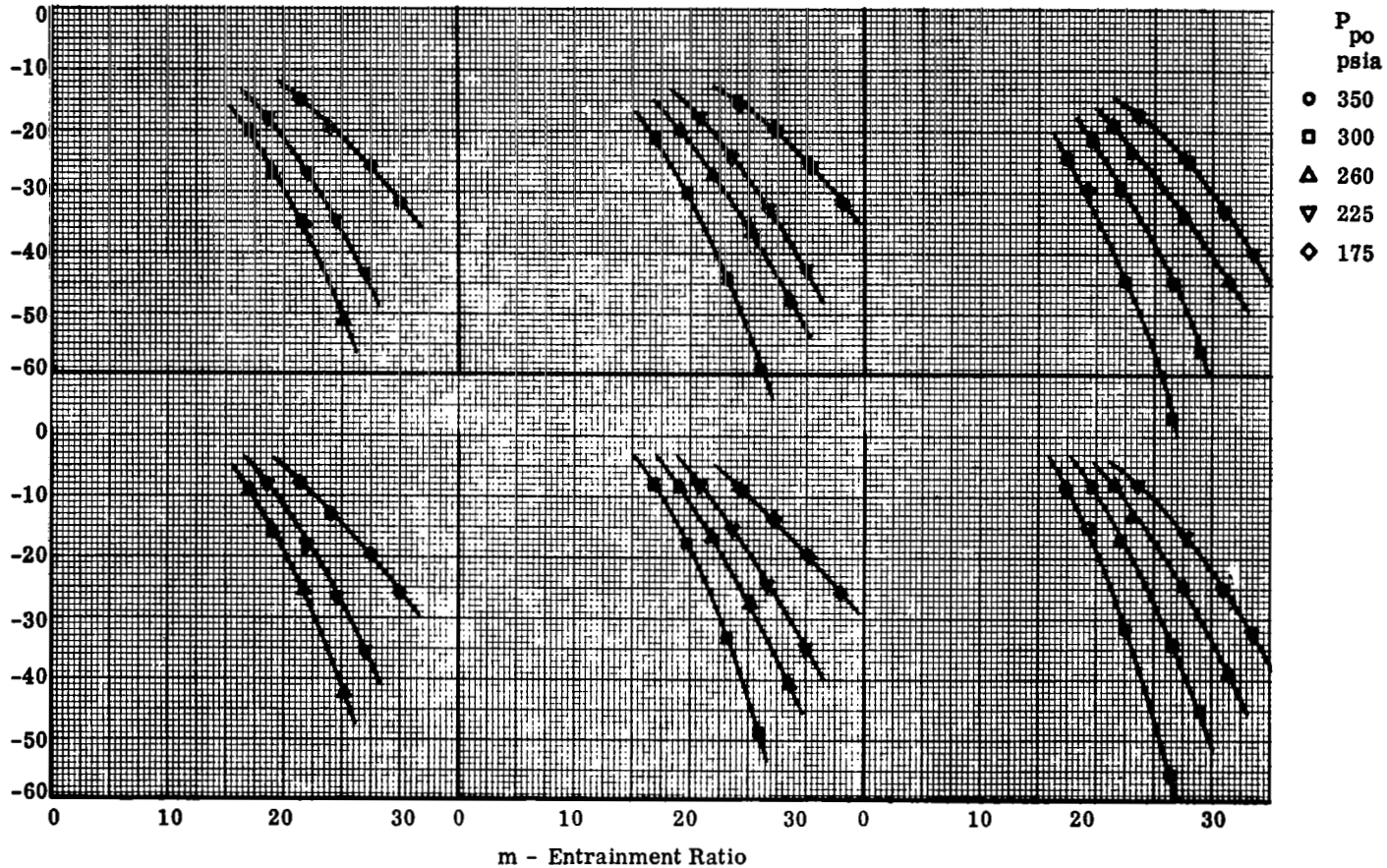
P - Static Pressure 0.81" downstream of primary nozzle discharge (tap #18)

P_{max} - Maximum Static Pressure In Mixing Tube - Inches Water Gage

T_{po} = 450°F
Runs 68 - 79

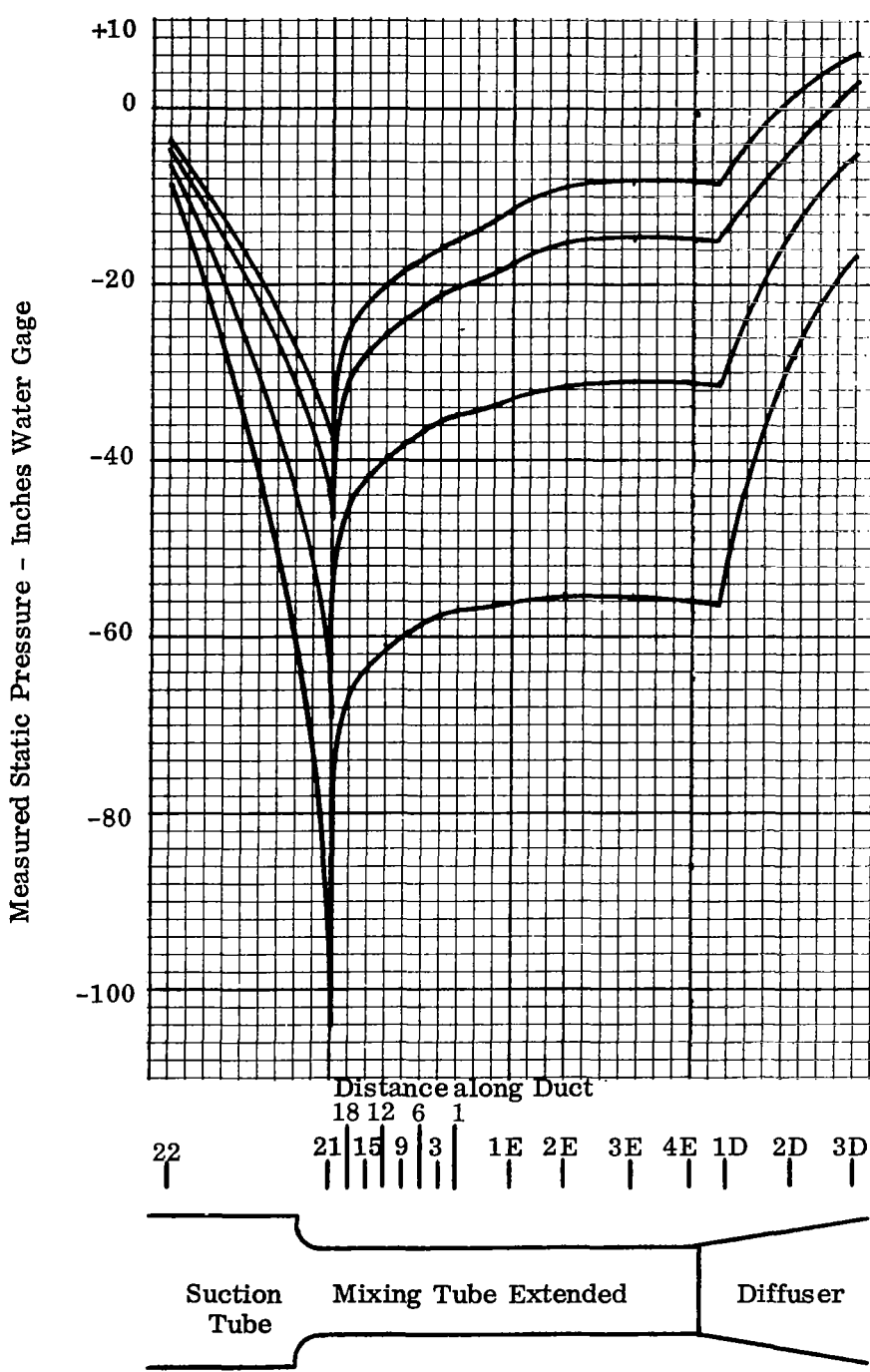
T_{po} = 750°F
Runs 80 - 95

T_{po} = 1100°-1200°F
Runs 96 - 111



Static Pressures in Extended Constant Area Mixing Tube
LD #1 Nozzle Cluster
Case 4 Nozzles

Figure 63



m Run No.

17.3 99

19.2 98

22.5 97

26.4 96

$P_{po} = 350$ psia

$T_{po} = 1112^{\circ}$ F

Figure 64

Variation of Static Pressure in Mixing Tube and Diffuser
 Extended Constant Area Mixing Tube
 LD #1 Nozzle Cluster - Case 4 Nozzles

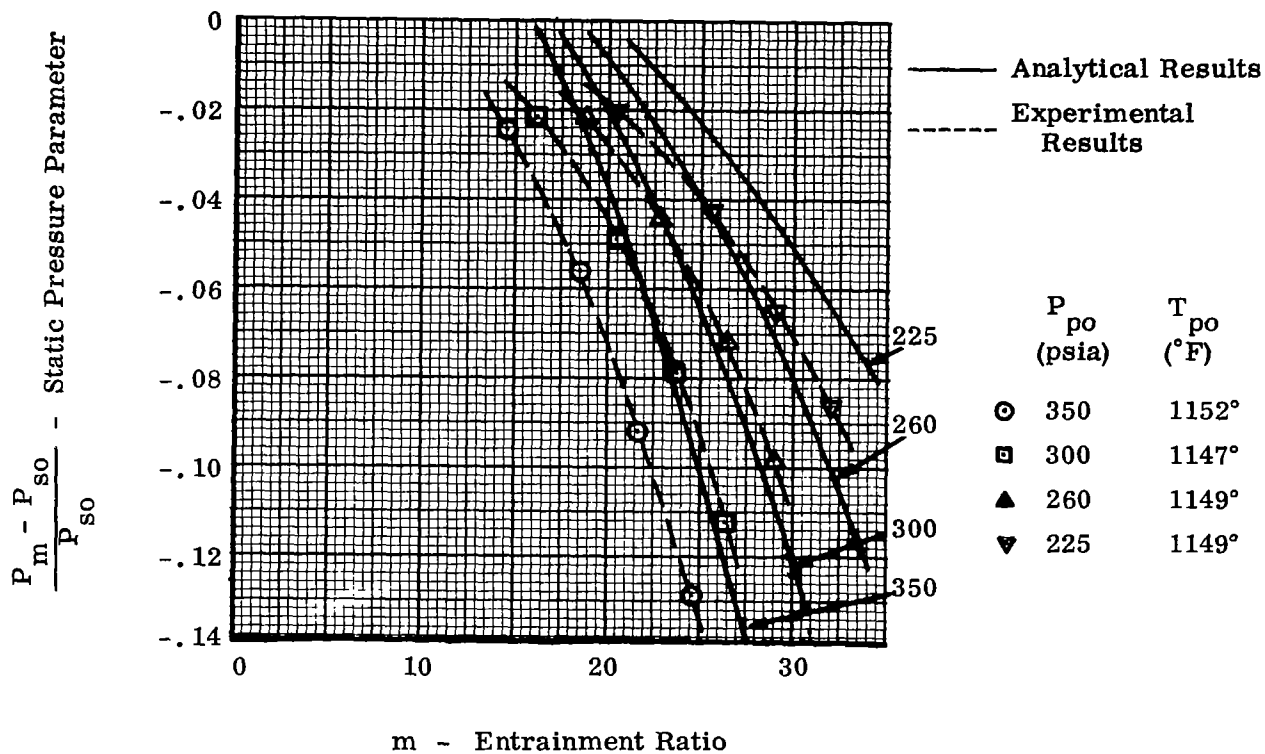


Figure 65

Jet Pump Static Pressure Parameter Calculated
 At the Mixing Tube Discharge
 Short Constant Area Mixing Tube
 LD #1 Nozzle Cluster - Case 4A Nozzles

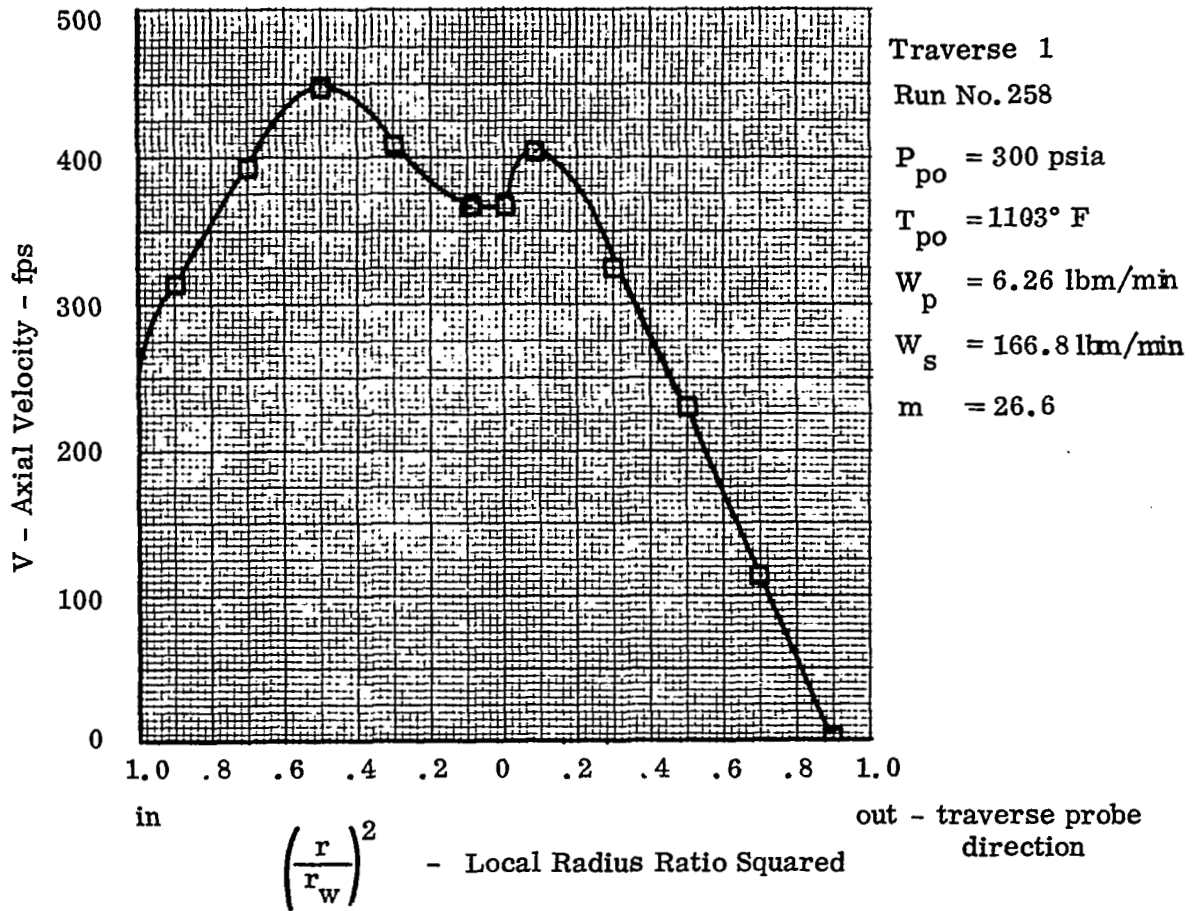


Figure 66

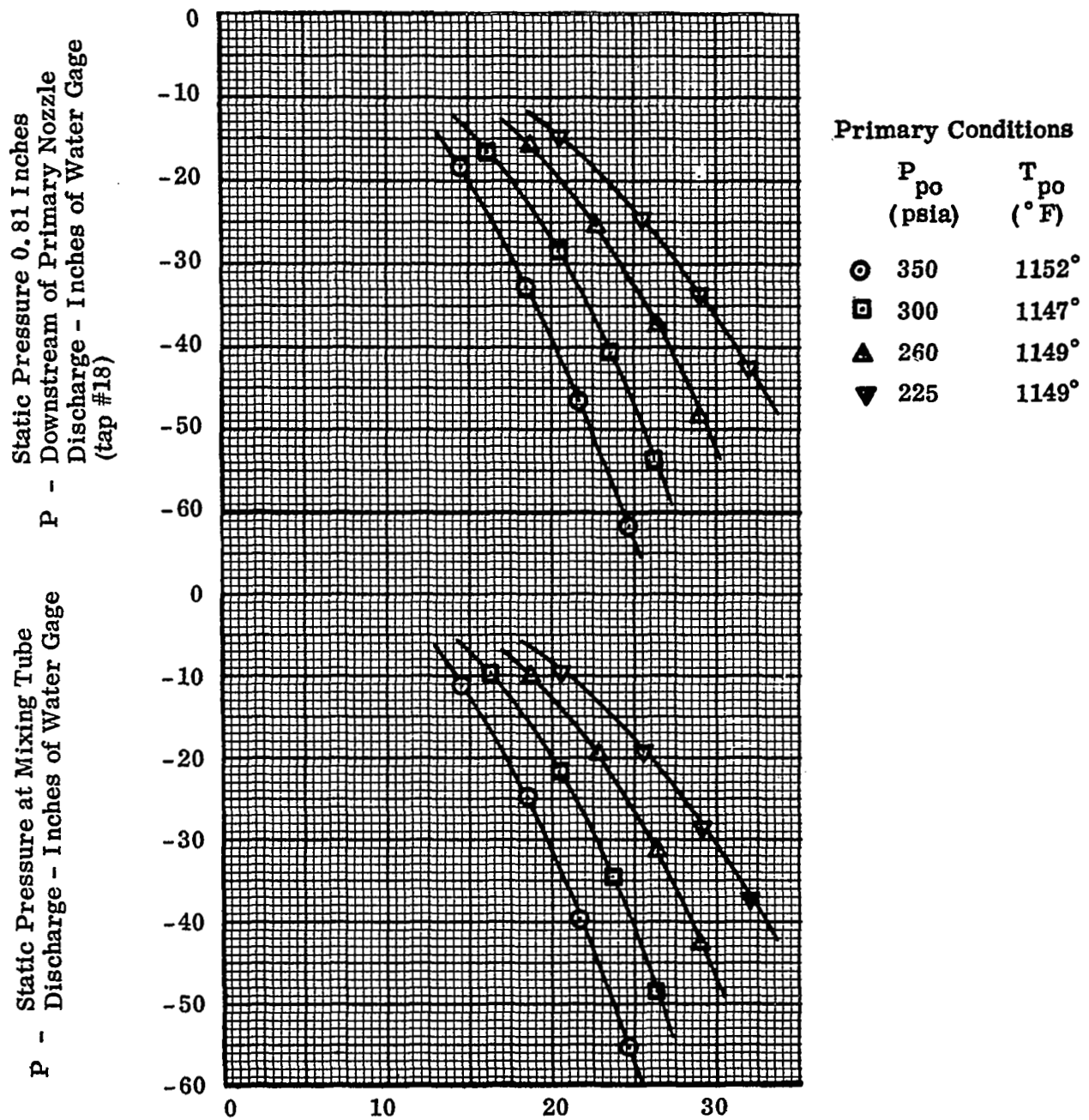
Velocity Profiles at Diffuser Discharge

$$d = 5.087''$$

$$A_d/A_m = 1.61$$

Short Constant Area Mixing Tube

LD #1 Nozzle Cluster - Case 4A Nozzles



m - Entrainment Ratio

Figure 67

Static Pressures in Mixing Tube
Short Constant Area Mixing Tube
LD #1 Nozzle Cluster
Case 4A Nozzles

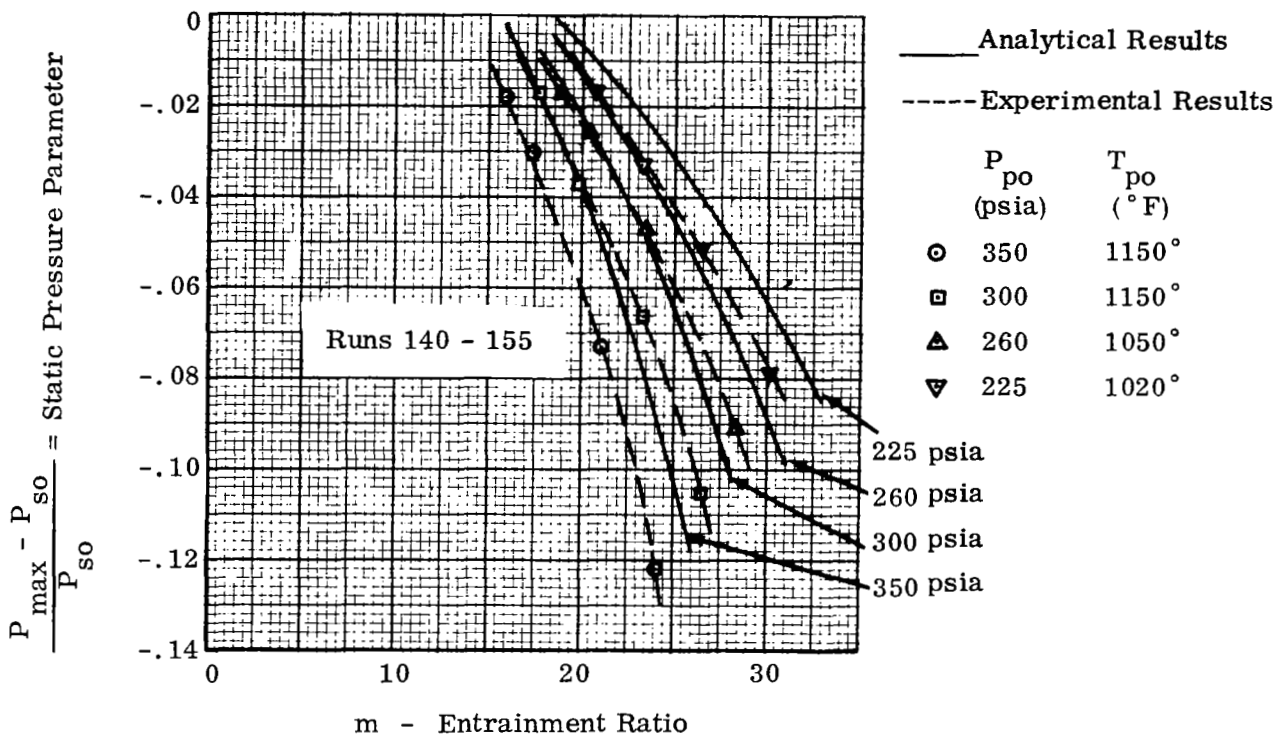


Figure 68

Jet Pump Static Pressure Parameter

Extended Constant Area Mixing Tube
LD #1 Nozzle Cluster

Case 4A Nozzles

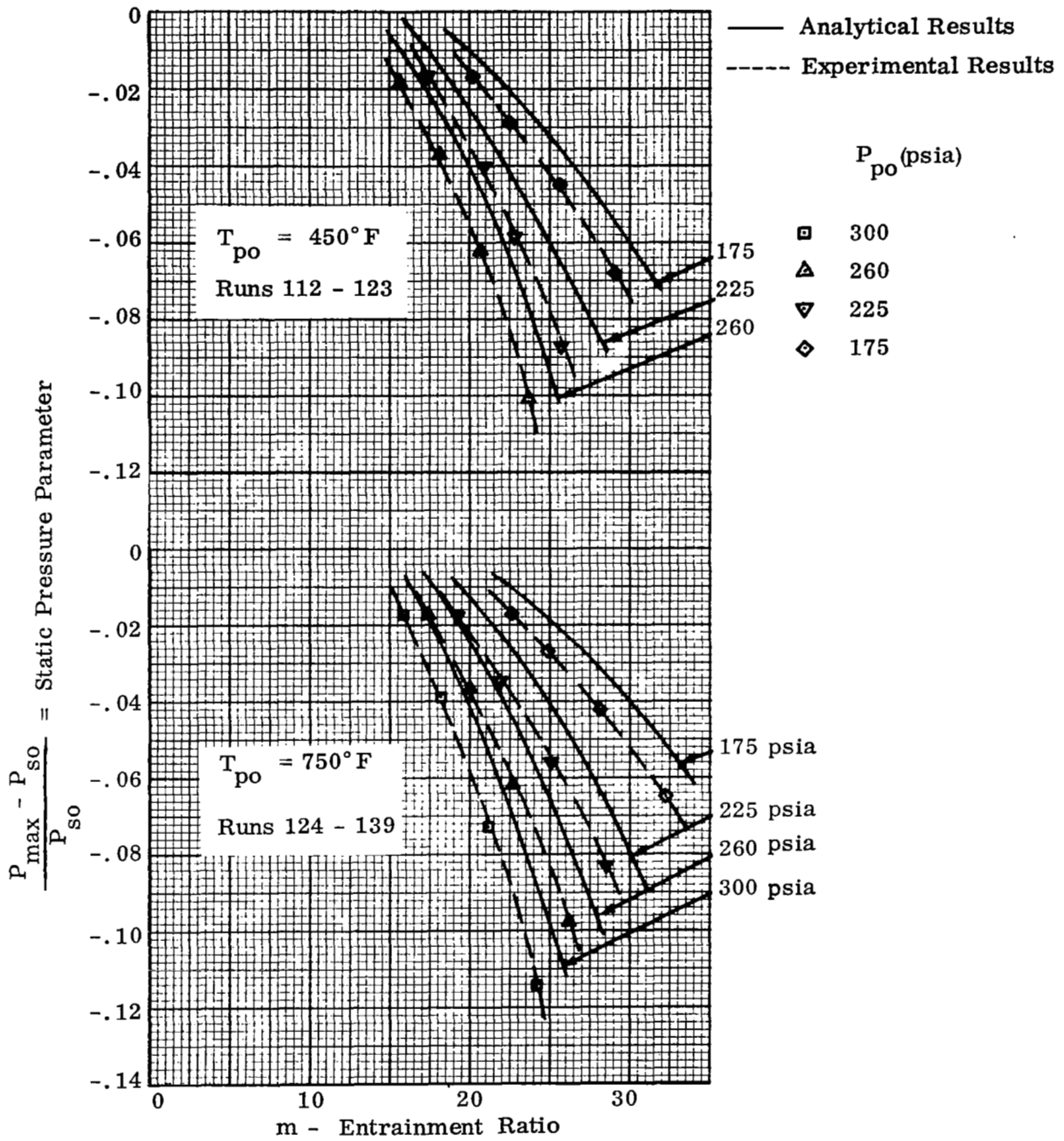


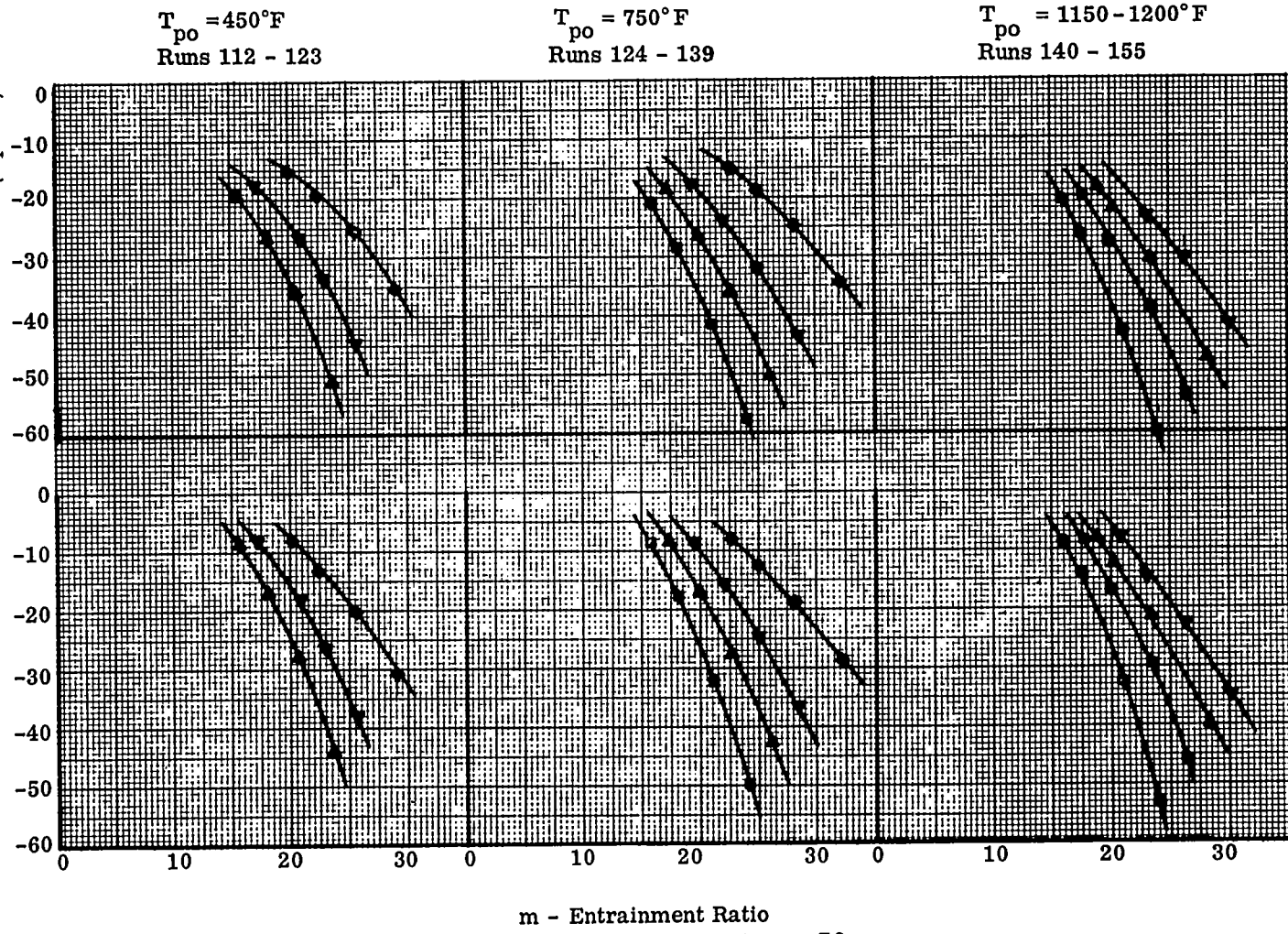
Figure 69
 Jet Pump Static Pressure Parameter
 Extended Constant Area Mixing Tube
 LD#1 Nozzle Cluster
 Case 4A Nozzles

Static Pressure, 0.81 Inches
Downstream of Primary Nozzle
Discharge - Inches Water Gage
(tap #18)

P -

Maximum Static Pressure In
Mixing Tube - Inches Water Gage

P_{max} -



P_{po}
psia

- 350
- 300
- △ 260
- ▽ 225
- ◇ 175

m - Entrainment Ratio

Figure 70

Static Pressures in Extended Constant Area Mixing Tube
LD #1 Nozzle Cluster - Case 4A Nozzles

Measured Static Pressure - Inches of Water Gage

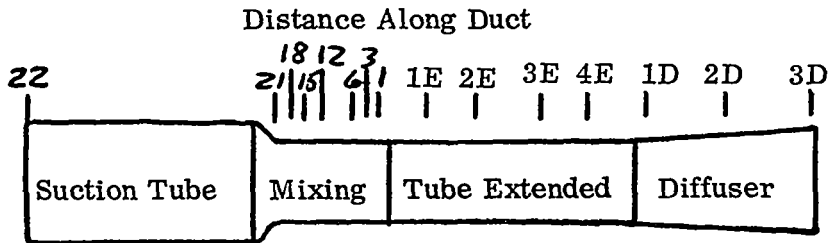
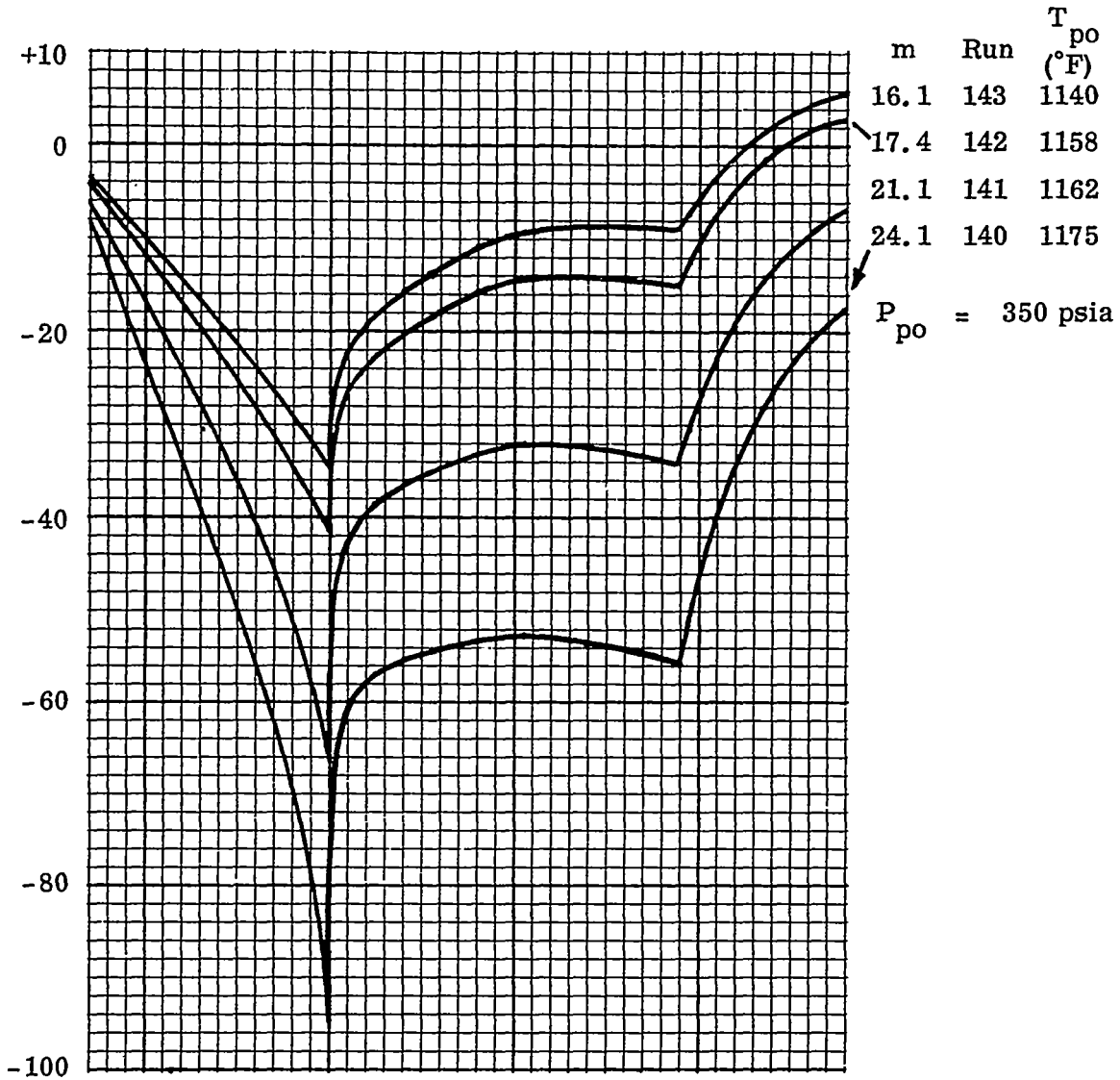


Figure 71

Variation of Static Pressure in Mixing Tube and Diffuser
 Extended Constant Area Mixing Tube
 LD #1 Nozzle Cluster
 Case 4A Nozzles

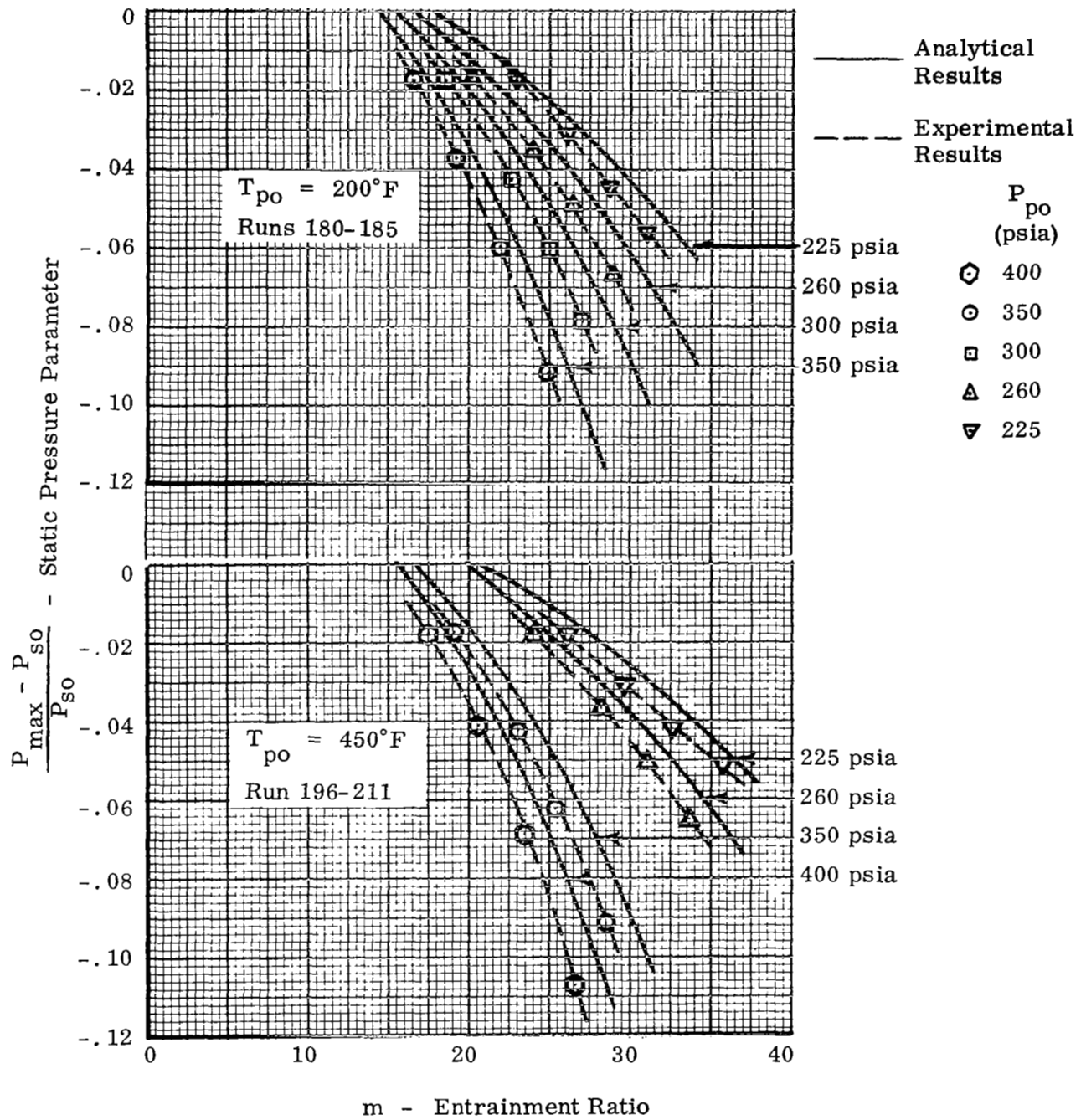


Figure 72

Jet Pump Static Pressure Parameter
 Extended Constant Area Mixing Tube
 LD#1 Nozzle Cluster - Case 2 Nozzles

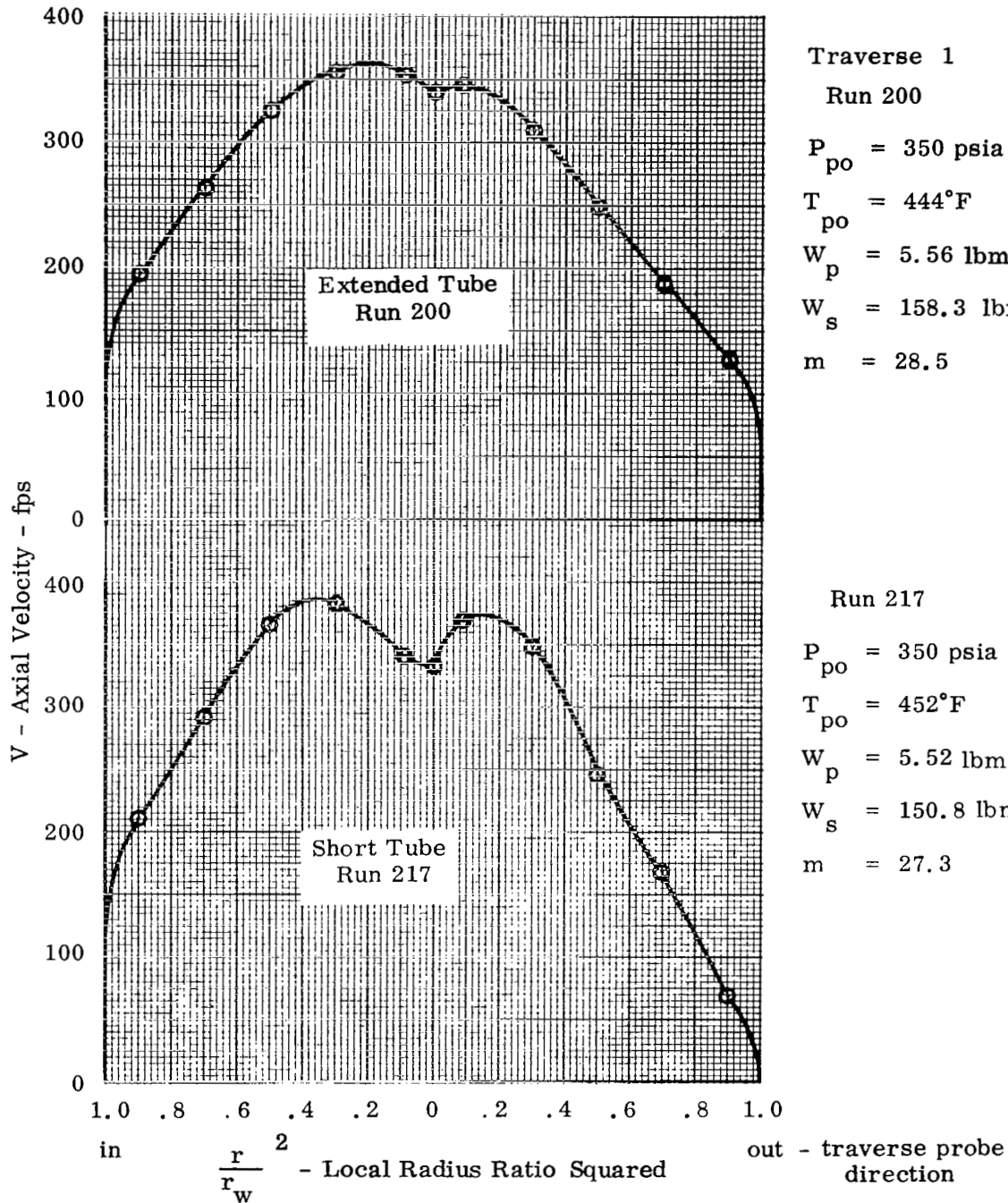


Figure 73

Velocity Profiles at Diffuser Discharge

$$d = 5.084'' \quad \frac{A_d}{A_m} = 1.61$$

Short and Extended Constant Area Mixing Tube
LD#1 Nozzle Cluster
Case 2 Nozzles

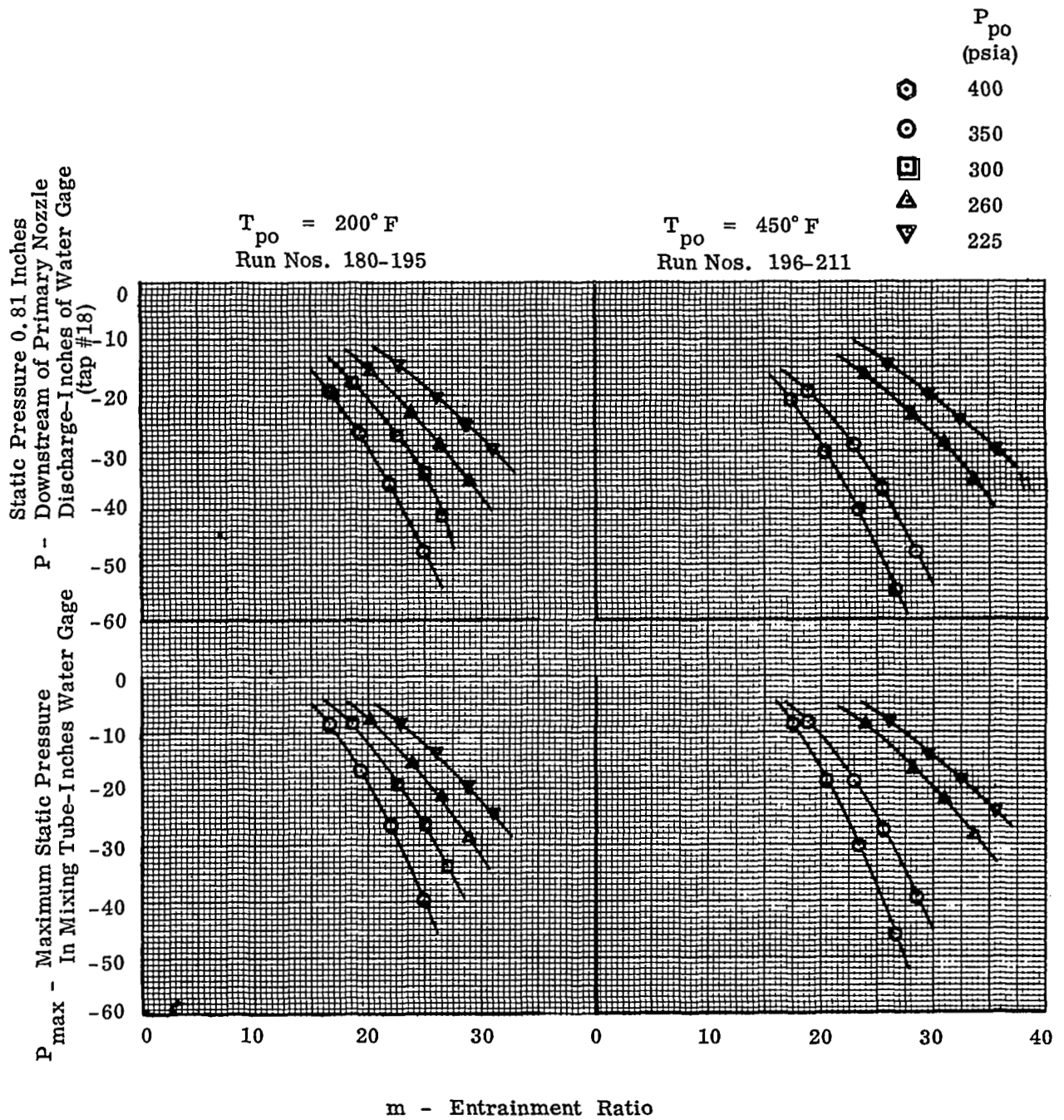


Figure 74

Static Pressures in Extended Constant Area Mixing Tube
LD #1 Nozzle Cluster
Case 2 Nozzles

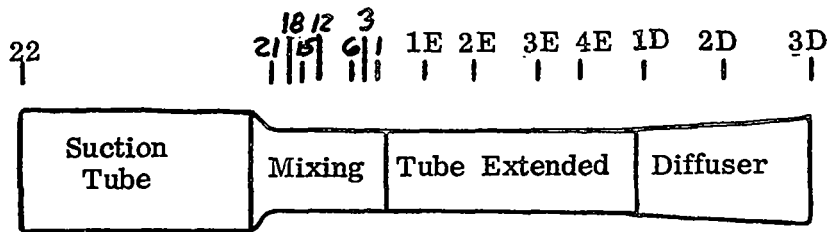
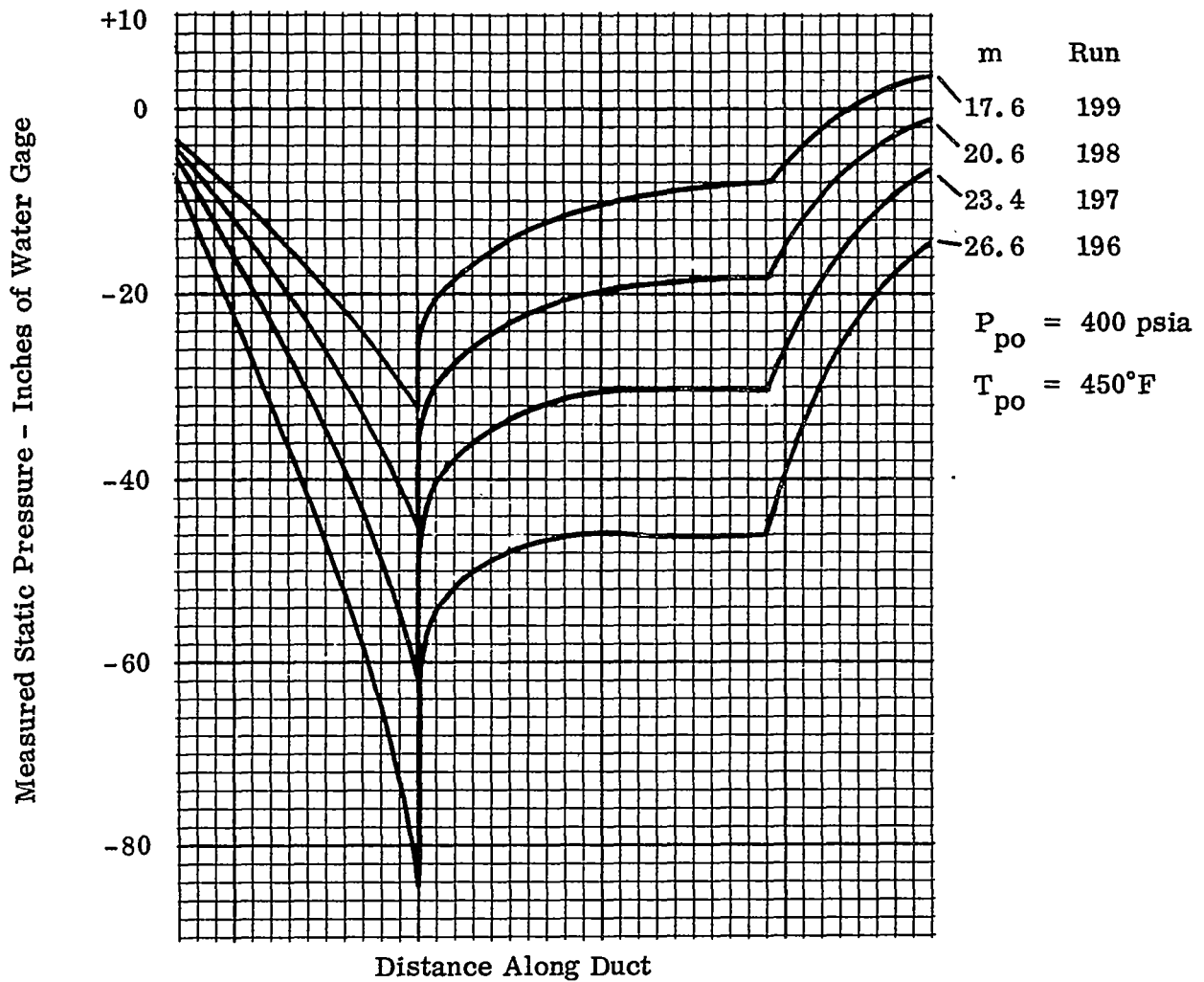


Figure 75

Variation of Static Pressure in Mixing Tube and Diffuser
 Extended Constant Area Mixing Tube
 LD #1 Nozzle Cluster - Case 2 Nozzles

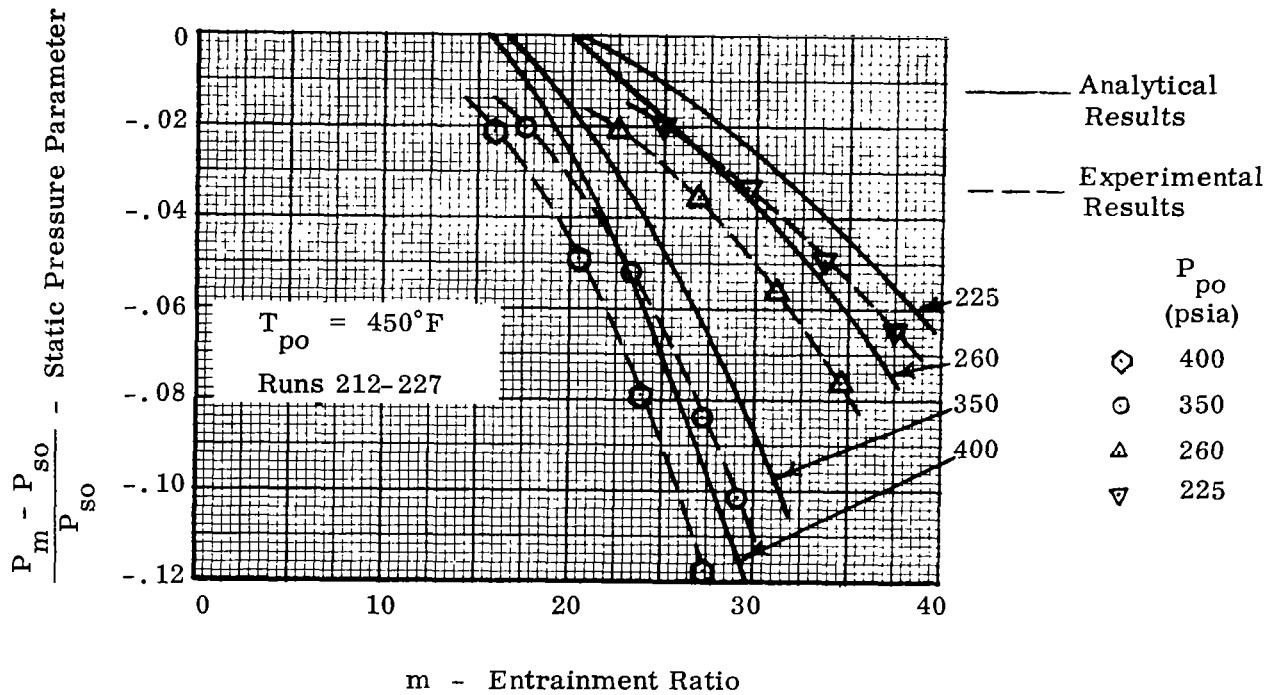


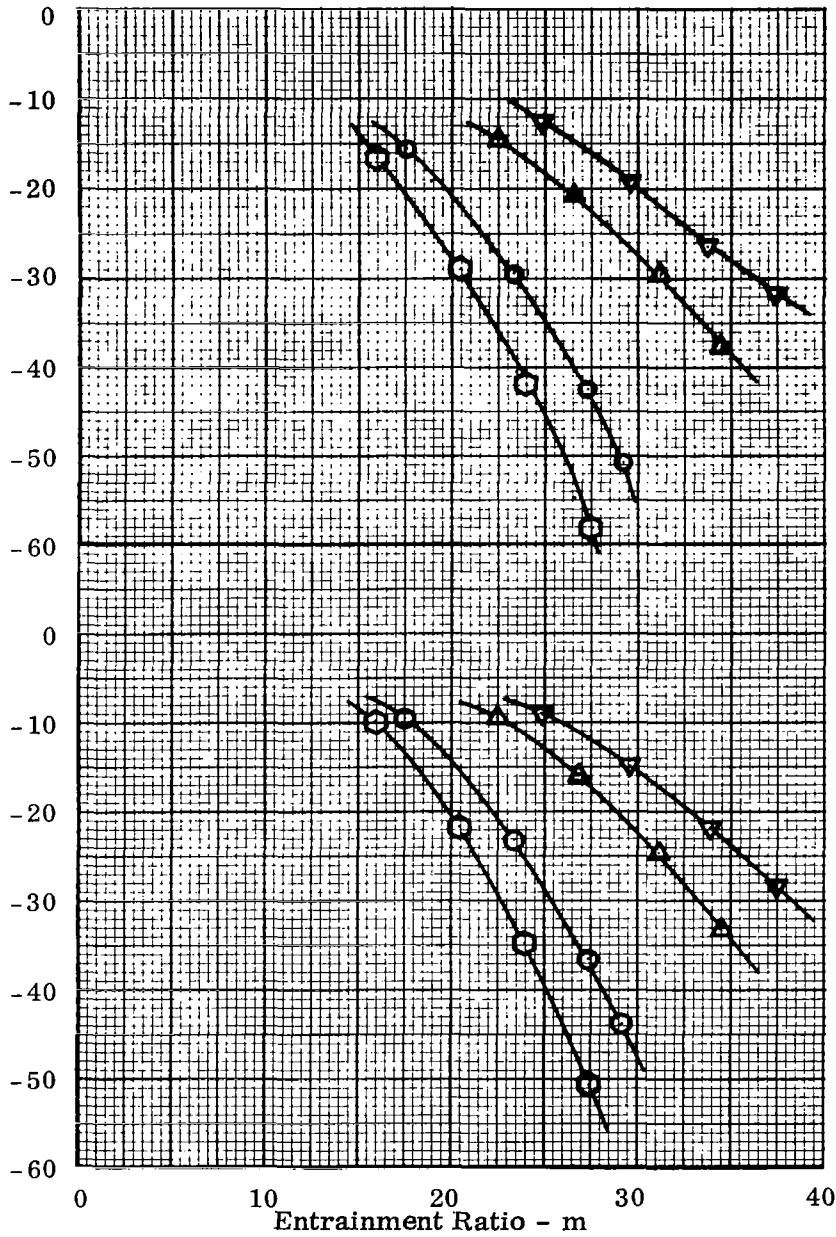
Figure 76

Jet Pump Static Pressure Parameter Calculated
 at the Mixing Tube Discharge
 Short Constant Area Mixing Tube

LD #1 Nozzle Cluster
 Case 2 Nozzles

Static Pressure 0.81 Inches Downstream
of Primary Nozzle Discharge-Inches of
Water Gage (tap #18)

Static Pressure at Mixing Tube
Discharge-Inches of Water Gage



Run Nos. 212-227

Primary Conditions

	P_{po} (psia)	T_{po} (°F)
⊙	400	458°
○	350	454°
△	260	451°
▽	225	448°

Figure 77
Static Pressures in Mixing Tube
Short Constant Area Mixing Tube
LD #1 Nozzle Cluster
Case 2 Nozzles

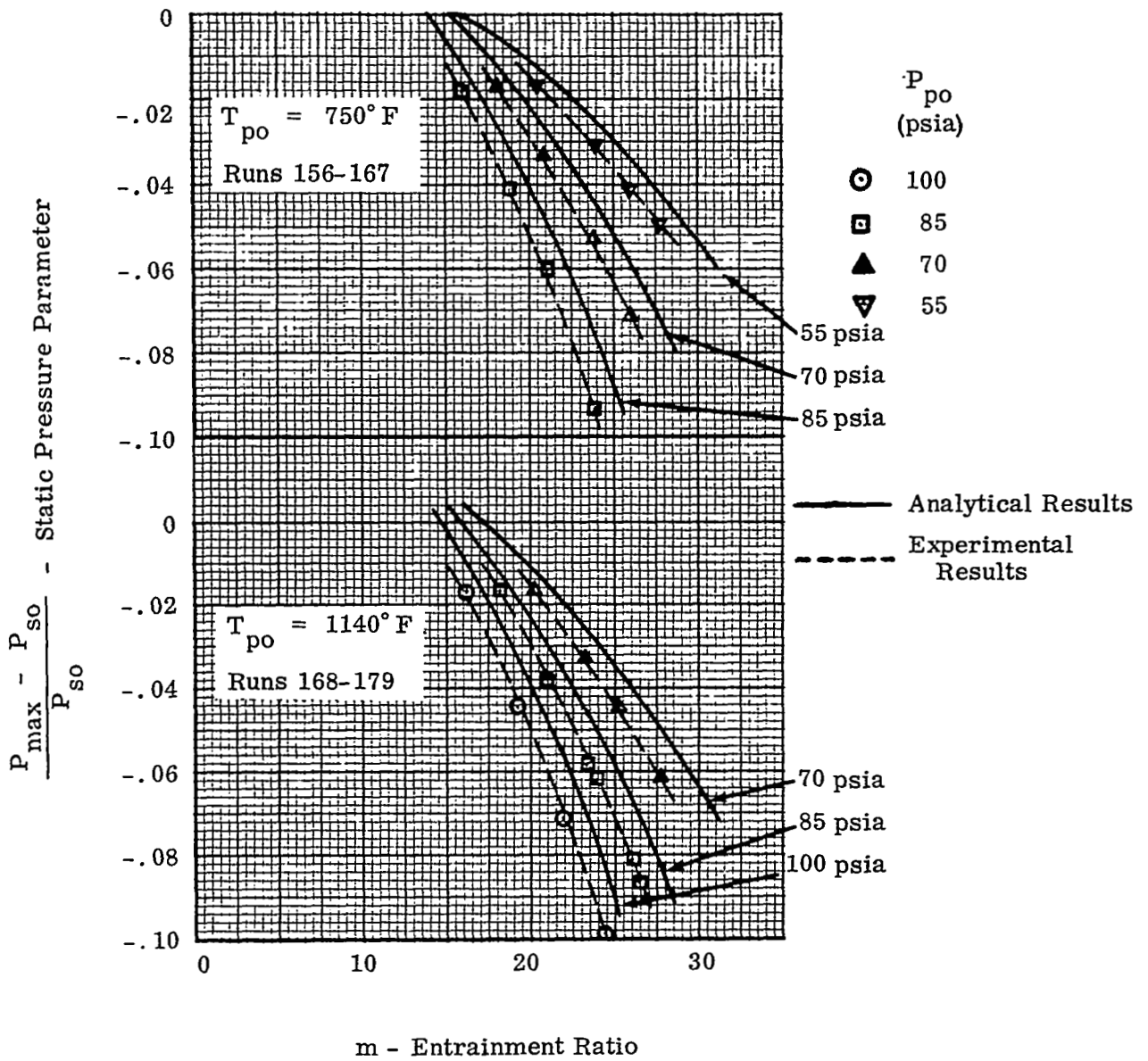


Figure 78
 Jet Pump Static Pressure Parameter
 Extended Constant Area Mixing Tube
 LD #1 Nozzle Cluster
 Case 3 Nozzles

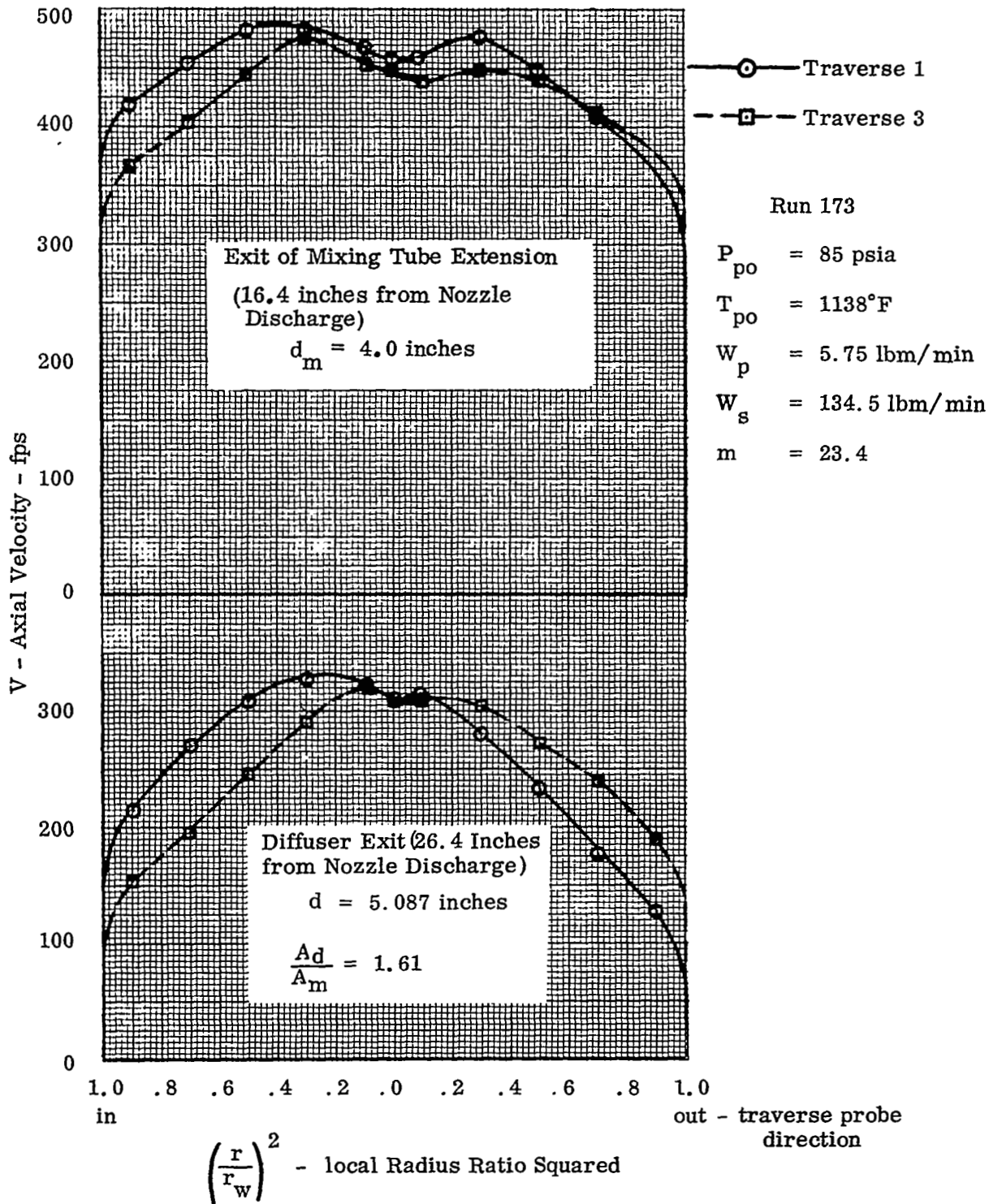


Figure 79
 Velocity Profiles
 Extended Constant Area Mixing Tube
 LD#1 Nozzle Cluster
 Case 3 Nozzles

Static Pressure 0.81 Inches
 P - Downstream of Primary Nozzle Discharge
 -Inches Water Gage (tap #18)

Maximum Static Pressure
 In Mixing Tube
 P_{max} - Inches Water Gage

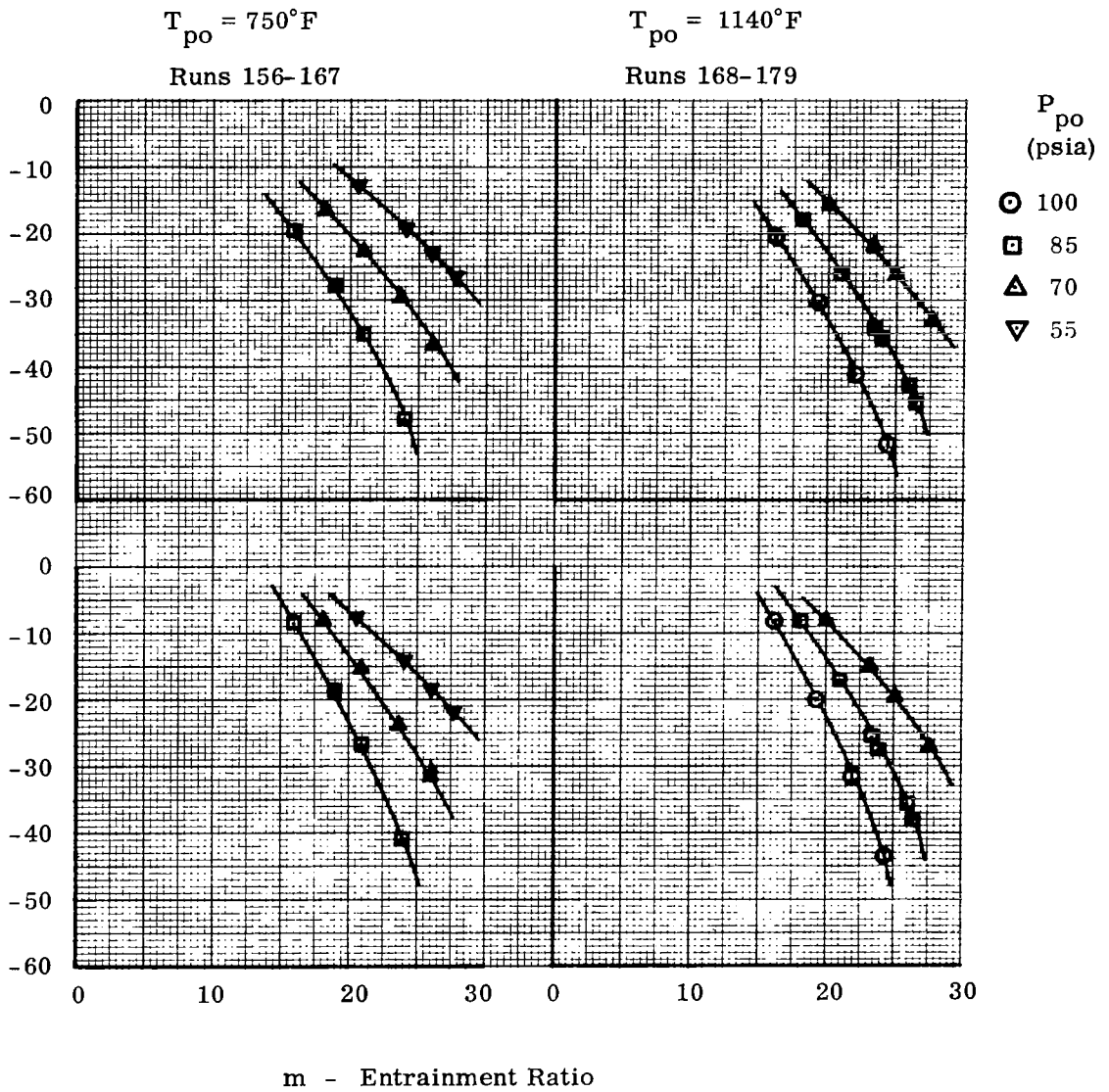


Figure 80

Static Pressures in Extended Constant Area Mixing Tube
 LD #1 Nozzle Cluster
 Case 3 Nozzles

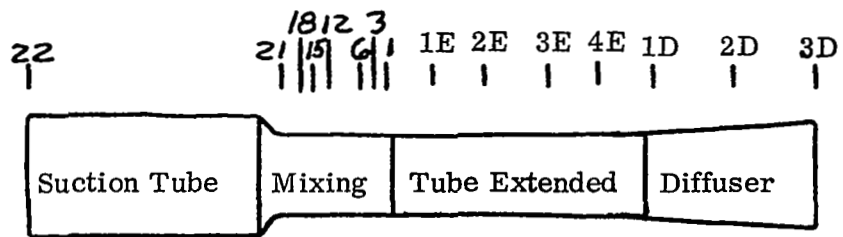
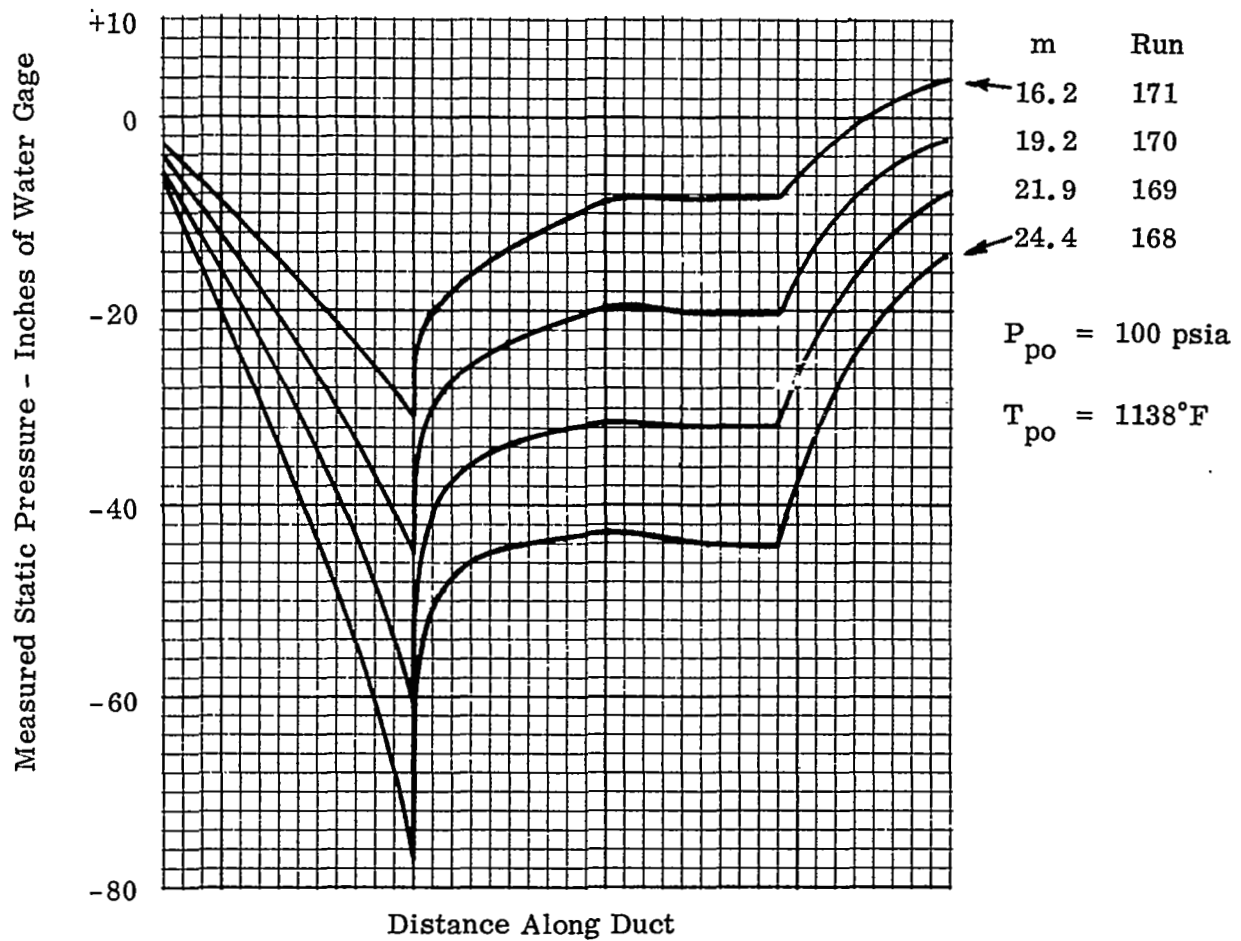


Figure 81

Variation of Static Pressure in Mixing Tube and Diffuser
 Extended Constant Area Mixing Tube

LD #1 Nozzle Cluster
 Case 3 Nozzles

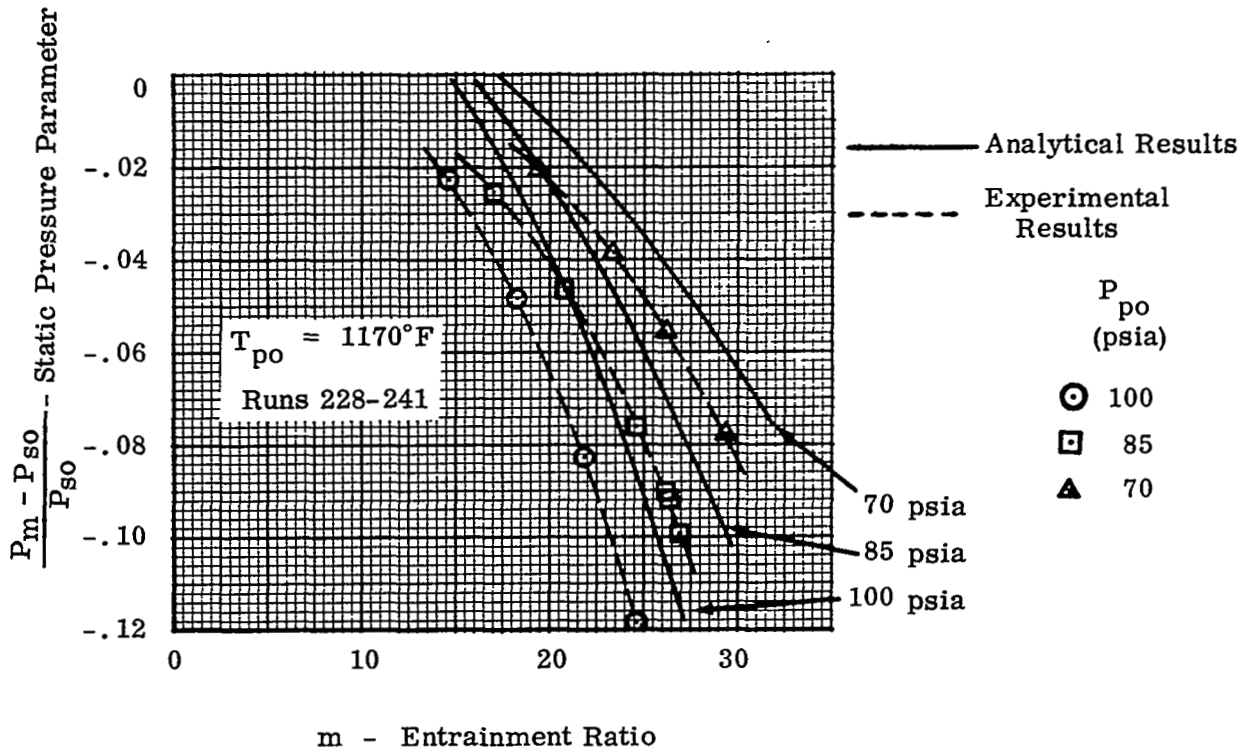
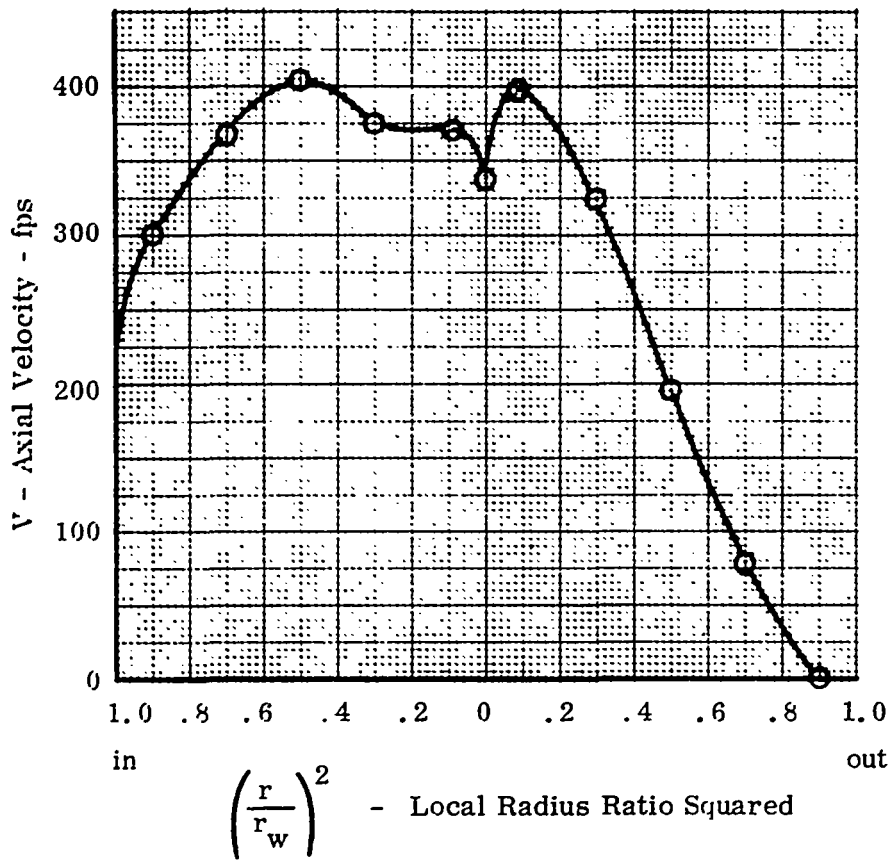


Figure 82
 Jet Pump Static Pressure Parameter Calculated at
 Mixing Tube Discharge

Short Constant Area Mixing Tube
 LD #1 Nozzle Cluster
 Case 3 Nozzles



Traverse 1

Run No. 240

$P_{po} = 85 \text{ psia}$

$T_{po} = 1159^\circ\text{F}$

$W_p = 5.73 \text{ lbm/min}$

$W_s = 150.4 \text{ lbm/min}$

$m = 26.3$

Figure 83

Velocity Profiles at Diffuser Discharge
Short Constant Area Mixing Tube

$d = 5.084'' \quad A_d/A_m = 1.61$

LD #1 Nozzle Cluster

Case 3 Nozzles

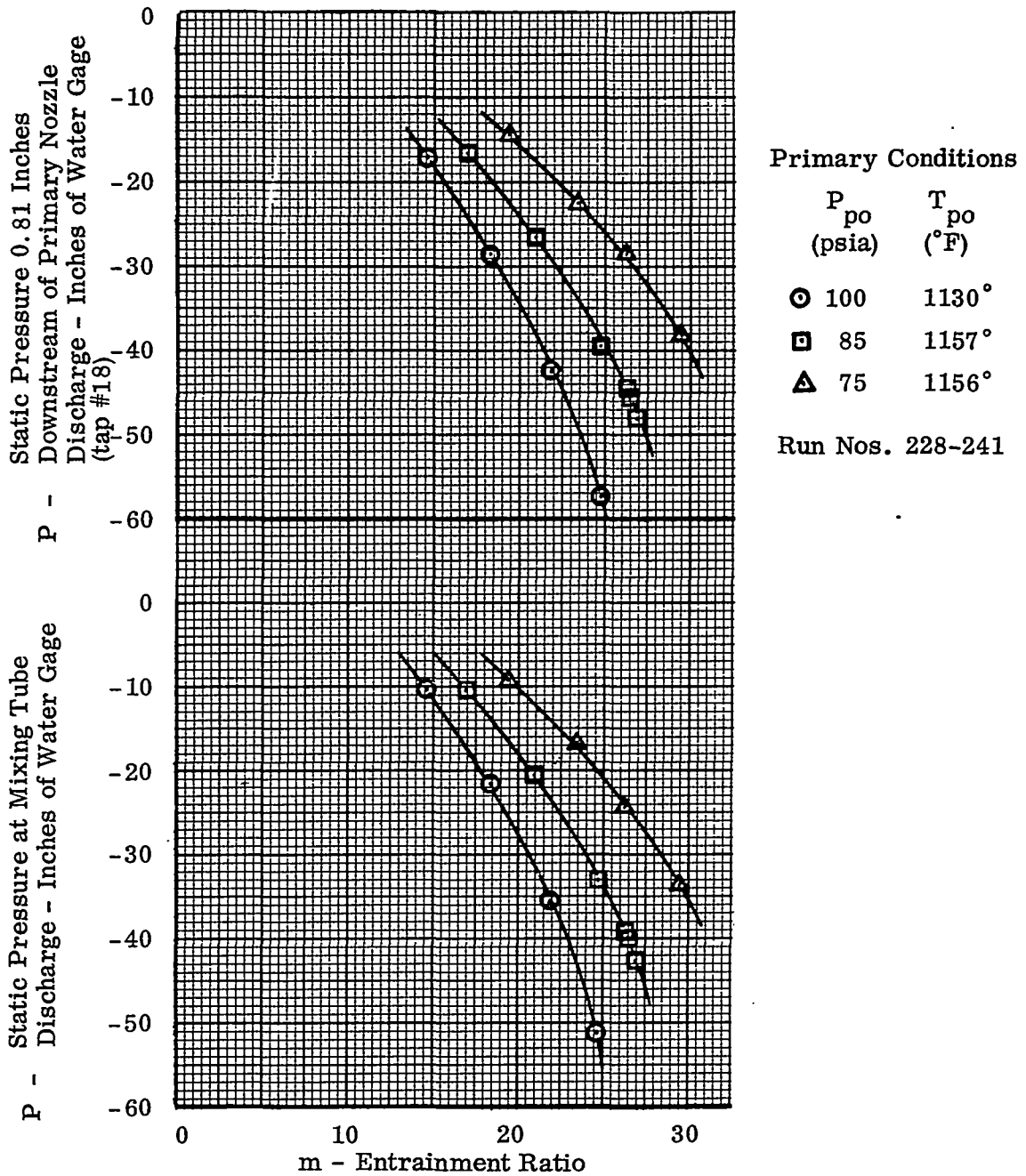
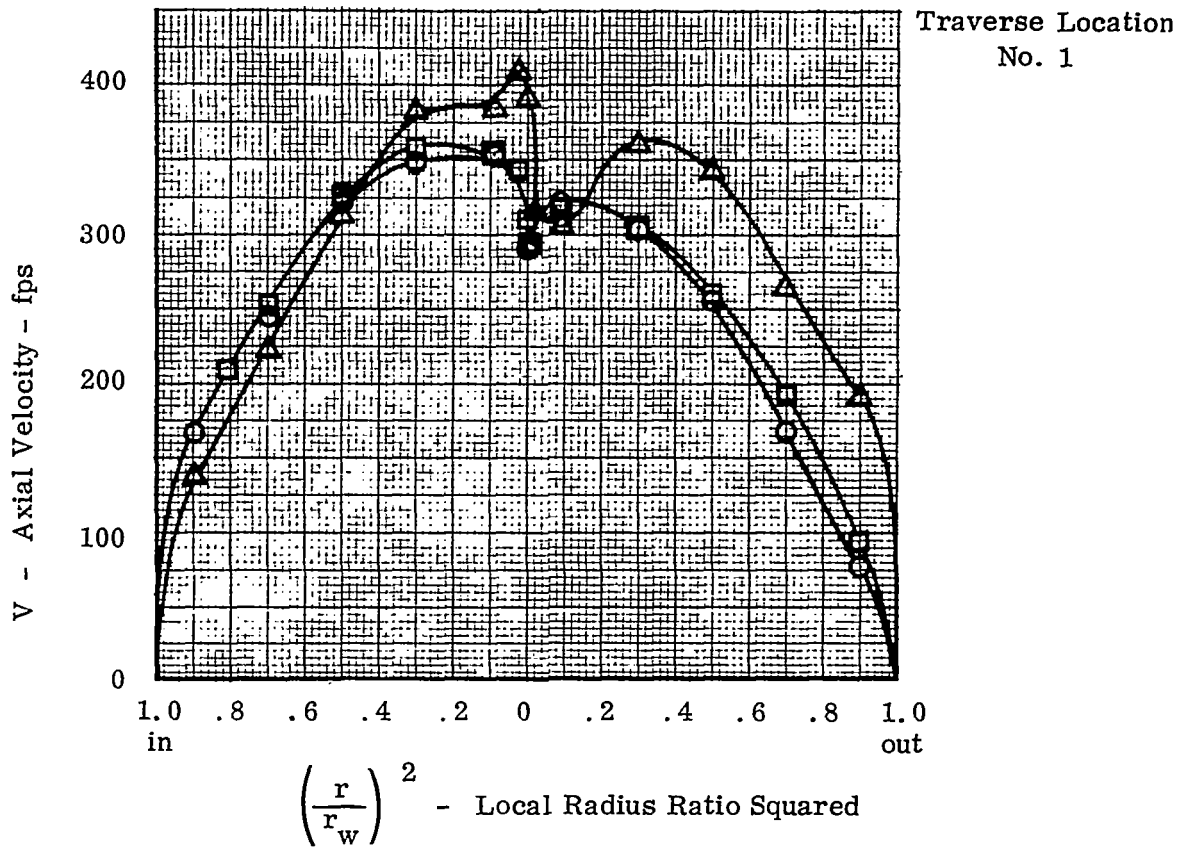


Figure 84

Static Pressures in Mixing Tube
Short Constant Area Mixing Tube
LD #1 Nozzle Cluster
Case 3 Nozzles



Test	P_{po} psia	T_{po} °F	W_p lbm/min	T_{so} °F	W_s lbm/min	m	Probe	Nozzles
○	313	140	5.95	71	146.9	24.7	Kiel	9 Case 2
◻	313	218	5.75	70	146.0	25.4	Wedge	9 Case 2
△	313	223	6.04	79	154.9	25.6	Kiel	8 Case 2 1 Case 4 in center

Figure 85
Velocity Profiles with Unheated Primary Flow
Short Constant-Area Mixing Tube
LD#1 Nozzle Cluster

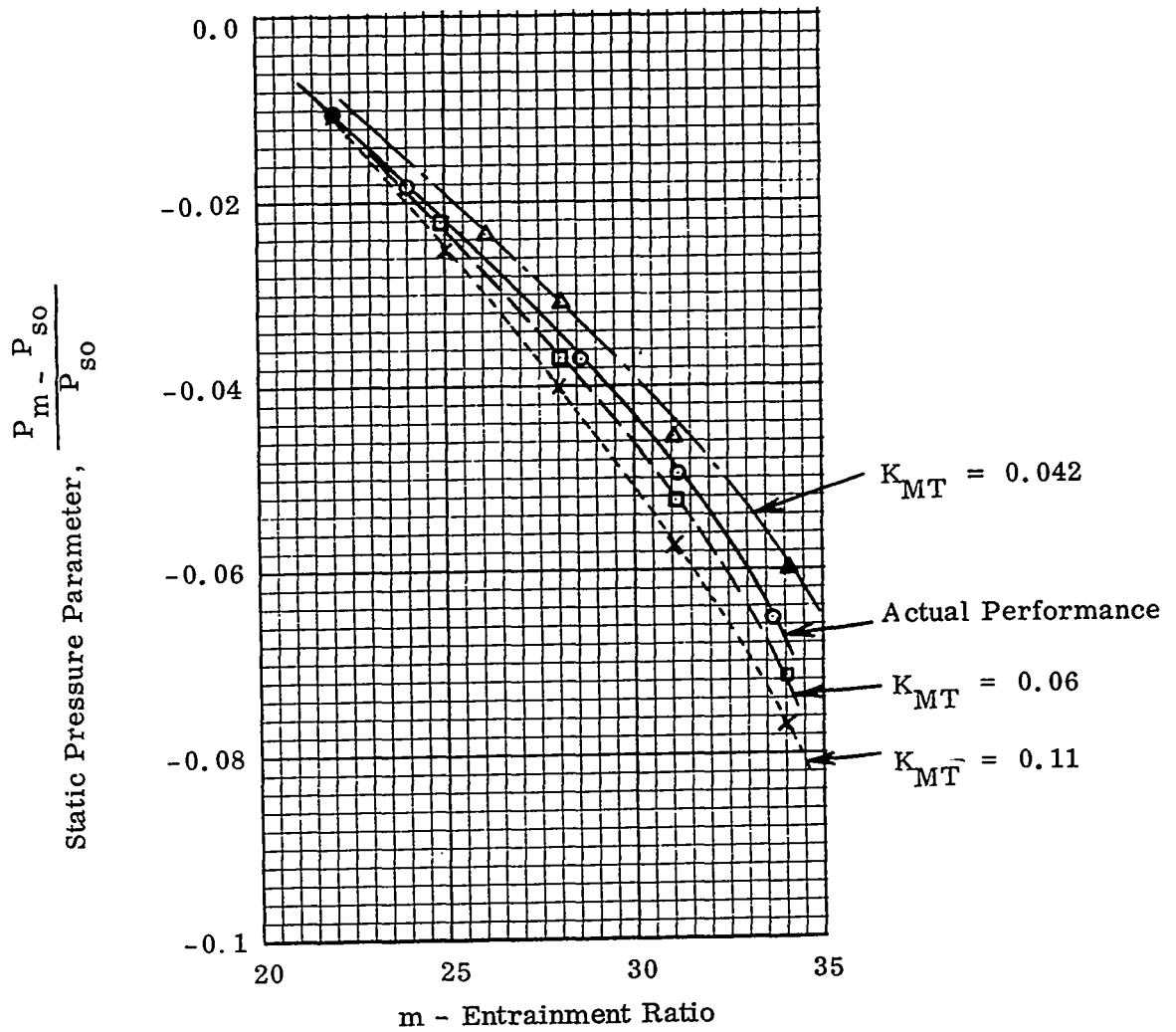


Figure 86

Influence of Duct Loss Coefficient Upon
Predicted Jet Pump Performance

Case 2 Nozzle, Extended Mixing Tube

$\bar{P} = 17.7$, $P_{po} = 260$ psia

$\bar{T} = 1.678$, $T_{po} = 455^\circ\text{F}$